

Glacial to Holocene development of Baffin Bay sedimentary systems: processes, provenances, and patterns

Dissertation

zur Erlangung des Doktorgrades der Naturwissenschaften (Dr. rer. nat.)
im Fachbereich Geowissenschaften der Universität Bremen/

submitted for the Doctoral Degree in Natural Sciences
at the Faculty of Geosciences, University of Bremen

vorgelegt von/

by

Emmanuel Okuma

Bremen, October 2023

Erstgutachter / 1st Reviewer: Prof. Dr. Dierk Hebbeln
Universität Bremen

Zweitgutachterin / 2nd Reviewer: Prof. Dr. Marit-Solveig Seidenkrantz
Aarhus University

Tag des Prüfungskolloquiums / Date of PhD Defence: 20th, December 2023

“The Arctic is our planet's refrigerator, and as we warm it, we're essentially leaving the fridge door open, affecting the entire climate system. It's time to take bold action to preserve this icy wonderland, for in its preservation lies hope for a balanced and stable world.”

Dr. James Hansen

Glacial to Holocene development of Baffin
Bay sedimentary systems: processes,
provenances, and patterns

Summary

Ongoing climate warming puts the Arctic in a perilous condition, as it now warms at least twice as fast as other regions in a process called Arctic Amplification. Rising atmospheric and ocean temperatures have forced the dramatic loss of Arctic ice observed in the last decades, with direct implications also for mid- to low-latitude regions via numerous atmospheric and oceanic connections. Understanding past Arctic ice (sheet)-dynamics related to changing climate and ocean conditions is instrumental in constraining numerical model-based projections of future environmental conditions better.

Baffin Bay, a narrow oceanic basin between Canada and Greenland connecting the Arctic and North Atlantic Oceans, is one of the ideal settings for studying past atmosphere-ice-ocean interactions in the northern high latitudes. Three major Northern Hemisphere ice sheets (the Laurentide, Innuitian, and Greenland ice sheets) partly surrounded Baffin Bay during the Last Glacial Maximum (LGM). These large ice sheets remained marine-based on Baffin Bay shelves until the early Holocene. Several studies reconstructing the sedimentary history of Baffin Bay have provided valuable insights into past ice sheet dynamics and paleoenvironmental changes in the region. However, most of these studies are concentrated on eastern Baffin Bay (i.e., the Greenland side), leaving the past ice-margin dynamics and paleoenvironmental conditions in western Baffin Bay poorly understood. In this thesis, we carried out multi-proxy analyses on five marine sediment cores in three separate studies with the aim of contributing to a better understanding of deglacial to Holocene sediment and ice sheet dynamics in western Baffin Bay.

In the first two studies (Chapters 4 and 5), AMS radiocarbon, sedimentological (computed tomography imaging and grain size analysis), mineralogical, and radiogenic isotope analyses of gravity core GeoB22336-4 raised from the mouth of the Lancaster Sound trough and gravity cores GeoB22346-3 and GeoB22357-3 recovered from the Clyde Inlet fjord and Clyde trough, respectively, allowed the reconstruction of local changes in sediment dynamics and provenances since the last deglaciation. These provided new insights into the retreat pattern of the Laurentide and Innuitian ice sheets from western Baffin Bay and subsequent paleoenvironmental developments. In the deeper Lancaster Sound trough in northern Baffin Bay, our study (Chapter 4) improved the retreat chronology of the Lancaster Sound Ice Stream, draining the confluent Laurentide and Innuitian ice sheets. AMS radiocarbon dating of the basal till ($> \sim 14.5$ ka BP) suggests the presence of a grounded ice stream in northern Baffin Bay until the start of the Bølling-Allerød interstadial. The prevailing presence of the Lancaster Sound Ice Stream during the Younger Dryas stadial enabled the rapid deposition of detrital carbonate-rich glaciomarine sediments eroded from proximal sources. Meanwhile, the basal till in the sediment core from the Clyde trough (Chapter 5) in western Baffin Bay most likely indicates a Younger Dryas mid-shelf stillstand (or re-advance) of the Clyde Ice Stream (draining the Laurentide Ice Sheet).

In the following early Holocene warming, ice streams of surrounding ice sheets rapidly retreated from marine-terminating to land-terminating positions. Radiogenic isotope data reveal the final deglaciation of the Lancaster Sound (~10.4 – 9.9 ka BP) and Nares Strait (~8.5 ka BP) and the re-establishment of Baffin Bay as an Arctic-Atlantic throughflow, also documenting the impacts of the Arctic gateways opening on sediment routing and deposition. The Clyde Inlet fjord core data show that the Laurentide Ice Sheet was already land-based in this region by ~9.5 ka BP, where the continuous decrease in meltwater discharge to the core site (into mid-Holocene) reflects the further collapse of the ice sheet. In northern Baffin Bay, this substantial reduction in meltwater input as ice sheets shrunk toward their minimum extent during the mid-Holocene probably permitted the deeper Atlantic-sourced warmer waters transported by the West Greenland Current to exert a stronger influence on surface waters. This interaction favored the intense melting of sea ice entering northern Baffin Bay, and the consequent release of sea ice-rafted debris most likely enabled the rapid accumulation of fine-grained sediments observed here.

In the late Holocene, the Neoglacial cooling trend observed in the Arctic, possibly in response to the combined decline in summer insolation and northward oceanic heat transport, is evident in the data from the cores from Clyde Inlet fjord and off Lancaster Sound. This cooling is most prominently displayed by the increase in iceberg-rafted large clasts in the last approximately two millennia, indicating the re-advance of regional glaciers.

In light of the new insights into the close coupling of sediment and ice-sheet dynamics in western Baffin Bay, the third study (Chapter 6) was conducted to compare spatial and temporal trends in sedimentation patterns across the entire Baffin Bay since the LGM. This study is based on the compilation of radiocarbon-derived sedimentation rates from the three sediment cores used in the first two studies (and the remaining two cores here), together with those from previously unpublished and published records from Baffin Bay, totaling 79 sediment cores. This Baffin Bay-wide data compilation shows that during the LGM and up until ~15 ka BP, the deep basin and slope were the only active sediment depocenters as ice sheets likely occupied the surrounding shelves. It highlights the transition from relatively low glacial sedimentation in the deep basin and slope to enhanced deglacial sedimentation on the shelves following the landward retreat of ice sheets from Baffin Bay. Furthermore, the data collated for the West Greenland shelf was converted into subglacial erosion rates, providing for the first time sedimentation rate-based erosion rates for the West Greenland Ice Sheet.

Overall, the present study demonstrates the usefulness of marine sedimentary archives from high-latitude glaciated margins for reconstructing paleo-ice sheet(s) dynamics closely linked to changing atmospheric and oceanic temperatures. The findings of this thesis significantly improve our understanding of the depositional history of Baffin Bay through the last major global warming, the last deglaciation, and provide an analogue of the Arctic ecosystem response to present and future global climate change.

Kurzfassung

Die fortschreitende Klimaerwärmung bringt die Arktis in eine gefährliche Lage, da sie sich inzwischen mindestens doppelt so schnell erwärmt wie andere Regionen, ein Prozess, der als arktische Verstärkung bezeichnet wird. Der Anstieg der atmosphärischen und ozeanischen Temperaturen hat zu dem dramatischen Verlust des arktischen Eises geführt, der in den letzten Jahrzehnten zu beobachten war, und der über zahlreiche atmosphärische und ozeanische Verbindungen auch für Regionen in mittleren und niedrigen Breitengraden fatale Folgen hat. Das Verständnis der vergangenen Eis(schild)dynamik in der Arktis im Zusammenhang mit den sich ändernden Klima- und Ozeanbedingungen ist von entscheidender Bedeutung, um Projektionen zukünftiger Umweltbedingungen anhand numerischer Modelle verbessern zu können.

Die Baffin Bay, ein enges ozeanisches Becken zwischen Kanada und Grönland, das den Arktischen und den Nordatlantischen Ozean miteinander verbindet, ist ein ideale Lokation für die Untersuchung vergangener Wechselwirkungen zwischen Atmosphäre, Eis und Ozean in den hohen nördlichen Breitengraden. Drei große Eisschilde der nördlichen Hemisphäre (der Laurentid-, der Inuit- und der Grönland-Eisschild) umgaben die Baffin Bay während des letzten glazialen Maximums (LGM) teilweise. Diese großen Eisschilde erstreckten sich bis zum frühen Holozän auf die Schelfe der Baffin Bay. Mehrere Studien zur Rekonstruktion der Sedimentationsgeschichte der Baffin Bay haben wertvolle Einblicke in die frühere Eisschilddynamik und die paläoökologischen Veränderungen in der Region geliefert. Die meisten dieser Studien konzentrieren sich jedoch auf die östliche Baffin Bay (d. h. die grönländische Seite), so dass die frühere Eisranddynamik und die Paläoumweltbedingungen in der westlichen Baffin Bay nur unzureichend bekannt sind. Im Rahmen dieser Dissertation wurden in drei separaten Studien Multi-Proxy-Analysen an fünf marinen Sedimentkernen durchgeführt, um zu einem besseren Verständnis der deglazialen bis holozänen Sediment- und Eisschilddynamik in der westlichen Baffin Bay beizutragen.

In den ersten beiden Studien (Kapitel 4 und 5) ermöglichten AMS-Radiokohlenstoff-, sedimentologische (Computertomographie und Korngrößenanalyse), mineralogische und radiogene Isotopenanalysen des Schwerelotkerns GeoB22336-4, der aus der Mündung des Lancaster Sound Trogs gewonnen wurde, sowie der Schwerelotkerne GeoB22346-3 und GeoB22357-3, die aus dem Clyde Inlet Fjord bzw. dem Clyde Trog geborgen wurden, die Rekonstruktion lokaler Veränderungen der Sedimentdynamik und der Sedimentherkunft seit der letzten Deglaziation. Dies lieferte neue Erkenntnisse über den Rückzug der Laurentid- und Inuit-Eisschilde aus der westlichen Baffin Bay und die nachfolgenden paläoökologischen Entwicklungen. Im tieferen Lancaster Sound Trog in der nördlichen Baffin Bay verbesserte diese Studie (Kapitel 4) die Rückzugschronologie des Lancaster Sound Eisstroms, der die zusammenfließenden Laurentid- und Inuit-Eisschilde entwässert. Die AMS-Radiokohlenstoffdatierung des basalen Till ($> \sim 14,5$ ka BP) deutet auf das Vorhandensein eines am

Boden liegenden Eisstroms in der nördlichen Baffin Bay bis zum Beginn des Bølling-Allerød-Interstadials hin. Die anhaltende Präsenz des Lancaster Sound Ice Stream während des Younger Dryas Stadials ermöglichte die schnelle Ablagerung von detritischen, karbonatreichen glaziomarinen Sedimenten, die von nahe gelegenen Quellen erodiert wurden. Der basale Geschiebelehm im Sedimentkern des Clyde-Trogs (Kapitel 5) in der westlichen Baffin Bay deutet höchstwahrscheinlich auf einen Stillstand (oder ein erneutes Vordringen) des Clyde-Eisstroms (der den Laurentid-Eisschild entwässert) in der Mitte der Jüngeren Dryas hin.

In der darauffolgenden Erwärmung des frühen Holozäns zogen sich die Eisströme der umliegenden Eisschilde rasch von marinen zu landgebundenen Positionen zurück. Radiogene Isotopendaten zeigen die endgültige Deglaziation des Lancaster Sound (~10,4 - 9,9 ka BP) und der Nares Strait (~8,5 ka BP) und somit die Wiederherstellung der Baffin Bay als arktisch-atlantischer Durchfluss an, was auch die Auswirkungen der Öffnung dieser arktischen Durchlässe auf die Sedimentführung und -ablagerung dokumentiert. Die Daten aus dem Fjordkern von Clyde Inlet zeigen, dass der Laurentid-Eisschild in dieser Region sich bereits um ~9,5 ka BP an Land zurückgezogen hat, wo der kontinuierliche Rückgang des Schmelzwasserabflusses zur Kernposition (bis ins mittlere Holozän) den weiteren Zusammenbruch des Eisschildes widerspiegelt. Als die Eisschilde während des mittleren Holozäns auf ihre minimale Ausdehnung schrumpften, ermöglichte wahrscheinlich die daraus resultierende erhebliche Verringerung des Schmelzwassereintrags in die nördliche Baffin Bay, dass das tiefere, aus dem Atlantik stammende wärmere Wasser, das vom Westgrönlandstrom transportiert wurde, einen stärkeren Einfluss auf das Oberflächenwasser ausübte. Diese Wechselwirkung begünstigte das intensive Schmelzen des Meereises in der nördlichen Baffin Bay, und die daraus resultierende Freisetzung von auf dem Meereis transportierten Sedimenten führte höchstwahrscheinlich zu der hier beobachteten raschen Anhäufung von feinkörnigen Sedimenten am Meeresboden.

Im späten Holozän ist der in der Arktis beobachtete neoglaziale Abkühlungstrend, der möglicherweise auf den kombinierten Rückgang der sommerlichen Sonneneinstrahlung und des nordwärts gerichteten ozeanischen Wärmetransport zurückzuführen ist, in den Daten der Bohrkerne aus dem Clyde Inlet Fjord und vor dem Lancaster Sound offensichtlich. Diese Abkühlung zeigt sich am deutlichsten in der Zunahme großer, von Eisbergen stammender Klasten in den letzten zwei Jahrtausenden, was auf ein erneutes Vordringen der regionalen Gletscher hinweist.

Angesichts der neuen Erkenntnisse über die enge Kopplung von Sediment- und Eisschilddynamik in der westlichen Baffin Bay wurde die dritte Studie (Kapitel 6) durchgeführt, um die räumlichen und zeitlichen Trends der Sedimentationsmuster in der gesamten Baffin Bay seit dem LGM zu vergleichen. Diese Studie basiert auf der Zusammenstellung von aus Radiokohlenstoff abgeleiteten Sedimentationsraten aus den drei Sedimentkernen, die in den ersten beiden Studien verwendet wurden (und den verbleibenden zwei Kernen in dieser Dissertation) mit, zuvor unveröffentlichten und veröffentlichten Daten aus der Baffin Bay, so dass diese Studie auf insgesamt 79 Sedimentkernen

basiert. Diese Baffin Bay-weite Datenzusammenstellung zeigt, dass während des LGM und bis ~15 ka BP das tiefe Becken und der Hang die einzigen aktiven Sedimentdepotcenter waren, da die umliegenden Schelfe wahrscheinlich immer noch von den Eisschilden bedeckt waren. Sie verdeutlicht den Übergang von relativ geringer glazialer Sedimentation im tiefen Becken und am Hang zu verstärkter deglazialer Sedimentation auf den Schelfen nach dem landwärtigen Rückzug der Eisschilde aus der Baffin Bay. Darüber hinaus wurden die für den westgrönländischen Schelf gesammelten Daten in subglaziale Erosionsraten umgerechnet, so dass zum ersten Mal auf Sedimentationsraten basierende Erosionsraten für den westgrönländischen Eisschild ermittelt werden konnten.

Insgesamt zeigt die vorliegende Studie, wie nützlich marine Sedimentarchive von vergletscherten Kontinentalrändern in hohen Breitengraden sind, um die Dynamik von Paläo-Eisschilden zu rekonstruieren, die eng mit sich ändernden atmosphärischen und ozeanischen Temperaturen verbunden sind. Die Ergebnisse dieser Arbeit verbessern unser Verständnis der Ablagerungs- und Gletschergeschichte der Baffin Bay erheblich und bieten ein Analogon für die Reaktion des arktischen Ökosystems auf gegenwärtige und zukünftige globale Klimaänderungen.

Acknowledgments

It is often said that “a journey of a thousand miles starts with just one step,” but many fail to acknowledge the powerful forces that set the steps in motion in the first place. So, I’ll start from the beginning. I want to thank my master’s thesis supervisor, Matthias Zabel, for drawing my attention to this PhD offer and for your subsequent motivating words that encouraged me to embark on this dream PhD-journey.

What can I say? Phew! This PhD journey has been the most thrilling experience of my life, filled with many excitements, opportunities, interesting and stressful challenges, frustrations during Corona times, and delightful moments. Trust me, this thesis would not have come to fruition without the incredible support and assistance of many people in various ways to whom I’m really indebted.

First and foremost, I would like to express my profound gratitude to my supervisor, Dierk Hebbeln, for giving me the opportunity to join your research group and thus making it possible for me to conduct this project at a state-of-the-art research institute like MARUM (Uni Bremen) in the first place. My biggest support: thank you, Dierk, for the excellent guidance, the ever-open doors, and your patience in the last four years of this project. For the countless advice, discussions, comments, ideas, encouragements, and the enormous time you invested in me, I sincerely appreciate them all. Thanks a lot, Dierk, as I always say 😊

Special thanks go to Markus Kienast for co-supervising this PhD work as our project partner from ArcTrain Canada. Thank you for your continuous support, advice, comments, and ideas; they were indeed of invaluable help, keeping me motivated throughout the years.

Another strong pillar in making this PhD project a reality is Jürgen Titschack, whom I would call my third supervisor. I am very thankful for your dedicated efforts and patience in introducing me to the CT measurements and processing of the CT data and for your guidance in the lab during the grain-size analysis. Thank you for always keeping your office door open for impromptu discussions, answering my questions, your attention to detail, and insightful comments and ideas on my manuscripts. Also, for going above and beyond to provide needed support in many ways in my personal and non-academic matters, Jürgen, I’m eternally grateful to you.

I would like to thankfully appreciate my thesis committee, Rüdiger Stein, Matthias Zabel, Dierk Hebbeln, Markus Kienast, and Jürgen Titschack, for your enormous support, critical discussions, and valuable advice on both scientific and career issues during our numerous meetings. Thank you all for your time!

Many thanks to my co-authors, Johanna Hingst, Lina Madaj, Simone Kasemann, Claude Hillaire-Marcel, Christoph Vogt, Alexandre Normandeau, Jens Weiser, Jürgen Titschack, Markus Kienast, and Dierk Hebbeln, for your swift responses and helpful comments on conference abstracts, posters, presentation slides, and your valuable contributions to improving our manuscripts. And Johanna, it’s

been a pleasure to closely share this PhD experience with you in our joint works, and I greatly appreciate/thank you for all the discussions and your time.

I want to thank Marit-Solveig Seidenkrantz for accepting to be the second reviewer of my thesis on such short notice, and with this comes the attendance of my thesis defense. Thanks for your helpful and motivating feedback after my conference presentation during the EGU General Assembly 2023.

To my wonderful colleagues (both past and present) in AG Hebbeln and AG Mohtadi, Dierk, Mahyar, Claudia, Jens, Jürgen, Jasmin, Rodrigo, Henrik, Luis, Leonardo, Martina, Chelsea, Christina (Klose), Christina (Gnade), Sinah, and Ziye (this list is by no means exhaustive), it has been a privilege and absolute pleasure to work with you all and to enjoy all the scientific meetings, coffee (and cookies) breaks, lunch breaks, birthday and paper cakes, occasional beer outings, Christmas dinners. Thank you all for the friendly atmosphere, incredible support, pleasant conversations, and good laughs. Jens, you deserve special thanks for being very welcoming from the very first days I stepped into our office and for all your subsequent support and discussions in helping me, a newcomer to Arctic research, settle in as quickly and easily as possible.

I also appreciate Christina Gnade, Volker Diekamp, Vera Bender, Vera Lukies, Jutta Bülten, Jasmin Ricks, Carmen Murken, Christina Klose, and Sinah Teumer for the numerous lab, IT, administrative, and GLOMAR Early-Carrier Researcher support. I am very much thankful for all your advice and assistance.

This PhD project was conducted as one of many projects within the international graduate school ArcTrain (Processes and impacts of climate change in the North Atlantic Ocean and the Canadian Arctic), a research partnership between the University of Bremen and eight Canadian Universities, and I'm very grateful to have immensely benefitted from the ArcTrain program. Of course, I acknowledge none of these projects would have happened without the funding from the Deutsche Forschungsgemeinschaft (DFG; IRTG 1904 ArcTrain). I appreciate the financial support from ArcTrain (and graduate school GLOMAR) that made possible my participation in several excursions, conferences, seminars, workshops, meetings, and retreats in Bremen and Canada. My special thanks go to Michal Kucera, Anne de Vernal, Maren Walter, Michael Siccha, and ArcTrain PhD (Bremen and Canada) students' representatives for all their efforts and time expended on administrative support, providing networking opportunities, coordinating annual meetings and retreats, and organizing courses, workshops, and monthly research seminars, in making ArcTrain a truly fascinating and growth experience all round for us all. To my fellow ArcTrain (and associate) members, thanks for all the wonderful time and scientific exchanges during our excursions, conferences, seminars, meetings, relaxing lunch breaks, dinners, drinks, karaoke nights, bowling, and chats, and also for creating a fantastic, enjoyable, and supportive environment to work in.

Many thanks to my friends, Awais, Angela, Azuka, Cyril, Hani, Martin, Nelson, Francine, Lilia, Sandro, Great, Trust, and the rest, for your care and concern and for supporting and encouraging me throughout these past years. You all have helped me in so many ways you may have thought lightly of: thanks for providing the needed distractions to forget my frustrations and stress, your listening ears and keen interest whenever I'm rambling about the joys and struggles of my PhD life, the after-work meals, wines/beers/softs, and cinemas, the get-away trips, the runnings, hikes and cycling tours, for the lovely gifts to put smiles on my face, and so much more fun times.

Last but not least, my deepest gratitude goes to my Mum, Dad, and dear siblings for your ever-present unconditional love, devotion, and support, as well as your, understanding, prayers, optimism, and advice that got me through this PhD years and made my dream come true. Miriam, thanks a lot for your tremendous energy in doing the hard work of almost single-handedly raising lovely Malia through these years and for all the great times we've all shared. To my "beautiful" wife, Uche, I can't thank you enough for the endless love, care, patience, understanding, and support I've enjoyed from you in the latter half of my PhD years, which, if I try to enumerate, would perhaps need thesis-thick pages to document. Thank you so much for taking care of everything especially when I wasn't looking and for being that one true shoulder I rely on.

Preface

This thesis was submitted to the Faculty of Geosciences (FB5) at the University of Bremen in partial fulfillment of the requirements for the degree of Doctor of Natural Sciences (Dr. rer. nat.). The PhD project was conducted as part of the International Research Training Group ArcTrain which is focused on studying the processes and impacts of climate change in the North Atlantic Ocean and the Canadian Arctic and was fully funded by the Deutsche Forschungsgemeinschaft (DFG). This research was supervised by Prof. Dr. Dierk Hebbeln and was carried out within the Marine Sedimentology Group at MARUM - Centre for Marine Environmental Sciences and the Faculty of Geosciences, University of Bremen, Germany. Co-supervision was provided by Prof. Dr. Markus Kienast at the Department of Oceanography, Dalhousie University, Halifax, Canada. This thesis is presented in a cumulative format and the main body is formed by three individual manuscripts (two first- and one co-authorship) that are either published, submitted, or in preparation for submission to an international, peer-reviewed, scientific journal. A brief overview of the contents of each chapter is given below.

Chapter 1 briefly defines the scientific motivation, provides general background knowledge, introduces the research area, its modern environmental and geological settings, glacial and oceanographic history, and the research objectives.

Chapter 2 presents the sample materials and the analytical methods used in this project.

Chapter 3 provides an overview of the three manuscripts and outlines the author's contributions to the manuscripts.

Chapter 4 contains the first manuscript titled Deglacial and Holocene sediment dynamics and provenances off Lancaster Sound: Implications for paleoenvironmental conditions in northern Baffin Bay. This manuscript is published in *Quaternary Science Reviews*, 2023.

Chapter 5 contains the second manuscript titled Proximal recordings of the NE Laurentide Ice Sheet retreat in Clyde Inlet (Baffin Island). This manuscript is in preparation for submission to a scientific journal.

Chapter 6 contains the third manuscript titled Shifting sediment depocenters track ice-margin retreat in Baffin Bay. This manuscript is submitted to *Communications Earth & Environment*, 2023.

Chapter 7 summarizes the main conclusions drawn from the individual manuscripts and presents the outlook for future research.

Contents

Summary	iv
Kurzfassung.....	vii
Acknowledgments	x
Preface.....	xiii
Contents.....	xiv
1. Introduction	1
1.1 Motivation: the Arctic – a critical component of the global climate system.....	1
1.2 Sedimentary archives off glaciated margins.....	3
1.3 Glacial-marine sedimentation off northern high-latitude glaciated margins.....	5
1.4 Research Area.....	6
1.4.1 Baffin Bay: modern physiographic and oceanographic setting.....	6
1.4.2 Geological setting.....	9
1.4.3 Baffin Bay paleo-environments since the LGM.....	10
1.5 Scientific objectives.....	11
2. Materials and Methods	13
2.1 Sediment cores used in this project	13
2.2 Methods	14
2.2.1 Chronology: radiocarbon analysis and age calibration.....	14
2.2.2 Sedimentological analyses.....	14
2.2.3 X-Ray Diffraction (XRD) mineralogical analysis.....	15
2.2.4 Additional analyses	15
3. Research overview and author contributions to the manuscripts	18
3.1 Manuscript I (Chapter 4)	18
3.2 Manuscript II (Chapter 5).....	19
3.2 Manuscript III (Chapter 6).....	21
4. Deglacial and Holocene sediment dynamics and provenances off Lancaster Sound: Implications for paleoenvironmental conditions in northern Baffin Bay	24
Abstract	24
4.1 Introduction	24
4.2 Regional Setting	27
4.2.1 Environment and Oceanography	27
4.2.2 Surrounding geology and related radiogenic isotope signatures	28
4.3 Material and Methods.....	29
4.3.1 Sediment core and location.....	29
4.3.2 Chronology	29
4.3.3 Sedimentological analyses.....	31

4.3.4 X-ray diffraction (XRD) mineral assemblage and pattern analyses	33
4.3.5 Radiogenic isotope analyses	33
4.3.6 Characterization of sediment provenance based on radiogenic isotope signatures	34
4.4 Results	35
4.4.1 Age model and sedimentation rates	35
4.4.2 Computed tomography and stratigraphic units	35
4.4.3 Grain-size distributions	37
4.4.4 Mineralogical association	38
4.4.5 Radiogenic Nd and Sr isotope composition	39
4.5 Discussion	40
4.5.1 Ice stream retreat and deglacial sediment dynamics (~14.5 to 10.3 ka BP)	40
4.5.2 Early-Holocene postglacial transition and the establishment of Arctic-Atlantic throughflow (10.3 to 8.5 ka BP)	42
4.5.3 Rapid fine-grained sedimentation in northern Baffin Bay during the HTM (8.5 to 5.8 ka BP)	45
4.5.4 Reduced sedimentation during the late Holocene (<5.8 ka BP)	47
4.6 Conclusions	48
Supplementary figure	50
5. Proximal recordings of the NE Laurentide Ice Sheet retreat in Clyde Inlet (Baffin Island)	52
Abstract	52
5.1 Introduction	52
5.2 Regional Setting	54
5.2.1 Oceanography and sea ice conditions	55
5.2.2 Geology, lithology, and related radiogenic isotope signatures	56
5.3 Materials and Methods	57
5.3.1 Chronology	57
5.3.2 Computed tomography	58
5.3.3 X-ray diffraction (XRD)	59
5.3.4 Radiogenic isotope analysis	59
5.4 Results	60
5.4.1 Age model and sedimentation rates	60
5.4.2 Stratigraphic units and computed tomography	62
5.4.3 Relative mineralogical composition (XRD)	63
5.4.4 Sr, Nd, and Pb isotope composition	63
5.5 Discussion	65
5.5.1 Outlet glacier retreat from the NE Baffin Island shelf into the Clyde Inlet during the Late Pleistocene to early Holocene	65
5.5.2 Early to late Holocene ice sheet retreat and glacier variability on NE Baffin Island as reflected in sediment data from the Clyde Inlet head (GeoB22346-3)	68
5.5.3 Radiogenic Sr, Nd, and Pb isotope composition of GeoB22346-3 – interpretation and challenges	70

5.6 Conclusion.....	72
6. Shifting sediment depocenters track ice-margin retreat in Baffin Bay.....	75
Abstract	75
6.1 Introduction	75
6.2 Sedimentation in Baffin Bay over the last 25,000 years	76
6.3 Discussion	80
6.4 Methods.....	84
6.4.1 Age calibration and sedimentation rates.....	84
6.4.2 Cores with basal till.....	85
6.4.3 Estimating subglacial erosion rates	85
Supplementary figures.....	87
7. Conclusions and Outlook	90
7.1 Conclusions	90
7.2 Outlook.....	92
8. Bibliography.....	95
9. Appendices	115
9.1 Supplement to Manuscript I (Chapter 4)	115
9.2 Supplement to Manuscript II (Chapter 5).....	122
9.3 Supplement to Manuscript III (Chapter 6)	126
Versicherung an Eides Statt / <i>Affirmation in lieu of an oath</i>	215

Chapter one

1. Introduction

1.1 Motivation: the Arctic – a critical component of the global climate system

Today, the Arctic (the regions north of 65 °N) is in a perilous situation as global warming has accentuated faster than elsewhere at alarming rates in the last decades (Overland et al., 2019; AMAP, 2021; IPCC, 2022). The extreme sensitivity of the Arctic to rising, partly anthropogenic-induced, global temperatures of the ongoing climate change is often highlighted by the phenomenon referred to as Arctic Amplification (Ding et al., 2014, 2019; Notz & Stroeve, 2016; Smith et al., 2019). Arctic Amplification describes the over twice-as-fast increase of near-surface temperature in this high latitude regions relative to those in mid to lower latitudes (Serreze & Francis, 2006; Serreze et al., 2009; England et al., 2021; Previdi et al., 2021). Rantanen et al. (2022), using satellite observational datasets over the last four decades, have shown that indeed the Arctic region has been warming almost four times faster than the rest of the planet (Fig. 1.1). Such faster warming rate in recent decades has huge environmental implications for the Arctic, most prominently expressed by the positive feedback of dramatic decline in (sea-)ice extent, thickness, and duration (and age) that have been observed in the field (Comiso, 2002, 2012; Nghiem et al., 2007; Polyakov et al., 2012; Screen et al., 2012; Box et al., 2019; Yadav et al., 2020) and simulated by various climate models (Holland & Bitz, 2003; Stroeve et al., 2012; Notz & Community, 2020; Rantanen et al., 2022). While the loss of sea-ice cover could open new marine shipping routes (e.g., the northwest passage; Smith & Stephenson, 2013; Melia et al., 2016), the associated reduction in albedo promotes enhanced oceanic heating as the ocean surfaces can absorb more of the incoming radiative solar energy than the more reflective sea ice (Jenkins & Dai, 2021). Furthermore, sea ice loss leads to diminished insulation which allows for more enhanced ocean heat (moisture and gas) transferred into the atmosphere, further amplifying Arctic warming and driving the rapid melting of sea ice, permafrost, ice caps, glaciers, and the ice sheets (Comiso, 2002; Miller et al., 2010; Yadav et al., 2020; Slater & Straneo, 2022), with compounding effects on global ice volume, climate, weather patterns, ocean circulation, and sea level (Holland et al., 2001; Cohen et al., 2014, 2018a, 2018b; Jung et al., 2015; Francis & Skific, 2015; Francis et al., 2017).

Locally, summer sea ice extent has been declining at a rapid rate of over 11% per decade since the late 1970s (Polyakov et al., 2012). In addition to the shrinking extent, the portion of multiyear sea ice (at least two years old) in the Arctic has decreased from 50–60% during the 1980s to only 15% in 2010

(Comiso, 2012; Polyakov et al., 2012). At these drastic rates, a seasonal sea ice-free Arctic will likely occur before the mid-21st century (Shen et al., 2023).

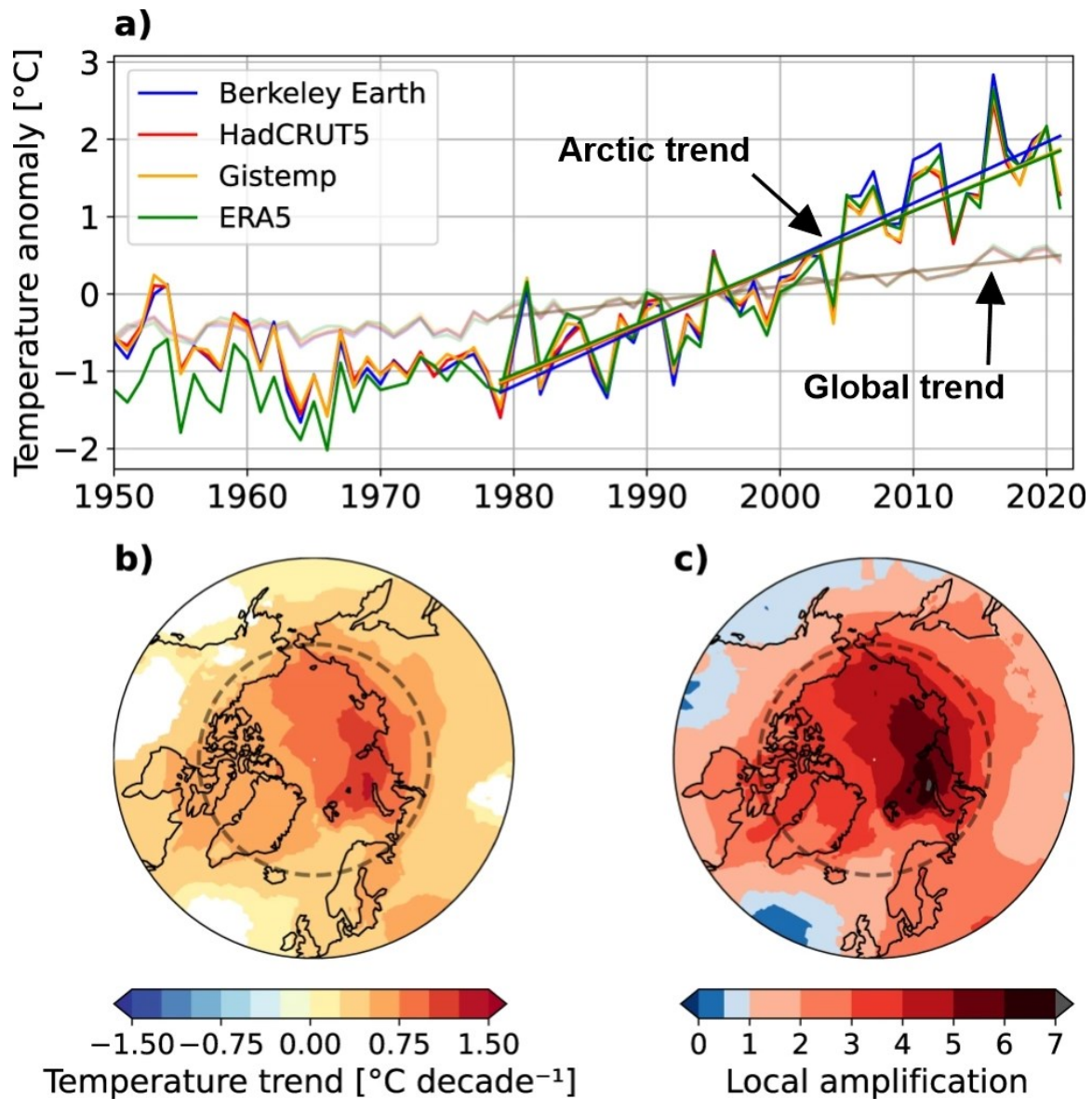


Figure 1.1: (A) Observed annual mean Arctic and global temperature anomalies from 1950 to 2021. The anomalies were calculated relative to the 30-year standard period (1981–2010). Arctic and global trends since 1979 are highlighted with black arrows. (B) Year 1979 to 2021 annual mean temperature trends based on the average of the observational datasets. Areas with a statistically insignificant change are depicted in white. (C) Local amplification ratio calculated for the same period. The dashed lines in (B) and (C) mark the Arctic Circle (modified after Rantanen et al., 2022).

Moreover, the Greenland Ice Sheet (GIS) and associated outlet glaciers and the smaller ice caps in the Canadian Arctic Archipelago (CAA), which are the most important freshwater reservoirs in the Arctic, have been undergoing tremendous mass loss in the last few decades in tandem with increased air and ocean temperatures (Rignot & Kanagaratnam, 2006; Stearns & Hamilton, 2007; Holland et al., 2008;

Bamber et al., 2012; Bjørk et al., 2012; King et al., 2020). This mass loss poses disastrous consequences for the Arctic cryosphere, terrestrial, and marine ecosystems (Hauser et al., 2018), as well as Arctic residents, especially indigenous peoples (Box et al., 2019), and beyond (IPCC, 2022). Unfortunately, as there continue to be increased emissions of greenhouse gases, the magnitude of earth warming is projected to increase throughout the 21st century, promoting further amplification of Arctic (and Antarctic) warming, forcing global cryospheric changes involving even greater and more rapid ice loss (Holland et al., 2006; Wang & Overland, 2012; Radić et al., 2014; Notz & Stroeve, 2018; Smith et al., 2019). By extension, this can potentially trigger dramatic perturbations in the atmospheric and oceanic systems in lower latitudes (Jacob et al., 2012).

Historical observational datasets since the (pre) satellite era have been immensely useful in furthering our understanding of Arctic ice (sheet)-dynamics, among others, connected to accelerated warming, which climate models have struggled to simulate (Box et al., 2019; Rantanen et al., 2022). However, these direct observations are limited to only short-term time scales (e.g., Alley et al., 2010; Bjørk et al., 2012; Hanna et al., 2013) and are inadequate bases for forecasting future climate changes and effects. In order to better constrain these future projections, reconstructing past environmental changes and ice sheet evolution (waxing and waning) on longer geological time scales provide indispensable clues for improved understanding, which enables well-informed and more realistic predictions (Stokes et al., 2015). To achieve this long-term perspective, we often rely on the proxy data from lacustrine and marine sedimentary archives off glaciated margins (e.g., Kaufman et al., 2004; Stein, 2008a; Simon et al., 2014; McKay et al., 2018; Seidenkrantz et al., 2019; Thomas et al., 2023), where evidence is better preserved from subsequent glacial erosion. In this thesis work, the sedimentological, mineralogical, geochemical, and micropaleontological (chronological) investigation of marine sediment cores from Baffin Bay elucidated sediment provenances, transport and depositional processes, and input rates that offer new insights into past ice sheet dynamics and paleoenvironmental conditions since the Last Glacial Maximum (LGM).

1.2 Sedimentary archives off glaciated margins

The Arctic marine environment is a valuable resource filled with clues for unveiling the northern high latitude Quaternary (i.e., the last ~2.6 Ma, divided into the Pleistocene and the Holocene) climate and ice sheet fluctuations (glacial-interglacial cycles; see Berger et al., 2005). Given that large continental ice sheets expanded onto adjacent northern high-latitude shelves during repeated Pleistocene glaciations (Batchelor et al., 2019), marine sedimentary deposits off these glaciated margins potentially serve as valuable recorders (archives) of paleoenvironmental conditions, thus making these areas attractive sites for the reconstruction of northern high latitude Quaternary climate and ice sheet dynamics.

Generally, the growth and decay of the Northern Hemisphere ice sheets throughout the Quaternary (Bowen et al., 1986; Batchelor et al., 2019) caused significant environmental changes (the same is true for the Southern Hemisphere ice, cf. Clapperton, 1990), including, for example, the respective fall and rise in the global sea level and the tectonic subsidence and uplift, due to (glacio-isostatic) loading and unloading, as the ice sheets grew and melted. The expansion of ice over large areas of land and adjacent continental shelves in the northern high latitudes resulted in the extensive reworking of the (pre- and) Quaternary landscapes and submarine environments (Dowdeswell et al., 2016a; Ottesen et al., 2022) and facilitated direct and substantial glacial-sediment delivery to and beyond the shelves (Heinrich, 1988; Hodell et al., 2008). Enhanced freshwater inputs (meltwater discharges) into the North Atlantic due to large-scale melting of continental ice sheets following peak glacial conditions (the so-called Heinrich events; Hodell et al., 2008) likely triggered the weakening or shutdown of the North Atlantic Deep Water (NADW) formation (Bohm et al., 2015). This essentially led to the destabilization and collapse of the Atlantic Meridional Overturning Circulation (AMOC) (Bohm et al., 2015), which by extension holds serious consequences for global ocean circulation and climate that exerts pressures on other Earth's ecosystems (Screen, 2017).

In today's present interglacial, the Arctic Ocean is also connected to the North Atlantic Ocean via the various channels of the CAA (e.g., Nares and Barrow Straits; Tang et al., 2004). However, these Arctic connections may have been totally blocked or partially restricted by marine-based ice during periods of full-glacial conditions (Batchelor et al., 2019; Dalton et al., 2022), obstructing these important pathways for Arctic-Atlantic water mass exchange and thus influencing (paleo-)oceanographic conditions (circulation pattern and water-mass composition) in the region (Aksu, 1983).

The most recent major ice advance (i.e., the Last Glacial Period) began at ~115 ka, with most ice sheets reaching their maximum extents during the LGM, largely between ~25 and 18 ka BP, and this is followed by the Last Deglaciation Period (Stokes et al., 2012; Dalton et al., 2020, 2022). The reconstruction of ice-margin dynamics prior to and from LGM-limits, which remains in part enigmatic, is essential to understanding the long-term behavior of the GIS margin (and Antarctica Ice Sheet) with respect to global climatic trends (Stokes et al., 2012; Briner et al., 2020). Off the previously and present-day high-latitude glaciated continental margins, past ice-margin dynamics can be deduced from a combination of seafloor geomorphology and environmental indicators (proxies) contained in the marine sediments (e.g., Aksu & Piper, 1987; Li et al., 2011; Simon et al., 2012, 2014; Dowdeswell et al., 2016b; Slabon et al., 2016; Brouard & Lajeunesse, 2017, 2019a).

1.3 Glacial-marine sedimentation off northern high-latitude glaciated margins

In terms of glacial-marine sedimentation off northern high-latitude glaciated margins, distinct types (pattern and mode) of sediment input and depositional environment are characteristic of full glacial (ice growth) and interglacial (ice decay) climatic conditions (Dowdeswell et al., 2016a). Moreover, the main area of sediment delivery and deposition (depocenters) markedly shifted across high-latitude fjords, shelves, slopes, and deep basins, as well as the sedimentary facies, between full glacial and interglacial periods (Dowdeswell et al., 2016a).

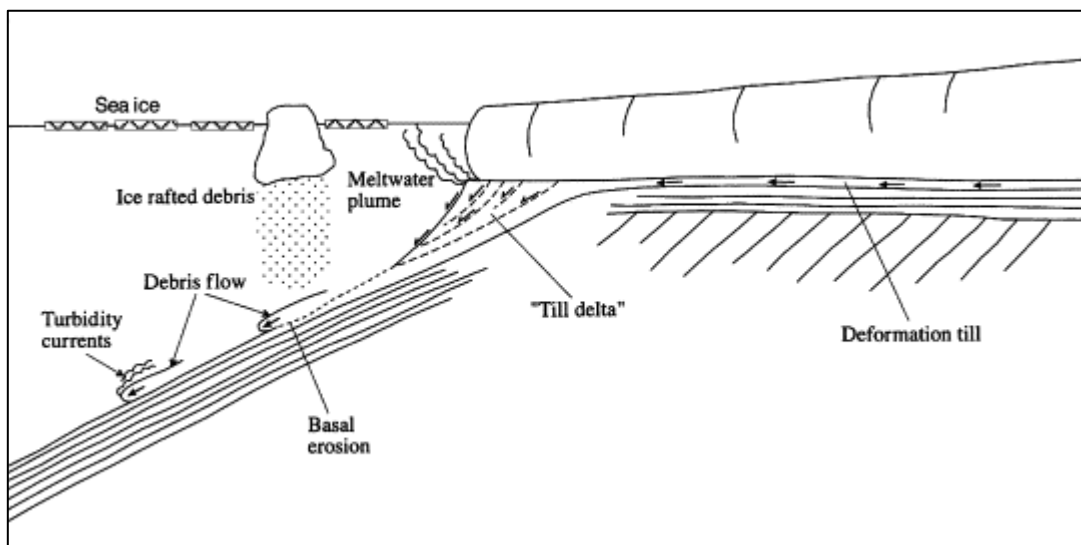


Figure 1.2: Simplified schematic showing the main sedimentological processes on glaciated margins during the presence of an ice sheet at the shelf edge (adapted from Stein, 2008b, who modified after Laberg & Vorren, 1995).

During the last glacial period, ice sheets expanded and the fast-flowing ice streams draining them advanced seaward, through connecting fjords and inter-island channels, over continental shelf-troughs transporting enormous amounts of glacially-eroded detrital and marine sediments (Syvitski, 1991; Dowdeswell et al., 2016a). Highly compacted subglacial- and unsorted lodgment- till sediments (units) are usually deposited at the base of shelf-crossing grounded ice (Fig. 1.2; Syvitski, 1991). Rapid accumulation of glacial debris (coarse-grained and poorly sorted sediments) may occur proximal to the grounding line or ice terminus (as part of ice proximal sedimentation), which can build up to form laterally extensive grounding zone wedges (GZWs), indicating periods and position of ice margin still-stands (Dowdeswell & Fugelli, 2012; Batchelor & Dowdeswell, 2015). Substantial amounts of these diamictic debris delivered by the ice stream to the shelf edge may be redistributed further downslope by mass-wasting processes triggered plausibly by ice sheet-related instability and sediment overloading (Dowdeswell et al., 1998; Ó Cofaigh et al., 2013a). Glacial debris flows (GDFs) are one of the most effective ways, after slumping and sliding, of transporting vast amounts of sediment to the slopes,

beyond trough mouths, whose deposits stack up on the slope to form the glacial-influenced trough-mouth fans (TMFs; Piper et al., 1985; Aksu & Hiscott, 1989; Vorren et al., 1998; Ó Cofaigh et al., 2003, 2013b; Batchelor & Dowdeswell, 2014). Turbidity currents also play an important role in sediment redistribution downslope for fan development (Ó Cofaigh et al., 2013b). In addition, iceberg rafting may disperse previously entrained sediments (e.g., dropstones) over large distances (ice distal) upon melting, as well as sediment transport by turbid glacial meltwater plumes (Aksu & Piper, 1987; Syvitski, 1991; Stein, 2008b; Ó Cofaigh et al., 2013a).

Upon deglaciation and landward retreat of the grounding line from the shelf edge, the ice-contact (basal till) deposits are progressively exposed to be covered by the ensuing rapid glaciomarine sedimentation (iceberg-rafted debris (IRD) and meltwater plumes) and mass-wasting deposits (e.g., Hogan et al., 2012; Streuff et al., 2017). The intensity of glaciomarine sedimentation decreases with increasing distance between the ice margin and the depocenter, and increasingly ice-distal deposition may be reflected by decreasing IRD content in the sediment record (Syvitski, 1991). As the ice (stream) retreats further into the adjacent fjords and hinterlands (during interglacial period), glacial-influenced sedimentation generally decreases, leaving the seafloor predominantly draped by slower accumulating (normal) hemipelagic post-glacial sediments that are relatively more bioturbated (Aksu & Piper, 1987; Syvitski, 1991; Ó Cofaigh et al., 2013a). Post-glacial marine sediments in the northern high latitudes' shelves contain comparatively less IRD, but the contribution from sea ice-rafting and meltwater plumes (especially from nearby tidewater-glacier outlets) can be significant (Hasholt, 1996; Hebbeln, 2000; Stein, 2008b; Overeem et al., 2017).

1.4 Research Area

1.4.1 Baffin Bay: modern physiographic and oceanographic setting

Baffin Bay is a narrow, semi-enclosed oceanic basin between Canada (Baffin Island and CAA) and Greenland, extending from latitude $\sim 67^{\circ}\text{N}$ to 76°N (Fig. 1.3). This 450 km wide, about 1300 km long ($\sim 689,000 \text{ km}^2$), and >2000 m deep bay connects the Arctic Ocean to the Labrador Sea/North Atlantic Ocean (Muench, 1973; Aksu, 1983; Aksu & Piper, 1987). The continental shelf off West Greenland is comparatively wider (on average 250 km wide) than that off Baffin Island (25–50 km) (Andrews, 1987; Tang et al., 2004; Andrews et al., 2014; Simon et al., 2014). The shelves around Baffin Bay (up to 500 m deep) are dissected by almost U-shaped, over-deepened cross-shelf troughs, extending from the coast to the shelf edges, and are connected to the TMFs on the slopes (Li et al., 2011; Ó Cofaigh et al., 2013b; Batchelor & Dowdeswell, 2014; Knutz et al., 2019).

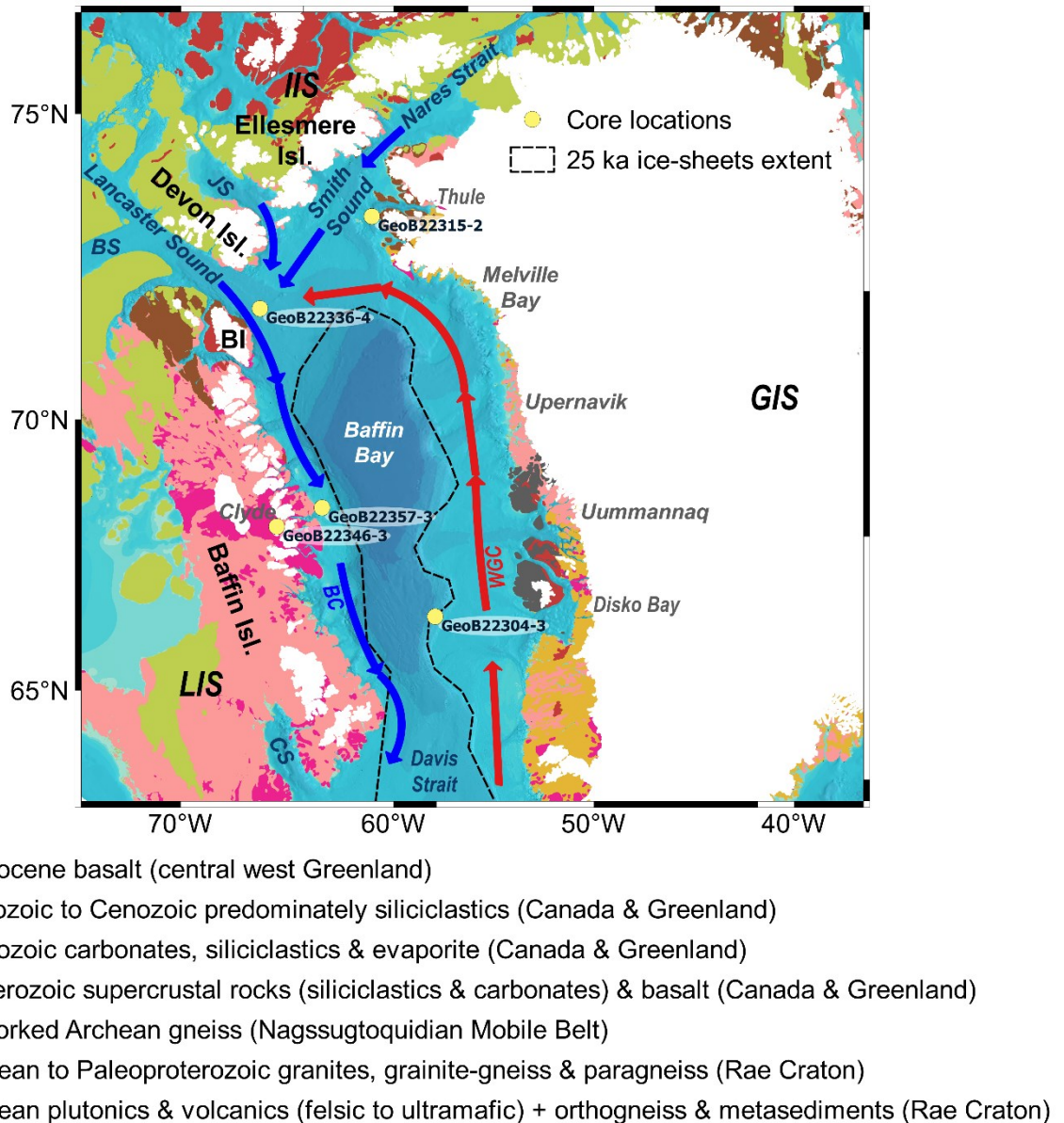


Figure 1.3: Location of Baffin Bay and the main oceanographic currents in the region, the Last Glacial Maximum (25 ka) ice sheet extent in Baffin Bay (black dashed line; Dalton et al., 2022), as well as simplified geology of the surrounding landmasses (after Harrison et al., 2011b). GeoB core sites are shown in yellow dots. BC = Baffin Current, WGC = West Greenland Current; LIS = Laurentide Ice Sheet, IIS = Innuitian Ice Sheet, GIS = Greenland Ice Sheet; BI = Baffin Island, Isl. = Island; BS = Boothia Sound, CS = Cumberland Sound, JS = Jones Sound. Map data from IBCAOv3 (Jakobsson et al., 2012).

The surface circulation in Baffin Bay is a counter-clockwise flow driven by two main current systems (Fig. 1.3), the West Greenland Current (WGC) and the Baffin Current (BC). The WGC is an admixture of Atlantic-sourced Irminger (warmer and more saline) and Arctic-sourced East Greenland (cooler and fresher) Currents which enters Baffin Bay from the south via Davis Strait and carries a relatively warm and saline water mass northward along the West Greenland coast (Tang et al., 2004; Dunlap & Tang, 2006; Münchow et al., 2015). In northern Baffin Bay, the WGC mixes with the southward-flowing BC

transporting relatively fresh and cold Arctic-sourced waters exiting the CAA channels of Lancaster Sound (connected to Barrow Strait), Jones Sound, and Smith Sound (connected to Nares Strait). The BC flow continues along the Baffin Island coast and beyond Davis Strait into the Labrador Sea, an important location for deep-water formation in the North Atlantic and crucial for global overturning circulation and climate modulation (Tang et al., 2004; Münchow et al., 2015).

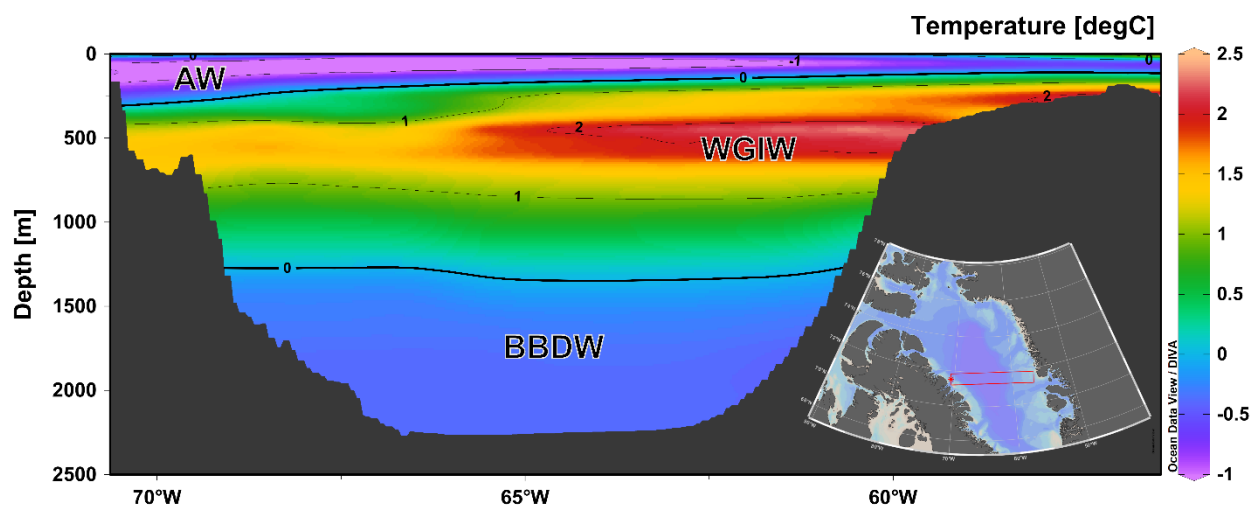


Figure 1.4: Overview (west-east) section of the main water masses defined in Baffin Bay (Tang et al., 2004) based on water temperatures. Temperature data is from Garcia et al. (2019): AW: Arctic Water, WGIW: West Greenland Intermediate Water, BBDW: Baffin bay Deep Water. Vertical section was generated using Ocean Data View v.5.2 (Schlitzer, 2019), and bathymetry data is from the General Bathymetric Chart of the Oceans (GEBCO_ 2014; Weatherall et al., 2015).

Three main water masses have been identified in Baffin Bay based on the spatial (horizontal-vertical) distribution of temperatures and salinities (Fig. 1.4; Tang et al., 2004): The topmost Arctic Water (AW), characterized by sub-zero temperatures and low salinity, forms the surface layer present throughout Baffin Bay, reaching down to 300 m in the western parts of the bay and shoals toward the eastern side (to about 100 m). This AW primarily consists of winter-cooled waters entering northwestern Baffin Bay from the CAA channels and meltwater input mainly from the GIS; the West Greenland Intermediate Water (WGIW) directly underlies the upper layer. This WGIW is typified by relatively higher temperatures ($> 0^{\circ}\text{C}$) and salinities ($S > 34$) and is usually found between 300 – 800 m water depths. The warmer WGC inflow via Davis Strait is the dominant contributor to the WGIW, which cools as it travels up north further into Baffin Bay; The Baffin Bay Deep Water (BBDW) floors the central part of Baffin Bay at depths below 1200 m, and is slightly colder and fresher than the overlying WGIW. The origin of BBDW is unclear since the sill depths of the CAA channels and Davis Strait are quite shallow (< 700 m) to allow direct connection to the Arctic and Atlantic Oceans (Tang et al., 2004).

It may be important to note that the present-day carbonate compensation depth (CCD) in Baffin Bay lies between ~ 600 and 900 m and, below this interval, the bottom water is very corrosive, resulting in intense

carbonate dissolution (Aksu, 1983), essentially rendering Baffin Bay deep sediments free of biogenic carbonates (e.g., foraminifera, ostracods, etc.). This has probably led to serious challenges in establishing radiocarbon chronological control on sediment records from deep Baffin Bay (e.g., Hiscott et al., 1989; Simon et al., 2012, 2014; Gibb et al., 2014). In addition, the inflow of Arctic waters, having a low (calcite) saturation state, through the CAA channels potentially promotes poor biogenic carbonate preservation off Baffin Island along western Baffin Bay (Azetsu-Scott et al., 2010). This is perhaps the reason why fewer paleoenvironmental studies (climate and ice-sheet dynamics) have been conducted on sediments from western Baffin Bay compared to the eastern part.

Baffin Bay is covered by sea ice for most of the year, except in the southeastern region, where the inflow of warmer WGC prevents the formation of any thick ice cover (Tang et al., 2004). Sea ice starts to form in October in the northwestern part of Baffin Bay and, from here, steadily spreads south as it reaches its maximum extent in March. Ice melt begins in April, initially in the North Water Polynya (NOW) and on the Greenland coast, and from August to September, the entire bay is mostly ice-free. Icebergs in Baffin Bay are mostly calved from West Greenland outlet glaciers, particularly areas around Disko and Uummannaq Bays, and some of these are drifted northward by the WGC before being redirected southwards by the BC to enter Davis Strait (Tang et al., 2004).

1.4.2 Geological setting

The Baffin Bay basin is a product of the North Atlantic-Labrador Sea rift system (Maclean et al., 1990). As a result, largely similar bedrocks can be observed along the bordering continental margins (Dawes, 2009; St-Onge et al., 2009; Andrews et al., 2018; Knutz et al., 2021). The bedrock geology of the landmasses surrounding Baffin Bay is composed of some of the oldest rocks on Earth: Archean to Paleoproterozoic granitic and gneissic rocks are exposed on the eastern Canadian (Baffin, Bylot, Devon, and southern Ellesmere Islands) and west Greenland margins, collectively referred to as the Rae Craton (Harrison et al., 2011b). Early Proterozoic reworked Archean blocks of the Nagssugtoquidian Mobile Belt are found around the coast of central west Greenland (Harrison et al., 2011b; Simon et al., 2014). These basement rocks are partly overlain by Proterozoic siliciclastic (also containing red beds and shales) and carbonate rocks, and minor basalt in northeastern Baffin Island and northwestern and northern Greenland (Harrison et al., 2011b).

Around northern Baffin Bay, the CAA channels are bordered by extensive Paleozoic carbonate (limestones and dolostones), siliciclastic, and evaporite outcrops (Hiscott et al., 1989; Harrison et al., 2011b). Younger Mesozoic – Cenozoic siliciclastics (with small amounts of coal and carbonates) can be found in the interior parts of the CAA (Harrison et al., 2011b). Paleocene basalts are observed along Disko and Uummannaq Bays in west Greenland (Harrison et al., 2011b; Simon et al., 2014).

1.4.3 Baffin Bay paleo-environments since the LGM

During the LGM, Baffin Bay was partly surrounded by the marine-terminating Laurentide Ice Sheet (LIS), Inuitian Ice Sheet (IIS), and GIS which coalesced in the north to form a continuous belt of (grounded) ice (England, 1999; Dyke et al., 2002; Funder et al., 2011), blocking Arctic water inflow through the northern gateways of the CAA channels (Fig. 1.3; Zreda et al., 1999; Knudsen et al., 2008; Jennings et al., 2011; Pieńkowski et al., 2012, 2014). This northern (ice) coalescence likely culminated in a thick floating ice shelf in northern Baffin Bay (Couette et al., 2022, 2023), while the rest of the bay is thought to be under heavy to pervasive sea ice cover (Gibb et al., 2015; Simon et al., 2016; Jennings et al., 2018). Several geomorphological and sedimentological evidence from Baffin Bay suggests that the margins of these ice sheets extended to the continental shelf breaks off Baffin Island and west Greenland (Ó Cofaigh et al., 2013b; Slabon et al., 2016; Newton et al., 2017; Brouard & Lajeunesse, 2017; Jennings et al., 2017; Lévesque et al., 2020). Moreover, glacial-ice stream was grounded deeper (in ~1300 m water depth) at the Lancaster Sound TMF in northern Baffin Bay (Harrison et al., 2011a; Li et al., 2011; Bennett et al., 2014; MacLean et al., 2017). However, rather less extensive ice margins on the Baffin Bay inner shelves (near-shore) have also been proposed by other studies (e.g., Dyke et al., 2002; England et al., 2006; Briner et al., 2007; Funder et al., 2011; Vasskog et al., 2015). Albeit, the widespread deposition of GDF deposits, diamictons, and turbidites on the slopes represent downslope redistributions (redeposition) of glacially eroded materials and indicate the presence of LGM ice streams at the shelf edges (Ó Cofaigh et al., 2013a,b; Dowdeswell et al., 2014; Campbell et al., 2017; Jennings et al., 2017; Jenner et al., 2018).

The onset of the LIS, IIS, and GIS collapse and subsequent landward retreat was probably asynchronous across Baffin Bay, but the timings remain poorly constrained (Jackson et al., 2017; Ownsworth et al., 2023). The incursion of warm Atlantic-sourced sub-surface waters likely forced the initial retreat of the GIS margin around central-west Greenland between 17.1 and 16.2 ka BP (Jennings et al., 2017), earlier than the onset at ~15 ka BP previously suggested (Ó Cofaigh et al., 2013b; Dowdeswell et al., 2014; Sheldon et al., 2016). Although not well constrained, the LIS retreat is believed to have been underway by ~16 ka BP (Brouard & Lajeunesse, 2017; Dalton et al., 2020), which is roughly coeval with the onset of ice-shelf break-up in northern Baffin Bay (~16.5 ka BP, Couette et al., 2022). In northwestern Baffin Bay, the Lancaster Sound Ice Stream, draining the coalesced LIS and IIS, is thought to have retreated from the trough-mouth into inner Lancaster Sound by ~15.3 ka BP (Kelleher et al., 2022), in contrast to a more outer (ice) position suggested around this time (Li et al., 2011; Dalton et al., 2020).

The landward retreat of the LIS and GIS was likely punctuated by periods of stillstand or transient readvances during the YD cooling as indicated by GZWs found on the mid-shelf areas of Baffin Bay (e.g., Hogan et al., 2016; Sheldon et al., 2016; Slabon et al., 2016; Couette et al., 2023). The following early-Holocene climate warming caused further retreat of these marine-terminating ice margins to

predominantly land-terminating positions, remaining close to their present-day near-minimum extent mostly onshore since mid-Holocene (Kaufman et al., 2004; Batchelor et al., 2019; Dalton et al., 2020). The deglaciation of Barrow Strait was probably completed between 10.6 and 10.4 ka BP (Kelleher et al., 2022; Pieńkowski et al., 2014), much earlier than Nares Strait which possibly opened between 8.5 and 8.2 ka BP (Knudsen et al., 2008; Jennings et al., 2011; Georgiadis et al., 2018; Kelleher et al., 2022). The retreat of glacial-ice from these CAA channels led to the early-Holocene reconnection of Baffin Bay to the Arctic Ocean (Jennings et al., 2011; Pieńkowski et al., 2012, 2014). Generally, deglacial sediment facies in Baffin Bay are mainly characterized by rapidly deposited pebble- and sandy-rich glaciomarine (IRDs and meltwater plumes) and mass-wasting deposits, whereas hemipelagic deposits predominate over the last 10-8 kyr only experiencing slight increase in IRD contribution during Neoglacial ice-advance (e.g., Aksu & Piper, 1987; Ó Cofaigh et al., 2013a,b; Hogan et al., 2016; Jennings et al., 2017; Kelleher et al., 2022; Weiser et al., 2023).

1.5 Scientific objectives

In the last decades, there has been an increase in the number of studies reconstructing past ice-sheet dynamics in the Baffin Bay region, and its paleoenvironmental impacts on oceanographic conditions, sedimentation pattern, and sediment provenance. Although Baffin Bay has indeed received a lot of attention, these efforts are quantitatively and qualitatively skewed toward the eastern part of the bay (off west Greenland), resulting in a comparatively poor understanding of paleoenvironmental conditions in northern Baffin Bay and western Baffin Bay (off Baffin Island). Taking this bias into consideration, our investigation set out to first address this knowledge deficit in two separate exploratory studies in northern and western Baffin Bay to test the general hypothesis that the sedimentation patterns in Baffin Bay since the LGM are predominantly controlled by the dynamics of surrounding ice sheets in a third study. Thus, this approach leads to the three key scientific objectives outlined below:

- 1) To reconstruct sediment and ice (stream) margin dynamics in northern Baffin Bay since the last deglaciation and throughout the Holocene, using a combination of proxy data and robust radiocarbon dating from a continuous sediment record, to assess the timing of ice-margin retreat and paleoenvironmental developments (sedimentation pattern and sediment provenances) following deglaciation.
- 2) To reconstruct sediment dynamics in the Clyde Inlet area of western Baffin Bay and its coupling to Laurentide Ice Sheet Holocene variability using multiproxy data from two well-radiocarbon-dated sediment records.
- 3) To reconstruct the overall sedimentation pattern in Baffin Bay since the LGM by compiling radiocarbon-derived sedimentation rates from sediment cores used in this study and other published records to assess overall changes in sediment input and the link to surrounding ice-sheet dynamics.

Chapter two

2. Materials and Methods

2.1 Sediment cores used in this project

A total of five gravity cores (GeoB22315-2, GeoB22336-4, GeoB22346-3, GeoB22357-3, and GeoB22304-3), recovered from across Baffin Bay, primarily used in this thesis (Fig. 1.3; Table 2.1) were provided by the GeoB Core Repository at MARUM – Center for Marine Environmental Science, University of Bremen, Germany. All sediment cores were taken in 2017 during Cruise MSM66 (WESTBAFF), also aimed at obtaining high-resolution sediment records from western Baffin Bay, aboard *R/V Maria S. Merian* (Dorschel et al., 2017). Cores GeoB22315-2 (Inglefield Bredning Fjord, Thule region) and GeoB22336-4 (mouth of Lancaster Sound) are from northern Baffin Bay, whereas cores GeoB22346-3 (Clyde Inlet fjord) and GeoB22357-3 (Clyde Trough) are from the western side of Baffin Bay. GeoB22304-3 is from the Disko Bay TMF in southern Baffin Bay.

Table 2.1: Details of sediment cores used in this thesis. All gravity cores were raised in Baffin Bay during the MSM66 Cruise in 2017 (Dorschel et al., 2017). Trough-mouth fan = TMF.

Core ID	Region	Latitude (N)	Longitude (W)	Length (cm)	Water depth (m)
GeoB22315-2	Thule	76° 55.11'	71° 57.68'	758	907
GeoB22336-4	Lancaster Sound	74° 04.43'	77° 26.99'	613	839
GeoB22346-3	Clyde Inlet	69° 54.18'	70° 13.54'	783	203
GeoB22357-3	Clyde Trough	70° 36.28'	67° 53.63'	902	315
GeoB22304-3	Disko Bay TMF	68° 54.18'	59° 28.62'	1144	1149

The data from core GeoB22336-4 form the basis of the first manuscript (Chapter 4), while cores GeoB22346-3 and GeoB22357-3 were investigated in the second manuscript (Chapter 5). Data from core GeoB22304-3 and other cores here, together with published records, were compiled and used in the third manuscript (Chapter 6). A number of analyses were performed on these cores, and some of the individual procedures are briefly described in the following methods section in order to avoid repetition, as detailed descriptions of some of the applied methods are given in the individual manuscripts.

2.2 Methods

2.2.1 Chronology: radiocarbon analysis and age calibration

Accelerator Mass Spectrometry (AMS) radiocarbon (^{14}C) dating of biogenic material retrieved from these sediment cores was fundamental in the establishment of chronological control providing the temporal context for the interpretations of changing sedimentation process (sediment transport and deposition), rates of sediment delivery, and sediment provenance. A detailed coverage of the main principles and challenges of the ^{14}C dating technique for age determination in paleoenvironmental studies is given by Skinner & Bard (2022).

For age determinations in the various cores, several syringe samples (~10 ml) of bulk sediments were taken at 5 to 20-cm intervals and then freeze-dried, wet-sieved to retain the 63-150 μm and >150 μm size fractions, and finally, the sediment fractions were oven-dried (at 50 $^{\circ}\text{C}$). Also, the weights of the samples were collected between each processing step (this provided preliminary data on grain-size distributions). Foraminifera (and ostracod) shells were hand-picked from the >150 μm size-fraction, with the aid of a binocular microscope, and the biogenic samples were sent for ^{14}C dating at the MICADAS (MIni CARbon Dating System) laboratory, Alfred Wegener Institute (AWI) in Bremerhaven, Germany. All ^{14}C ages obtained for each core were calibrated to calendar ages (stated in this thesis as 'ka BP') within the age-depth modeling process in UNDATABLE software (Lougheed & Obrochta, 2019) programmed in MATLAB, applying the Marine20 calibration datasets (Heaton et al., 2020) and variable marine reservoir age correction (ΔR) values outlined in the individual manuscript (Chapters 4 – 6).

2.2.2 Sedimentological analyses

2.2.2.1 Computed tomography

Non-destructive computed tomography (CT)-imaging of the archive halves of all cores was performed in order to obtain detailed 3D information on the overall lithofacies characteristics (internal structures), useful in the reconstruction of environmental and depositional conditions. The X-ray imaging of the cores was done using a CT scanning device (Philips Brilliance iCT Elite 256) at the hospital Klinikum Bremen-Mitte, Bremen, Germany. Information on the processing steps applied to the raw CT scans of the cores are described in Chapter 4. All CT scans but core GeoB22304-3 have been processed. The CT imaging of the cores in this thesis enabled the quantification of ice-rafted debris (IRD), bioturbation traces, and the identification of core intervals containing mass-wasting deposits.

2.2.2.2 Grain-size analysis

Standard grain-size analysis is routinely carried out on disaggregated inorganic sediment to determine the size distribution of particles in a sediment sample, which allows us to understand the underlying sedimentation processes, such as transport pathways, current speeds, and depositional conditions. Here, these measurements were performed using a Beckman Coulter Laser Diffraction Particle Size Analyzer LS 13320, and the sample preparation procedure and device set-up are fully described in Chapter 4. Laser grain-size analysis was only done on cores GeoB22315-2 and GeoB22336-4 to study sediment dynamics in northern Baffin Bay.

2.2.3 X-Ray Diffraction (XRD) mineralogical analysis

In order to gain insights into downcore changes in sediment provenances, the mineralogical composition of some of the sediment cores was determined through the X-ray diffraction method. The mineral assemblage and pattern analyses were carried out by Dr. Christoph Vogt in the lab of the Crystallography and Geomaterials Research Group belonging to the Faculty of Geosciences at the University of Bremen, Germany. The XRD measurements were performed using the Bruker D8 Discover diffractometer, and the approach employed here is described in Chapter 4. For cores GeoB22315-2 and GeoB22336-4, ~6 g samples of bulk sediments (every 20 cm), after freeze-drying, were wholly pulverized and homogenized to fine particles (<20 μm size) before measurement. Additional pulverized samples from cores GeoB22346-3 and GeoB22357-3 were sent by Johanna Hingst (Isotope Geochemistry Research Group) for XRD measurements as part of her PhD project, but these sediment samples were first wet-sieved to retain the finer < 63 μm fraction used. Mineralogical assemblages of the < 63 μm size fraction of these cores were determined in order to evaluate the possible influence of sediment mineralogy on radiogenic isotope compositions.

2.2.4 Additional analyses

2.2.4.1 Radiogenic isotope analysis

Just like XRD analysis for mineral composition, the analysis of radiogenic isotopic composition (e.g., Sr and Nd) of sediment samples can help to pinpoint the provenance of the sediments. This analysis was carried out on the < 63 μm grain-size fraction of cores GeoB22336-4, GeoB22346-3, and GeoB22357-3 by Johanna Hingst as part of her PhD work. The measurements were done using a Thermo-Fisher Scientific TRITON Plus thermal ionization mass spectrometer in the lab of the Isotope Geochemistry Research Group at MARUM, University of Bremen, Germany. The sample preparation and measurement procedures are also described in Chapters 4 and 5.

2.2.4.2 X-Ray fluorescence (XRF) core scanning and data calibration

Non-destructive XRF-scanning of all sediment cores was performed to determine the (geochemical) elemental composition of the records, useful in identifying changes in lithological units depicting varying depositional and environmental conditions and sediment sources. The XRF runs (10 and 30 kV) were conducted at 2 cm resolution using the XRF Core Scanner II (AVAATECH Serial No. 2) at MARUM, University of Bremen, Germany. The elemental data was acquired using a rhodium (Rh) tube, a Canberra X-PIPS Silicon Drift Detector, and a Canberra Digital Spectrum Analyzer. Raw data spectra were processed by the analysis of X-ray spectra by the Iterative Least square software (WIN AXIL) package from Canberra Eurisys.

XRF core scanning provides high-resolution and relatively rapid semi-quantitative measurements of elemental composition in split sediment cores. But the result is heavily biased towards lighter elements (e.g., Al and Si) due to the effects of differing porosity, water content, and grain size in the entire record, and have to be calibrated against elemental concentrations obtained using standard analytical methods (Tjallingii et al., 2007; Weltje & Tjallingii, 2008; Lyle et al., 2012; Boxberg et al., 2020). To calibrate the XRF core-scanner data into concentrations, 10 discrete sediment samples (~5 ml) were taken at arbitrary core depths, covering the range and trends of XRF elemental counts for cores GeoB22315-2 and GeoB22336-4. In order to quantify elemental concentrations (mg/kg), these samples were freeze-dried, pulverized, and then analyzed using PANalytical epsilon3-XL energy-dispersive XRF spectrometer in the lab of the Sediment Geochemistry Research Group at MARUM, University of Bremen, Germany. Instrument calibration is based on certified standard materials and analytical precision of replicate analyses on samples is found to be better than 1.8% for major elements.

These data are uploaded to the PANGAEA depository. Calibration of XRF scanner elemental intensities to “absolute” concentrations (%) can be done utilizing the XELERATE software package, employing, for example, the multivariate log-ratio calibration (MLC) algorithm (for details on this technique and prediction, see Weltje et al., 2015).

Chapter three

3. Research overview and author contributions to the manuscripts

The main body of this dissertation is prepared in a cumulative format, consisting of three individual manuscripts presented in the following Chapters 4, 5, and 6. These manuscripts, developed in collaboration with other scientific researchers, are either published, submitted (under review), or in preparation for submission to international peer-reviewed scientific journals. A brief overview of the individual studies, along with the various author contributions according to the format of Contributor Roles Taxonomy (CRediT; Allen et al., 2019), is given below.

3.1 Manuscript I (Chapter 4)

Deglacial and Holocene sediment dynamics and provenances off Lancaster Sound: Implications for paleoenvironmental conditions in northern Baffin Bay

Emmanuel Okuma^a, Johanna Hingst^a, Jens Weiser^a, Lina Madaj^b, Jürgen Titschack^{a,c}, Christoph Vogt^a, Markus Kienast^d, Claude Hillaire-Marcel^e, Dierk Hebbeln^a, and Simone A. Kasemann^a

^aMARUM - Centre for Marine Environmental Science and Faculty of Geoscience, University of Bremen, Germany

^bDepartment of Earth Sciences, Vrije Universiteit Amsterdam, Amsterdam, The Netherlands

^cSenckenberg am Meer, Marine Research Department, Wilhelmshaven, Germany

^dDepartment of Oceanography, Dalhousie University, Halifax, Canada

^eGeotop - Centre de recherche sur la dynamique du système Terre, Université du Québec à Montréal, Canada

Status: published in *Quaternary Science Reviews* 2023, Volume 309,

doi:10.1016/j.quascirev.2023.108101

The first study used a combination of sedimentological, mineralogical, and radiogenic isotope data from a well-radiocarbon-dated sediment core GeoB22336-4 from the mouth of the Lancaster Sound to reconstruct deglacial and Holocene sediment and ice-margin dynamics in northern Baffin Bay and assess the impacts of the deglaciation and opening of Arctic gateways (Lancaster Sound and Nares Strait) on environmental conditions and sediment routing. A basal till deposit in the core documents the presence of a grounded ice stream in northern Baffin Bay at ~14.5 ka BP, and subsequent retreat resulted in the deposition of thick glaciomarine units. Our data reveal changes in sediment provenances and dominant

sedimentation patterns linked to ice recession and the opening of Lancaster Sound (~10.4 – 9.9 ka BP) and Nares Strait (~8.5 – 8.2 ka BP).

Author contributions:

Emmanuel Okuma: Investigation, Formal analysis, Data curation, Methodology, Visualization, Writing - original draft, Writing - review & editing

My contributions include the collection (where necessary) and processing of samples (freeze-drying, wet-sieving, oven-drying, and weighing) and hand-picking of foraminifera for ¹⁴C-dating, developing the age model, CT-scanning/data-processing, collection and sample preparation/grain-size analysis, collection and sample preparation (freeze-drying, grinding, and weighing) for XRD-analysis, data analysis, preparation of figures/table, writing of initial draft, and writing of the final manuscript, together with Johanna Hingst, incorporating the advice, comments, and suggestions from other authors

Johanna Hingst: Investigation, Formal analysis, Data curation, Methodology, Visualization, Writing - original draft, Writing - review & editing

Jens Weiser: Visualization, Writing - review & editing

Lina Madaj: Data curation, Writing - review & editing

Jürgen Titschack: Resources, Data curation, Writing - review & editing, Supervision

Christoph Vogt: Investigation, Formal analysis, Writing - review & editing

Markus Kienast: Writing - review & editing, Supervision

Claude Hillaire-Marcel: Writing - review & editing, Supervision

Dierk Hebbeln: Conceptualization, Resources, Investigation, Writing - review & editing, Supervision, Funding acquisition, Project administration

Simone A. Kasemann: Conceptualization, Resources, Investigation, Writing - review & editing, Supervision, Funding acquisition, Project administration.

3.2 Manuscript II (Chapter 5)

Proximal recordings of the NE Laurentide Ice Sheet retreat in Clyde Inlet (Baffin Island)

Johanna Hingst^a, Emmanuel Okuma^a, Dierk Hebbeln^a, Claude Hillaire-Marcel^b, Friedrich Lucassen^a, Christoph Vogt^a, and Simone A. Kasemann^a

^aMARUM – Centre for Marine Environmental Science and Faculty of Geoscience, University of Bremen, Germany

^bGeotop - Centre de recherche sur la dynamique du système Terre, Université du Québec à Montréal, Canada

Status: in preparation for submission to an international journal

The second study presents sedimentological, mineralogical, and radiogenic isotope data on two radiocarbon-dated sediment cores from the Clyde Fjord (GeoB22346-3) and Trough (GeoB22357-3) system off Baffin Island. A basal till (in GeoB22357-3) and rapidly accumulated glaciomarine deposits in these records track the early-Holocene retreat of the Clyde Ice Stream (draining the northeastern Laurentide Ice Sheet) from western Baffin Bay (mid) shelf to the adjacent fjord head, and the complete shelf trough-fjord deglaciation occurred already by 9.5 ka BP. Strongly reduced glaciomarine sedimentation characterized the times since the mid-Holocene, in keeping with a fully disintegrated Laurentide Ice Sheet, until the last ~2 ka BP where our data indicates neoglacial re-advance of local glaciers.

Author contributions:

Johanna Hingst: Investigation, Formal analysis, Data curation, Methodology, Visualization, Writing - original draft, Writing - review & editing

Emmanuel Okuma: Investigation, Formal analysis, Data curation, Methodology, Visualization, Writing - review & editing

My contributions include the collection of syringe sediment samples from both cores, processing (freeze-drying, wet-sieving, oven-drying, and weighing) and subsequent hand-picking of foraminifera for ¹⁴C-dating, construction of the age models for both cores, CT-scanning of both cores and data-processing, analysis of the results, supported in the drafting of the methods section, data visualization, data interpretation, and data discussion, and contributed to reviewing and editing the manuscript in order to improve the original draft (by Johanna Hingst). This manuscript draft is still a work in progress.

Dierk Hebbeln: Conceptualization, Resources, Investigation, Supervision, Funding acquisition, Project administration

Claude Hillaire-Marcel: Conceptualization, Supervision, Writing - review & editing

Friedrich Lucassen: Conceptualization, Supervision, Writing - review & editing

Christoph Vogt: Investigation, Formal analysis

Simone A. Kasemann: Conceptualization, Resources, Investigation, Supervision, Funding acquisition, Project administration

3.2 Manuscript III (Chapter 6)

Shifting sediment depocenters track ice-margin retreat in Baffin Bay

Emmanuel Okuma^a, Jürgen Titschack^{a,b}, Jens Weiser^a, Alexandre Normandeau^c, Markus Kienast^d, and Dierk Hebbeln^a

^aMARUM - Centre for Marine Environmental Science and Faculty of Geoscience, University of Bremen, Germany

^bSenckenberg am Meer, Marine Research Department, Wilhelmshaven, Germany

^cGeological Survey of Canada (Atlantic), Natural Resources Canada, Dartmouth, Nova Scotia, Canada

^dDepartment of Oceanography, Dalhousie University, Halifax, Canada

Status: under review, submitted to *Communications Earth & Environment*, September 2023

(Manuscript Number: COMMSENV-23-1478-T)

The third study presents an overview of spatio-temporal variability in the pattern of sedimentation (input rates and deposition) in Baffin Bay coupled with the fluctuations of surrounding LIS, IIS, and GIS since the LGM. This research is based on the compilation of ¹⁴C-derived sedimentation rates from the sediment cores used in this PhD project, as well as from unpublished and published records. The results show that sedimentation in Baffin Bay probably occurred only beyond the shelves as they were likely occupied by extended marine-terminating ice sheets from the LGM until ~15 ka BP. Ice-margin retreat exposed new depocenters on the shelves which were fully deglaciated between 12-11 ka BP. These findings throw more light on the pattern of sedimentation in Baffin Bay and show strong controls exerted by ice-margin dynamics.

Author contributions:

Emmanuel Okuma: Investigation, Formal analysis, Data curation, Methodology, Visualization, Writing - original draft, Writing - review & editing

My contributions include the collection of syringe sediment samples primary cores used in this project, processing (freeze-drying, wet-sieving, oven-drying, and weighing) and subsequent hand-picking of foraminifera for ¹⁴C-dating, compilation of ¹⁴C ages of published and unpublished records, construction of all age models and sedimentation rates, analysis of the results, preparation of figures/tables, writing of original draft, and writing of the final manuscript (incorporating the advice, comments, and suggestions from other authors).

Jürgen Titschack: Writing - review & editing, Supervision

Jens Weiser: Data curation, Writing - review & editing

Alexandre Normandeau: Data curation, Writing - review & editing

Markus Kienast: Writing - review & editing, Supervision

Dierk Hebbeln: Conceptualization, Investigation, Supervision, Funding acquisition, Project administration

Chapter four

4. Deglacial and Holocene sediment dynamics and provenances off Lancaster Sound: Implications for paleoenvironmental conditions in northern Baffin Bay

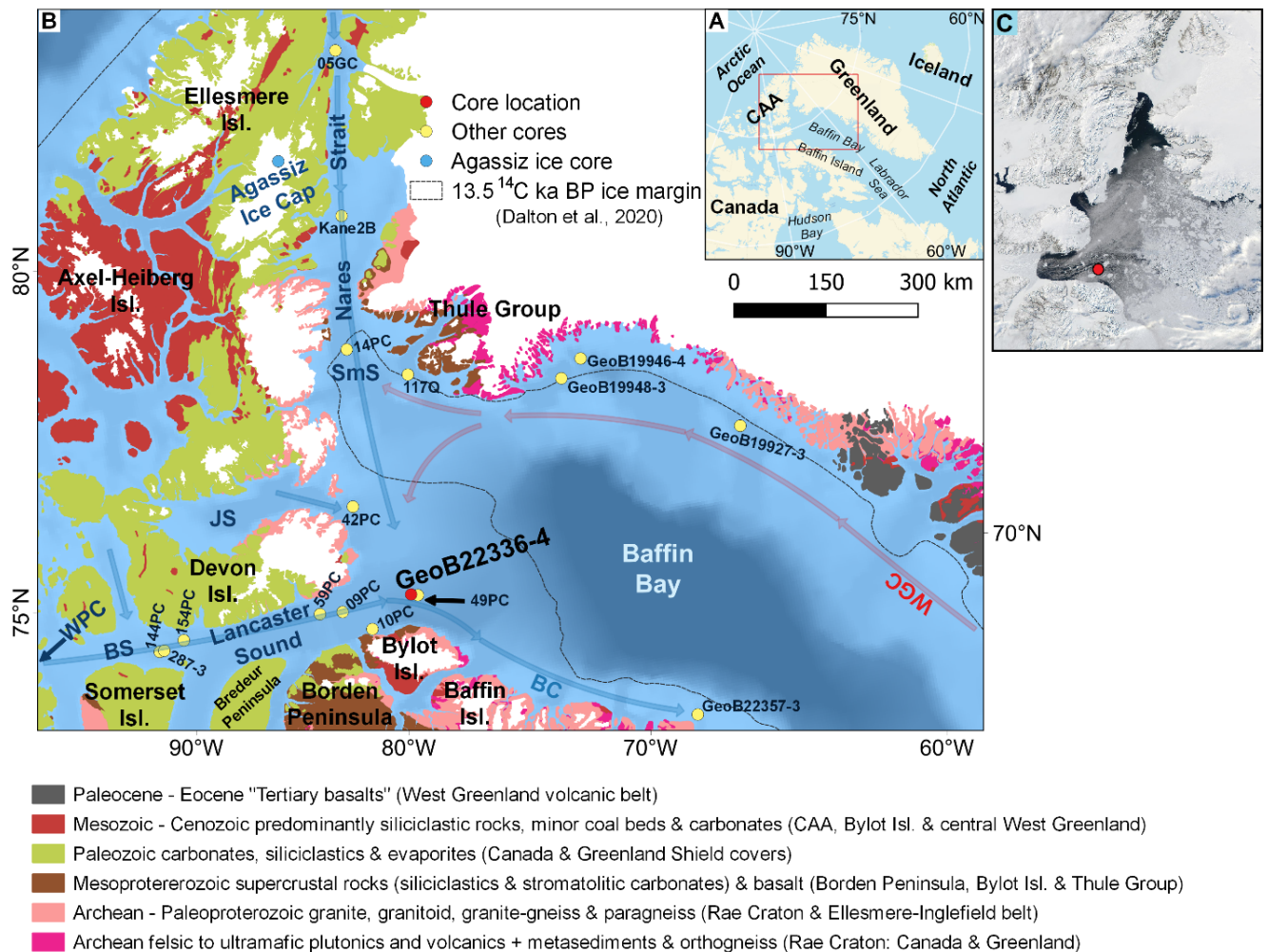
Abstract

Since the last deglaciation, Baffin Bay between Greenland and Canada developed from an isolated marginal sea to a major Arctic-Atlantic throughflow closely linked to the North Atlantic circulation. While the initial steps of gateway openings through Lancaster Sound and Nares Strait to northern Baffin Bay are reasonably well documented, far less is known about related regional deglacial-to-Holocene changes in sediment sources and depositional processes due to a lack of continuous and well-dated paleoenvironmental records from northern Baffin Bay. Sedimentological, mineralogical, and radiogenic isotope data of the well-dated sediment core GeoB22336-4 from the mouth of Lancaster Sound provide new insights on the impacts of ice-sheet retreat and opening of the gateways to the Arctic Ocean on the depositional setting. Basal subglacial till deposits point to a grounded ice stream at the mouth of Lancaster Sound before ~14.5 ka BP. Subsequent glaciomarine sedimentation is characterized by the input of ice-rafted detritus (IRD), bioturbation traces, and foraminifera shells. Decreasing sediment supply and input of IRD through time reflects a period of ice-sheet recession to predominantly land-terminating positions during the Early Holocene. Changes in radiogenic isotope signatures reveal the openings of Lancaster Sound between ~10.4 – 9.9 ka BP and of Nares Strait between 8.5 and 8.2 ka BP, in alignment with earlier studies. The rapid mid-Holocene (up to ~5.8 ka BP) deposition of fine-grained sediments is most likely caused by enhanced sea ice-rafted sediment input released under a strong West Greenland Current influence. Finally, a slight increase in IRD input during the last ~2 ka BP is linked to the neoglacial re-advance of regional glaciers.

4.1 Introduction

Today, Baffin Bay serves as a major Arctic-Atlantic throughflow, between Greenland and Canada, and constitutes an important component of the North Atlantic circulation (Holland et al., 2001; Tang et al., 2004; Jennings et al., 2019). Due to its proximity to major Quaternary ice sheets, it is a well-suited area to study ice margin and sea ice dynamics and their coupling to changes in late Quaternary climate and oceanography (e.g., Aksu & Piper, 1987; Andrews et al., 1998; Simon et al., 2014). During the Last Glacial Maximum (LGM), Baffin Bay was partly surrounded by grounded glacial ice of the extended Laurentide (LIS), Innuitian (IIS), and Greenland (GIS) ice sheets (England, 1999; Zreda et al., 1999;

Dyke et al., 2002; Dalton et al., 2020; Couette et al., 2022). The margins of the LIS, IIS, and GIS persisted on Baffin Bay shelves into the early Holocene and formed a continuous belt of ice over the Lancaster Sound, Nares Strait, and other smaller channels of the Canadian Arctic Archipelago (CAA) north of Baffin Bay (Fig. 4.1; Dalton et al., 2020). The blocking of these Arctic gateways prevented the inflow of Arctic Ocean water and ice into Baffin Bay (Dyke et al., 2002; Knudsen et al., 2008; Jennings et al., 2011; Pieńkowski et al., 2012, 2014).



Agassiz Ice Cap location. The red circle indicates the location of core GeoB22336-4 investigated in this study. Yellow circles represent the locations of other cores discussed or data shown in this study.

Past climate warming and the increasing influence of relatively warm Atlantic waters in the region likely forced the final collapse of the LIS, IIS, and GIS and their retreat from marine-terminating portions during the early Holocene (Dyke et al., 2002; Kaufman et al., 2004; Jennings et al., 2014, 2017; Dalton et al., 2020). Eventually, this led to the reconnection of the Arctic Ocean to Baffin Bay. The final separation of the coalescent LIS and IIS in the central Barrow Strait was probably completed between 10.6 and 10.4 ka BP (Pieńkowski et al., 2012, 2014; Kelleher et al., 2022), whereas the eventual severance of the IIS and GIS and the resulting opening of Nares Strait likely occurred much later between 8.5 and 8.2 ka BP (Knudsen et al., 2008; Jennings et al., 2011, 2019, 2022; Georgiadis et al., 2018; Kelleher et al., 2022). The deglaciation of these northern gateways controlled the connectivity of Baffin Bay to the Arctic Ocean (e.g., Jennings et al., 2011; Pieńkowski et al., 2012, 2014) and probably the sedimentary dynamics, particularly in northern Baffin Bay during the Early Holocene.

While the deglaciation pattern and subsequent opening of the Arctic gateways are fairly well documented based on marine geophysical and sediment core data (e.g., Zreda et al., 1999; England et al., 2006; Harrison et al., 2011a; Jennings et al., 2011; Li et al., 2011; Pieńkowski et al., 2012, 2014; Bennett et al., 2014; MacLean et al., 2017; Furze et al., 2018; Georgiadis et al., 2018; Kelleher et al., 2022), the impacts of ice-ocean interactions on paleoenvironmental and paleoceanographic conditions, especially in northern Baffin Bay, remain, in part, enigmatic. This is partly due to the lack of continuous records from northern Baffin Bay documenting environmental and oceanographic developments since the last deglaciation and throughout the Holocene. Previous studies reconstructing such developments in northern Baffin Bay are largely based on sediment records covering either the Holocene only (e.g., Ledu et al., 2008; Knudsen et al., 2008; St-Onge & St-Onge, 2014; Caron et al., 2019; Jennings et al., 2019; Stevenard et al., 2021) or the late Pleistocene to early Holocene (Furze et al., 2018; Kelleher et al., 2022). For instance, a recently published paleoenvironmental reconstruction from northern Baffin Bay partly based on core 49PC (Kelleher et al., 2022), taken close to the core location presented here (Fig. 4.1), suffers from an incomplete record and lacks radiocarbon age control for the most likely middle to late-Holocene sediment sequence. Thus, a continuous well-dated sedimentary record capturing the environmental conditions since the retreat of ice streams from the marine realm and the opening of Arctic gateways is so far unavailable from this region.

In the last decades, analyses of the mineral composition of Baffin Bay late Quaternary sediments have proven to be very useful in the differentiation of sediment provenance and the reconstruction of ice-sheet dynamics around Baffin Bay (e.g., Andrews & Eberl, 2011; Andrews et al., 2018; Andrews & Piper, 2022). Additionally, it has been shown that the strontium (Sr) and neodymium (Nd) radiogenic isotope composition of the detrital sediment fraction can serve as a reliable tracer for sediment source areas and as a valuable addition to the mineral data (e.g., Andrews et al., 2015). Indeed, the analyses of

the radiogenic isotope composition (Sr, Nd, and lead (Pb)) of sediment cores from Baffin Bay and the Labrador Sea provided additional insights into the history of LIS and GIS (Farmer et al., 2003; Colville et al., 2011; Reyes et al., 2014; Andrews et al., 2015; Filippova et al., 2023). Although radiogenic isotope studies in northern Baffin Bay have the potential to increase our understanding of glacial erosion and sediment transport processes during past glacial and interglacial cycles, such studies are still unavailable in this region. The only radiogenic isotope data from northern Baffin Bay are contained in a PhD Thesis (Madaj, 2021). Further, there included radiogenic isotope data of a sediment core from Nares Strait revealed changing sediment transport patterns and source distributions during the Holocene potentially providing new information on the stepwise deglaciation pattern and the final opening of this Arctic gateway.

This study is focused on the impacts of the retreat of Lancaster Sound ice stream and surrounding ice margins on environmental conditions and the sediment routing system in northern Baffin Bay. We document changes in sedimentation patterns related to the reconnection of the Arctic Ocean and Baffin Bay after the opening of Barrow and Nares Straits and the establishment of modern oceanographic conditions. To investigate temporal changes in (i) sedimentation pattern and (ii) sediment provenances, we analyzed the sedimentological characteristics (computerized tomography and grain size) and mineralogical and radiogenic isotope compositions from a new well radiocarbon-dated sediment core (spanning the last ~14.5 ka BP) recovered from northern Baffin Bay (GeoB22336-4; Fig. 4.1).

4.2 Regional Setting

4.2.1 Environment and Oceanography

Baffin Bay is a narrow, semi-enclosed ocean basin between west Greenland and northeastern Canada (Fig. 4.1). The basin is bordered by islands of the CAA at its northern end and to the south by the Davis Strait, an ocean passage connecting Baffin Bay to the Labrador Sea and the North Atlantic Ocean. The CAA channels, namely Lancaster Sound linked to Barrow Strait, Jones Sound (JS), and Smith Sound (SmS) linked to Nares Strait, connect the northern Baffin Bay to the Arctic Ocean.

In the northern Baffin Bay, the northward-flowing West Greenland Current (WGC), partly transporting relatively warm and saline Atlantic waters, meets the south-flowing cold Arctic surface waters that form the Baffin Current (BC; Fig. 4.1). The latter is dominated by relatively fresh water (and ice) coming from the Arctic Ocean through the CAA gateways. A majority of the WGC is deflected west- and southward in northern Baffin Bay to join the BC's southward flow (Tang et al., 2004; Dunlap & Tang, 2006; Münchow et al., 2015). The interaction of these ocean currents, as well as the presence of the northern and southern ice arches (or bridges) across Nares Strait, influences the formation and extent of sea ice (Tang et al., 2004), and the formation and persistence of the highly productive North Water Polynya (NOW) in the northernmost Baffin Bay (Melling et al., 2001; Ingram et al., 2002; Barber &

Massom, 2007; Jennings et al., 2011; Jackson et al., 2021; Ren et al., 2022). Today, sea ice covers almost all of northern Baffin Bay in winter (Tang et al., 2004). Between April and July, however, strong northerly winds, occasionally causing upwelling of warmer Atlantic water transported via the WGC near the Greenland coast, and the southward-flowing currents maintain the thin-ice-cover to open-water areas of the NOW (Fig. 4.1b) until September, when most of northern Baffin Bay is ice-free (Melling et al., 2001; Tang et al., 2004; Barber & Massom, 2007).

Besides the reoccurring NOW in the surface waters of northern Baffin Bay, another prominent feature is a complex submarine sediment fan system fed by former ice streams in the Lancaster, Jones, and Smith Sounds (Dyke et al., 2002; Harrison et al., 2011a). Particularly, the Lancaster Sound Trough Mouth Fan (TMF) is a large sediment fan that was formed by the delivery of glacially eroded materials by shelf-crossing Lancaster Sound ice streams during the Pleistocene (Harrison et al., 2011a; Li et al., 2011; Bennett et al., 2014; MacLean et al., 2017). These sediments and seafloor erosion patterns indicated by subglacial bedforms provide insights into the history of glacial erosion of surrounding landmasses and CAA channels (Li et al., 2011; Simon et al., 2014, 2016; Furze et al., 2018). Modern sediment transport to Baffin Bay occurs primarily through fluvial and meltwater plumes, icebergs and sea-ice rafting (Andrews, 1990; Andrews et al., 2018).

4.2.2 Surrounding geology and related radiogenic isotope signatures

The bedrock geologic units of the surrounding hinterlands bordering Baffin Bay and the channels of the CAA vary in age from Archean to (early) Cenozoic (Fig. 4.1; Harrison et al., 2011b). Archean to Paleoproterozoic crystalline shield rocks (mainly granite, granite-gneiss, and paragneiss), hence rich in quartz, plagioclase, K-feldspar, and clay minerals like mica and illites, are exposed in the ice-free areas of the still mostly glaciated west Greenland margin. Similar bedrocks are found on the Canadian side of Baffin, Bylot, Devon, and southeastern Ellesmere islands, which, together with the Greenland side, constitute the Rae Craton (Harrison et al., 2011b). Parts of this crystalline basement are still covered by several CAA glaciers and ice caps. Mesoproterozoic siliciclastics (including red beds and shales), carbonates, and volcanic (basalt) rocks of the Borden Peninsula, Bylot Island, and the Thule Group overlie parts of the Rae Craton (Harrison et al., 2011b). Extensive Paleozoic carbonates (dolostones and limestones), siliciclastics, and evaporites crop out on the adjacent land areas on either side of Barrow Strait to Lancaster Sound, Jones Sound, and northern Nares Strait and cover much of the Precambrian basement (Scott & de Kemp, 1998; Harrison et al., 2011b). In addition, Mesozoic to Cenozoic siliciclastics (with minor coal beds and carbonates) are found on the western side of Bylot and Ellesmere islands, and the so-called “Tertiary basalts” (e.g., Simon et al., 2014) occur along the shores of central west Greenland.

Information on the radiogenic isotope composition of the bedrocks bordering northern Baffin Bay and the CAA channels is rare, but measurements on nearby fluvial and detrital marine sediments (including

sediment cores) provide a range of Nd ($^{143}\text{Nd}/^{144}\text{Nd}$, expressed in ϵ_{Nd} values; see section 4.3.5) and Sr ($^{87}\text{Sr}/^{86}\text{Sr}$) isotope values, which are used as a reference to characterize these geological terrains. Generally, the old bedrock of the Rae Craton corresponds to unradiogenic ϵ_{Nd} values and more radiogenic Sr isotope signatures. For example, radiogenic isotope data from shelf sediments off northwest Greenland, bordered by Archean to Paleoproterozoic rocks, show ϵ_{Nd} and $^{87}\text{Sr}/^{86}\text{Sr}$ values ranging from -36 to -21 and 0.73 to 0.77, respectively (Madaj, 2021). Also, stream sediment (silts) data from southwest and central west Greenland near Precambrian bedrock yield ϵ_{Nd} values between -41 and -15 and $^{87}\text{Sr}/^{86}\text{Sr}$ values between 0.70 and 0.74 (Colville et al., 2011; Reyes et al., 2014). Composite bedrock data from the crystalline basement on eastern Baffin Island show an ϵ_{Nd} value of -32 and a $^{87}\text{Sr}/^{86}\text{Sr}$ value of 0.76 (McCulloch & Wasserburg, 1978). Younger rocks are usually characterized by more radiogenic ϵ_{Nd} and relatively unradiogenic Sr isotope signatures, as reflected by higher ϵ_{Nd} (-19 to -12) and lower $^{87}\text{Sr}/^{86}\text{Sr}$ (0.72 to 0.74) values observed in surface sediments from around the CAA (Maccali et al., 2018).

4.3 Material and Methods

4.3.1 Sediment core and location

This study is based on gravity core GeoB22336-4 (74° 04.43' N, 77° 26.99' W; 839 m water depth; 613 cm core length) retrieved from the mouth of Lancaster Sound approximately 50 km off Bylot Island in northern Baffin Bay during cruise MSM 66 onboard RV Maria S. Merian in 2017 (Dorschel et al., 2017, Fig. 4.1). This core site is ideally situated to record the influence of Arctic gateways (mainly the Lancaster Sound and Nares Strait) on sedimentation patterns and sediment provenance in northern Baffin Bay. According to the initial visual core description, the sediment consists of an upper olive-brown to olive-grey silty mud and transitions to a light brownish-grey, silty-muddy sand interval and a dark brownish-grey, sandy mud at the bottom of the core (Dorschel et al., 2017).

4.3.2 Chronology

4.3.2.1 Radiocarbon dating

Chronostratigraphic control for core GeoB22336-4 is achieved by obtaining several Accelerator Mass Spectrometry (AMS) ^{14}C -datings from mixed planktic and benthic (e.g., *Islandiella norcrossi*, *Nonionella labradorica*, *Cassidulina neoteretis*) foraminifera and ostracods conducted at the MICADAS (Mini CARbon Dating System) ^{14}C laboratory, Alfred Wegener Institute (AWI) in Bremerhaven, Germany. Since biogenic carbonate was rare, especially in the upper part of the sediment core, several subsamples at different adjacent depths were required to obtain sufficient material for dating. Foraminifera (and ostracods) were picked from the >150 μm size fraction after the original samples were

freeze-dried and wet-sieved. AMS ^{14}C measurements were carried out on 13 samples (Table 4.1). Due to the small sample size ($\leq 100 \mu\text{g C}$), the AMS measurements were performed with the acid hydrolysis (CO_2 gas) preparation method (for details see Mollenhauer et al., 2021).

4.3.2.2 Age model and calibration

The 13 AMS ^{14}C dates were calibrated using the open-source software UNDATABLE in MATLAB (Lougheed & Obrochta, 2019; settings: $\text{nsim} = 10^5$, $\text{bootpc} = 30$, $\text{xfactor} = 0.1$), which considers age-depth uncertainty in its rapid Bayesian approach in determining the best possible downcore age-depth relationship, applying the Marine20 calibration curve (Heaton et al., 2020). UNDATABLE uses the MatCal function (Lougheed & Obrochta, 2016) in MATLAB for the ^{14}C age calibration. In addition, we applied a regional marine reservoir age correction (ΔR) of 81 ± 18 years, proposed for NE Baffin Island by Pieńkowski et al. (2022), for the calibration of mid and late-Holocene ages (Table 4.1), assuming largely similar oceanographic conditions for these periods. For the calibration of early Holocene and deglacial dates, we adopted the regional ΔR values calculated from benthic and planktic paired dates according to Kelleher et al. (2022). They calibrated ^{14}C dates from benthic organisms between 10.2 and 8.1 ka using linearly decreasing ΔR values from 550 to 235 years, and a constant ΔR value of 550 years for dates older than this interval. These ΔR values were derived considering the previously proposed ΔR of 220 ± 20 years for the NE Baffin Island region (Coulthard et al., 2010), which is only valid for Marine13 calibration curve (Reimer et al., 2013). Here, using the updated regional ΔR (81 ± 18 years; Pieńkowski et al., 2022), valid for Marine20 calibration curve, as the base for additional reservoir correction, we employ ΔR values decreasing linearly from approximately 411 to 96 years for the calibration of ^{14}C ages between 10.2 and 8.1 ka. For ^{14}C dates obtained here from mixed benthic and planktic organisms, we used the mean value between planktic ΔR (81 years) and the corresponding benthic ΔR values. Furthermore, we use linear extrapolation to extend the age model outside ^{14}C -dated intervals, with the top of the core assumed to be ‘present’ or 0 years (1950 on the radiocarbon age scale).

We note that the applicability of the Marine20 global-average calibration curve is rather limited for samples from polar regions as it does not consider extreme local fluctuations in marine ^{14}C pools in response to rapid shifts in climatic and oceanographic conditions (Heaton et al., 2020). Nevertheless, Marine20 calibration curve provides significant improvements over previous marine calibration curves (Heaton et al., 2023a, 2020). Applying this calibration curve and the assumption of a constant ΔR over time potentially introduces unquantified uncertainty in the age model (Butzin et al., 2017). The appropriate regional marine reservoir offset (ΔR) values through time may differ from those used here (e.g., Heaton et al., 2023b), and thus the calibrated ages presented in this study should be used as best estimates.

Table 4.1. List of AMS ^{14}C dates obtained from core GeoB22336-4. All ^{14}C ages were calibrated within the age-modeling UNDATABLE software (Lougheed & Obrochta, 2019) using Marine20 dataset (Heaton et al., 2020) and applying a regional reservoir correction (ΔR) of 81 ± 18 years (after Pieńkowski et al., 2022) for mid and late-Holocene ages and variable ΔR values, described in the text, for older ages (after Kelleher et al., 2022). Calibrated ages are simply the median probability ages and 95% confidence interval (2 sigma: minimum and maximum age) based on the MatCal 3.1 ^{14}C age calibration software (Lougheed & Obrochta, 2016). Abbreviations: MBF, mixed benthic foraminifera; MBPF, mixed benthic and planktic foraminifera; O, ostracods.

Lab ID	Depth interval (cm)	Material	^{14}C Age		ΔR (yrs)	Calibrated age (yrs BP)		
			(yrs)	\pm		Min.	Max.	Median
6220.1.1	65–69	MBF	2513	65	81 ± 18	1691	2119	1898
5488.1.1	108–109	MBPF	3736	69	81 ± 18	3178	3622	3399
5489.1.1	109.5–110.5	MBPF	3640	69	81 ± 18	3051	3494	3282
5490.1.1	198–199	MBPF	6004	79	81 ± 18	5914	6350	6141
5491.1.1	258–259	MBPF	7111	79	81 ± 18	7150	7543	7340
5492.1.1	273–274	MBPF	7493	84	81 ± 18	7499	7913	7693
1724.1.1	290–291	MBF	7729	120	81 ± 18	7646	8213	7927
6221.1.1	323–324	MBPF	8696	92	134 ± 50	8645	9304	8997
5493.1.1	353–354	MBPF	9655	84	206 ± 50	9778	10424	10114
7625.1.1	443–444	MBF	10904	126	411 ± 50	11168	12006	11561
5494.1.1	473–474	MBF & O	10945	104	411 ± 50	11230	12004	11616
1725.1.1	498–499	MBF	11811	136	411 ± 50	12463	13068	12750
5495.1.1	568–569	MBPF	12968	119	246 ± 50	13833	14791	14265

4.3.3 Sedimentological analyses

4.3.3.1 Computed tomography

To gain insights into downcore variability in lithofacies characteristics, the archive halves of core GeoB22336-4 were scanned using a Philips computer tomography (CT) Brilliance iCT Elite 256 at the hospital Klinikum Bremen-Mitte, Bremen, Germany. This CT device is equipped with an X-ray source

voltage of 120 kV and a current of 300 mA. Core scanning was done at a resolution of 0.293 mm in the x and y directions and 0.625 mm resolution in the z -direction (0.3 mm reconstruction interval). The scans were reconstructed using the filtered Back Projection (fBP) mode and a bone kernel (YB (Enhanced)) and exported as DICOM data.

Further processing of the CT data was performed using the ZIB edition of the Amira software (version 2021.08; Stalling et al., 2005), partly following the processing approach described previously in Bartels et al. (2017). Similar x-ray density threshold values of >1500, 601 to 1499, 1 to 600, and <1 Hounsfield units (HU) were used for the segmentation of the >1 mm dense constituents (including iceberg-rafted debris (IRD) and lithified/pyritized bioturbation traces), open bioturbation (air- and water-filled) traces, matrix sediments, and the surrounding background (air and water), respectively. For the core interval 580 to 613 cm, the uppermost threshold value had to be adjusted to a slightly lower value (HU=1400) to properly segment the dense constituents from the matrix sediments. For the separation of the dense constituents into lithified/pyritized bioturbation traces and lithic clasts (IRDs), shape information had to be considered. Dense constituents with lengths >3 mm, a length/width ratio >2.6, and a length/volume ratio >0.1 are considered lithified bioturbation traces (parameters were calculated with the *Label Analysis* module and filtered with the *AnalysisFilter* module). Subsequently, touching IRD clasts were separated by running the *ContourTreeSegmentation* module (persistence mode: adaptive; persistent values: 0.003) on the distance map of the IRD segmentation (*DistanceMap* module). Afterwards, all IRD particles within and touching an ~1 cm thick analyzing window (33 CT slices) were automatically counted and divided by the total sediment volume within the respective interval to obtain IRD clasts cm^{-3} . The analyzing window was moved slice by slice, and the obtained results were written to a spreadsheet at the central slice position. In addition, each sediment constituent (IRD, bioturbation traces, and matrix sediments) was quantified using the *MaterialStatistics* module (volume per slice). Finally, the whole core (archive half) mean X-ray attenuation of the matrix sediment (unit: HU) of every CT was computed with the *MaterialStatistics* module (statistic per slice and label) as a proxy for the sediment density, in the following referred to as mean sediment density (MSD).

4.3.3.2 Grain-size analysis

Grain-size measurements were performed every 10 cm on ~0.5 ml bulk sediment in the Particle-Size Laboratory at MARUM – Center for Marine Environmental Sciences, University of Bremen, using a Beckman Coulter Laser Diffraction Particle Size Analyzer LS 13320. Sample preparation and measurements were carried out with deionized, degassed, and filtered water (filter mesh size: 0.2 μm) to reduce the potential influence of gas bubbles or particles within the water. Following the protocol outlined in McGregor et al. (2009), sample preparation to isolate the terrigenous sediment fractions entail a stepwise removal of organic carbon, biogenic carbonate, and biogenic opal by boiling the samples (in about 200 ml water) with 10 ml of H_2O_2 (35 %; until the reaction stopped), 10 ml of HCl (10 %; 1 min)

and 6 g of NaOH (10 min). Finally, ~ 0.3 g of tetrasodium diphosphate decahydrate ($\text{Na}_4\text{P}_2\text{O}_7 \cdot 10\text{H}_2\text{O}$) was added to the samples and then boiled for 3 min to disaggregate the remaining particles. After each preparation step, the samples were diluted with water (dilution factor: > 25). Prior to the measurements, each sample was sieved to remove the >2 mm sediment fraction. The grain-size distributions obtained with the particle size analyzer range from 0.04 to 2000 μm and are divided into 116 size classes. The calculation of the grain-size range is based on the polarization intensity differential scattering (PIDS; particles from 0.04 to 0.4 μm) and the Fraunhofer diffraction theory (particles from 0.4 to 2000 μm). The repeatability is checked regularly through replicate analyses of three internal glass-bead standards and is found to be better than $\pm 0.7 \mu\text{m}$ for the mean and $\pm 0.6 \mu\text{m}$ for the median grain size (1 SD). The average standard deviation integrated over all size classes is better than $\pm 4 \text{ vol.}\%$ (note that the standard deviation of the individual size classes is not distributed uniformly). Downcore particle size distributions and statistical parameters (including mean grain sizes) were derived by using geometric statistics.

4.3.4 X-ray diffraction (XRD) mineral assemblage and pattern analyses

To determine the mineral composition of core GeoB22336-4, X-ray diffraction pattern analyses were conducted on pulverized sediment samples (~6 g of <20 μm particle size, every 20 cm) in the laboratory of the Crystallography & Geomaterials Research Group (Faculty of Geosciences, University of Bremen). The samples were measured on a Bruker D8 Discover diffractometer equipped with a Cu-tube (k-alpha 1.541 \AA , 40 kV, 40 mA), a fixed divergence slit of $\frac{1}{4}^\circ$, and a monochromator (via Linxeye detector system). The measurements involve a continuous scan from $3 - 65^\circ 2\theta$, with a calculated step size of 0.016° . Mineral identification was performed utilizing the Philips software X'Pert HighScore™, and identification of sheet silicates was done with the freely available Apple MacIntosh X-ray diffraction interpretation software MacDiff 4.25 (<http://www.geologie.uni-frankfurt.de/Staff/Homepages/Petschick/Rainer.html#MacDiff>; Petschick et al., 1996). This was followed by a full quantification of mineral assemblages of the bulk fraction via the QUAX full pattern method (c.f. Vogt et al., 2002). The main mineral composition (and relative errors (2SD)) of the samples include carbonates ($\pm 1 \text{ wt.}\%$), quartz ($\pm 1 \text{ wt.}\%$), feldspars (± 2 to $5 \text{ wt.}\%$), and clay minerals ($\pm 5 \text{ wt.}\%$).

4.3.5 Radiogenic isotope analyses

Radiogenic isotope ratios of Sr and Nd were analyzed in the laboratories of the Isotope Geochemistry Group at MARUM – Center for Marine Environmental Sciences, University of Bremen. Approximately 2 g of wet sediment samples (taken at 10 to 40 cm intervals) were initially washed twice with Milli Q water (18.2 M Ω) to remove the soluble fraction and residual pore water and wet-sieved to obtain the <63 μm grain-size fraction used for further analysis. To remove carbonate from the silicate fraction and dissolve potential authigenic Fe-Mn oxyhydroxide coatings on the sediment, samples were leached with a solution of hydroxylamine hydrochloride and 15 % acetic acid (CH_3COOH), buffered with NaOH (for

3 hours; adapted from Gutjahr et al., 2007). The remaining detrital samples were washed with Milli Q water (twice) and dried, after which 100 mg of the siliciclastic fraction was transferred into 15 ml Teflon Savillex® beakers for sample digestion in several steps (modified after Höppner et al., 2018). Samples were dissolved in 3 ml of a concentrated HF:HNO₃ (5:1) mixture at 140 °C (at least 48 hours), dried, and re-dissolved in 3 ml of aqua regia (3:1, 6 N HCl: concentrated HNO₃) at 120 °C for two days. To remove organic matter, 100 µl of H₂O₂ was added to the samples (4 to 5 times) until the reaction stopped. Afterwards, 1 ml of concentrated HNO₃ was added to each sample, and the samples were placed on the hotplate (70 °C) overnight to dissolve again, dried, and re-dissolved in 3 ml 6 N HCl. Finally, the samples were dried and re-dissolved in 1100 µl 2 N HNO₃ for further chemical separation. Column chemistry was performed to separate Nd and Sr from the sample matrix. Sr was separated using 70 µl of Sr.spec™ resin, following a modified method after Deniel and Pin (2001). Nd was isolated in two steps using TRU.spec™ for light rare earth elements and LN.spec™ for Nd separation (Eichrom®) (method after Pin et al., 1994).

Isotope ratios were measured with a Thermo-Fisher Scientific TRITON Plus thermal ionization mass spectrometer (TIMS). Sr isotope composition was measured using a single filament, a Ta activator, and the static multicollection mode, whereas Nd isotope composition was analyzed on double filaments in a static multicollection mode. The stable ratio of ⁸⁶Sr/⁸⁸Sr (= 0.1194) was used to correct the instrumental mass fractionation that occurs during Sr isotope analysis. To assess the analytical accuracy and repeatability of the ⁸⁷Sr/⁸⁶Sr data, the reference material NIST SRM 987 was used with an analyzed value of 0.710246 ± 0.000018 (2SD_{mean}, n = 5), which is within the range of values analyzed by TIMS and published in the GeoRem database of 0.710250±0.000034 (2SD_{mean}, n= 1711, data <0.7102 and >0.7103 are discarded) (<http://georem.mpch-mainz.gwdg.de/>, 2022). During Nd analysis, instrumental mass fractionation was corrected to ¹⁴⁶Nd/¹⁴⁴Nd (= 0.7219). The analytical accuracy and repeatability for ¹⁴³Nd/¹⁴⁴Nd were monitored by the reference material JNdi-1, which yielded a value of 0.512111 ± 0.000022 (2SD_{mean}, n = 3) and agrees with the published values of 0.512107±0.000024 (2SD_{mean}, n= 414, data <0.51204 and >0.51217 are discarded) analyzed by TIMS (GeoRem database, <http://georem.mpch-mainz.gwdg.de/>, 2022). The ¹⁴³Nd/¹⁴⁴Nd ratio is reported in the ε_{Nd} notation relative to the Chondritic Uniform Reservoir (CHUR) value (¹⁴³Nd/¹⁴⁴Nd = 0.512638; Jacobsen & Wasserburg, 1980) to emphasize changes in radiogenic Nd isotope composition.

4.3.6 Characterization of sediment provenance based on radiogenic isotope signatures

For sediment provenance reconstructions, the Sr and Nd isotopic signatures from core GeoB22336-4 are compared with available reference data describing the characteristic radiogenic isotope composition of adjacent geological terrains. Due to the paucity of reference radiogenic isotope data, especially from the CAA and Baffin Island regions, we incorporate two additional data sets from sediment cores from

Barrow Strait (PS72/287-3; Jokat, 2009; Appendix Table 9.1.2) and the Baffin Island shelf (GeoB22357-3; Dorschel et al., 2017; Appendix Table 9.1.3; Fig. 4.1). These additional samples were analyzed in the laboratories of the Isotope Geochemistry Group at MARUM, following similar preparation and analytical steps described above (Section 4.3.5). The radiogenic isotope data from the Holocene part of the core PS72/287-3 (chronology is based on parasound data and correlation with the ^{14}C dated core ARC-3; Vare et al., 2009; Stein et al., 2009; Niessen et al., 2010) form a distinct cluster and are representative of sediments deposited in this area under postglacial conditions. For sediment provenance discussion, they are used here as an end-member to track sediments from the Barrow Strait area. Additionally, the radiogenic isotope data obtained from core GeoB22357-3 from Baffin Island shelf are grouped with the data from cores GeoB19927-3 and GeoB19946-4 from the northwestern Greenland shelf (Madaj, 2021), also analyzed at MARUM following similar procedure as mentioned above, to represent the Sr and Nd isotope signatures of the proximal Rae Craton (Archean and Archean to Paleoproterozoic are differentiated).

4.4 Results

4.4.1 Age model and sedimentation rates

The final age-depth model of sediment core GeoB22336-4 is based on 13 calibrated AMS ^{14}C dates and indicates that the entire core record extends to ~ 14.5 ka BP, spanning from the last deglaciation through the Holocene (Fig. 4.2). The sedimentation rates between calibrated ages primarily range from 27 to 73 cm ka^{-1} . Exceptions are the lowest (22 cm ka^{-1}) and highest (545 cm ka^{-1}) values observed near a turbidite interval, which was identified in the deglacial part of this core (see section 4.4.2). The deglacial period is characterized by a moderate sedimentation rate of 46 cm ka^{-1} to over 62 cm ka^{-1} , followed by a drop to lower rates of 27 to 31 cm ka^{-1} during the early Holocene. During the mid-Holocene, sedimentation rates increased to moderate to high values of 42 to 73 cm ka^{-1} , and during the neoglacial period (late-Holocene), the rates dropped again towards lower values of ~ 31 cm ka^{-1} .

4.4.2 Computed tomography and stratigraphic units

Analyses of the CT-scans of core GeoB22336-4 reveal downcore changes in sediment characteristics, which in relation to the age model, allow the differentiation of five main stratigraphic units (Fig. 4.2): Unit 1: the lowermost unit characterized by high IRD content and a very high matrix sediment density from 613 to 580 cm ($> \sim 14.5$ ka BP); Unit 2: a rapidly deposited deglacial IRD-rich unit from 580 to 370 cm ($\sim 14.5 - 10.3$ ka BP); Unit 3: a slowly accumulated early-Holocene transitional unit with significantly reduced IRD contents from 370 to 309 cm (10.3 – 8.5 ka BP); Unit 4: a mid-Holocene rapidly deposited IRD-free interval between 309 and 189 cm (8.5 – 5.8 ka BP); and Unit 5: a heavily

bioturbated, slowly accumulated, and low IRD neoglacial sediment interval in the upper 189 cm of the core (< 5.8 ka BP).

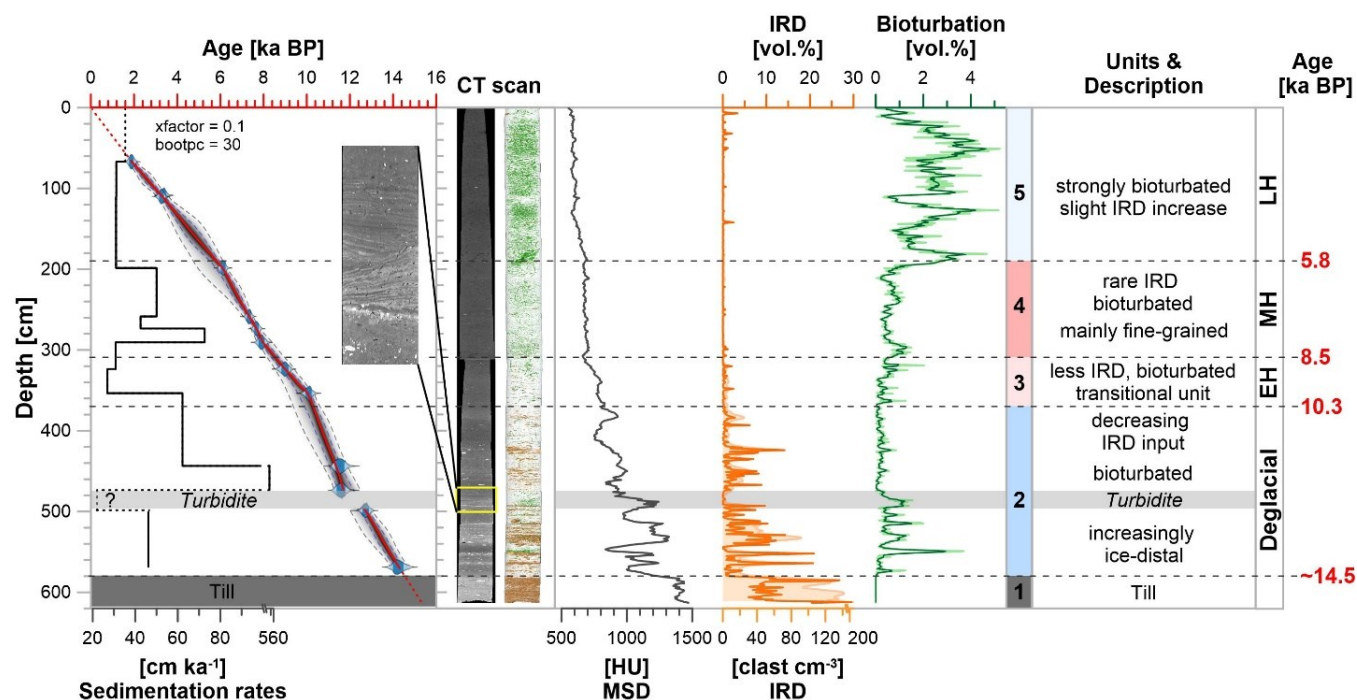


Figure 4.2: Age-depth model and calculated sedimentation rates (left) and processed CT scan and associated downcore quantification of the mean matrix sediment density (MSD) and ice-rafted debris (IRD) and bioturbation content (right) with a brief description of stratigraphic units 1-5 of core GeoB22336-4. Left to right: the solid black step line represents the sedimentation rates between calibrated ages; the solid red line connects the modeled ages (dashed red lines show depths outside radiocarbon-dated intervals where linear extrapolation is applied), and the blue and grey dashed lines represent the 68% (1σ) and 95% (2σ) probability intervals; the yellow rectangle on the CT scan marks the turbidite interval enlarged to the right; the brown, green and light-grey colors on the interpreted CT image respectively highlight IRD (clasts > 1 mm), bioturbation, and the matrix sediments.

The basal interval from 613 to 580 cm (Unit 1; > ~14.5 ka BP) constitutes a relatively dense and IRD-rich interval with many clasts reaching gravel size (Fig. 4.2). Maximum MSD (~1400 HU) and IRD concentrations (mean: 11.4 vol.%; 120.3 clasts cm⁻³) are recorded here. This massive (unstratified) and over-compacted unit lacks any bioturbation, although some internal cracks are visible, which appear to be an artifact of the coring or subsequent processing of these dense deposits. Based on these observations, the basal sediments are classified as till deposits. Throughout Unit 2, between 580 and 370 cm (14.5 – 10.3 ka BP), there is a continuous trend (although with some fluctuations) toward decreasing MSDs and IRD contents (mean: 985 HU; 2.6 vol.%; 21.8 clasts cm⁻³). Thin cross- to planar-bedded sediment layers with basal erosional contacts are visible in the CT data between 495 and 474 cm, with low quantities of IRD, and are classified as a turbidite (Fig. 4.2). Bioturbation is enhanced in low-IRD layers in the older and denser part of Unit 2, but in the younger part bioturbation is typically low even when IRD content is low (mean: 0.4 vol.%). In Unit 3, the IRD contributions are low in an even less

dense matrix (mean: 762 HU; 0.3 vol.%; 4.2 clasts cm⁻³), while volume percentages of bioturbation portray an increasing trend (mean: 0.4 vol.%). Bioturbation is only marginally increased in Unit 4 (mean: 0.7 vol.%), where hardly any IRD is observed. The uppermost Unit 5 displays an over three-fold higher proportion of bioturbated sediments (mean: 2.2 vol.%) and shows rare occurrences of isolated IRD mainly towards the core top. The lowest MSD values are obtained in the upper Units 4 and 5 (decreasing from 710 to 552 HU). In the following sections, subsequent data from core GeoB22336-4 are presented exclusively against calibrated ages (i.e., the age model).

4.4.3 Grain-size distributions

The grain-size distributions of the <2 mm terrigenous sediment fraction of core GeoB22336-4 are polymodal and can generally be classified as sandy to silty mud, showing an upward fining sequence (Fig. 4.3). Multiple modes can be observed in the silt- and sand-sized fractions (8 to 0 ϕ) with the volume percentages of the sand-sized modes largely decreasing towards the core top. A finer mode of $\sim 7.5 \phi$ ($\sim 5.4 \mu\text{m}$) is relatively stable and remained present in all samples downcore. Based on the grain-size distributions, the 6 ϕ ($\sim 16 \mu\text{m}$) line is used to separate the unimodal $<16 \mu\text{m}$ (fine) fraction from the polymodal $>16 \mu\text{m}$ (coarse) fraction (orange demarcation line in Fig. 4.3).

In general, downcore changes in the proportion of the fine-grained sediments (and inversely of the coarse fraction), as well as the calculated mean-grain sizes, largely fit the previously defined units (Units 1 – 5; Fig. 4.3). The lowermost section of the core (Unit 1; $> \sim 14.5$ ka BP) is associated with a rather stable mean grain size of around $19 \mu\text{m}$ and consistently low contents (~ 45 vol.%) of fine-grained material (FGM; i.e. sediments $< 16 \mu\text{m}$). The following Unit 2 (14.5 – 10.3 ka BP) is initially characterized by strong fluctuations in mean grain size (mean: $10.5 \mu\text{m}$), mirrored by variable FGM contents (mean: 62 vol.%). Above the turbidite, the record is marked by a less variable mean grain size (mean: $4.6 \mu\text{m}$) but more variable and higher FGM contents (mean: 79 vol.%). In Unit 3 (10.3 – 8.5 ka BP), a very slight increase in the mean grain size (mean: $4.9 \mu\text{m}$) and a drop in the FGM content (mean: 78 vol.%) indicate slightly coarser sediments. A fining-upward trend is reflected by the decreasing mean grain sizes and increasing FGM contents towards the upper part of this unit. This trend continues into Unit 4 (8.5 – 5.8 ka BP), which shows the finest sediments with the smallest mean grain sizes (mean: $3.7 \mu\text{m}$) and highest FGM contents (mean: 87 vol.%). The transition to Unit 5 (< 5.8 ka BP) is marked by a small decrease in FGM contents (mean: 83 vol.%). Across this unit, the overall rather stable grain-size distribution is overlain by a weak long-term trend towards slightly coarser compositions, which becomes most obvious during the last 2 ka by increasing mean grain size (mean: $4.4 \mu\text{m}$) and decreasing FGM contents (mean: 82 vol.%).

4.4.4 Mineralogical association

The XRD analyses of the sediments in core GeoB22336-4 show that, on average, carbonates (dolomite and calcite), quartz, K-feldspar, plagioclase, and clay minerals (mica and illites) constitute 81% of the total mineral assemblages. The remaining background composition is dominated by chlorite, kaolinite, pyroxene, and smectites. The basal till unit shows a mixed mineral composition with variable contents of total carbonates (dolomite and calcite; mean: 34 wt.%), the sums of illites and mica (SIM; mean: 16 wt.%) and quartz, plagioclase, and K-feldspars (SQF; mean: 36 wt.%; Fig. 4.3). In the overlying units, the XRD data reveal an anti-correlation of detrital dolomite and SIM. This anti-correlation demonstrates a pronounced shift from dolomite-dominated deglacial deposits (Unit 2; mean: dolomite = 31 wt.%, SIM = 12 wt.%), through transitional Unit 3 (mean: dolomite = 26 wt.%, SIM = 20 wt.%), to SIM-rich mid-late Holocene sediments (Unit 4 and 5; mean: dolomite = 20 wt.%, SIM = 24 wt.% and dolomite = 22 wt.%, SIM = 21 wt.%, respectively). In addition, Unit 2 sediments are associated with relatively high calcite (mean: 11 wt.%) and variable SQF (mean: 34 wt.%) contents. In Unit 3, calcite abundance steadily decreases from 11 wt.% mean value, observed in the lower unit, to ~1 wt.% at the top of this unit, while SQF content shows only a slight relative drop (mean: 28 wt.%). Calcite remained nearly absent (mostly below 1 wt.%) in Units 4 and 5 sediments. SQF values gradually increase from the onset of Unit 4 up to about 37 wt.% at ~6.7 ka BP. The SQF values stay around this level until the core top except for the central part in Unit 5 (4.5 to 2 ka BP), when these decrease to <32 wt.%.

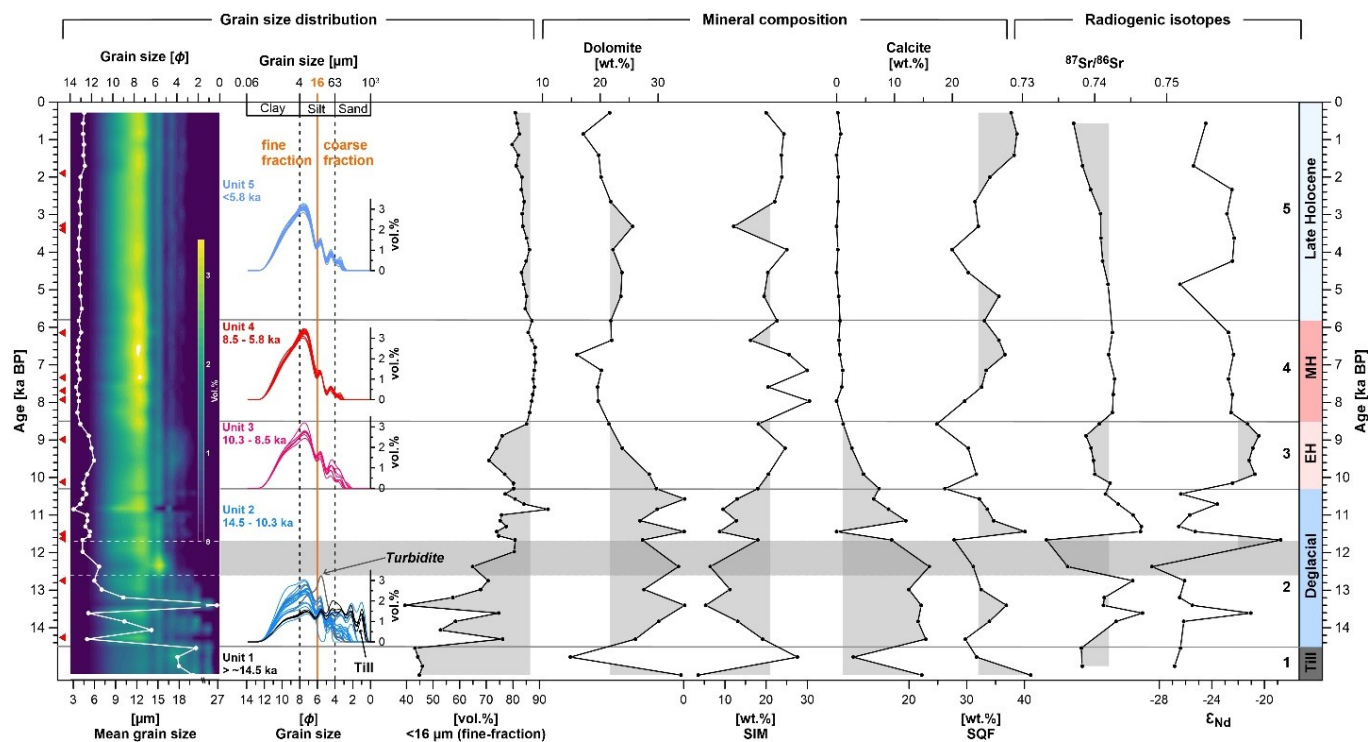


Figure 4.3: Contour plot of the downcore grain-size distributions overlain by the mean grain size (white line), grain-size distribution of individual samples associated with stratigraphic units 1–5 (orange line separates the fine and coarse fractions), downcore abundance of the fine-grained (<16 μm) fraction, as well as mineralogical and

radiogenic isotope composition of core GeoB22336-4. Grey lines mark the boundary of the different units; red triangles indicate intervals with age control; SIM (sum of illites and mica), SQF (sum of quartz, plagioclase, and K-feldspars); grey shading is added to highlight the most prominent patterns in grain size, mineralogical and radiogenic isotope composition; EH (early-Holocene); MH (mid-Holocene).

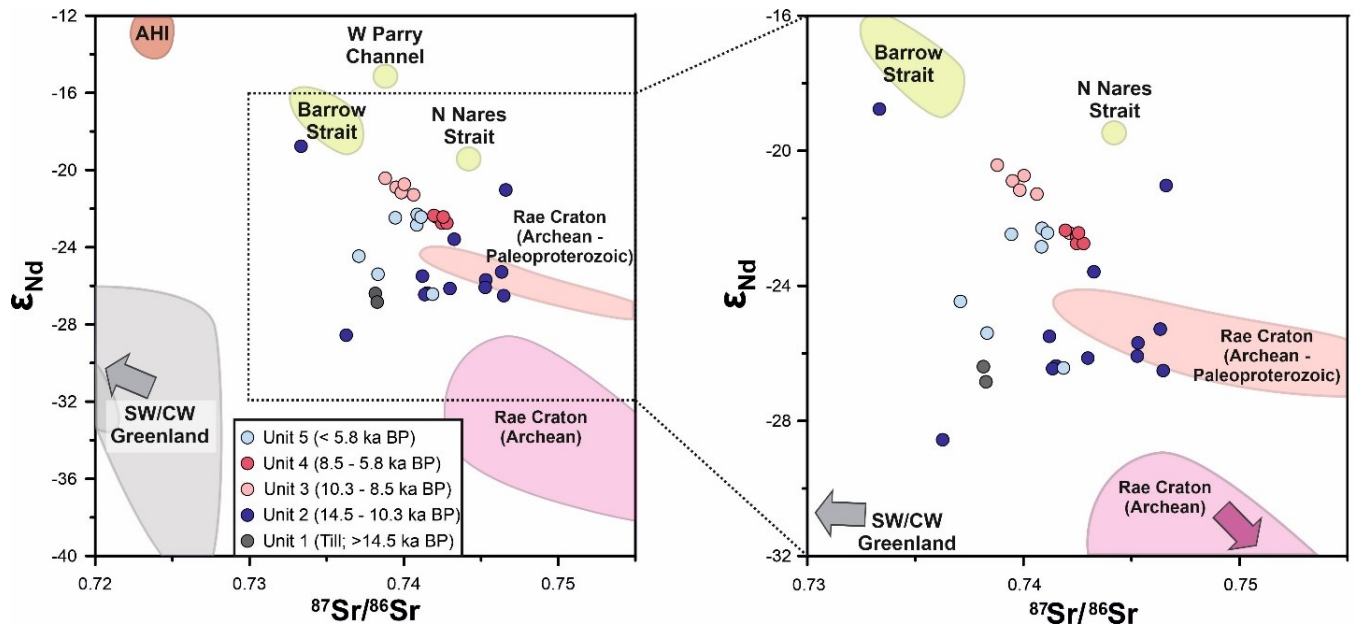


Figure 4.4: The $^{87}\text{Sr}/^{86}\text{Sr}$ versus ϵ_{Nd} isotope plot for core GeoB22336-4. Data points have colors corresponding to their age and the five stratigraphic units identified in the text. Background isotope signatures from different geological terrains are shown for comparison. The colors of the background data are adapted to the colors used in Figure 4.1. Background data are from marine sediment analyses of different studies: Rae Craton (Archean – Paleoproterozoic; light pink): sediment core (GeoB19927-3) from the western Greenland shelf (Madaj, 2021), Rae Craton (Archean; dark pink): sediment core (GeoB19946-4) from the northwestern Greenland shelf (Madaj, 2021) as well as from the northeastern Baffin Island shelf (data from GeoB22357-3, Appendix Table 9.1.3), Barrow Strait (light green): Holocene isotope signatures of core PS72/287-3 (Appendix Table 9.1.2), western Parry Channel, northern Nares Strait (light green), and Axel-Heiberg Island (AHI; red): surface sediment data (Maccali et al., 2018), and southwest (SW) and central west (CW) Greenland: stream sediment data (Colville et al., 2011; Reyes et al., 2014).

4.4.5 Radiogenic Nd and Sr isotope composition

Varying radiogenic Nd and Sr isotope compositions of the $<63 \mu\text{m}$ siliciclastic sediment fraction of core GeoB22336-4 (Fig. 4.3; Appendix Table 9.1.1) reflect changes in contributions of source rocks, which have different ages and mineral compositions. The $^{87}\text{Sr}/^{86}\text{Sr}$ versus ϵ_{Nd} plot (Fig. 4.4) sets the isotope signatures into context with potential source areas of the siliciclastic sediment fraction. The radiogenic isotope data show uniform compositions in the basal Unit 1 (>14.5 ka BP), having $^{87}\text{Sr}/^{86}\text{Sr}$ and ϵ_{Nd} values of 0.738 and ~ 26.6 , respectively (Fig. 4.3). The highest variability with both the highest and lowest $^{87}\text{Sr}/^{86}\text{Sr}$ and ϵ_{Nd} values is recorded in Unit 2. Within this unit, $^{87}\text{Sr}/^{86}\text{Sr}$ values range from 0.733

to 0.747 and ϵ_{Nd} values from -28.6 to -18.8. The most extreme $^{87}Sr/^{86}Sr$ and ϵ_{Nd} values occur within or close to the turbidite layer. The Sr-Nd isotope plot (Fig. 4.4) also reveals a larger scatter in Unit 2. In Unit 3, the isotope patterns of Sr and Nd change significantly to relatively stable values around 0.74 and -21, respectively (Fig. 4.3). Data from this unit form a more defined cluster in the Sr-Nd isotope plot. At the onset of Unit 4, $^{87}Sr/^{86}Sr$ (ϵ_{Nd}) values slightly increase (decrease) toward relatively uniform compositions within this unit, concentrating around 0.742 and -22.6, respectively (Fig. 4.3). This unit also shows a well-defined cluster in the Sr-Nd isotope plot (Fig. 4.4), which differs from the previous unit and is again closer to the radiogenic isotope signatures of Units 1 and 2. Within the uppermost Unit 5, the $^{87}Sr/^{86}Sr$ ratios show a continuous upward decrease from \sim 0.742 to 0.737 (Fig. 4.3). This change toward lesser radiogenic Sr values is initially gradual and becomes more pronounced after \sim 2.3 ka BP. In contrast, until \sim 2.3 ka BP, ϵ_{Nd} values remain largely (with one exception at the beginning of this unit at \sim 4.9 ka BP) at Unit 4 levels (-22) before values decrease to around -25. These youngest Nd isotope signatures are in a similar range as observed in the much older Units 1 and 2.

4.5 Discussion

Variations in sedimentological properties and mineralogical and radiogenic isotopic composition of the five stratigraphic units of core GeoB22336-4 (Fig. 4.2, 4.3) provide a continuous record of the changing depositional and environmental conditions and sediment provenances in northern Baffin Bay since the last deglaciation. These are discussed in the following sections from paleoclimatic and palaeoceanographic perspectives.

4.5.1 Ice stream retreat and deglacial sediment dynamics (\sim 14.5 to 10.3 ka BP)

During the LGM, the LIS, IIS, and GIS advanced across the continental shelves surrounding Baffin Bay (England, 1999; Dyke et al., 2002; England et al., 2006; MacLean et al., 2017). The coalescing of the LIS and GIS with the IIS formed marine-terminating grounded ice shelves blocking the connections between the Arctic Ocean and Baffin Bay, which presently exist (mainly) through Lancaster Sound and Nares Strait (Blake et al., 1996; England, 1999; Dyke, 1999; Dyke et al., 2002; Niessen et al., 2010; MacLean et al., 2017; Dalton et al., 2020). The glacial-ice stream draining the coalescent LIS and IIS advanced eastward into Baffin Bay and was grounded on the seabed approximately 270 km from the mouth of Lancaster Sound in \sim 1300 m water depth (Li et al., 2011; Harrison et al., 2011a; Bennett et al., 2014). The glacial-ice margins were likely buttressed by an ice shelf that extended partly (Jennings et al., 2018; Couette et al., 2022) or entirely across Baffin Bay (Gibb et al., 2015; Simon et al., 2016).

In core GeoB22336-4, the massive, very dense, highly homogenized, and burrow-free gravelly and sandy mud in the oldest Unit 1 ($>$ \sim 14.5 ka BP) is indicative of subglacial till deposits (Figs. 4.2, 4.3). The variability and composition in mineral assemblages of the till unit suggest highly mixed sediment provenances (Fig. 4.3), probably materials eroded from northeastern Baffin Island (Bylot Island and

Borden Peninsula) and Devon Island and adjacent channels transported by the Lancaster Sound ice stream toward the core site. In contrast, the radiogenic isotope signatures in the till unit are rather stable, also pointing to a mixture of various source regions (Fig. 4.4). The presence of these till deposits indicates that the Lancaster Sound ice stream was still grounded at the mouth of Lancaster Sound until 14.5 ka BP.

In contrast, based on three ^{14}C -dated sediment cores (incl. core 49PC collected ~11 km from our core site), Kelleher et al. (2022) suggested that the ice stream had already retreated to central Lancaster Sound (to site 59PC; Fig. 4.1) by ~15.3 ka BP, much earlier than previously thought (e.g., Dyke et al., 2002; MacLean et al., 2017; Furze et al., 2018; Dalton et al., 2020). However, this interpretation is based on linear age extrapolations for sediments older than ~11.6 and 11.1 ka BP, without considering probable higher sedimentation rates in the older parts of the cores deposited under more ice proximal conditions, which would support younger lift-off ages. As the presence of the Lancaster Sound ice stream at site GeoB22336-4 until ~14.5 ka BP (last calibrated ^{14}C age of 14.3 ka BP obtained 10 cm above the till) is also consistent with an extensive ice margin close or even seaward of our core site around ~13.5 ^{14}C ka (~14.5 ka BP; Dalton et al. (2020); Fig. 4.1), there is clear evidence that grounded ice indeed extended to the outer Lancaster Sound until the start of the Bølling-Allerød interstadial (Naughton et al., 2023).

These basal till deposits are overlain by a slightly bioturbated, gravel-bearing sandy-silty mud with an intercalated turbidite (Unit 2; 14.5 – 10.3 ka BP; Figs. 4.2, 4.3), suggesting variable sediment delivery also by iceberg rafting and mass-wasting. Decreasing but variable IRD input at the core site and nearby site 49PC (Kelleher et al., 2022) probably reflects the change from ice proximal to increasingly distal glaciomarine sedimentation. Ice sheet retreat into cross-shelf troughs nearby (e.g., Scott Trough) around this time was also postulated by Couette et al. (2022). Ice-proximal sediments containing abundant large clasts have been widely described along Baffin Bay surrounding shelves and slopes (e.g., Ó Cofaigh et al., 2013a, 2013b; Dowdeswell et al., 2014; Jennings et al., 2017; Jenner et al., 2018; Kelleher et al., 2022). In addition, some bioturbation traces in our core (Fig. 4.2) and the presence of foraminifera (available for radiocarbon dating and also found in cores 49PC and 10PC; Furze et al., 2018; Kelleher et al., 2022) point to more open water conditions. These glaciomarine conditions prevailed until ~10.3 ka BP, as also found in other cores in the region (Bennett et al., 2014; Kelleher et al., 2022).

Decreasing sedimentation rates in Unit 2 from ~11.7 ka BP (in addition to the generally decreasing IRD inputs, Fig. 4.2) probably reflect the fast westward recession of the Lancaster Sound ice stream (e.g., Dyke, 1999; Pieńkowski et al., 2014; MacLean et al., 2017). In addition to the maximum northern latitude summer insolation at that time (Berger & Loutre, 1991; Laskar et al., 2004), the ice stream recession might have been accelerated by the gradual strengthening northward flow of comparably warm Atlantic Water via the WGC at this time (Fig. 4.5; Weiser et al., 2021). Enhanced Atlantic water influence inferred from foraminifera assemblages has been reported from several sites along the west Greenland shelf (e.g., Sheldon et al., 2016; Jennings et al., 2014, 2017) up to northern Baffin Bay (e.g.,

Knudsen et al., 2008; Jennings et al., 2019; Jackson et al., 2021) and into Lancaster Sound and the CAA channels (e.g., Pieńkowski et al., 2012, 2013, 2014; Furze et al., 2018; Kelleher et al., 2022). During this time, the Arctic Ocean-Baffin Bay connections through the Lancaster Sound, Nares Strait, and other CAA channels remained shut by grounded glacial ice (Dyke et al., 1991, 2003; England, 1999; England et al., 2006), permitting an enhanced northward penetration of warm Atlantic Water forming the dominant water mass in Baffin Bay, accompanied by meltwater input from surrounding ice sheets.

The moderate to rapid deposition of this ~2-m thick IRD-rich deglacial interval (Unit 2; ~ 14.5 to 10.3 ka BP), also rich in carbonates (mean: ~42 wt.%; Figs. 4.2, 4.5), points to a high sediment input from ice stream activities in Lancaster Sound transporting regional Paleozoic carbonates to site GeoB22336-4, as well as sites 49PC and 59PC (Kelleher et al., 2022). The deposition of this deglacial carbonate- and IRD-rich sediments also spans the various timing of the well-documented Baffin Bay Detrital Carbonate (BBDC) Events 1 (~14.5 to ~13.0 ka BP) and 0 (~12.5 – ~10.9 ka BP) further south in Baffin Bay (Aksu & Piper, 1987; Simon et al., 2012, 2014; Jennings et al., 2014; Jackson et al., 2017; Jenner et al., 2018; Andrews et al., 2020; Ownsworth et al., 2023; and many others). Significant amounts of SQF and radiogenic ϵ_{Nd} values ranging mainly between -24 and -28 and $^{87}\text{Sr}/^{86}\text{Sr}$ isotope signatures between 0.741 and 0.747 (Fig. 4.3), further indicate a significant contribution of older Archean to Paleoproterozoic granitic and gneissic rocks of the Rae Craton, probably from nearby eastern Devon Island and/or the west coast of Smith Sound (Figs. 4.1, 4.4). Despite the lack of Sr and Nd isotope reference data from sites proximal to the core site, the general bedrock lithology of eastern Devon Island and the west coast of Smith Sound is similar to that of the Rae Craton on Greenland and Baffin Island and, thus, is expected to provide comparable Sr and Nd isotopic signatures. Furthermore, ϵ_{Nd} values between -32.1 and -30.8 measured in samples from rivers draining Bylot Island (Grenier et al., 2022) could argue for Bylot Island as an additional source area for parts of Unit 2 sediments.

4.5.2 Early-Holocene postglacial transition and the establishment of Arctic-Atlantic throughflow (10.3 to 8.5 ka BP)

A marked shift from deglacial conditions to the early-Holocene transitional environment is recorded in Unit 3 (10.3 – 8.5 ka BP). This transition is characterized by a pronounced drop in sedimentation rates suggesting largely reduced sediment delivery to the core site (Fig. 4.2), accompanied by a significant change towards more radiogenic ϵ_{Nd} values and a less pronounced shift towards less radiogenic $^{87}\text{Sr}/^{86}\text{Sr}$ values and SQF mean content (Fig. 4.3). In addition, coarse-grained sediments (>16 μm) still make up almost a quarter (on average) of the grain-size distributions during this interval (Fig. 4.3). The very low amounts of large iceberg-rafted clasts in this interval and decreasing contents of detrital carbonates (Fig. 4.5) might signify a switch from tidewater to predominately land-terminating glaciers during the late stage of LIS and IIS retreat (onset of postglacial conditions). This transition is similarly reflected in the largely reduced IRD input and decreasing detrital carbonate content in northern Baffin Bay cores 49PC

and 59PC around this time (Kelleher et al., 2022). However, still recognizable IRD inputs and enhanced contents of coarse-grained sediments in core GeoB22336-4 point to at least an occasional occurrence of iceberg rafting. The transition to postglacial conditions happens during a period of potentially high northward-heat transport by the early-Holocene WGC-speed maximum occurring synchronously with decreasing but high Agassiz meltwater release and high summer insolation (Fig. 4.5; Laskar et al., 2004; Fisher et al., 2012; Weiser et al., 2021). Still, reconstructions of summer sea-surface temperatures (SSTs) and seasonal sea ice conditions suggest mean sea surface temperatures $<2.5^{\circ}\text{C}$ and sea ice coverage for around 9.5 months at that time in northwestern Baffin Bay (Fig. 4.5; Ledu et al., 2008, 2010). Similarly, cold sea-surface conditions with extensive (spring) sea-ice cover is reconstructed for northeastern Baffin Bay (Fig. 4.5; Saini et al., 2020, 2022). Nevertheless, increasing bioturbation in core GeoB22336-4, which suggests an enhanced organic matter availability at the sea floor, hence primary production, hints at slightly more extensive (prolonged) open surface waters. The decrease in sediment delivery (sedimentation rates) during this period appears to be of a regional scale, observed in several records from Barrow Strait, Smith Sound, and Northern Baffin Bay (Pieńkowski et al., 2012, 2013; Jennings et al., 2019; Jackson et al., 2021; Fig. S4.1, Appendix Table 9.1.4).

In addition, the shift of Sr and Nd isotope compositions towards less and more radiogenic values (Fig. 4.3), respectively, and their placement between the Barrow Strait and Rae Craton isotope signature range (Fig. 4.4) indicates a weaker influence of sediments from proximal Devon Island and west coast of Smith Sound (i.e., Rae Craton) and a stronger input from the Barrow Strait area during this interval. The radiogenic ϵ_{Nd} signature of the Barrow Strait region indicated by sediment core PS72/287-3 (Appendix Table 9.1.2) is further supported by radiogenic ϵ_{Nd} values of -15.1 and -16.1 obtained from river samples draining into Barrow Strait (Grenier et al., 2022). However, the dolomite content indicating the detrital carbonate input, which is also seen as an indicator for material coming from the Barrow Strait region, continues to decrease at the same time in core GeoB22336-4 (Fig. 4.3) and other cores (e.g., 49PC; Kelleher et al., 2022), thus, seemingly contradicting the interpretation of increased sediment delivery from this region. The long-term decrease in dolomite coincides with a similar reduction in IRD input (Fig. 4.5), pointing to a predominant iceberg transport of the dolomite. Thus, with the transition from tidewater to land-terminating glaciers, the dolomite input to the Lancaster Trough Mouth fan decreased, giving space for the delivery of finer materials of different mineralogies from the Barrow Strait area and the wider CAA. Consequently, the observed shift in sediment provenance and the marked drop in sedimentation rates at our core site (and others, also in Barrow Strait; Fig. S4.1) is interpreted as the final deglaciation of Lancaster Sound and Barrow Strait and the establishment of an open marine connection between the Arctic Ocean and Baffin Bay via the main channels of the CAA around this time. According to our results, this opening happened approximately between 10.4 and 9.9 ka BP in agreement with previous studies (e.g., Pieńkowski et al., 2012, 2014).

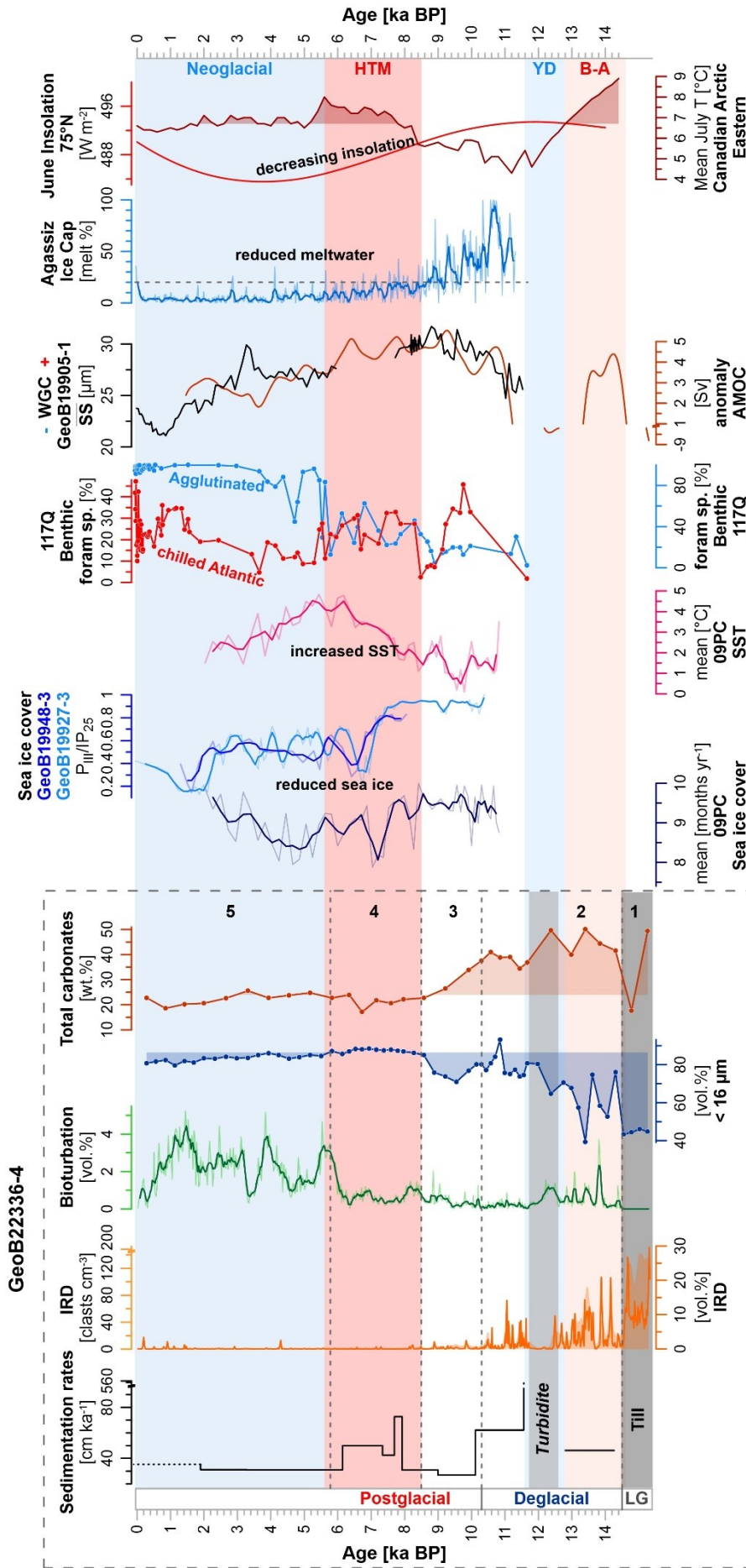


Figure 4.5: Comparison of selected proxies from core GeoB22336-4 with other paleoenvironmental data from northern Baffin Bay. From left to right: Core GeoB22336-4 data on sedimentation rates, contents ice-rafted debris (IRD), bioturbation traces, fine material <16µm and total carbonate (= sum of dolomite and calcite). The black numbers 1-5 indicate the five units discussed in the text. The grey dashed line marks the transition from deglacial to postglacial conditions in core GeoB22336-4. Further paleoenvironmental data include Holocene sea-ice conditions and sea surface temperatures in northern Baffin Bay from core 09PC (Ledu et al., 2010) and cores GeoB19948-3 and GeoB19927-3 (Saini et al., 2020, 2022) and benthic foraminifera abundance in core 117Q (Jackson et al., 2021), reconstructed Atlantic Meridional Overturning Circulation (AMOC) anomaly (Ritz et al., 2013), West Greenland Current (WGC) strength from mean sortable silt record in core GeoB19905-1 (Weiser et al., 2021), the melt record from the Agassiz Ice Cap (Fisher et al., 2012), mean July temperatures for the eastern Canadian Arctic (Gajewski, 2015), and the June solar insolation at 75°N (Laskar et al., 2004). LG = Late Glacial; B-A = Bølling-Allerød; YD = Younger Dryas; HTM = Holocene Thermal Maximum.

A shift in trend towards increased contribution of fine-grained sediments (with increasing SIM and SQF contents), more radiogenic $^{87}\text{Sr}/^{86}\text{Sr}$, and less radiogenic ϵ_{Nd} values at the core site started at ~8.5 ka BP at the end of Unit 3 (Fig. 4.3). The timing coincides with the opening of the Nares Strait connection between the Arctic Ocean and Baffin Bay, fully unblocked between 8.5 and 8.2 ka BP (Dyke et al., 2002; Jennings et al., 2011, 2019, 2022; Georgiadis et al., 2018; Kelleher et al., 2022). The potential link between Nares Strait deglaciation and a reorganization of the sediment routing system in northern Baffin Bay is discussed in the following section.

4.5.3 Rapid fine-grained sedimentation in northern Baffin Bay during the HTM (8.5 to 5.8 ka BP)

The most conspicuous feature of Unit 4 (8.5 – 5.8 ka BP) is the rapid deposition of predominantly fine-grained sediments (up to 73 cm ka⁻¹) and the virtual absence of IRD that follows slight changes in sediment composition (highest mean SIM and SQF contents, lowest dolomite content) in this interval (Figs. 4.2, 4.3). Just after 8.5 ka BP, also a shift towards consistently less radiogenic ϵ_{Nd} and more radiogenic $^{87}\text{Sr}/^{86}\text{Sr}$ values (Fig. 4.3) point to a relatively pronounced input of material originating from the Rae Craton. Since the timing of the transition roughly coincides with the opening of Nares Strait between 8.5 and 8.2 ka BP (Dyke et al., 2002; Jennings et al., 2011, 2019, 2022; Georgiadis et al., 2018; Kelleher et al., 2022), these shifts in our records might point to a reconfiguration of the sediment routing system. A change in surface ocean circulation due to additional Arctic waters entering northern Baffin Bay via Nares Strait could cause intensive sediment transport from the mouth of Jones Sound to the core site. Enhanced sediment input from eastern Devon Island or the west coast of Smith South, which originate predominantly from rocks of the Rae craton, could potentially drive Nd and Sr isotope composition towards the values observed in Unit 4 (Fig. 4.4).

While at first glance, such a change in provenance might also be a reason for the observed increase in sediment accumulation, this appears rather unlikely here as towards the end of Unit 4, sedimentation rates decrease by ~50 % without any major change in sediment composition (Figs. 4.3, 4.5). Consequently, the sedimentation rates of Unit 4, which are associated with over 85 vol.% of fine-grained sediments, most likely reflect a change in the dominant sedimentation process. Interestingly, such increases in sedimentation rates by 2 to >5 fold are a common feature in Northern Baffin Bay during this time window (Fig. S4.1), which roughly coincided with the regional Holocene Thermal Maximum (HTM; broadly spanning from ~8.5 to ~5 ka BP; Kaufman et al., 2004; Jennings et al., 2011; Gajewski, 2015; Briner et al., 2016). Accordingly, St-Onge and St-Onge (2014) attributed similar observations of predominately fine-grained sediments in core 42PC to sedimentation from suspension settling (hemipelagic origin). This interpretation may be supported by warmer and wetter Arctic conditions during the mid-Holocene (Thomas et al., 2018; Chen et al., 2022). Such environmental conditions would have favored increased terrestrial freshwater runoffs, resulting in enhanced delivery of suspended sediments (suspension cloud) mainly to the nearby fjords and shelves around northern Baffin Bay, as observed today along the west Greenland coastline (Overeem et al., 2017). However, the bordering LIS, IIS, and GIS approached their minimum areal extent after 8.5 ka BP (Dyke et al., 2003; Funder et al., 2011; Dalton et al., 2020), coinciding with decreasing Arctic summer solar insolation (Laskar et al., 2004) and low melting rates (e.g., Agassiz melt record, Fisher et al., 2012) (Fig. 4.5). Thus, resulting low amounts of meltwater and, hence, reduced sediment discharge is clearly in conflict with the above interpretation.

Recent model simulations revealed that reduced meltwater input to Baffin Bay results in the thinning of the freshwater lens capping the underlying warmer WGC waters and, consequently, in the weakening of water-column stratification (weaker halocline), which would allow for enhanced vertical heat flux and ocean-atmosphere heat exchange (Castro De La Guardia et al., 2015). Even today, with a much weaker WGC (Weiser et al., 2021), wind-driven upwelling of warmer WGC water along the northwestern Greenland shelf (Melling et al., 2001) can provide heat to melt sea ice and cause the prolongation of sea ice melt season in northern Baffin Bay as observed in recent decades (Ballinger et al., 2022).

Such a scenario can also be assumed for the period between ~8.5 and 5.8 ka BP. During this time, a strong WGC, forced by a strong AMOC, transported sensible heat northward (Ritz et al., 2013; Weiser et al., 2021). This process probably contributed to decreasing sea-ice cover (increasing SSTs) in northwestern (Ledu et al., 2010) and northeastern (Saini et al., 2020, 2022) Baffin Bay (Fig. 4.5). Contemporaneously increasing air temperatures documented from the eastern Canadian Arctic (Gajewski, 2015; Fig. 4.5) might also be interpreted as consequences due to a weakened halocline and enhanced heat exchange with the atmosphere. These conditions most likely favored a very high turnover of sediment-laden sea ice and the release of fine-grained sediments entrained in the sea ice (Nürnberg et al., 1994; Eicken et al., 2000; Dethleff, 2005). Consequently, this scenario could explain the regional

pattern of high sedimentation rates in northern Baffin Bay observed for several sites (Fig. S4.1). In contrast, the relatively low and stable postglacial sedimentation rates in Barrow Strait (sites 144PC and 154PC; Pieńkowski et al., 2012, 2014) and Nares Strait (sites 05GC and Kane2B; Jennings et al., 2011; Georgiadis et al., 2018, 2020; Fig. S4.1) could accordingly be explained by a much weaker influence of the WGC at these locations far off the northern Baffin Bay, which likely resulted in more extensive (permanent) sea ice cover.

Independent evidence for this scenario is provided from a comparable setting in the eastern Fram Strait, where sea-ice-covered Arctic waters meet the relatively warm waters (>0 °C) of the West Spitsbergen Current (Hebbeln, 2000). Sediment trap studies (1987-1990) revealed a four- to six-fold increase in particle flux attributed to the release of sea ice-rafted debris, mainly sediment particles <40 μm (Hebbeln, 2000). This observation is in line with the observed increase in sedimentation rates as well as the predominance of fine-grained sediments in core GeoB22336-4 (Fig. 4.5). The incorporation of large amounts of fine-grained sediment into sea ice commonly occurs in shallow shelf areas, often within polynyas, as e.g., in the Laptev Sea (Nürnberg et al., 1994). In northern Baffin Bay, the most extensive shelves occur right beneath the NOW along the coasts of Ellesmere and Devon Islands, whose coasts are characterized by rocks of the Rae Craton (Fig. 4.1). Thus, sea ice produced on the shelves of these islands would have the potential to carry high amounts of sediments with a distinct and stable radiogenic isotope signature as found in our core GeoB22336-4. Interestingly, the observed accumulation rates of 40 to 73 $\text{g cm}^{-2} \text{ka}^{-1}$ in this core (assuming a dry bulk density of ~ 1 g cm^{-3}) are almost in the same order of magnitude as the seabed accumulation rates of ~ 30 $\text{g cm}^{-2} \text{ka}^{-1}$ extrapolated from the sediment trap study in the Fram Strait (Hebbeln, 2000), pointing to the potential of the process suggested here to explain the observed high sedimentation rates). Thus, for the period from 8.5 to 5.8 ka BP, a relatively strong heat supply via the WGC, predominantly controlled by the AMOC (Weiser et al., 2021), probably enabled the intense melting of sea ice due to a weak halocline, resulting in the enhanced sediment accumulation of sea ice-transported fine-grained sediment (<16 μm) at our core site.

4.5.4 Reduced sedimentation during the late Holocene (<5.8 ka BP)

The decrease of the fine-grained sediment input at the onset of Unit 5 (~ 5.8 ka BP) towards pre-HTM levels coincides with a significant reduction in sedimentation rates to ~ 31 cm ka^{-1} (Fig. 4.5). At the same time, the amount of bioturbation in the sediments shows an ~ 3 -fold increase. This suggests a sudden decline in the input of sea ice-rafted fine-grained sediments at site GeoB22336-4 (see section 4.5.3), probably triggered by the weakening of the WGC after ~ 6 ka BP (Fig. 4.5; see Weiser et al., 2021). As neither regional SSTs nor sea ice cover data show any marked shift at ~ 5.8 ka BP (Ledu et al., 2008, 2010; Saini et al., 2020, 2022), the observed increase in bioturbation might be, at least partly, related to the decrease in sedimentation rates resulting in prolonged exposure of surface sediments to bioturbating organisms. A decreasing influence of Atlantic-sourced waters at this time is further supported by a strong

increase in relative abundances of agglutinated foraminifera in core 117Q from northern Baffin Bay (Fig. 4.5; Jackson et al., 2021). Also, Caron et al. (2019) observed decreasing proportions of ‘North Atlantic’ indicator dinocyst taxa south of the west Greenland coast, suggesting decreasing SSTs after ~5 ka BP with intensified cooling in the last ~2 ka BP.

During the following millennia, sedimentation in northern Baffin Bay showed little variation. Most notable are long-term trends in the mineralogical and radiogenic isotope composition and the IRD input. Less radiogenic ϵ_{Nd} and Sr signatures and high SQF values, especially for the last ~2 ka BP (Fig. 4.3), suggest an increased influence of sediments originating from the rocks of the Rae Craton of eastern Devon Island and the west coast of Smith Sound. For the same period, a slight coarsening of the sediments (Fig. 4.3) and an increase in IRD (Fig. 4.5) point to glacier advance and an increasing number of tidewater glaciers in the region, which might be sourced rather proximal, e.g., eastern Devon Island, as suggested by the radiogenic isotope and SQF data. The suggested glacier advance is likely linked to the Neoglacial cooling, an Arctic-wide shift in paleoclimatic and paleoceanographic conditions documented in numerous terrestrial- and marine records and climate simulations (e.g., Miller et al., 2005; Briner et al., 2009, 2016; McKay et al., 2018). In northern Baffin Bay, these conditions are most prominently expressed over the last 3 ka BP (e.g., Briner et al., 2016). The shift toward cooler conditions in this region has been explained (e.g., Briner et al., 2016) as a response to (i) the minimum Arctic summer insolation at ~3 ka BP (Laskar et al., 2004) and (ii) the decline in northward oceanic heat transport via the AMOC-controlled WGC (Ritz et al., 2013; Weiser et al., 2021; Fig. 4.5). Deteriorating conditions linked to this cooling also might have reduced productivity, as indicated by decreasing bioturbation observed in core GeoB22336-4 (Fig. 4.5). However, the chronostratigraphy in the upper 60 cm (the last ~2 ka) of this core is weak due to the lack of datable material (age control), which hampers more detailed reconstructions.

4.6 Conclusions

Based on data from radiocarbon-dated sediment core GeoB22336-4, we investigated changing depositional regimes related to past ice-sheet dynamics and varying oceanographic conditions in northern Baffin Bay for the last ~14.5 ka BP. For the time prior to 14.5 ka BP, the sediment record provides evidence of grounded glacial ice at the mouth of Lancaster Sound. This reconstruction puts the grounding line of the Lancaster Sound ice stream farther out of Lancaster Sound at this time, in contrast to prior suggestions of a tentative inner Lancaster Sound position at ~15.3 ka BP. The prevailing proximity of the ice stream between 14.5 and 10.3 ka BP enabled efficient delivery of IRD, predominantly comprised of material from regional Paleozoic carbonates accompanied by materials from the proximal eastern Devon and southeastern Ellesmere Islands, as identified by radiogenic Sr and Nd isotope compositions. The early Holocene postglacial interval is marked by the opening of the Barrow Strait-Lancaster Sound gateway between ~10.4 and 9.9 ka BP, which resulted in an initial

Arctic-Atlantic throughflow documented by enhanced sediment supply from Barrow Strait. After the Nares Strait opening at ~8.5 ka BP, the mid-Holocene interval (up to 5.8 ka BP) is characterized by the rapid deposition of fine-grained, sea-ice-rafted sediments. Reduced meltwater input to northern Baffin Bay after the ice sheets had reached their Holocene minimum extent likely led to a weaker halocline, allowing the heat supplied by a strong WGC to trigger intense melting of sediment-laden sea ice during this time. The weakening WGC influence in the region around ~5.8 ka BP resulted in a reduced input of sea-ice-rafted material and a corresponding significant drop in sedimentation rates, which probably enabled the strong bioturbation of the late Holocene sediments deposited thereafter. During the last ~2 ka BP, increasing IRD inputs and continuously changing source areas inferred from radiogenic isotope data, suggest regional glacier re-advances, probably in response to Neoglacial cooling.

Declaration of competing interest

The authors declare that they have no known competing financial interests or personal relationships that could have appeared to influence the work reported in this paper.

Data availability

All data presented here are available at the PANGAEA online data repository (<https://www.pangaea.de/>).

Acknowledgments

We gratefully acknowledge the master and crew of the R/V Maria S. Merian for their work during cruise MSM66. Sample material has been provided by the GeoB Core Repository at the MARUM – Center for Marine Environmental Sciences, University of Bremen, Germany. We gratefully acknowledge Klinikum Bremen-Mitte and Christian Timann and Arne-Jörn Lemke for supporting the CT measurements in their facilities. Thanks to Ruediger Stein and the Alfred Wegener Institute Helmholtz Centre for Polar and Marine Research for providing sediment samples from Core PS72/287-3 recovered during Polarstern Expedition ARK-XXIII/3 in 2008. We also thank the XRD Lab Team of Johannes Birkenstock, Ella Schmidt, and Reinhard Fischer for keeping the XRD machines always online. This project was supported by the Deutsche Forschungsgemeinschaft (DFG) through the International Research Training Group “Processes and impacts of climate change in the North Atlantic Ocean and the Canadian Arctic” (IRTG 1904 ArcTrain).

Supplementary figure

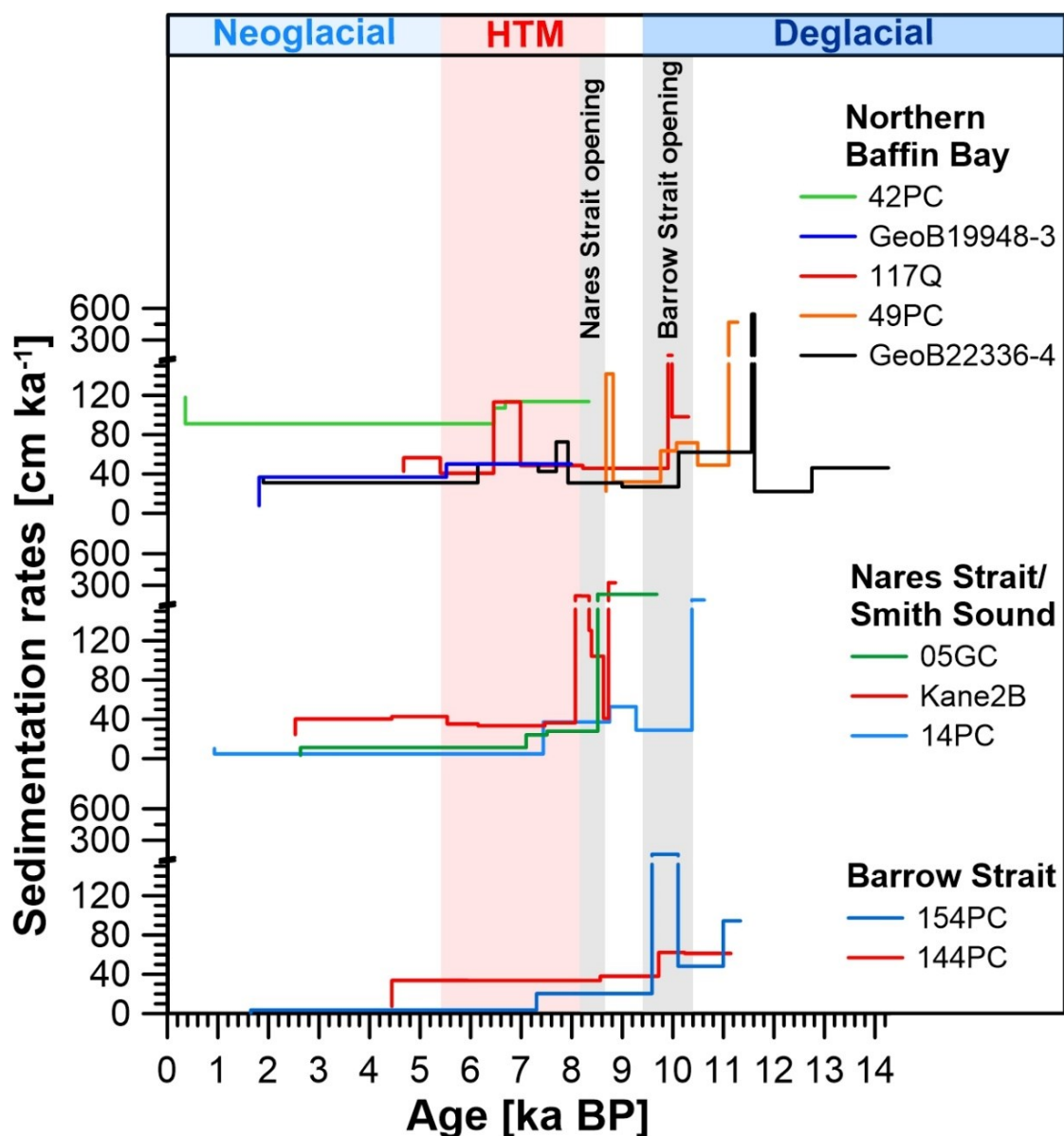


Figure S4.1: Compilation of sedimentation rates from published sediment cores from Barrow Strait: 144PC (Pieńkowski et al., 2012), 154PC (Pieńkowski et al., 2014); Nares Strait: Kane2B (Georgiadis et al., 2018), 05GC (Jennings et al., 2011); Smith Sound: 14PC (Jennings et al., 2019); and Northern Baffin Bay: GeoB22336-4 (this study), 49PC (Jenner et al., 2018; Kelleher et al., 2022), 42PC (St-Onge & St-Onge, 2014), 117Q (Jackson et al., 2021), GeoB19948-3 (Saini et al., 2022). Radiocarbon ages from the published sediment cores are calibrated using Calib 8.20 (Stuiver & Reimer, 1993), and the median ages and 95% confidence intervals are given in Appendix Table 9.1.4. Grey bars indicate the entire interval for Barrow and Nares Straits opening based on the sediment records. HTM = Holocene Thermal Maximum (see Fig. 4.1 for core locations).

Chapter five

5. Proximal recordings of the NE Laurentide Ice Sheet retreat in Clyde Inlet (Baffin Island)

Abstract

The reconstruction of ice sheet fluctuations during the last deglaciation and the Holocene helps to understand the response of past and present ice sheets to a changing climate. The large-scale spatial and temporal variations of the Foxe Basin-Baffin Island ice dome (NE Laurentide Ice Sheet, Canada) are relatively well documented. However, information on its final decay mode is still restricted. Here, we reconstruct ice margin fluctuations of one of its eastern outlet glaciers in the Clyde Inlet (NE Baffin Island) using two radiocarbon-dated marine sediment cores retrieved from the Clyde fjord (GeoB22346-3) and the associated cross-shelf trough in western Baffin Bay (GeoB22357-3). High-resolution computed tomographic data, radiogenic isotope compositions (Sr-Pb-Nd), and mineral assemblages of the siliciclastic sediment fraction provide new insights into the sediment dynamics, ice margin fluctuations, and the spatial and temporal variations in meltwater discharge. A subglacial till at the bottom of the shelf core suggests that grounded ice was still present during the Younger Dryas. Above, major changes in physical sediment properties, their radiogenic isotope and mineralogical compositions, are dated at ~ 11.1 ka BP. They document the transition from an ice-proximal to an ice-distal environment, which accompanied the retreat of the Clyde Inlet ice stream to the adjacent fjord. Above this transition, higher carbonate contents and steadily rising ϵ_{Nd} values are observed. They are associated with enhanced relative sediment fluxes from northern Baffin Bay, probably related to the deglaciation of the Lancaster Sound. Radiocarbon ages in the fjord core suggest land-terminating ice positions already set at ~ 9.5 ka BP. The following early- to mid-Holocene environmental conditions were initially characterized by intense meltwater discharge, which attained a minimum between ~ 6 and 3 ka BP coeval with a minimum alpine-type glacier extent. Finally, sediment, radiogenic isotope, and mineralogical compositions suggest the re-advance of alpine glaciers in the last ~ 2 ka BP, marking the neoglacial cooling.

5.1 Introduction

The mass balance of ice sheets is highly influenced by the behavior and stability of outlet glaciers and ice streams, as they are responsible for the main ice and sediment discharge (Bamber et al., 2000; Bennett, 2003). Besides the observation of today's ice sheet behavior and their variability, past ice stream and ice sheet reconstructions are a helpful tool to better understand their long-term response to a

changing climate (e.g., Briner et al., 2020; Kaufman et al., 2004). The Laurentide Ice Sheet (LIS) covered large parts of Canada during the last glacial period, with several ice streams draining into the Arctic Ocean, Baffin Bay, and the northwestern North Atlantic (Margold et al., 2015). The retreat of its marine-terminating margins during the last deglaciation shows similarities to the present-day retreat of Greenland and West Antarctic ice sheets (Briner et al., 2009a). Therefore, the deglaciation history of LIS, particularly its outlet glaciers and ice streams, is of great interest.

One of the multiple outlet glaciers of the northeastern LIS occupied the Clyde Inlet, a 120 km long fjord on northeastern Baffin Island (Fig. 5.1), during the Last Glacial Maximum (LGM) (Margold et al., 2015). Several studies provide an outline of the northeastern LIS's decay. Couette et al. (2023) recently identified the maximum extent and the retreat chronology of the LIS in the Clyde Inlet fjord and trough system using detailed bathymetry, seismic stratigraphy, and marine sediment core data. Specific glaciomarine landforms close to the shelf edge revealed that the LIS extended onto the Baffin Shelf during the LGM, though it has not reached the shelf edge (Couette et al., 2023). The onset of deglaciation started between 16 and 14 ka BP (Briner et al., 2005, 2007) and was characterized by the collapse of the Clyde ice shelf and the subsequent rapid retreat of the LIS (Couette et al., 2023). Cosmogenic ages of a moraine from the coastal lowlands date its deglaciation to around 12.5 ka BP (Briner et al., 2007), and a moraine system at the mouth of the Clyde Inlet indicates that the ice has reached it at the onset of the Holocene (Couette et al., 2023). Several moraines in the central part of the Clyde trough suggest that the initial ice retreat was interrupted by re-advances, probably during the Younger Dryas (~12.9 to 11.7 ka BP) (Couette et al., 2023). The following retreat of the LIS from the Clyde Inlet was described to happen rapidly, starting at the outer fjord at ~ 10 ka BP and reaching the fjord head at ~ 9.3 to 9.1 ka BP (Briner et al., 2007). However, several moraine deposits in the middle section and head of the Clyde fjord have been interpreted as the interruption of overall deglaciation or re-advances related to cooler periods, in particular the Cockburn Substage between 9.5 and 8.3 ka BP and the 8.2 ka cold event (Andrews & Ives, 1978; Couette et al., 2023). Additionally, Briner et al. (2007) identified some re-advances of the LIS during the early Holocene, which do not correlate with specific cold events but could have been caused by increased winter precipitation related to the influence of warm waters in Baffin Bay. The rapid retreat of the LIS from the Clyde Inlet coincided with the Holocene Thermal Maximum of Arctic Canada dated between ~ 10 and 7 ka BP, in a period with warmer-than-present temperatures (Fisher et al., 1995; Briner et al., 2006). As indicated by the strong connection between climate variability and ice sheet dynamics, the regional climate was the main driver of the Clyde Inlet deglaciation, although its specific pattern was also influenced by the local topography (Couette et al., 2023). After its retreat from the multiple fjords on central to northeastern Baffin Island, the remnant of the LIS over the Foxe basin collapsed, and the remaining Foxe Dome became isolated, and reduced to the Barnes Ice Cap (Fig. 5.1) (Briner et al., 2009b). This ice cap steadily shrank throughout the mid to late Holocene, reaching its current size at about ~2 to 1 ka BP (Briner et al., 2009b). As inferred from proglacial lake studies, alpine glaciers on

northeastern Baffin Island likely survived the Holocene Thermal Maximum (HTM) and had their minimum extent between ~6 to 3 ka BP (Thomas et al., 2010). Thomas et al. (2010) suggest that the survival of the alpine glaciers during the early Holocene was likely caused by a stronger seasonality and the presence of the residual LIS but also by increased precipitation associated with warmer surface ocean waters. Finally, lake sediment records reveal that the most pronounced advance of alpine glaciers on Baffin Island after 14 ka BP occurred during the Little Ice Age (LIA) between 1500 and 1900 CE (Andrews & Barnett, 1979) in response to cold temperatures and high precipitation (e.g., Miller et al., 2005; Briner et al., 2009b; Thomas et al., 2010).

In this study, we intend to improve the present understanding of the LIS deglaciation history on Baffin Island, with attention paid to the specificity of the ice retreat in Clyde Inlet and, more generally, to the evolution of the Baffin Island ice cover. Sedimentary sequences from the fjord (core GeoB22346-3) and the adjacent shelf (GeoB22357-3) are used for this purpose. Our approach involves performing computer tomography and radiogenic isotopes (Sr, Pb, Nd) and mineralogical analyses to identify past sediment sources and dynamics. These data are also used to trace the spatially-focused freshwater pulses from changing catchment geologies into the ocean, thereby providing valuable information about the chronology of spatial glacier dynamics.

5.2 Regional Setting

Baffin Bay is an oceanic basin delimited by Greenland, Ellesmere Island, the Canadian Arctic Archipelago (CAA), and Baffin Island. Presently, it connects the northwest Atlantic Ocean and the Arctic Ocean (Fig. 5.1). During the last glaciation, prior to the opening of Nares Strait and the CAA channels (e.g., Jennings et al., 2011; Pieńkowski et al., 2014; Stevenard et al., 2022), connections with the Arctic were interrupted, and the basin was exclusively linked to the North Atlantic through the Labrador Sea. The bay is about 1300 km long and 450 km wide, with water depth reaching 2000 - 2500 m in the deep central basin. In contrast to the broad western Greenland shelf (> 250 km), the continental shelf off Baffin Island is relatively narrow (50 to 60 km wide) (Bennett et al., 2013). The Baffin shelf is cut by several transverse troughs located offshore major fjord systems (Brouard & Lajeunesse, 2017), which are the results of glacial erosion by outlet glaciers and sediment reworking during Quaternary glaciations (Bennett et al., 2013; Brouard & Lajeunesse, 2017). Onshore, the study area is characterized by long fjords, which dissect the eastern coastal mountains of Baffin Island with gently descending forelands on the outer part of some inter-fjord peninsulas (Praeg et al., 2007). To the west of the eastern coastal mountains and the study area, the Barnes Ice Cap, a remnant of the LIS, covers the interior uplands of Baffin Island (Praeg et al., 2007).

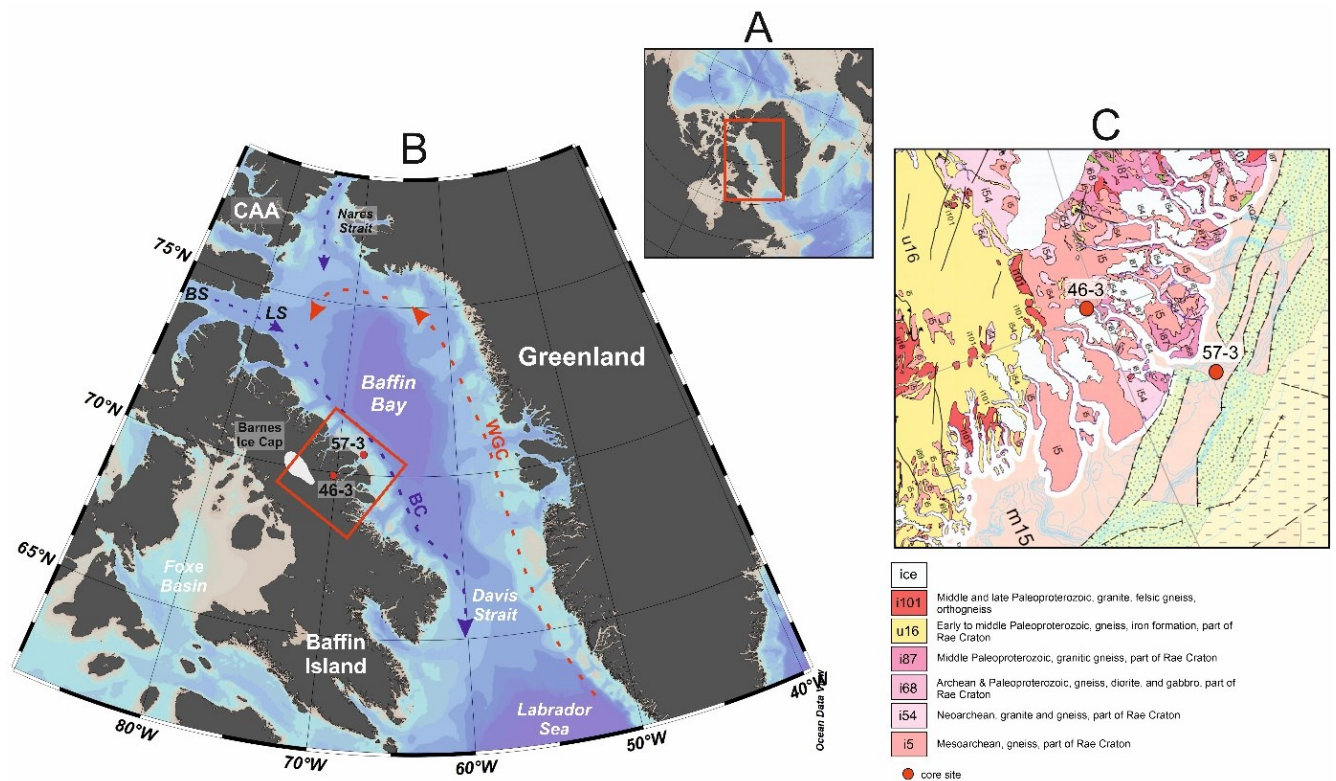


Figure 5.1: (A) Overview map showing the location of Baffin Bay. (B) Map of the research area including the locations (red circles) of sediment cores GeoB22346-3 and GeoB22357-3 from the Clyde area and simplified present-day oceanography including the West Greenland Current (WGC) transporting relatively warm waters towards northern Baffin Bay and the Baffin Current (BC) that transports cold Arctic waters southwards towards Labrador Sea. CAA: Canadian Arctic Archipelago, LS: Lancaster Sound, BS: Barrow Strait. Map created with Ocean Data View (Schlitzer, 2019). (C) Detailed geological map of the Clyde Inlet area showing core locations and present-day ice coverage. Map modified after Harrison et al. (2011b).

5.2.1 Oceanography and sea ice conditions

In the eastern part of the Baffin Bay, the West Greenland Current (WGC) transports relatively warm and saline Atlantic waters northward along the western Greenland margin (Fig. 5.1; Tang et al., 2004). Cold Arctic waters can enter the basin via Nares Strait, the Barrow Strait, and smaller gateways of the CAA and feed the Baffin Current (BC), which transports relatively cold and fresh water along western Baffin Bay (the eastern Baffin Island coast) through the Davis Strait into the Labrador Sea and the North Atlantic (Tang et al., 2004). This counter-clockwise circulation pattern with warm northward flowing waters in the east and cold southward flowing waters in the west strongly influences the seasonal sea ice distribution in the basin. Until recently, most of the year, sea ice was present in Baffin Bay with a minimum extent to complete disappearance in August and September (Tang et al., 2004). Full ice cover was typically reached during March, with the exception of the eastern Davis Strait, where the relatively warm waters of the WGC inhibited any thick sea ice formation. Recent warming has modified this regime with a significant reduction in the sea-ice cover, notably in the fall (Ballinger et al., 2022).

Icebergs transiting Baffin Bay are mainly provided by the Greenland Ice Sheet (GIS) and in smaller amounts, by tidewater glaciers on the northern CAA.

5.2.2 Geology, lithology, and related radiogenic isotope signatures

The northern part of Baffin Island mainly consists of Archean to Paleoproterozoic crystalline shield rocks of the Committee Belt ascribed to the Rae craton (Harrison et al., 2011b). The Committee Belt extends from northern Baffin Island to northwestern Greenland. Thus, similar geological units and related radiogenic isotopic signatures occur on both sides of northern Baffin Bay. On northern Baffin Island, Mesoproterozoic siliciclastic rocks interbedded with some shales, limestones, and dolostones of the Borden Peninsula and Bylot Island overlie parts of the Rae Craton (Harrison et al., 2011b). The CAA is dominated by large outcrops of Paleozoic dolostones and limestones, siliciclastics, and evaporites that cover the Precambrian basement (Scott & de Kemp, 1998; Harrison et al., 2011). In detail, the geology around the outer Clyde Inlet and at the fjord head is dominated by Mesoarchean quartzo-feldspathic gneisses of the Rae craton, including undifferentiated deformed granitic intrusions (Fig. 5.1c) (Jackson & Berman, 2000; Harrison et al., 2011). Around the middle part of the fjord and on the Clyde Inlet forelands, slightly younger Archean to Paleoproterozoic migmatites occur. Southwest of the Clyde Inlet head, between the southern Barnes ice cap and the fjord, there are again outcrops of Archean to Paleoproterozoic migmatites and small areas of outcropping Paleoproterozoic quartzites, marbles, and the rusty schist iron formation (Jackson & Berman, 2000; Harrison et al., 2011b).

A few studies have conducted radiogenic isotope analysis on bedrock samples from Baffin Island or the Clyde Inlet area. McCulloch and Wasserburg (1978) measured the radiogenic Nd and Sr isotope composition on a composite sample from Baffin Island, which showed unradiogenic ϵ_{Nd} values of -31.7 and radiogenic $^{87}Sr/^{86}Sr$ values of 0.76. In general, the Pb isotope signatures of old crystalline rocks tend to be relatively radiogenic. While information on the bedrocks is scarce, measurements were conducted on marine surface sediments and cores from northern Baffin Bay and the northwestern Greenland shelf that provide a range of Nd, Sr, and Pb isotope values. These can be used for sediment provenance discussion because they represent very similar sources compared to Baffin Island. Radiogenic isotope measurements on shelf sediments (surface sediments) off northwest Greenland, close to Archean to Paleoproterozoic rocks, show ϵ_{Nd} , $^{87}Sr/^{86}Sr$, and $^{206}Pb/^{204}Pb$ values ranging from -36 to -21, 0.73 to 0.77, and 18 to 19, respectively (Madaj, 2021). In contrast to the old crystalline rocks on Baffin Island and Greenland, younger rocks usually have higher ϵ_{Nd} and lower $^{87}Sr/^{86}Sr$ and $^{206}Pb/^{204}Pb$ values. Isotope analysis of a sediment surface sample from west of the Barrow Strait, surrounded mainly by carbonate rocks, yielded higher ϵ_{Nd} (-19 to -12) and lower $^{87}Sr/^{86}Sr$ (0.72 to 0.74) values (Maccali et al., 2018). Similarly, the Holocene radiogenic isotope composition from a sediment core from Barrow Strait shows $^{87}Sr/^{86}Sr$ values ranging from 0.73 to 0.74, ϵ_{Nd} values around -17.6, and $^{206}Pb/^{204}Pb$ values around 19.0 (Hingst et al., in review).

5.3 Materials and Methods

The two selected marine sediment cores GeoB22346-3 and GeoB22357-3, hereafter named 46-3 and 57-3, were collected with a gravity corer during the 2017 RV Maria S. Merian cruise MSM66 within (proximal) the Clyde Inlet and distal, in front of the Clyde Inlet, on the shelf of northeastern Baffin Island, respectively (Dorschel et al., 2017). Sediment core 46-3 (69° 54.18'N / 70° 13.54'W; 203 m water depth) has a recovery length of 783 cm, whereas core 57-3 (70° 36.28'N / 67°53.63'W; 315 m water depth) has a total length of 902 cm.

For the radiogenic isotope and mineral analyses of the present study, 24 samples from core 57-3 and 12 samples from core 46-3 were collected, with each sample weighing approximately 5 g. Lithological descriptions of the two cores can be found in the cruise report (Dorschel et al., 2017) and are further discussed in Couette et al. (2023). Furthermore, bathymetric data, seismic and acoustic profiles of the research area, and elemental compositions of the two sediment cores are presented in Couette et al. (2023).

5.3.1 Chronology

The age models of cores 57-3 and 46-3 are based on 6 and 7 Acceleration Mass Spectrometry (AMS) ¹⁴C dates, respectively (Figs 5.2, 5.3; Tables 5.1, 5.2). The AMS measurements were carried out on mixed foraminifera and mollusk shell samples at the MICADAS (MIni CARbon Dating System) ¹⁴C laboratory of the Alfred Wegener Institute (AWI) in Bremerhaven, Germany. The age calibration and age-depth model were performed using the age-modeling UNDATABLE software (Lougheed & Obrochta, 2019) and applying the Marine20 dataset (Heaton et al., 2020). For the ¹⁴C age calibration, a regional reservoir age correction (ΔR) for northeastern Baffin Island of 81 ± 18 years was applied (Pieńkowski et al., 2022). The age model was extended by linear extrapolating the sedimentation rates outside the ¹⁴C dating points.

Table 5.1: AMS ¹⁴C dates from core GeoB22357-3. Calibrated ages are the median probability ages and 95% confidence interval (minimum and maximum age) obtained with Calib 8.2 (Stuiver & Reimer, 1993). MBF: Mixed Benthic Foraminifera.

Lab ID	Depth interval (cm)	Dated material	¹⁴ C Age		Reservoir Age (yrs)	Calibrated Ages (yrs BP)		
			yrs	±		Min.	Max.	Median
6229.1.1	128 - 129	MBF	9044	99	81 ± 18	9191	9788	9475
6230.1.1	218 - 219	MBF	9915	98	81 ± 18	10297	11009	10637

6231.1.1	248 - 249	MBF	9894	38	81 ± 18	10383	10795	10598
6232.1.1	308 - 309	MBF	10025	33	81 ± 18	10601	11043	10804
6233.1.1	368 - 369	MBF	10442	95	81 ± 18	11101	11714	11374
6234.1.1	398 - 399	MBF	10246	36	81 ± 18	10898	11255	11118

Table 5.2: AMS ¹⁴C dates from core GeoB22346-3. Calibrated ages are the median probability ages and 95% confidence interval (minimum and maximum age) obtained with Calib 8.2 (Stuiver & Reimer, 1993). Samples marked with a * are from Couette et al. (2023). MBF: Mixed Benthic Foraminifera.

Lab ID	Depth interval (cm)	Dated material	¹⁴ C Age		Reservoir Age (yrs)	Calibrated Ages (yrs BP)		
			yrs	±		Min.	Max.	Median
6226.1.1	32 - 36	MBF	2688	212	81 ± 18	1606	2679	2120
6223.1.1	152 - 155	MBF	2442	71	81 ± 18	1586	2039	1812
6224.1.1	243 - 245	MBF	3614	71	81 ± 18	3011	3459	3253
1726.1.1*	387	Mollusc shell	5929	51	81 ± 18	5898	6252	6066
6225.1.1	483 - 485	MBF	6833	85	81 ± 18	6805	7282	7057
6226.1.1	603 - 604	MBF	8471	91	81 ± 18	8462	9027	8763
6227.1.1	723 - 724	MBF	8421	102	81 ± 18	8408	8993	8701
1727.1.1*	767 - 768	Foraminifera	8902	193	81 ± 18	8769	9845	9303

5.3.2 Computed tomography

Computed tomography (CT) scanning is a non-destructive method to gain detailed information on sedimentary facies and structures. CT scanning of the archive halves of both sediment cores was performed at the hospital Klinikum Bremen-Mitte, Bremen, Germany, using a Philips CT Brilliance iCT Elite 256 equipped with a current of 300 mA and a 120 kV X-ray source voltage. The resolution used for core scanning was 0.293 mm in the x and y dimensions and 0.625 mm in the z-direction (0.3 mm reconstruction unit). The scans were rebuilt using a bone kernel (YB (Enhanced)) and the filtered Back Projection (fBP) mode before being exported as DICOM data. The CT data was processed using the Amira software (version 2021.08) (Stalling et al., 2005). Processing of the CT data of both cores enabled quantitative determinations of the concentrations of ice-rafted debris (IRD; lithic clasts with grain size

>1 mm; unit: vol. %), the mean matrix sediment densities (MSD; unit: HU), and the concentrations of sediment bioturbation (unit: vol. %). More information about data processing can be found in Okuma et al. (2023).

5.3.3 X-ray diffraction (XRD)

The bulk mineralogical assemblages of 17 samples of core 57-3 and twelve samples of core 46-3 were determined by X-ray diffraction (XRD). For this, the sediment fine fraction (< 63 μm) obtained by wet sieving was ground manually with an agate mortar to reach an approximate grain size of < 2 μm . XRD measurements were performed on a Bruker D8 Discover diffractometer at the laboratory of the Crystallography Research Group, Faculty of Geosciences, University of Bremen, Germany.

5.3.4 Radiogenic isotope analysis

Sr, Nd, and Pb isotope compositions were analyzed in the laboratory of the Isotope Geochemistry Group at MARUM – Center for Marine Environmental Sciences, University of Bremen, Germany. Approximately 2 g of wet sediment was filled into 15 ml centrifuge tubes and washed twice with Milli Q water (18.2 M Ω) to remove the soluble fraction and pore water from the sample. For further analysis, the < 63 μm grain size fraction was separated by wet sieving. After drying, samples were homogenized and ground with an agate mortar. The dried, coarse sediment fraction (>63 μm) was weighted to estimate the approximate grain size distribution within the sediment sample. To remove potential marine carbonates and authigenic Fe-Mn oxyhydroxide coatings, sediment samples were leached with acetic acid and/or a NaOH-buffered solution of hydroxylamine hydrochloride and 15 % acetic acid for 3 hours. The supernatants of each sample were saved in 40 ml PP containers. Leached samples were washed twice with Milli Q water and dried at 110°C in the oven.

To dissolve the siliciclastic sediment fraction (modified after Höppner et al., 2018), 100 mg of each decarbonated sample was transferred into 15 ml Teflon Savillex® beakers. In the first step, 3 ml of a concentrated HF-HNO₃ mixture was added to the samples (dissolution on the hotplate at 140°C for at least 48 hours). After drying, samples were re-dissolved in 3 ml aqua regia (3:1, 6 N HCl: concentrated HNO₃) for two days at 120°C. To remove organic matter, 100 μl H₂O₂ was added to the samples four to five times until the reaction stopped. After each repetition, samples were left on the hotplate for ~ 1 hour at 70°C. Afterward, 1 ml concentrated HNO₃ was added and samples were placed on the hotplate at 70°C overnight for dissolution. In the last dissolution step, 3 ml HCl was added to the dry samples, which were then placed on the hotplate at 70°C overnight. Finally, the samples were dried again for chemical separation and re-dissolved in 1100 μl 2M HNO₃.

Sr and Pb were separated on the same column using 70 μl Sr.specTM resin following a modified method after Deniel & Pin (2001). Nd separation was performed in two steps using TRU.specTM for light rare earth elements and LN.specTM for Nd isolation (method after Pin et al., 1994).

Sr, Nd, and Pb isotope ratios were measured with a Thermo-Fisher Scientific TRITON Plus thermal ionization mass spectrometer (TIMS) at the Isotope Geochemistry Laboratory at MARUM. Sr and Pb were measured on a single filament in the static multicollection mode, using a Ta and Si activator, respectively. For Nd analyses, a double filament was used and the measurements were conducted in a static multicollection mode. For the correction of the instrumental mass fractionation during Sr and Nd isotope analysis, the stable isotope ratios $^{86}\text{Sr}/^{88}\text{Sr}$ (=0.1194) and $^{146}\text{Nd}/^{144}\text{Nd}$ (=0.7219) were used, respectively. During Pb isotope analysis, instrumental mass fractionation was corrected by applying a factor of 1.001 per atomic mass unit. To record the analytical accuracy and repeatability, reference material NIST SRM 987 was used for $^{87}\text{Sr}/^{86}\text{Sr}$, NIST SRM 981 for Pb isotope ratios, and JNd-1 for $^{143}\text{Nd}/^{144}\text{Nd}$. The analyzed values are in the range of values analyzed by TIMS and published in the GeoReM database (<http://georem.mpch-mainz.gwdg.de/>, query November 2022, March 2023): NIST SRM987: 0.710242 ± 0.000032 (2SD_{mean} , $n=15$), 0.710250 ± 0.000040 (GeoReM; 2SD_{mean} , $n=1711$, data <0.7102 and >0.7103 are discarded); JNd-1: 0.512113 ± 0.000024 (2SD_{mean} , $n=12$), 0.512107 ± 0.000024 (GeoReM; 2SD_{mean} , $n=414$, data <0.51204 and >0.51217 are discarded); NIST SRM 981: 16.9004 ± 0.0133 ($^{206}\text{Pb}/^{204}\text{Pb}$; 2SD_{mean} , $n=12$), 16.9211 ± 0.0423 ($^{206}\text{Pb}/^{204}\text{Pb}$; GeoReM; 2SD_{mean} , $n=290$, data >17 are discarded). Nd isotope ratios are presented in the ϵ_{Nd} notation using the Chondritic Uniform Reservoir (CHUR) value of $^{143}\text{Nd}/^{144}\text{Nd} = 0.512638$ (Jacobsen & Wasserburg, 1980).

5.4 Results

5.4.1 Age model and sedimentation rates

The final age model of core 57-3 is based on six calibrated ^{14}C dates taken within the upper four meters of the core (Fig. 5.2). The age model suggests that the core covers the time interval between 8.1 and 13 ka BP and allows estimation of sedimentation rates on the shelf, offshore the Clyde Inlet. The calculated sedimentation rates in core 57-3 range from 90 to 290 cm ka^{-1} . Sedimentation rates are high prior to ~ 10.6 ka BP at ~ 250 cm (~ 280 to 290 cm ka^{-1}) before they drop and stay on a lower level at ~ 90 to 105 cm ka^{-1} .

The age model of core 46-3 is based on seven calibrated ^{14}C dates (Fig. 5.3) and indicates that the sediment record from the Clyde Inlet head covers the last ~ 9.5 ka BP, capturing most of the Holocene period. The calculated sedimentation rates range from ~ 50 to a maximum of 150 cm ka^{-1} , with the highest values in the lower parts of the core. Above ~ 500 cm core depth, sedimentation rates initially

decrease to moderate values ($\sim 100 \text{ cm ka}^{-1}$) before the lowest sedimentation rates ($\sim 50 \text{ cm ka}^{-1}$) occur between ~ 380 and 240 cm . Sedimentation rates slightly increased ($\sim 85 \text{ cm ka}^{-1}$) towards the core top.

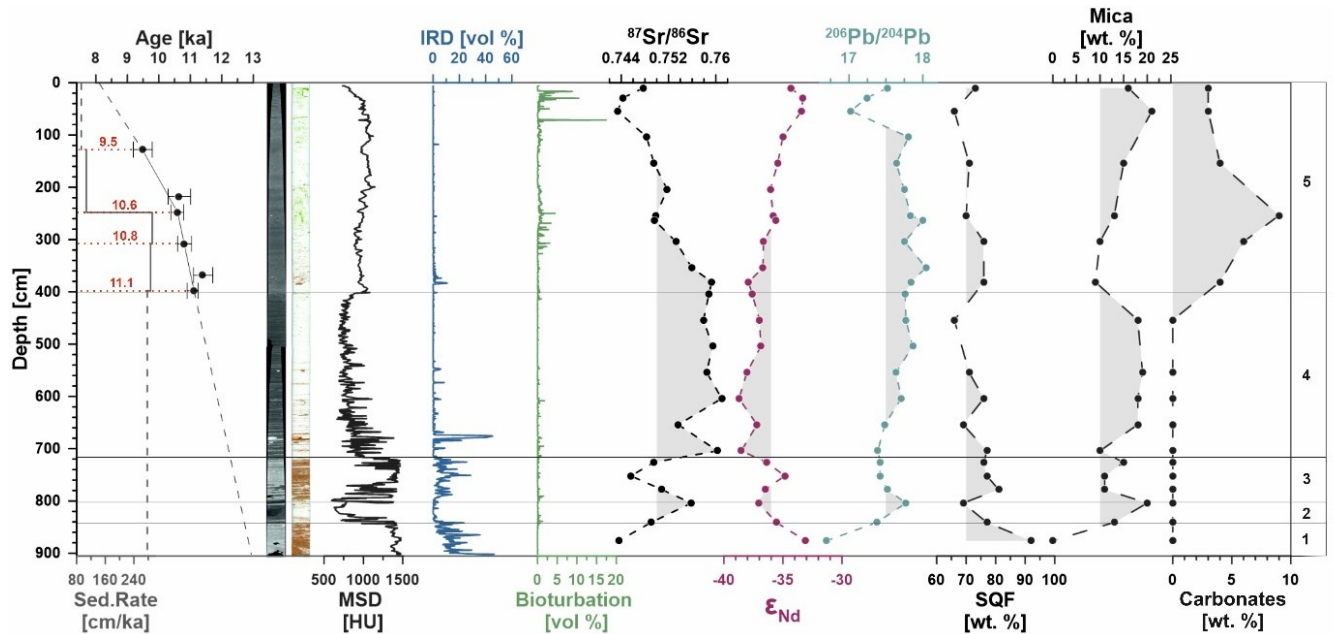


Figure 5.2: Age-depth model and calculated sedimentation rates, processed CT scans (brown, green, and white colours indicate clasts $>1 \text{ mm}$, bioturbation, and background sediments, respectively), and downcore quantification of the mean matrix sediment density (MSD), ice-rafted debris (IRD, i.e., clasts $>1 \text{ mm}$), and bioturbation content, as well as radiogenic isotope, and mineralogical compositions of core GeoB22357-3. Radiocarbon dating points are marked with dotted lines (in red) with corresponding calibrated ages given in ka BP. Sedimentation rates outside of the radiocarbon-dated intervals were linearly interpolated and are displayed as dashed lines. SQF is the sum of quartz and feldspar. Horizontal lines mark the identified stratigraphic Units 1 to 5.

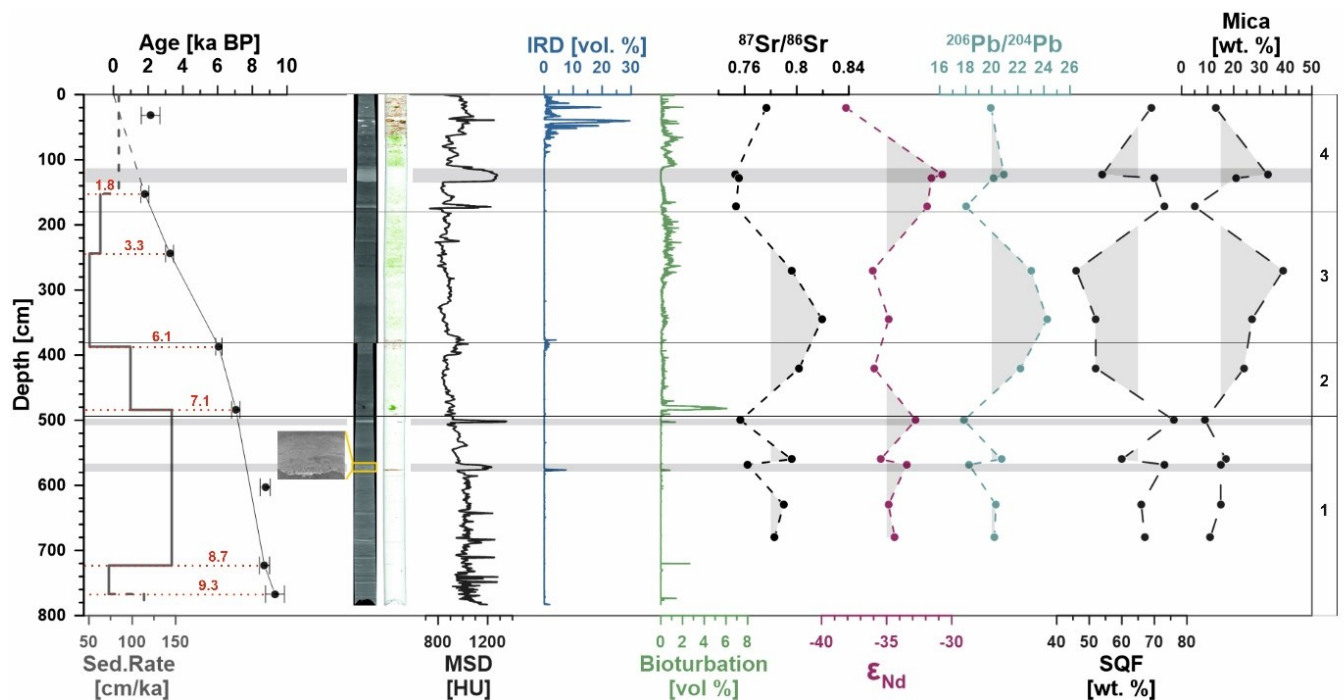


Figure 5.3: Age-depth model and calculated sedimentation rates, processed CT scans (brown, green, and white colours indicate clasts >1 mm, bioturbation, and background sediments, respectively), and downcore quantification of the mean matrix sediment density (MSD), ice-rafted debris (IRD, i.e., clasts >1 mm), and bioturbation content, as well as radiogenic isotope and mineralogical compositions of core GeoB22346-3. Radiocarbon dating points are marked with dotted lines (in red) with corresponding calibrated ages given in ka BP. Sedimentation rates outside of the radiocarbon-dated intervals were linearly interpolated and are displayed as dashed lines. Prominent turbidite layers are highlighted with horizontal grey bars, and an example interval is enlarged to the left. SQF is the sum of quartz and feldspar. Horizontal lines mark the identified stratigraphic Units 1 to 4.

5.4.2 Stratigraphic units and computed tomography

Based mainly on the interpretation of CT data of cores 57-3 and 46-3, different stratigraphic units have been identified for the two cores (Figs 5.2, 5.3). Although the identified units here are largely comparable to the lithological units previously described by Couette et al. (2023), the additional CT data provide further details in downcore changes of sediment characteristics.

Five different stratigraphic units can be identified in core 57-3 (Fig. 5.2). Unit 1 is a dense and IRD-rich lowermost layer, from the core bottom to ~ 840 cm, and is interpreted as a till. Here, maximum MSD values (~ 1470 HU) and IRD values of up to ~ 46 vol.% (901 cm) are recorded, with no traces of bioturbation in this highly compacted layer with abundant clasts. Unit 2 is a thin layer, between ~ 840 and 800 cm, characterized by low IRD content, significantly reduced sediment densities, and minor amounts of bioturbation. Unit 3 is another layer characterized by high, but more variable, sediment densities (up to ~ 1450 HU) and occurs between ~ 800 and ~ 720 cm. This unit is slightly laminated and bioturbated, IRD content is high, reaching up to 28 vol.%, and contains mainly smaller clasts compared to Unit 1. Unit 4 is characterized by a continuously decreasing and less variable MSD (~ 830 HU) and highly reduced IRD content (~ 1 vol.%) towards the top of this unit (~ 400 cm). This unit shows strong lamination with minor bioturbation and scattered large clasts. The transition to Unit 5 is marked by an increasing MSD, which stays mostly uniform (~ 1000 HU) in the rest of the unit, only dropping again in the uppermost ~ 35 cm. Small amounts of IRD can be observed in the lower part of this unit, while bioturbation increases up-core with the highest concentrations in the uppermost ~ 70 cm.

Core 46-3 can be subdivided into four different stratigraphic units (Fig. 5.3). Unit 1 extends from the core bottom to ~ 500 cm and consists of laminated mud interbedded with thin-to-thick (sandy) turbidite layers. MSD generally varies between approximately 880 and 1340 HU in this unit, showing distinct peaks within the turbidite layers. Almost no IRD or bioturbation is recorded in this relatively rapidly deposited interval. Unit 2 (~ 500 to 380 cm) is associated with intermediate sedimentation rates. This unit is marked by slightly higher bioturbation, lower MSD values, and no to minor amounts of IRD at the top of the unit. Unit 3, between ~ 380 and 180 cm, shows increasing values of bioturbation towards the top. This unit has almost no IRD, and MSD is constantly low (~ 870 HU). Unit 4 is the uppermost

interval of the core (< 180 cm) and is characterized by the occurrence of lamination and thick-and-thin sandy layers marked by higher sediment densities and lower bioturbation. The uppermost meter shows increased IRD content with values up to ~ 27 vol. % and several large clasts.

5.4.3 Relative mineralogical composition (XRD)

The mineralogical composition of core 57-3 (Fig. 5.2) can be divided into two different sections. The lower section of the core, from the core bottom to a depth of about 550 cm, is characterized by varying relative mineral abundances. Even if the quartz (on average ~34 %) and plagioclase (on average ~26 %) dominate over the entire core, the lower section exhibits the highest and lowest relative concentrations of these minerals. In contrast, the upper section, 550 cm to the core top, shows more uniform relative mineralogy, only interrupted by a small layer at 304 to 381 cm with enhanced quartz or K-feldspar concentrations but depleted relative abundances of mica. Within the upper section (10 - 380 cm), a relative abundance of 3 - 9 % of dolomite can be detected. Relative abundances of amphibole and pyroxene vary in both sections between 2 % and 9 %.

The XRD analysis of core 46-3 shows significant variations in the mineralogical composition down-core (Fig. 5.3). The mineralogy is mainly dominated by quartz, whose relative contribution varies between 21 % and 36 %, with low values mainly observed in Units 2 and 3, between 270 cm and 420 cm, and two peaks at 172 cm and 500 cm. In addition, 46-3 is rich in mica and plagioclase, with values up to 39 % and 36 %, respectively. However, relative mica concentrations are highly variable, with the highest concentrations in Unit 3. Other clay minerals like chlorite and kaolinite play a minor role in the down-core mineralogy with maximum relative concentrations of 8 %. Relative K-feldspar concentrations are, on average, 11 %, with the highest value of 17 % at 345 cm. There are almost no carbonates detected by the XRD measurements (1 % at 630 cm).

5.4.4 Sr, Nd, and Pb isotope composition

In general, the range of radiogenic isotope values in core 57-3 is smaller than in the core from the fjord head, with the Sr isotope composition ranging between 0.74 and 0.76 (Fig. 5.4). In the lower part of the core, in Units 1 to 3, the fluctuation of Sr isotope values is strongest (Fig. 5.2). Higher and more constant Sr isotope values occur in Unit 4, before the Sr isotope composition is initially just slightly decreasing before values drop more rapidly in Unit 5 towards 0.74. In the upper ~ 50 cm of the core, $^{87}\text{Sr}/^{86}\text{Sr}$ values are slightly increasing again. Variations in the Nd isotope records occur parallel to the fluctuations in the Sr isotope composition but anticorrelate. The highest variability occurs in Units 1 to 3, with ϵ_{Nd} values ranging between -37.1 and -33.1. Nd isotope values are highest in Unit 4, staying more uniform around -37.7. In Unit 5, ϵ_{Nd} values increase with smaller variations towards -33.4 at ~30 cm before they slightly drop again. $^{206}\text{Pb}/^{204}\text{Pb}$ values vary between 16.7 and 18 (Fig. 5.2). The Pb isotope record shows a steep increase between the core bottom and ~ 800 cm and afterward, an overall smoothly increasing

trend towards ~260 cm. Between 260 cm and 50 cm, values drop before increasing again towards the core top.

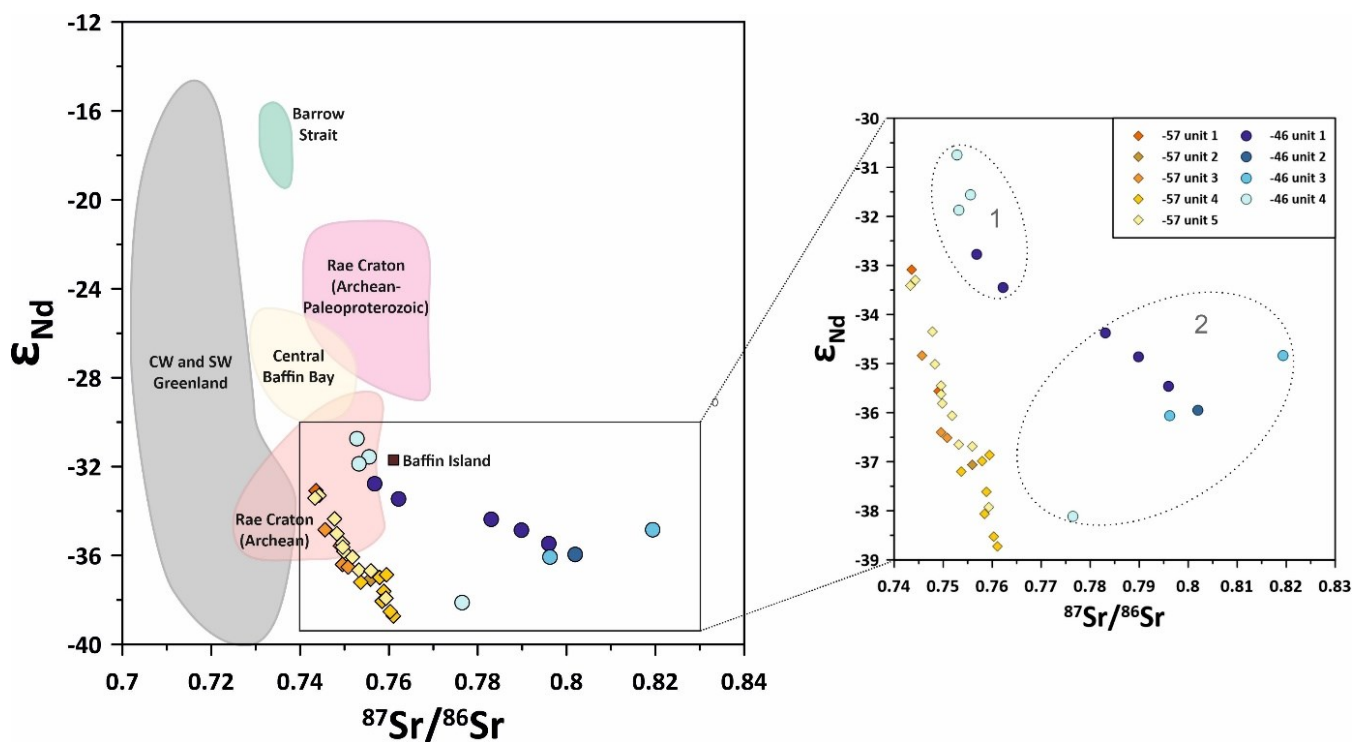


Figure 5.4: $^{87}\text{Sr}/^{86}\text{Sr}$ vs. ϵ_{Nd} plot of GeoB22346-3 and GeoB22357-3. Additionally, reference isotope signatures from different geological regions in Baffin Bay are included for provenance discussion. The colors of the background data are adapted to the colors used in Figure 5.1. Areas not displayed in Figure 5.1 are marked in grey. Background data are from marine sediment analyses of different studies: Rae Craton (Archean – Paleoproterozoic; light pink): sediment core (GeoB19927-3) from the western Greenland shelf (Madaj, 2021), Rae Craton (Archean; dark pink): sediment core (GeoB19946-4) from the northwestern Greenland shelf (Madaj, 2021), Baffin Island (dark-brown square; McCulloch & Wasserburg, 1978), Barrow Strait (light green): Holocene isotope signatures of core PS72/287-3 (Hingst et al., in review), and southwest (SW) and central west (CW) Greenland (grey): stream sediment data (Colville et al., 2011; Reyes et al., 2014), central Baffin Bay (yellow): isotope signatures of core PC16 (Kirillova, 2017). The zoomed-in section to the right shows the two data clusters highlighted in circles.

In the Sr-Nd isotope plot, the data of core 57-3 form a distinct cluster, which does not overlap with the data from the Clyde Inlet head. Specifically, the radiogenic isotope data for Units 1, 3, and 5 are generally less radiogenic in the Sr isotope composition and more radiogenic in the Nd isotope composition (Fig. 5.4). Conversely, the isotope data for Unit 4 have predominantly more radiogenic Sr isotope values and less radiogenic Nd isotope values. Data with higher Nd isotope compositions overlap with reference isotope signatures measures close to the Rae Craton (Paleoproterozoic) in NW Greenland, similar to some data points of the core 46-3 (Fig. 5.4).

The radiogenic Sr isotope composition of core 46-3 is highly variable, ranging from 0.75 to 0.82 (Fig. 5.3). In Unit 1, $^{87}\text{Sr}/^{86}\text{Sr}$ values fluctuate between 0.76 and 0.79, whereas lower Sr isotope values occur

within the identified turbidite layers. The highest $^{87}\text{Sr}/^{86}\text{Sr}$ values are reached in Units 2 and 3 (0.8 to 0.82) before Sr isotope values decrease again towards Unit 4 (0.75 and 0.78). ϵ_{Nd} values of the detrital material are more uniform with just small variations mainly in Unit 1, which occur again within the turbidite layers. In Unit 4, ϵ_{Nd} values initially rise to values of up to -31 before the most unradiogenic ϵ_{Nd} value of about -38 is reached at the core top. The most radiogenic ϵ_{Nd} value is reached in the turbidite layer in Unit 4. The $^{206}\text{Pb}/^{204}\text{Pb}$ measured on the detrital sediment fraction are variable and these changes follow the variation in the Sr isotope record, except in Unit 4. $^{206}\text{Pb}/^{204}\text{Pb}$ values range from 17.9 to 24.2 (Fig. 5.3).

Sr and Nd isotope data of the Clyde Inlet core 46-3 plot in two groups (Fig. 5.4). Data points between 7.8 and 7.1 ka BP and 2.1 and 1.5 ka BP show rather unradiogenic Sr isotope values and more radiogenic Nd isotope compositions, while the group of data points from 8.6 to 7.7 ka BP and 6.2 to 3.8 ka BP, as well as the from 0.2 ka BP are characterized by more radiogenic $^{87}\text{Sr}/^{86}\text{Sr}$ values and less radiogenic ϵ_{Nd} values. The data points of the first group are closest to the bedrock reference data from Baffin Island (McCulloch & Wasserburg, 1978) and overlap with available isotope signatures measured close to the Rae Craton (Paleoproterozoic) in NW Greenland (Madaj, 2021). The isotope signatures of the second group are not close to any known reference isotope signatures from the Baffin Bay area.

5.5 Discussion

5.5.1 Outlet glacier retreat from the NE Baffin Island shelf into the Clyde Inlet during the Late Pleistocene to early Holocene

The location of the sediment core 57-3 on the cross-shelf trough, with its connection to the Clyde Inlet, allows the reconstruction of changing sediment input from Baffin Island and related meltwater and transport processes during the last deglaciation. Moreover, radiogenic isotope composition and mineral assemblages could identify material from other source regions in Baffin Bay transported to the core site by ocean currents. Even if the age model of the core is limited, by extrapolation it suggests that the sediment record covers approximately the period ~13 to 8.1 ka BP. The enclosed time interval likely covers parts of the initial Clyde shelf deglaciation, between 16 and 11.7 ka BP, and the early Holocene step-wise retreat of the ice margin into the fjord (Couette et al., 2023). Thus, the 57-3 core can provide valuable information about the early LIS deglaciation processes and related sediment dynamics on the Baffin Island shelf (Fig. 5.5).

Couette et al. (2023) already presented the lithology and selected element ratios of core 57-3. However, this study does not include ^{14}C dates for this core, as they did for core 46-3. In addition to the CT scanning of the sediment cores, the presented ^{14}C dates here are a valuable addition to the above-mentioned study, providing better temporal constraints to sedimentological changes observed in the cores, further improving paleoenvironmental interpretations. According to Couette et al. (2023), the base of core 57-

3 is characterized by two diamicton layers, interpreted as glaciogenic debris-flows deposited during ice stillstands. However, the consistently high sediment density indicates over-compaction of the lowermost interval (our Unit 1), with an extrapolated age of 12.7 ka BP (Fig. 5.5), suggesting that this unit is most likely a subglacial till deposit. This till indicates the presence of grounded ice in the cross-shelf trough during the Younger Dryas cold stadial. CT images of the second compacted layer above (Unit 3; Fig. 5.2) reveal some lamination, which is not present in Unit 1. However, the high but variable MSD values and a high IRD content suggest ice proximal conditions and probably ice re-advance, leading to the deposition of this glaciogenic debris during the mid-Younger Dryas. Couette et al. (2023) describe that these two dense layers are interrupted and overlain by ice-proximal glaciomarine deposits. The short interval of lower sediment density and IRD identified in Unit 2 (Fig. 5.2) supports the assumption of ice proximal, glaciomarine conditions, and constantly decreasing MSD and IRD in Unit 4 (Fig. 5.2) likely reveals the steady ice retreat until ~ 11.1 ka BP (Fig. 5.5). At ~ 11.1 ka BP (the transition from Unit 4 to 5), CT data, radiogenic isotope, and mineralogical compositions as well as XRF data (Couette et al., 2023) show a clear shift probably marking the transition from an ice-proximal to an ice-distal environment (Fig. 5.5). This timing is later than previously assumed based on different ages from cores collected along the Clyde Trough, which set this transition and the ice margin retreat into the fjord at ~ 11.7 - 11.5 ka BP (Couette et al., 2023).

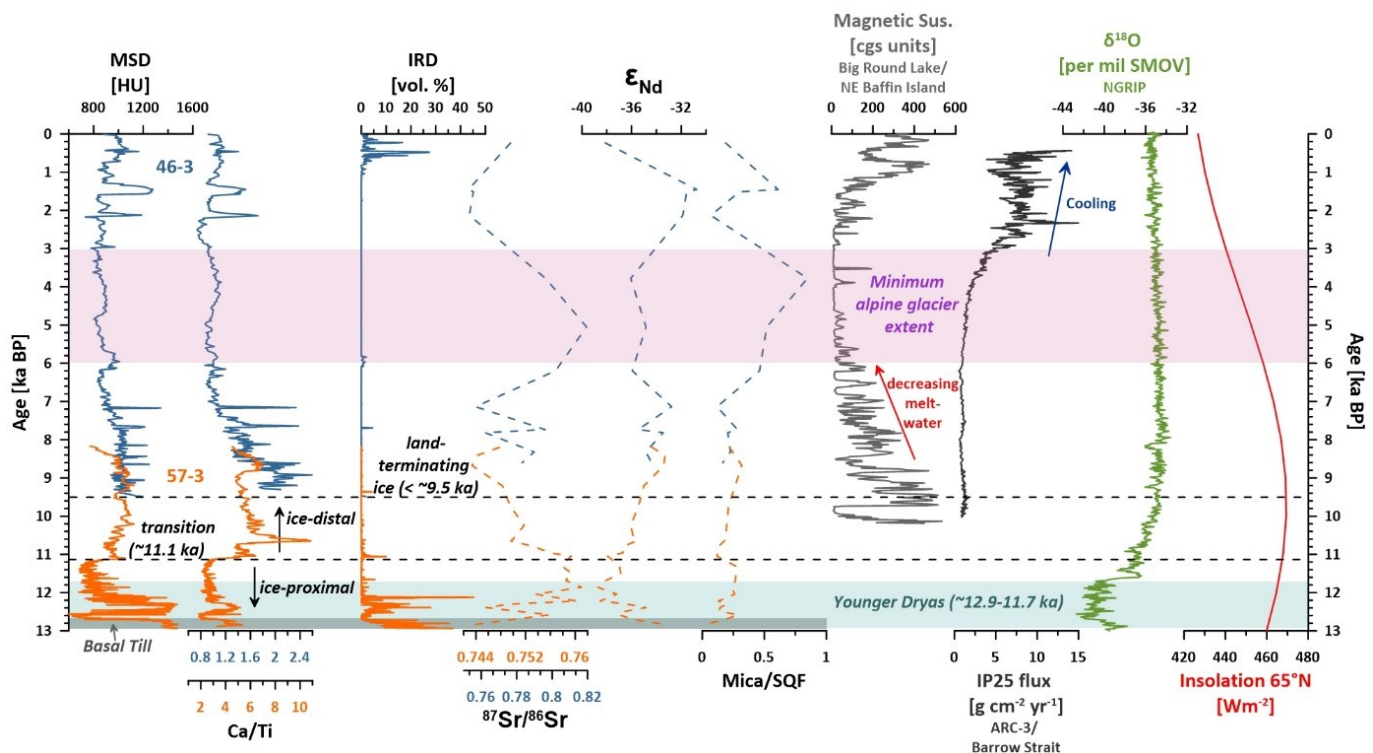


Figure 5.5: Selected data from cores GeoB22357-3 and GeoB22346-3 in comparison with different regional paleoenvironmental data. From left to right: core 46-3 (blue) and core 57-3 (orange) data: mean sediment density (MSD), Ca/Ti ratio (Couette et al., 2023), ice-rafted debris (IRD) content, Sr and Nd isotope compositions, and ratio of micas and the sum of quartz and feldspar (SQF). The grey bar marks the basal till. Additional data that are

shown: Magnetic susceptibility measured on lacustrine sediments of the Big Round Lake (NE Baffin Island) (Thomas et al., 2010), IP25 flux measured on the marine sediment core ARC-3 from Barrow Strait to reconstruct sea-ice conditions (Vare et al., 2009), oxygen isotope record ($\delta^{18}\text{O}$) from NGRIP project (Vinther et al., 2006), and July solar insolation at 65°N (Berger & Loutre, 1991).

The uppermost ~ 4 meters consists of ice-distal predominantly hemipelagic sediments, which can also be found at the top of most other cores in the Clyde Inlet region (Couette et al., 2023). That seems to be contradictory to the age model suggesting that sediments from the last ~ 8 kyrs are missing. There are three radiocarbon ages, ranging between 9.5 and 10.6 ka BP dated at 130 cm to 250 cm sediment depth (Fig. 5.3), situated within the upper layer of sediment identified by Couette et al. (2023). This could mean that the sediment of the uppermost 1.3 m was either deposited steadily after 9 ka BP but, at some point, with a meager sedimentation rate or that some sediment was eroded during this time interval due to ocean bottom currents. The analysis of multiple sediment cores from the northeast Baffin margin shows similar depositional patterns (Jenner et al., 2018). For example, radiocarbon analysis from sediments of core 64PC from the upper continental slope of Baffin Island, north of the Buchan Trough, suggests ages at 138 cm of 9.46 ka BP and 111 cm of 8.72 ka BP (Campbell et al., 2017; Kelleher et al., 2022). In general, Jenner et al. (2018) conclude that the lithological features of the different cores suggest that in Baffin Bay, the direct glacial supply is more significant for sedimentation than the effect of glacial meltwater. Therefore, we assume that the sediment top (~1 m) was slowly deposited during the interval when the ice stream had retreated behind the Clyde Inlet head after its last re-advance at ~7.9 ka BP (Briner et al., 2007) and meltwater runoff predominantly delivered sediment to the Clyde Inlet fjord and only minor amounts to the shelf.

Radiogenic isotope data of core 57-3 suggest minor variations in sediment provenance on the Baffin Island shelf during the last deglaciation and the Holocene. The slight differences in continental bedrock geology in the research area may have caused the small changes in the isotope signatures. While the Clyde foreland and some areas close to the fjord head are predominantly characterized by the occurrence of the slightly younger Paleoproterozoic igneous and metamorphic rocks, the hinterland and more distal regions are mainly composed of the Archean rocks (Fig. 5.1). The range of Sr and Nd isotope signatures of the core generally fit with the expected values for the nearby Rae Craton, the main sediment source area. The variable radiogenic isotope data in the lower parts of the core (Units 1-3) was likely caused by the retreating ice shelf, while less variable radiogenic isotope values in Unit 4 are likely caused by less iceberg discharge and a more distal ice margin during that time. After ~11.1 ka BP, radiogenic Sr and Nd isotope data decrease and increase, respectively, within Unit 5. According to the age model, which is robust due to the abundance of dating points in Unit 5 (Fig. 5.2), this gradual change occurred between 11.1 and 8.9 ka BP. The interval fits with the rapid retreat of the ice margin into the fjord and the subsequent deglaciation of the Clyde Inlet (Couette et al., 2023). Hence, the gradually decreasing $^{87}\text{Sr}/^{86}\text{Sr}$ and increasing ϵ_{Nd} values likely reflect the increasing distance of the ice margin to the core site

and the decreasing influence of sediment originating from the Clyde Inlet area on the shelf. In addition to the sediment from the nearby land, material transported by ocean currents could be deposited on the shelf during post-glacial periods, leading to mixed radiogenic isotope signals of different source areas.

Couette et al. (2023) argued that the elevated Ca/Ti ratios in the upper part of core 57-3 are probably related to the increased accumulation of detrital carbonates originating from northern Baffin Bay. The Baffin Bay detrital carbonate events (BBDC) are carbonate-rich layers, which can be found in multiple sediment cores from Baffin Bay and which are associated with the iceberg and meltwater discharge from Lancaster Sound through northern Baffin Bay (Aksu & Piper, 1987; Hiscott et al., 1989; Andrews et al., 1998). The timing of the last event, BBDC 0, is around 12.7 to 11 ka BP (Jackson et al., 2017). While the high Ca/Ti ratios in the upper part of the core occurred after ~ 11.1 ka BP (with a maximum at ~ 10.6), which is slightly after the BBDC 0, they are likely related to the final decay of the Lancaster Sound ice stream during the early Holocene, which resulted in the opening of the Barrow Strait and the onset of the Arctic-Atlantic throughflow at between 11 and 10 ka BP (Pieńkowski et al., 2014; Kelleher et al., 2022). In addition, reference isotope signatures from Barrow Strait show significantly higher ϵ_{Nd} values in an area surrounded by detrital carbonates than what we observed in core 57-3. Even though the ϵ_{Nd} values slightly increase after ~ 11 ka BP, they do not show maxima that could be related to distinct peaks of carbonate layers. Thus, they are probably related to an enhanced input of sediment originating from northern Baffin Bay after the deglaciation of the Barrow Strait. Additionally, mineralogical data show an increasing carbonate content from the upper end of Unit 4 and into Unit 5 (Fig. 5.2), suggesting a stronger sediment input from northern Baffin Bay.

5.5.2 Early to late Holocene ice sheet retreat and glacier variability on NE Baffin Island as reflected in sediment data from the Clyde Inlet head (GeoB22346-3)

According to the age model, core 46-3 covers the last ~ 9.5 ka BP (Fig. 5.3) and potentially records the final period of the rapid deglaciation of NE Baffin Island fjords and the breakup of the Barnes Ice Cap during the middle Holocene (Briner et al., 2009b). Based on the deglaciation chronology of the Clyde Inlet by Briner et al. (2007), the ice margin retreated from the outer fjord to the fjord head between ~ 10 ka BP and ~ 7.9 ka BP. This rapid melting occurred during a period of warmer-than-present temperatures, the HTM between ~ 10 to 7 ka BP, as a result of high boreal summer insolation (Fig. 5.5) (Briner et al., 2006; Axford et al., 2009). This warm period was interrupted by periods of pronounced cooling between 9.5 and 8 ka BP (Briner et al., 2006; Axford et al., 2009). In response to these cold events, the ice margin advanced or stopped several times in the fjord, as inferred from multiple moraines deposited between 9.4 and 8.8 ka BP (Briner et al., 2007; Couette et al., 2023). However, CT data of core 46-3 show almost no IRD content, except in the uppermost meter of the core (Fig. 5.3). While low IRD contents could be explained by high sediment accumulation rates from meltwater leading to a dilution of the signal (Olsen et al., 2022; Couette et al., 2023), this could also indicate the absence of marine-based ice in the Clyde

Inlet after ~ 9.5 ka BP, until the late Holocene. A strong lamination and sand layers in Unit 1 rather suggest a strong seasonality and changing meltwater inputs from the shrinking land-terminating glaciers and the Barnes Ice Cap. Turbidite layers in this section indicate sediment delivery by mass wasting as previously identified by Couette et al. (2023) as deposits by turbidity currents or turbid meltwaters. Thus, even though the Clyde Inlet was probably deglaciated at ~9.5 ka BP, short-term ice re-advances into the fjord between ~ 8 and 7 ka BP are also likely. This time interval does not coincide with the known ice advance around the 8.2 cold event (Young et al., 2012). However, the ~200 cm of sediment deposited between 7.1 and 8.7 ka BP might have been affected by sedimentation rate variations, possibly causing some inaccuracies of the age model within this period (Fig. 5.4). Thus, it would be very vague to discuss precise timings of ice margin dynamics during the early to mid-Holocene based on the available data and core chronology.

Decreasing sedimentation rates, less lamination, and higher bioturbation values in Unit 2 (Fig. 5.3) suggest changes in sediment deposition and environmental conditions after ~ 7 ka BP. This roughly agrees with the reported final retreat of the ice stream from the Clyde Inlet at around 7 ka BP (Briner et al., 2007). Less sediment accumulation and related enhanced bioturbation likely reveal the further retreat and more distal ice margin conditions between ~ 7 and 6 ka BP. In Unit 3 between ~ 6 and 2.3 ka BP, the lowest sedimentation rates and enhanced bioturbation (Fig. 5.3) are probably related to decreasing or no meltwater input. MSD, IRD, and XRF data are very uniform during this time interval, suggesting stable environmental conditions. During this time interval, lacustrine sediment data from northeastern Baffin Island (Big Round Lake; Fig. 5.5) were interpreted to reveal a minimum alpine glacier extent on northeastern Baffin Island (Thomas et al., 2010).

Multiple studies report about a re-advance of alpine glaciers on Baffin Island during the late Holocene due to the Neoglacial cooling (Briner et al., 2009b). As some studies indicate that a Neoglaciation already started at some sites on Baffin Island around 6 ka BP (Miller et al., 2005; Briner et al., 2009b), most alpine glaciers on Baffin Island began to expand after ~ 3.5 ka BP and reached their maximum Holocene extent during the Little Ice Age (LIA; ~ 1400 AD to 1900 AD) (Moore et al., 2001; Briner et al., 2009b; Thomas et al., 2010). Thomas et al. (2010) used proglacial lake sediments to observe changes in the alpine glacier extent on northeastern Baffin Island. Similar to one of their lake magnetic susceptibility records, the Ca/Ti data of core 46-3 start to increase and become more variable after ~ 2.2 ka BP (Fig. 5.5). A pronounced increase in IRD concentrations in core 46-3 occurs later at ~ 1.2 ka BP. Therefore, the high-resolution data of core 46-3 potentially reflects glacier re-advance in the Clyde Inlet region starting at ~2.2 ka BP, which becomes more intense after ~ 1.2 ka BP.

5.5.3 Radiogenic Sr, Nd, and Pb isotope composition of GeoB22346-3 – interpretation and challenges

While radiogenic isotopes can usually be used as reliable provenance tracers, there can also be challenges in their interpretation. Indeed, studies showed that Sr isotope variations could result from grain-size effects (Eisenhauer et al., 1999; Tütken et al., 2002). In contrast, ϵ_{Nd} values appeared to be unaffected by particle grain size because Sm-Nd isotopes are potentially not fractionated between different-sized mineral fractions (Tütken et al., 2002; Meyer et al., 2011). Moreover, radiogenic isotope studies on river sediments have shown that changing abundances of specific mineral species caused by mineral sorting processes during sediment transport can control the bulk Sr and Pb isotopic budget of river sediments without influencing the Nd isotope composition (Garçon et al., 2014). The effect of mineral species on the Sr isotope composition of sediments depends on the ability to incorporate rubidium in the mineral structure and the age of the source rocks. In old igneous and metamorphic rocks such minerals are micas and K-feldspars (Faure & Powell, 2012). Thus, the enrichment of micas in the sediment could lead to high $^{87}Sr/^{86}Sr$ values. The $^{206}Pb/^{204}Pb$ isotope composition is mainly influenced by Pb-rich clay minerals and K-feldspar, but also muscovite and plagioclase can affect the isotopic budget (Garçon et al., 2014). Garçon et al. (2014) also showed that extremely radiogenic heavy minerals like zircon, monazite, and allanite have a crucial impact on the $^{206}Pb/^{204}Pb$ isotope composition and are responsible for the highest $^{206}Pb/^{204}Pb$ values. Because micas can also include minerals like zircon, a high amount of micas could potentially lead to higher radiogenic Pb isotope compositions as well. This positive correlation between high mica concentrations and a radiogenic Sr and Pb isotope composition (Garçon et al., 2014) can be observed in the isotope and mineral data of core 46-3 (Fig. 5.3). Especially in Unit 3, where just minor variations in the IRD and Ca/Ti data suggest stable environmental conditions, the highest $^{87}Sr/^{86}Sr$ and $^{206}Pb/^{204}Pb$ values occur parallel to increasing mica concentrations. Changes in the ϵ_{Nd} record occur in parts parallel to the Sr and Pb isotope records but are generally less variable, especially in the middle part of the core. Since many studies have shown that ϵ_{Nd} signatures are a highly reliable tracer for the provenance reconstruction of continental detritus (e.g., Tütken et al., 2002; Garçon et al., 2014) and Sr and Pb isotopic records show in parts a different evolution than the ϵ_{Nd} record, we suggest that Sr and Pb isotope composition in core 46-3 are not only driven by the sediment source signature but are influenced by mineral abundances, mainly changing mica concentrations. It is likely that the variable mineral assemblage at the core 46-3 site is caused by hydrodynamic mineral sorting caused by changing meltwater flux intensities and/or varying transport distances, as has been previously observed in fluvial settings (Garçon et al., 2014). Correlations of radiogenic Sr and Pb isotope composition and meltwater conditions may thus be useful for reconstructing past glacial conditions in the Clyde Inlet region. In contrast, the isotopic and mineralogical composition of core 57-3 from the shelf is less variable, with lower $^{87}Sr/^{86}Sr$ and $^{206}Pb/^{204}Pb$ values. Even if mineralogical changes occur, the mineral composition does not seem to be the controlling factor of the radiogenic Sr and Pb isotope

composition from the Clyde Inlet shelf. In summary, these data potentially provide insights into the mechanisms that drive changes in radiogenic Sr and Pb isotope compositions in marine sediment records, which are close to river or meltwater systems in polar regions. Specifically, they allow the differentiation and identification of changing sediment sources and variations in meltwater fluxes.

With this knowledge, radiogenic isotope data of core 46-3 can be interpreted in terms of sediment provenance but also in terms of changing meltwater intensities and related glacier dynamics/conditions. In general, Sr and Pb isotope records are more variable than the ϵ_{Nd} record (Fig. 5.3). Moreover, the range of values for Sr and Pb isotopes is large, and the values are higher than expected for the surrounding, more or less, uniform geological terrain. In contrast, ϵ_{Nd} values are in a similar range to the data obtained from core 57-3 (Figs. 5.4, 5.5). Overall, the Sr and Pb isotope records show an increasing trend until ~ 5 ka BP, while the Nd isotope signatures stay relatively constant until ~ 3.8 ka BP (Fig. 5.5). Short-term variations in Sr, Pb, and Nd in Unit 1 occur parallel to the turbidite layers, intervals of reworked and sorted sediment, and should therefore be excluded from the interpretation. Mineralogical data reveal overall decreasing SQF and increasing mica concentrations until ~ 3.8 ka BP (Fig. 5.3), showing similar patterns to the Sr and Pb isotope records. These patterns potentially suggest an overall retreat of the ice margin until ~ 3.8 ka BP. Since the most radiogenic Sr and Pb isotope compositions during unit 3 (between 6.2 and 3.8 ka BP) are probably caused by the highest accumulation of clay minerals (mica of clay size or clay mineral smectite) in that interval, they can be associated with either weak meltwater intensities or a long sediment transport during that interval. Decreased meltwater discharge would agree with the minimum glacier extent between 6 and 3 ka BP on Baffin Island (Fig. 5.5; Thomas et al., 2010). Following the radiogenic Sr and Pb isotope compositions during the mid-Holocene, Sr and Pb isotope ratios significantly decrease after ~ 3.8 ka BP, before they slightly increase again towards the core top (Fig. 5.3). Parallel to it, Nd isotope composition slightly increases after 3.8 ka BP and then decrease again in the uppermost core part (Fig. 5.3). Isotope data from the turbidite layer in Unit 4 should be again excluded from the data interpretation. Since all three isotope systems show a shift after 3.8 ka BP, they likely reflect a change in sediment provenance. However, reference isotope signatures from Baffin Island are scarce, and the geology shows, in general, small variation, which makes it challenging to differentiate between the potential sediment sources in the Clyde region. However, we can at least speculate about a variation in the sediment source occurring after the mid-Holocene. This is most likely related to the advance of multiple glaciers around the Clyde Inlet during the late Holocene.

All in all, radiogenic Sr, Nd, and Pb isotope compositions in a glacially-influenced fjord system seem to be strongly affected by glacially-influenced sedimentation processes. In detail, the radiogenic isotope composition can be either controlled by changing sediment sources (Sr, Nd, and Pb), which can differ due to the retreat/advance of the ice margin, or by changing transport processes and energies that affect

the mineralogical composition of the bulk sediment. These relationships allow us to speculate about the timing of ice retreat and advance in the Clyde Inlet area.

5.6 Conclusion

Based on two radiocarbon-dated sediment cores from the head of the Clyde Inlet fjord (GeoB22346-3) and from the cross-shelf trough in front of it (GeoB22357-3), we reconstructed changing sedimentation processes and sediment provenances in the Clyde cross-shelf trough-fjord transect during the last deglaciation. We use CT-derived sedimentological data, radiogenic isotopes (Sr, Nd, and Pb), as well as mineralogical data of the two cores to investigate glacial dynamics and to assess, using the mineralogical assemblages, the different factors that control the radiogenic isotope composition in this fjord system.

- Data from core 57-3 shows a basal till at the bottom of the core, indicating the presence of grounded ice on the Baffin Island shelf during the Younger Dryas. Additionally, the data suggest a transition from ice-proximal to ice-distal conditions at around 11.1 ka BP, when the retreating ice margin reached the outer part of the Clyde Inlet. After this transition, higher carbonate contents and gradually increasing ϵ_{Nd} values likely reflect the stronger influence of along-shore transported sediments originating from northern Baffin Bay after the deglaciation of Lancaster Sound and the opening of the Parry Channel.
- Data from core 46-3 reveal a weakening meltwater discharge associated with a landward retreating ice margin towards the mid-Holocene, when glaciers reached their minimum extent (between ~ 6 and 3.8 ka BP), and a re-advance of alpine glaciers starting at 2.2 ka BP due to Neoglacial cooling.
- Highly variable Sr and Pb isotope data at the fjord head (core 46-3) seem to be strongly controlled by the sediment mineralogy. The variable radiogenic isotope and mineralogical compositions likely reflect changing meltwater fluxes related to fluctuations of the ice margin during the last deglaciation after the ice retreated out of the Clyde Inlet. Similar effects cannot be observed on the shelf where radiogenic isotope compositions are mainly controlled by sediment provenance.

Acknowledgements

We would like to thank the master and crew of the R/V Maria S. Merian for their work during expedition MSM66. Sample material has been provided by the GeoB Core Repository at the MARUM – Center for Marine Environmental Sciences, University of Bremen, Germany. We further gratefully acknowledge Klinikum Bremen-Mitte and Christian Timann and Arne-Jörn Lemke for supporting the CT measurements in their facilities. Additionally, we want to thank Catalina Gebhardt for providing the magnetic susceptibility data of the cores. This project was supported by the Deutsche

Forschungsgemeinschaft (DFG) through the International Research Training Group “Processes and impacts of climate change in the North Atlantic Ocean and the Canadian Arctic” (IRTG 1904 ArcTrain).

Chapter six

6. Shifting sediment depocenters track ice-margin retreat in Baffin Bay

Abstract

Reconstructing the depositional history of Baffin Bay allows insights into the deglacial retreat of the Laurentide, Innuitian, and Greenland ice sheets from their maximum extent during the Last Glacial Maximum (LGM). Here, we present ^{14}C -controlled sedimentation rates from Baffin Bay based on 79 sediment cores to assess spatio-temporal variability in sediment deposition since the LGM. This comprehensive dataset reveals that until ~ 15 ka BP the deep basin and slopes probably were the only active sediment depocenters in Baffin Bay, suggesting prolonged ice-margin stability near the shelf edge, much longer than previous studies suggested. Between 13 to 11 ka BP, most depocenters shifted quickly from the slope to the inner shelf, evidencing a very rapid ice-sheet retreat towards the coast. First sedimentation rate-based mean erosion rates (0.17 and 0.08 mm/yr) derived from the West Greenland Shelf underscore the high erosion capacity of the western Greenland Ice Sheet draining into Baffin Bay.

6.1 Introduction

Baffin Bay, located between Canada and Greenland, was flanked by three large continental ice sheets during the Last Glacial Maximum (LGM; Dyke et al., 2002; Margold et al., 2018; Batchelor et al., 2019; Dalton et al., 2022). The Laurentide (LIS), Innuitian (IIS), and Greenland (GIS) ice sheets advanced across the continental shelves surrounding Baffin Bay, reaching the shelf edge in many places (Fig. 6.1; Li et al., 2011; Brouard & Lajeunesse, 2017; Batchelor et al., 2019; Dalton et al., 2022). In northern Baffin Bay, the LIS and GIS merged with the IIS, forming a continuous ice sheet with an ice shelf (Couette et al., 2022). With the deglacial climate warming, the ice sheets retreated landward from their glacial marine-terminating ice margins to their present-day close-to-minimum extent, mainly being confined to onshore settings (Dyke, 2004; Dalton et al., 2020;).

Ice-sheet dynamics and the associated changes in the rate and pattern of erosion, and also the mode of sediment transport, had a strong control on sediment deposition in Baffin Bay since the last glacial period (Aksu & Piper, 1987; Jenner et al., 2018). However, the reconstruction of the LGM to modern sedimentation in Baffin Bay is limited by the scarcity of directly dated sediment cores due to the paucity of datable material in the sediments (Aksu, 1979, 1983; Andrews et al., 1985; Aksu & Piper, 1987; Andrews, 1987; Jenner et al., 2018). Because recent developments in Accelerator Mass Spectrometry (AMS) dating techniques reduced the amount of material needed for age determinations (Mollenhauer

et al., 2021), data availability is increasing rapidly (Saini et al., 2022; Okuma et al., 2023; Weiser et al., 2023).

Taking advantage of this, our study presents a new spatio-temporal analysis of radiocarbon-based sedimentation rate patterns across Baffin Bay since the LGM, based on an extensive collection of both previously published ($n = 68$) and new radiocarbon-dated sediment cores ($n = 11$). Besides documenting the successive activation of various depocenters, it provides detailed information on the pattern of ice margin retreat and new sedimentation rate-based estimates of subglacial erosion rates (for the GIS).

6.2 Sedimentation in Baffin Bay over the last 25,000 years

Baffin Bay is a >2000 m deep semi-enclosed oceanic basin between the Canadian Arctic Archipelago (CAA) and Greenland, connecting the Arctic Ocean to the North Atlantic Ocean (Fig. 6.1). Its continental shelves (up to 500 m deep) are largely dissected by U-shaped over-deepened cross-shelf troughs (up to 100 km wide and 950 m deep, Fig. 6.1), that were carved by fast-flowing ice streams associated with the repeated advance of the LIS, IIS, and GIS during previous glaciations (Praeg et al., 2007; Batchelor & Dowdeswell, 2014; Dalton et al., 2020, 2022). During full-glacial conditions, the advance of these paleo-ice streams through the cross-shelf troughs enabled the delivery of large volumes of eroded terrigenous and shelf material beyond the trough mouth, forming huge sediment aprons on the adjacent continental slopes, termed trough mouth fans (TMFs; Weidick & Bennike, 2007; Li et al., 2011; Ó Cofaigh et al., 2013a; Dowdeswell et al., 2014; Hofmann et al., 2016).

The new compilation of 79 ^{14}C -dated sediment cores from Baffin Bay (Fig. 6.1c and Appendix Table 9.3.1) comprises primarily previously published data, complemented by eleven new cores. Only cores with a minimum of two ^{14}C ages, all based on marine micro- and macro-fossil remains, were included in this compilation (See Methods and Appendix Table 9.3.2). Sedimentation rate (SR) in the majority (86 %) of cores in this compilation is constrained by at least three ^{14}C dates, with an overall range of two – twenty-six ^{14}C dates per core. Regionally, the 79 sediment cores are interpreted to represent six individual depocenters (Fig. 6.1c and Appendix Table 9.3.1): (1) the deep basin (7 cores), which largely comprises water depths >1500 m, termed as Central Baffin Bay (CBB); (2) the slope (15 cores) covering the water depth interval until the shelf break (~500 m), referred here as Baffin Bay Slope (BBS); (3) the Outer West Greenland Shelf (WGS) (3 cores); (4) the Mid WGS and Baffin Island Shelf (BIS) (8 cores); (5) the WGS and BIS Inner Shelves (30 cores, incl. 4 fjord sites); and (6) the Northern Baffin Bay (NBB) (16 cores), which is treated here as a separate depocenter due to its location beneath the confluence of the LIS, IIS, and GIS.

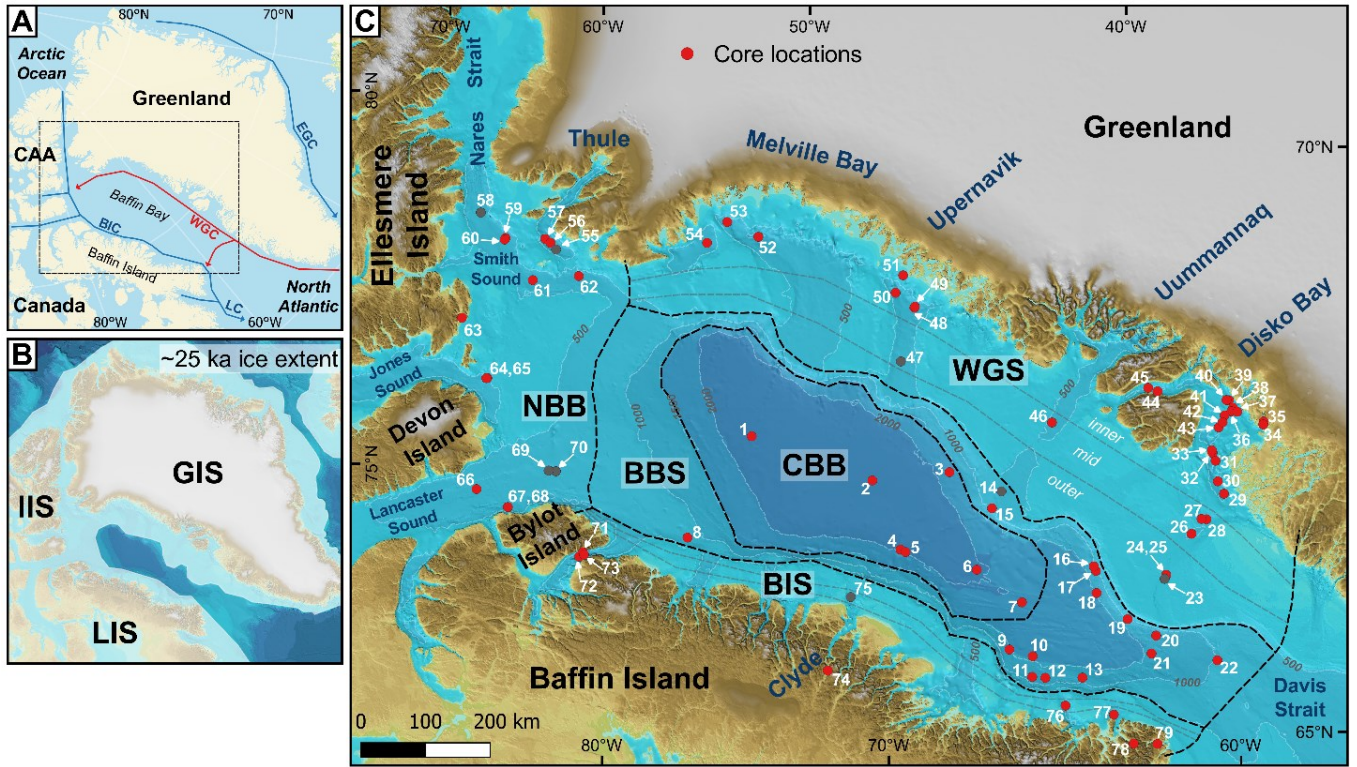


Figure 6.1: Overview maps showing the geographic location of Baffin Bay, its main oceanographic currents and glacial history, and core locations. (A) Baffin Bay is bordered to the north by the Canadian Arctic Archipelago (CAA), Baffin Island to the west, and Greenland to the east. The Baffin Island Current (BIC) transports colder and fresher waters originating from the Arctic Ocean southwards through Davis Strait, merging with the Labrador Current (LC) flowing into the North Atlantic Ocean. The West Greenland Current (WGC), an admixture of the Arctic-sourced East Greenland Current (EGC) and Atlantic-sourced Irminger Current, carries warmer and more saline waters into Baffin Bay along the west Greenland coast. (B) Reconstructed maximum extent of the Laurentide (LIS), Innuitian (IIS), and Greenland (GIS) ice sheets during the LGM (~25 ka; Batchelor et al., 2019; Dalton et al., 2022). (C) The location of the 79 radiocarbon-dated sediment cores (filled circles) compiled in this study (grey circles indicate cores with basal till, and red circles without) distributed into six depocenters (differentiated by black and grey dashed lines): (i) Central Baffin Bay (CBB), (ii) Baffin Bay Slope (BBS), (iii) Outer, (iv) Mid, (v) Inner Baffin Island Shelf (BIS) and West Greenland Shelf (WGS), and (vi) Northern Baffin Bay (NBB). The locations of cross-shelf troughs on the WGS (e.g., Melville Bay, Upernavik, Uummannaq, Disko Bay) are indicated. Bathymetric information in (B) and (C) is based on the International Bathymetric Chart of the Arctic Ocean Version 3.0 (Jakobsson et al., 2012).

The age-depth relationships for these 79 cores were constructed using the rapid Bayesian approach provided by the open-source software UNDATABLE in MATLAB (Lougheed & Obrochta, 2019). All ^{14}C dates were re-calibrated applying the Marine20 calibration curve (Heaton et al., 2020) and region-specific marine reservoir age corrections (Appendix Table 9.3.2). The resulting SRs were then binned into 1 ka time-slices (Fig. S6.1 and Appendix Table 9.3.3) and combined in a boxplot for all cores in

each depocenter (Fig. 6.2). In addition, mean SRs were calculated for each sediment core for the four time-intervals considered here (Fig. 6.3).

As only a few of the 79 sediment cores from the shelves penetrated the deglacial sediments and reached underlying tills (marked as grey circles in Fig. 6.1c; see Methods and Fig. S6.2), we note that the oldest ages retrieved from the cores only present minimum ages of the onset of sedimentation following ice retreat. Cores that did recover tills beneath dated sediments are of exceptional importance, as they permit temporal constraints of ice retreat and the onset of marine sedimentation at the respective site.

From the LGM to ~15 ka BP, sedimentation is only recorded in cores from the CBB and BBS (Fig. 6.2 and Fig. S6.1). During the LGM (~25 to ~18 ka BP), the binned median SRs were generally low in the CBB, averaging slightly below 10 cm ka⁻¹. In contrast, the BBS cores show higher rates of ~20 cm ka⁻¹ (Fig. 6.2). While rates mainly remained low in the CBB (~10 cm ka⁻¹) during the early deglaciation (~18 to ~12 ka BP), the BBS sites reveal faster accumulation between 30 and 50 cm ka⁻¹ (Fig. 6.2). The following late deglaciation (~12 to ~6 ka BP) is marked by a sharp decrease in the binned median SRs to <5 cm ka⁻¹ and ~10 cm ka⁻¹ in the CBB and BBS sites (Fig. 6.2), respectively, that remained rather constant through the following postglacial period (<6 ka BP).

The oldest outer shelf record from the WGS has a mean SR of ~200 cm ka⁻¹ and dates back to the end (12-13 ka BP) of the early deglaciation (Fig. 6.2 and Fig. S6.1). During the late deglaciation, binned median SRs in the outer shelf region drastically declined to ~10 cm ka⁻¹ to remain at this level throughout the postglacial. The earliest documented mid- and inner-shelf sedimentation on the BIS and WGS is documented for the late deglaciation (Fig. 6.2 and Fig. S6.1). On the mid-shelf, binned median SRs decreased from ~80 cm ka⁻¹ to a rather constant ~15 cm ka⁻¹ after ~8 ka BP. The inner-shelf binned median SRs revealed a similar decreasing trend through the late deglaciation, however, on a much higher level, decreasing from ~300 cm ka⁻¹ to ~80 cm ka⁻¹ (Fig. 6.2 and Fig. S6.1). Comparably high binned median SRs of ~50 cm ka⁻¹ also persisted throughout the postglacial.

In the NBB, sedimentation is documented since the early deglaciation interval at ~14.5 ka BP, much earlier than the shelf records from BIS and WGS (Fig. 6.2 and Fig. S6.1). Binned median SRs of ~40-70 cm ka⁻¹ lasted until about 10 ka BP when during the late deglaciation, the rates decreased to ~30-50 cm ka⁻¹, eventually becoming rather stable around 35 cm ka⁻¹ during the postglacial.

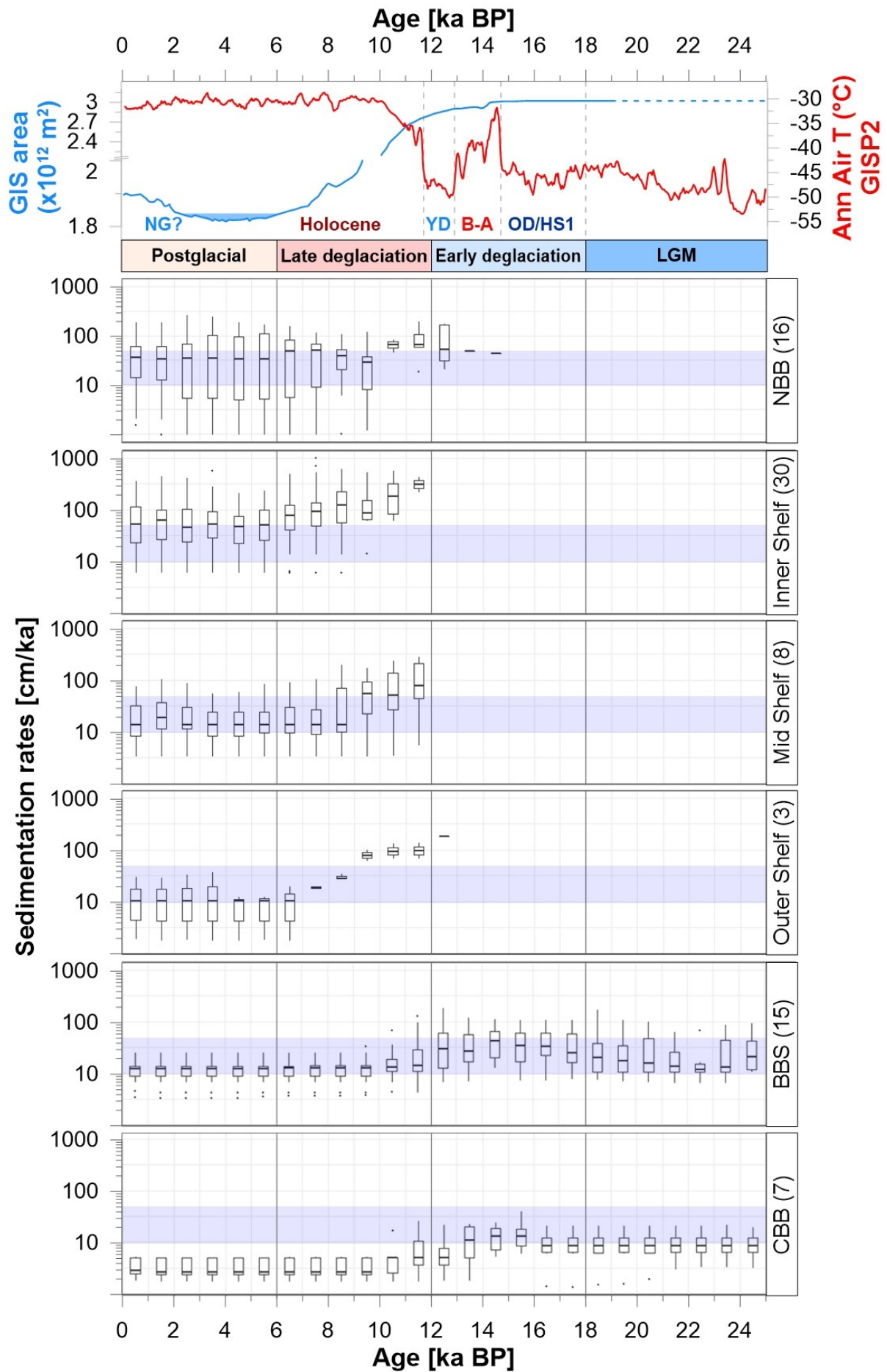


Figure 6.2: Binned sedimentation rates (1 kyr slices) derived from all sediment cores within a specific depocenter in Baffin Bay (below) compared with (top) model and proxy reconstructions of Greenland Ice Sheet (GIS) areal extent and air temperature evolution since the Last Glacial Maximum (LGM). Bottom: sedimentation rates are separated into the 6 depocenters delineated in Baffin Bay: (i) Central Baffin Bay (CBB), (ii) Baffin Bay Slope (BBS), (iii) Outer Shelf, (iv) Mid Shelf, (v) Inner Shelf, and (vi) Northern Baffin Bay (NBB). The number of cores in each depocenter is given in brackets. The light blue bars mark sedimentation rates interval of 10 to 50 cm/ka. Top: the LGM, early deglaciation, late deglaciation, and postglacial intervals are determined based on observed changes in GIS areal extent (Lecavalier et al., 2014) and annual air temperature from the GISP2 ice core record (Alley, 2000).

6.3 Discussion

Spatial sedimentation patterns in Baffin Bay have varied substantially (Figs. 6.2 and 6.3) since the LGM, when continental ice (LIS, IIS, & GIS) expanded onto the shelves of Baffin Bay (Fig. 6.1). When the continental ice sheets advanced to or near the shelf breaks during the LGM (Batchelor et al., 2019; Dalton et al., 2020, 2022), the CBB and BBS probably were the only accommodation space available as documented by the available sediment cores; therefore, they were most likely the only active depocenters in Baffin Bay (Figs. 6.2 and 6.3a). However, sedimentation rates of $<20 \text{ cm ka}^{-1}$ suggest low terrigenous sediment input into CBB (Figs. 6.2 and 6.3). The partly low amounts of ice-rafted detritus (IRD) in the deep basin records (Simon et al., 2014; Ownsworth et al., 2023) point to reduced iceberg rafting and imply sedimentation mainly from turbid meltwater plumes (Aksu & Piper, 1987; Ownsworth et al., 2023), which would be consistent with a perennial ice-covered (sea ice and ice-shelf) Baffin Bay during the LGM (Jennings et al., 2017; Couette et al., 2022). At the same time, the BBS received more sediment, particularly in the southeastern Baffin Bay off West Greenland (up to 10-fold more, Fig. 6.3a). There, common glacial debris flows (GDFs) and turbidity currents provided the TMFs with high amounts of sediment released from ice streams grounded at the mouths of cross-shelf troughs (Li et al., 2011; Jenner et al., 2018), accompanied by sediments delivered by turbid meltwater plumes (Ó Cofaigh et al., 2013b; Jennings et al., 2017).

The higher binned median SRs in the BBS records observed for the early deglaciation (Fig. 6.2) indicate faster-accumulating sediments during initial ice sheet recession (Fig. 6.3). These higher rates reflect the influence of IRD, GDFs, and meltwater-induced deposition (Ó Cofaigh et al., 2013b; Jennings et al., 2017). In contrast, SRs in the more distal CBB only show a slight increase between 13 and 16 ka BP (Fig. 6.2). During the LGM and the early deglaciation, the fastest deposition occurred at the Disko TMF in southern Baffin Bay (Fig. 6.3a,b), suggesting that the feeding glacier, Jakobshavn Isbrae, was most efficient in delivering sediments. This result aligns with present-day observations that indicate that this ice stream is by far the fastest-moving glacier of Greenland (Lemos et al., 2018).

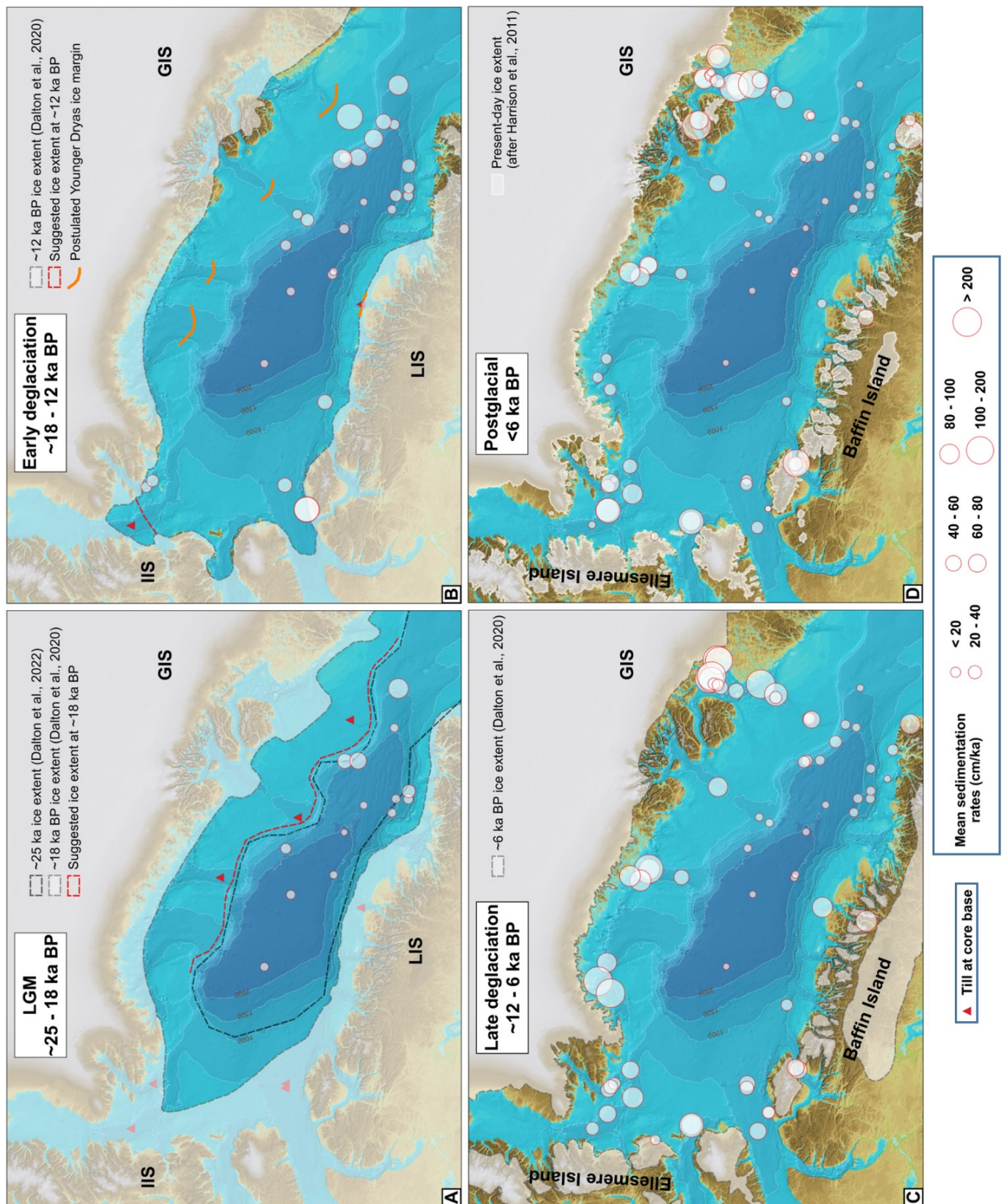


Figure 6.3: Spatio-temporal distribution of mean sedimentation rates for all individual sediment cores in Baffin Bay for the four time intervals (A-D) considered here and contemporary ice-margin reconstructions (Dalton et al., 2020, 2022). The red dashed lines highlight new ice margin positions for ~18 (in A) and ~12 ka BP (in B), respectively, as suggested in this study. The postulated Younger Dryas ice margin (orange lines in B) is based on

observed grounding zone wedges (GZWs) on the mid-shelf interpreted as periods of ice stillstand or short-term readvances (Ó Cofaigh et al., 2013b; Dowdeswell et al., 2014; Hogan et al., 2016; Sheldon et al., 2016; Slabon et al., 2016; Weiser et al., 2023).

The exclusivity of sedimentation in the CBB and BBS from the LGM to ~15 ka BP (Fig. 6.2) suggests prolonged ice sheet stability on the Baffin Bay shelves, most likely extending to near the shelf edges, at least within the cross-shelf troughs. This observation is consistent with empirical and model reconstructions of the GIS margin denoting close to the full-glacial maximum areal extent during this interval (Lecavalier et al., 2014; Leger et al., 2023). However, local changes in sedimentation style at the slope might indicate an initial small-scale retreat from the very shelf edge off West Greenland, possibly occurring as early as 17 ka BP (Jennings et al., 2017). Oldest marine sediments overlying a subglacial till were deposited on the upper slope at ~14.8 ka BP (Ó Cofaigh et al., 2013b), followed by outer shelf sedimentation around 13 ka BP (Fig. 6.2). In the NBB, the oldest sediments on till date back to ~14.5-15.3 ka BP (Kelleher et al., 2022; Okuma et al., 2023), coeval with the collapse of the up to 500 m thick ice shelf covering northern Baffin Bay (Couette et al., 2022). Ice sheet destabilization and the retreat from the shelf edges thus occurred during the relatively warm Bølling-Allerød interstadial (Naughton et al., 2023) and was probably forced by rising northern latitude summer insolation (Berger & Loutre, 1991; Laskar et al., 2004) and the strengthened advection of warmer waters into Baffin Bay triggered by the reinvigorated meridional heat transported by the Atlantic Meridional Overturning Circulation (AMOC; Ritz et al., 2013; Sheldon et al., 2016; Jennings et al., 2017). These data from West Greenland directly conflict with a proposed ice margin position close to the west Greenland coast at 18 ka BP (Dalton et al., 2020). The presence of tills and the absence of early-deglaciation sediments on the shelf rather suggest that at 18 ka BP the ice still extended to near the edge of the shelf (Fig. 6.3a).

At the end of the early deglaciation (13 to 11 ka BP), the main depocenters shifted very quickly from the BBS to the inner shelf (Fig. 6.2). Indeed, within less than 2 kyr, marine sedimentation progressed from the outer to the inner shelf (corresponding to 200 to 300 km on the WGS), indicating an extremely rapid retreat of the ice sheets from the shelf edge towards the coast (see Leger et al., 2023). This fast retreat of the LIS, IIS, and GIS was characterized by massive calving of icebergs leading to enhanced deposition of iceberg-rafted detritus in Baffin Bay, including the widely documented Baffin Bay Detrital Carbonate Layer 0 (Jackson et al., 2017, 2023; Couette et al., 2022).

Within the cross-shelf troughs, the retreating ice sheets opened new accommodation spaces and, therefore, facilitated shelf deposition that eventually caused sediment starvation in the CBB and BBS depocenters, beginning with the late deglaciation (Fig. 6.2), resulting in low binned median SRs for CBB (<5 cm ka⁻¹) and BBS (~10 cm ka⁻¹). During the Younger Dryas (YD; Rasmussen et al., 2014), ice sheet retreat was halted (or even reversed) as indicated by grounding zone wedges (GZWs) on the Baffin Island and West Greenland shelves (Dowdeswell et al., 2014; Hogan et al., 2016; Newton et al., 2017; Sheldon et al., 2016; Slabon et al., 2016; Couette et al., 2023; Weiser et al., 2023). During this YD mid-

shelf stillstand, SRs were highest at the outer shelf (Figs. 6.2 and 6.3b). Inner shelf deposition is only documented after the YD cold spell at ~11.5 ka BP (Fig. 6.2). Although no direct evidence exists, the west Greenland mid-shelf GZWs and the proposed later onset of inner-shelf sedimentation do not only challenge the 18 ka BP but also the 12 ka BP ice margin positions according to Dalton et al. (2020) (Fig. 6.3b,c). Thus, west Greenland shelf deglaciation probably occurred ~6 kyr later than previously suggested.

All shelf sections show initially very high SRs that continuously decreased until ~6 ka BP, with the dominant depocenter (i.e., fastest deposition) on the inner shelves (Fig. 6.2). The high SRs there are facilitated by the huge accommodation space provided by the over-deepened inner shelf troughs (Slabon et al., 2016), located most proximal to the remaining ice masses. The same pattern of decreasing sedimentation rates during this period is also observed in the NBB (Fig. 6.2; Kelleher et al., 2022; Okuma et al., 2023). As a consequence of the shelf deglaciation, sedimentation in Baffin Bay was dominated by hemipelagic sediments over the last 10-8 kyr, with only minor contributions from ice-rafted detritus until the beginning of Neoglacial (Couette et al., 2023; Okuma et al., 2023; Weiser et al., 2023).

During the subsequent postglacial period (<6 ka BP), sedimentation on the shelves leveled off in all areas (Fig. 6.2). At this time, the LIS and IIS had entirely disintegrated into smaller ice caps over Baffin Island and the CAA, whereas the GIS attained its Holocene minimum areal extent around this time (Lecavalier et al., 2014; Dalton et al., 2020; Leger et al., 2023). Thus, comparably low binned median SRs after ~6 ka BP were most likely triggered by reduced sediment input from land to the Baffin Bay shelves, probably due to decreasing sub-ice sheet erosion rates in the postglacial period. Still, the highest SRs (>50 cm ka⁻¹) occurred at the most ice proximal sites on the inner shelves (Figs. 6.2 and 6.3d). During the last ~3 ka BP, slightly enhanced binned median SRs are observed on the inner- and mid-shelves (Fig. 6.2), probably related to enhanced sediment input caused by Neoglacial re-advance of local glaciers as indicated by renewed IRD sedimentation (Caron et al., 2020; Couette et al., 2023; Okuma et al., 2023; Weiser et al., 2023).

Taking advantage of the very good database for the WGS (32 cores; Fig. 6.1c), we use this comprehensive overview of sedimentation rates to reconstruct erosion rates of the part of GIS draining into Baffin Bay for the late deglaciation (late deglacial) and postglacial periods. Based on the overall mean SR for all cores for these intervals from the four major cross-shelf troughs (Figs. 6.1c, 6.3), we calculated mean sediment accumulation rates for each trough (see Methods). Using the areal extents of the individual troughs and their paleo-ice stream drainages (Batchelor & Dowdeswell, 2014), estimated sediment mass fluxes were converted to approximate subglacial erosion rates (Appendix Table 9.3.4 and also see Andrews et al., 1994; Hogan et al., 2020).

Based on measured sediment accumulation rates, our estimated late deglacial (12-6 ka BP) bedrock erosion rates for West Greenland range from 0.08 mm yr⁻¹ (Uummannaq Trough) to 0.36 mm yr⁻¹ (Melville Bay), whereas postglacial rates range from 0.04 to 0.06 mm yr⁻¹, except for Disko Trough with 0.12 mm yr⁻¹ (Appendix Table 9.3.4). Although at the lower end, these results largely agree with estimates resulting from geophysical assessments of deglacial sediment volumes in Greenland shelf troughs (0.29-0.52 mm yr⁻¹, these are high estimates due to smaller effective drainage areas considered (Hogan et al., 2020)), from cosmogenic nuclide (¹⁰Be) analyses for centennial- (0.3-0.8 mm yr⁻¹) and orbital-scale (0.1-0.3 mm yr⁻¹) erosion rates (Young et al., 2016; Balter-Kennedy et al., 2021), and from a 10-year sediment load analysis in a southwest Greenland river (0.5 mm yr⁻¹; Hasholt et al., 2018). The consistency of these estimates based on various methods underlines the high erosion capacity of the GIS, as average subglacial erosion rates of 0.01-0.1 mm yr⁻¹ have been given for polar regions (Koppes et al., 2015).

Mean erosion rates derived from all four West Greenland shelf troughs decrease from 0.17 mm yr⁻¹ for the late deglacial to 0.08 mm yr⁻¹ for the postglacial, reflecting a roughly 55% reduction in subglacial erosion of West Greenland, a trend also observed off Petermann glacier entering Nares Strait (Hogan et al., 2020). This trend towards decreasing erosion rates probably reflects the transition from active deglacial (ice) retreat to relatively stable postglacial conditions.

6.4 Methods

6.4.1 Age calibration and sedimentation rates

All ¹⁴C dates from each core were re-calibrated individually within the age-depth modeling process of UNDATABLE (Lougheed & Obrochta, 2019; settings: nsim = 10⁵, bootpc = 30, xfactor = 0.1). For the age calibration, region-specific marine reservoir age correction (ΔR) values (Pieńkowski et al., 2022) were applied to Holocene and deglacial ¹⁴C ages (< 15,000 years) and a higher ΔR value (250 ± 100 years; Jackson et al., 2023) for ¹⁴C ages > 15,000 years from CBB and BBS (see Appendix Table 9.3.2). As the ¹⁴C ages obtained from bulk sediment organic matter and *Portlandia arctica*, due to the “Portlandia Effect,” often yield significantly older ages compared to other marine fossils (see Andrews et al., 1985; Coulthard, 2012; Giraudeau et al., 2020; Jackson et al., 2021; Pieńkowski et al., 2022), they were excluded from the age model constructions. In addition, the top of each core is assumed to be of recent age (i.e., 0 ka BP ± 50 years, with recent defined as the year 1950 AD), and the topmost (youngest) date for each core was excluded from the bootpc (bootstrapping process) to force the algorithm to include this date in the construction of the age-depth relationship. Note that the here presented SRs for the Baffin Bay cores were not corrected for any mass-transport deposits (MTDs) as these are usually only documented for those few cores analyzed by computer tomography (Okuma et al., 2023; Weiser et al., 2023; but see also Jenner et al., 2018), while for nearby cores with a similar stratigraphy such MTDs are

not documented (Caron et al., 2020; Giraudeau et al., 2020; Kelleher et al., 2022). Thus, to treat all records the same way, even the few documented cases (Jenner et al., 2018; Okuma et al., 2023; Weiser et al., 2023) have not been considered. As datings reveal that the sediment in such MTDs is of rather similar age as in the overlying deposits (Okuma et al., 2023), these MTDs are also considered to represent time-related sediment input associated with the retreat of ice sheets.

Besides computing the age-depth relationship, UNDATABLE calculates each sediment core's median SRs (in cm/ka). We binned these rates into one kiloyear time slices and wrote the mean values to the central position of each slice. The binned SRs are presented in logarithmic scale (\log_{10}) in Figure 6.2 to emphasize variability in areas (cores) with largely varying values. Alternatively, step-plots of the binned SRs for all cores are displayed in Supplementary Figure 6.1.

6.4.2 Cores with basal till

Sediment cores that have been interpreted to contain basal till deposits, indicative of paleo-ice extent on Baffin Bay, are indicated (grey-filled circles) in Figure 6.1c, including gravity core GeoB22357-3 from the Clyde Trough. The thick diamicton bed (LF2) identified at the bottom of core GeoB22357-3 was previously interpreted as GDFs (Couette et al., 2023). In light of the newly acquired computed tomographic data (see Okuma et al., 2023) revealing a rather massive and over-compacted basal diamicton and the absence of any internal structures consistent with GDFs (Fig. S6.2), this basal unit is re-interpreted here as ice-contact sediments. This presence of subglacial till, together with the presented ^{14}C dates, further substantiates evidence that the mid-shelf area of the Clyde shelf trough was glaciated (stillstand or LIS re-advance) by the Clyde Ice Stream during the YD stadial, as postulated by Couette et al. (2023).

6.4.3 Estimating subglacial erosion rates

Based on the available late deglacial and postglacial sedimentation rates, assuming an average dry bulk density of 0.8 g cm^{-3} for Greenland fjord and shelf sediments (Andrews et al., 1994) and considering the area covered by the four WGS troughs (Melville, Uummannaq, Upernavik, and Disko) (Batchelor & Dowdeswell, 2014), we calculated the total mass accumulation for these four troughs for the two time slices considered here (Appendix Table 9.3.4). As biogenic contributions (total organic carbon and biogenic carbonate) to the sediment accumulation are usually $<5\%$ (Perner et al., 2013; Limoges et al., 2020; Saini et al., 2022), these have been neglected. In a second step, the resulting mass accumulations were applied to the respective drainage areas (Batchelor & Dowdeswell, 2014) to calculate average denudation/erosion rates, thereby considering a density for the predominantly crystalline rocks of 2.7 g cm^{-3} (Andrews et al., 1994; Hogan et al., 2020). Mean erosion rates for West Greenland have been calculated by averaging the erosion rates of the individual drainage areas of the respective shelf troughs, thereby considering the size of the respective drainage basins.

Of course, there are several limitations to this approach: (1) the limited SR-data coverage for the various troughs on the WGS, as, for example, considering only proximal inner shelf records (e.g., Melville Bay) will lead to an overestimation of the sediment mass accumulation in a trough (and vice versa), (2) the late deglacial rates have to be considered as minimum estimates as most sediment cores considered here did not penetrate the entire deglacial sediment column, thus missing the fast accumulating ice proximal sediments deposited directly after the local deglaciation, and (3) neither sediment bypassing of the troughs, e.g., via iceberg rafting, nor input from the Canadian side is considered. Nevertheless, the consistency of the data from the various investigated cross-shelf troughs, as well as the alignment with estimates based on other methods, underlines the applicability of this approach (see Andrews et al., 1994).

Acknowledgments

We thank the masters and crew members of the various cruises who recovered the Baffin Bay sediment cores used in this study and those involved in the work to obtain radiocarbon ages. Sample materials have been provided by the GeoB Core Repository at the MARUM – Center for Marine Environmental Sciences, University of Bremen, Germany. We also thank Dr. Martin Bartels for sample preparation for radiocarbon dating and Dr. Lucas Jonkers and Dr. Michael Siccha for their support during the data analysis phase of this manuscript. This project was supported by the Deutsche Forschungsgemeinschaft (Bonn, Germany) through the International Research Training Group “Processes and impacts of climate change in the North Atlantic Ocean and the Canadian Arctic” (IRTG 1904 ArcTrain).

Supplementary figures

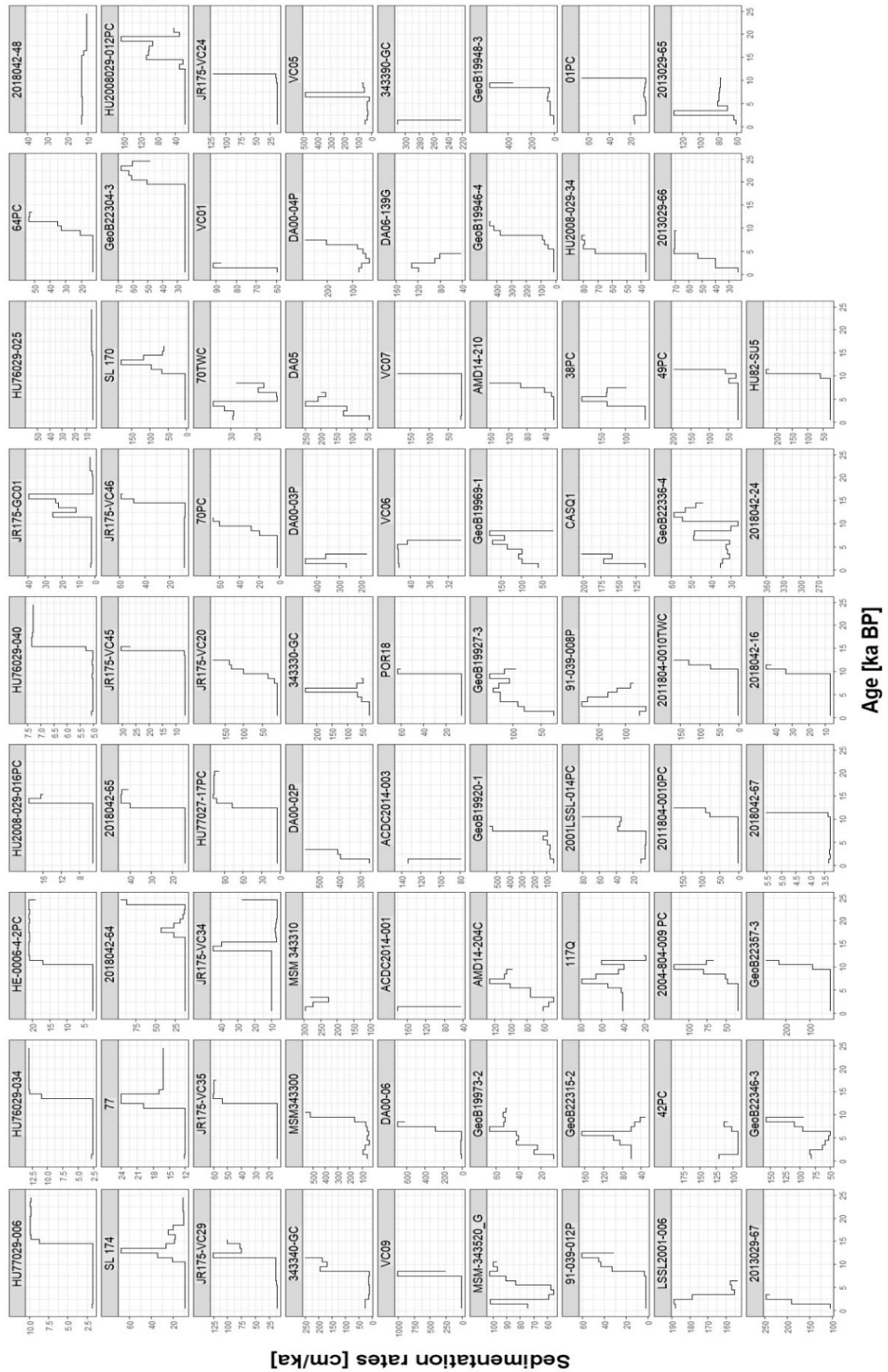


Figure S6.1: Step-plots of binned sedimentation rates for individual cores from Baffin Bay. The ^{14}C datings on core 2018042-24 (#78) only cover the last kilo year. Note that rates are truncated at 25 ka BP and are plotted in different Y-axis scales.

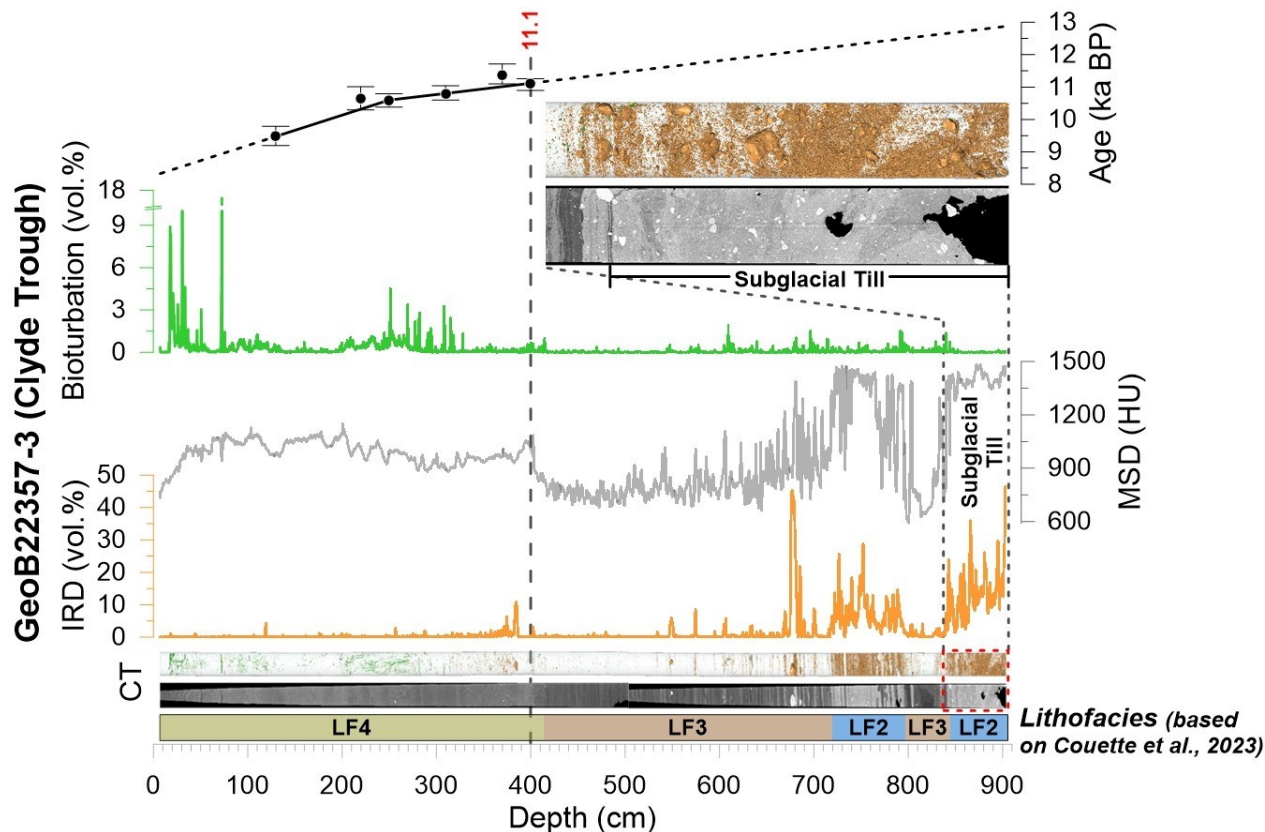


Figure S6.2: Processed computed tomographic (CT) data and calibrated ^{14}C ages (and 95% probability interval) for core GeoB22357-3 from the Clyde Trough in Baffin Bay shown against previously published lithofacies subdivision. The massive and over-compacted basal interval (LF2; denoted by the red dashed lines and enlarged at the top), previously interpreted as glaciogenic debris flows (GDFs) deposit (Couette et al., 2023), is re-interpreted here as subglacial till. Line plots and colors on interpreted CT image: iceberg-rafted debris (IRD; clasts > 1 mm) = brown; bioturbation = green; mean matrix sediment density (MSD) = light-grey.

Chapter seven

7. Conclusions and Outlook

7.1 Conclusions

The scientific objectives of this study (Chapter 1.5) were to reconstruct the deglacial to Holocene sediment and ice margin dynamics in (i) northern Baffin Bay, (ii) western Baffin Bay, and (iii) to decipher the overall changes in sedimentation pattern in Baffin Bay since the LGM. Since many of the paleoenvironmental studies done in Baffin Bay are concentrated on the West Greenland side, the understanding of sedimentation processes, ice-sheet dynamics, and paleoenvironmental conditions in northern Baffin Bay and the Baffin Island side remains comparably insufficient. This thesis filled this knowledge gap through the analyses and interpretation of acquired multiproxy-data (sedimentological, mineralogical, and radiogenic isotope composition) from sediment cores recovered from northern Baffin Bay (GeoB22336-4) and western Baffin Bay (GeoB22346-3 and GeoB22357-3, off northeastern Baffin Island), constrained by robust radiocarbon-dated chronology, with the findings and implications detailed in the first (Chapter 4) and second (Chapter 5) manuscripts, respectively. Overall, combining the knowledge gained and radiocarbon ages from the first and second manuscripts, together with unpublished and published records, we improved the current state of knowledge and understanding of the paleo-depositional history of Baffin Bay since maximum ice-sheet advance during the LGM (in Chapter 6).

In northern Baffin Bay, the first manuscript refined the tentative timing of the Lancaster Sound Ice Stream retreat. It reconstructed the ensuing deglacial and Holocene sediment dynamics and provenances related to changing ice-sheet extent and oceanographic conditions. Sedimentological data (till deposit) and radiocarbon chronology suggest the presence of a grounded ice stream beyond the mouth of Lancaster Sound, in the deep trough of northern Baffin Bay, and lift-off occurred at ~14.5 ka BP during the Bølling-Allerød warming, contrary to previous studies based on sediments lacking sound chronological control. Deglacial to early-Holocene shift in paleoenvironment from ice-proximal to ice-distal conditions between 14.5 and 10.3 ka BP likely marks the overall retreat of ice sheets from marine-terminating to land-terminating positions around northern Baffin Bay. Results documented changes in sediment routing associated with the opening of Lancaster Sound between ~10.4 and 9.9 ka BP and Nares Strait at ~8.5 ka BP, which led to the establishment of Arctic-Atlantic throughflow during an interval of strengthened inflow of relatively warmer WGC to the region. Reduced meltwater input during the mid-Holocene period, due to the largely retreated surrounding ice margins, allowed stronger WGC influence on sea-surface conditions in northern Baffin Bay, triggering intense sea-ice melt and release

of entrained sediment. Late-Holocene sediments with a pronounced increase in IRD content in the last ~2 ka BP provide evidence for Neoglacial cooling.

On the back of overall deglacial ice sheets retreat from Baffin Bay, multiproxy data from two sediment cores from the Clyde Trough (on western Baffin Bay) and adjacent Clyde Inlet (off northeastern Baffin Island) provided new insights into deglacial and Holocene variability of the LIS in our second study. Also, sedimentological data (till deposit) and radiocarbon ages in the core from the trough give credence to the previously postulated Clyde Ice Stream (draining the LIS) mid-shelf stillstand or re-advance during the Younger Dryas cooling. After this time, highly variable lithofacies, mineralogical, and radiogenic isotope compositions in the early-Holocene glaciomarine deposits indicate the progressive ice stream retreat (landward) from the trough site and probably reached the (fjord) mouth of the Clyde Inlet at ~11 ka BP, after which radiogenic isotope and mineralogical data suggest enhanced signal of sediments sourced from northern Baffin Bay. Complete deglaciation of the Clyde Inlet and LIS retreat to the fjord head likely happened before 9.5 ka BP during the early-Holocene warming characterized by high boreal summer insolation. There, rapidly accumulated laminated mud (bioturbation-free and rare IRD) with intercalated thin-to-thick sandy turbidites prevailed until ~6 ka BP and may have resulted from intense meltwater discharge from land-based ice. Subsequently, the relatively slow accumulation of predominately bioturbated mud during the mid-late Holocene points to reduced meltwater input as surrounding glaciers attained their minimum extent, but a re-advance, as documented by a pronounced increase in IRD supply, also occurred in the last ~2 ka BP as part of Neoglacial cooling of the region.

Based on a unique compilation of ^{14}C -derived sedimentation rates from 79 sediment cores from all over Baffin Bay, the third manuscript generally addressed spatio-temporal variability in sediment deposition in Baffin Bay, which appears to be closely linked to ice-margin dynamics since the LGM. Results of this compilation suggest that in Baffin Bay from the LGM until ~15 ka BP, the deep basin and slope were the only active sediment depocenters, pointing to a more prolonged presence of glacial ice near the shelf break than suggested by previous studies. Afterwards, sediment depocenters progressively shifted landward from the deeper to inner shelf settings following deglacial ice-margin retreat, which likely became predominantly coast-bound between 12-11 ka BP. Since the early-Holocene shelf deglaciation, most sediments delivered to Baffin Bay are deposited in the proximal inner shelf. In addition, an excellent database from the West Greenland Shelf provides the first sedimentation rate-based subglacial erosion rates for the West Greenland Ice Sheet, underlining its very efficient erosion.

Taken altogether, these studies (Chapters 4 – 6) show that the sediment dynamics (sediment input rates, transport, deposition, and provenance) in Baffin Bay were predominantly controlled by past ice sheet dynamics, which in turn were mainly influenced by variations in atmospheric and oceanic temperatures. This research highlights the role of atmosphere-ocean-ice interactions in shaping the depositional regimes off glaciated margins in polar environments. These data and the conclusions derived from this study will serve as a benchmark for future work addressing the deglacial development of Baffin Bay and

its adjacent coasts and – most likely – other high-latitude glaciated margins. Furthermore, it provides critical knowledge for numerical model-based paleo-ice sheet reconstructions and simulations of ice sheets' response to present and future global climate change.

7.2 Outlook

Despite the contributions of this study to the understanding of sedimentological processes (transport and deposition) on the western side of Baffin Bay and providing new insights into past sediment routing, ice-sheet dynamics, and environmental conditions, there remain potentially more avenues for further research in the future as this region is still relatively understudied compared to the eastern side. As evidenced by the compilation of (^{14}C) chronological data in Chapter 6, the relatively few ^{14}C ages obtained in sediments from the Baffin Island shelf inhibited the calculation of subglacial erosion rates for this branch of the LIS, which would have allowed a comparison with the erosion capacity of the western GIS. In other words, this scarcity of data prevented detailed shelf-to-shelf comparison of the evolution of sedimentation patterns (rates) on either side of Baffin Bay (i.e., the Baffin Island shelf vs. west Greenland shelf). Similar attention and efforts, as on the west Greenland shelf, should be given to extensive radiocarbon dating of sediment records from the Baffin Island shelf to establish better chronological controls, possibly supplemented by other dating methods (e.g., pollen stratigraphy, magneto-stratigraphy, tephra, radionuclide dating, etc.). This increased focus will be pretty helpful in bridging the knowledge gap on the Baffin Island side, making the Baffin Bay paleoenvironment reasonably well understood as a whole.

Our reconstructions of the evolution of sedimentation patterns in Baffin Bay (see Chapter 6) in this thesis were restricted to periods since the LGM. It would make sense to extend this compilation study to previous deglaciations, at least for the deeper slope and basin, to assess if the patterns (sediment and ice-margin dynamics) highlighted here are a reoccurring scenario or are different from the last deglaciation. Such a study would contribute to improving our understanding of sedimentation beyond Baffin Bay shelves and other previously glaciated Arctic shelves.

In this thesis, the application of CT-scanning of the sediment cores (see Chapters 4 and 5) allowed detailed lithofacies characterization, which provided new insights into sediment internal structures that enabled better interpretation of sediment transport and depositional processes in fairly complex and highly dynamic environmental settings. CT-scanning also enabled the identification of mass-wasting deposits in these cores that could have been easily missed by traditional split-surface line-scan imaging or during initial visual core description. Crucially, any subsequent sediment-base studies reconstructing paleoenvironmental conditions (e.g., sediment and ice-margin dynamics, sea-surface conditions, etc.) in the region should take advantage of the in-depth lithofacies information provided by CT-scanning, which

could effectively guide sampling strategy in choosing core intervals to obtain microfossils for ^{14}C dating and environmental proxy-data.

For each sediment core primarily used in this project, a minimum of four ^{14}C ages have been obtained downcore. These datings could serve as a basis for further proxy investigation aimed at paleoclimatic, paleoceanographic, and sea-ice reconstructions, such as foraminiferal analysis, palynomorph analysis, dinoflagellate cyst analysis, biomarker analysis, and stable isotope analysis.

The first (Chapter 4) and second (Chapter 5) manuscripts attempted provenance reconstruction of sediments delivered to western Baffin Bay by also using their radiogenic isotope compositions. This effort was somewhat hampered by the scarcity of suitable onshore and stream sediment reference data in the region for direct comparison to establish the source-to-sink relations. In the future, intensive investigation of surrounding bedrock radiogenic isotope signatures, as well as proximal river and stream sediments, could significantly improve provenance analysis tracking modern and past sediment export from eastern Canada and Greenland into Baffin Bay and Labrador Sea and as far as the North Atlantic Ocean. All in all, this is geared towards a better understanding of the northern hemisphere ice-sheet dynamics and responses to past, present, and future climate changes.

Chapter eight

8. Bibliography

- Aksu, A.E., 1983. Holocene and Pleistocene dissolution cycles in deep-sea cores of Baffin Bay and Davis Strait: Palaeoceanographic implications. *Mar. Geol.* 53, 331–348. [https://doi.org/10.1016/0025-3227\(83\)90049-X](https://doi.org/10.1016/0025-3227(83)90049-X)
- Aksu, A.E., 1979. Baffin Bay in the past 100,000 yr. *Geology* 7, 245–248. [https://doi.org/10.1130/0091-7613\(1979\)7<245:BBITPY>2.0.CO;2](https://doi.org/10.1130/0091-7613(1979)7<245:BBITPY>2.0.CO;2)
- Aksu, A.E., Hiscott, R.N., 1989. Slides and debris flows on the high-latitude continental slopes of Baffin Bay. *Geology* 17, 885–888. [https://doi.org/10.1130/0091-7613\(1989\)017<0885:SADFOT>2.3.CO;2](https://doi.org/10.1130/0091-7613(1989)017<0885:SADFOT>2.3.CO;2)
- Aksu, A.E., Piper, D.J.W., 1987. Late Quaternary sedimentation in Baffin Bay. *Can. J. Earth Sci.* 24, 1833–1846. <https://doi.org/10.1139/e87-174>
- Allen, L., O’Connell, A., Kiermer, V., 2019. How can we ensure visibility and diversity in research contributions? How the Contributor Role Taxonomy (CRediT) is helping the shift from authorship to contributorship. *Learn. Publ.* 32, 71–74. <https://doi.org/10.1002/leap.1210>
- Alley, R.B., 2000. The Younger Dryas cold interval as viewed from central Greenland. *Quat. Sci. Rev.* 19, 213–226. [https://doi.org/10.1016/S0277-3791\(99\)00062-1](https://doi.org/10.1016/S0277-3791(99)00062-1)
- Alley, R.B., Andrews, J.T., Brigham-Grette, J., Clarke, G.K.C., Cuffey, K.M., Fitzpatrick, J.J., Funder, S., Marshall, S.J., Miller, G.H., Mitrovica, J.X., Muhs, D.R., Otto-Bliesner, B.L., Polyak, L., White, J.W.C., 2010. History of the Greenland Ice Sheet: paleoclimatic insights. *Quat. Sci. Rev.* 29, 1728–1756. <https://doi.org/10.1016/j.quascirev.2010.02.007>
- AMAP, 2021. AMAP Arctic Climate Change Update 2021: Key Trends and Impacts. Arct. Monit. Assess. Program.
- Andrews, J.T., 1990. Fiord to Deep Sea Sediment Transfers along the Northeastern Canadian Continental Margin: Models and Data. *Géographie Phys. Quat.* 44, 55–70. <https://doi.org/10.7202/032798ar>
- Andrews, J.T., 1987. Late Quaternary marine sediment accumulation in fiord-shelf-deep-sea transects, Baffin Island to Baffin Bay. *Quat. Sci. Rev.* 6, 231–243. [https://doi.org/10.1016/0277-3791\(87\)90006-0](https://doi.org/10.1016/0277-3791(87)90006-0)
- Andrews, J.T., Barnett, D.M., 1979. Holocene (Neoglacial) moraine and proglacial lake chronology, Barnes Ice Cap, Canada. *Boreas* 8, 341–358. <https://doi.org/https://doi.org/10.1111/j.1502-3885.1979.tb00817.x>
- Andrews, J.T., Bjork, A.A., Eberl, D.D., Jennings, A.E., Verplanck, E.P., 2015. Significant differences in late Quaternary bedrock erosion and transport: East versus West Greenland ~70°N - evidence from the mineralogy of offshore glacial marine sediments. *J. Quat. Sci.* 30, 452–463. <https://doi.org/10.1002/jqs.2787>
- Andrews, J.T., Eberl, D.D., 2011. Surface (sea floor) and near-surface (box cores) sediment mineralogy in Baffin Bay as a key to sediment provenance and ice sheet variations. *Can. J. Earth Sci.* 48, 1307–1328. <https://doi.org/10.1139/e11-021>
- Andrews, J.T., Gibb, O.T., Jennings, A.E., Simon, Q., 2014. Variations in the provenance of sediment from ice sheets surrounding Baffin Bay during MIS 2 and 3 and export to the Labrador Shelf Sea: Site HU2008029-0008 Davis Strait. *J. Quat. Sci.* 29, 3–13. <https://doi.org/10.1002/jqs.2643>
- Andrews, J.T., Ives, J.D., 1978. “Cockburn” Nomenclature and the Late Quaternary History of the

- Eastern Canadian Arctic. *Arct. Alp. Res.* 10, 617–633. <https://doi.org/10.2307/1550683>
- Andrews, J.T., Jenner, K.A., Campbell, C., 2020. Linking marine core lithofacies and mineral and grain-size compositions on the baffin island margin: Changes in provenance and transport. *J. Sediment. Res.* 90, 763–775. <https://doi.org/10.2110/jsr.2020.50>
- Andrews, J.T., Jull, A.J.T., Donahue, D.J., Short, S.K., Osterman, L.E., 1985. Sedimentation rates in Baffin Island fiord cores from comparative radiocarbon dates (Canada). *Can. J. Earth Sci.* 22, 1827–1834. <https://doi.org/10.1139/e85-194>
- Andrews, J.T., Kirby, M.E., Aksu, A., Barber, D.C., Meese, D., 1998. Late quaternary detrital carbonate (DC-) layers in Baffin Bay marine sediments (67°-74°N): Correlation with Heinrich events in the North Atlantic? *Quat. Sci. Rev.* 17, 1125–1137. [https://doi.org/10.1016/S0277-3791\(97\)00064-4](https://doi.org/10.1016/S0277-3791(97)00064-4)
- Andrews, J.T., Klein, A.J., Jenner, K.A., Jennings, A.E., Campbell, C., 2018. The variability of Baffin Bay seafloor sediment mineralogy: The identification of discrete glacial sediment sources and application to Late Quaternary downcore analysis. *Can. J. Earth Sci.* 55, 620–639. <https://doi.org/10.1139/cjes-2017-0223>
- Andrews, J.T., Milliman, J.D., Jennings, A.E., Rynes, N., Dwyer, J., 1994. Sediment Thicknesses and Holocene Glacial Marine Sedimentation Rates in Three East Greenland Fjords (ca. 68°N) Author (s): J. T. Andrews, J. D. Milliman, A. E. Jennings, N. Rynes and J. Dwyer Published by: The University of Chicago Press. *J. Geol.* 102, 669–683.
- Andrews, J.T., Piper, D.J.W., 2022. Late Quaternary changes in sediment sources in the Labrador Sea, Canadian Journal of Earth Sciences. <https://doi.org/10.1139/cjes-2022-0026>
- Axford, Y., Briner, J.P., Miller, G.H., Francis, D.R., 2009. Paleocological evidence for abrupt cold reversals during peak Holocene warmth on Baffin Island, Arctic Canada. *Quat. Res.* 71, 142–149. <https://doi.org/DOI:10.1016/j.yqres.2008.09.006>
- Azetsu-Scott, K., Clarke, A., Falkner, K., Hamilton, J., Jones, E.P., Lee, C., Petrie, B., Prinsenberg, S., Starr, M., Yeats, P., 2010. Calcium carbonate saturation states in the waters of the Canadian Arctic Archipelago and the Labrador Sea. *J. Geophys. Res. Ocean.* 115, 1–18. <https://doi.org/10.1029/2009JC005917>
- Ballinger, T.J., Moore, G.W.K., Garcia-Quintana, Y., Myers, P.G., Imrit, A.A., Topál, D., Meier, W.N., 2022. Abrupt Northern Baffin Bay Autumn Warming and Sea-Ice Loss Since the Turn of the Twenty-First Century. *Geophys. Res. Lett.* 49. <https://doi.org/10.1029/2022gl101472>
- Balter-Kennedy, A., Young, N.E., Briner, J.P., Graham, B.L., Schaefer, J.M., 2021. Centennial- and Orbital-Scale Erosion Beneath the Greenland Ice Sheet Near Jakobshavn Isbræ. *J. Geophys. Res. Earth Surf.* 126, 1–27. <https://doi.org/10.1029/2021JF006429>
- Bamber, J., Van Den Broeke, M., Ettema, J., Lenaerts, J., Rignot, E., 2012. Recent large increases in freshwater fluxes from Greenland into the North Atlantic. *Geophys. Res. Lett.* 39, 8–11. <https://doi.org/10.1029/2012GL052552>
- Bamber, J.L., Vaughan, D.G., Joughin, I.I., 2000. Widespread complex flow in the interior of the antarctic ice sheet. *Science* (80-). 287, 1248–1250. <https://doi.org/10.1126/science.287.5456.1248>
- Barber, D.G., Massom, R.A., 2007. Chapter 1 The Role of Sea Ice in Arctic and Antarctic Polynyas. Elsevier Oceanogr. Ser. 74, 1–54. [https://doi.org/10.1016/S0422-9894\(06\)74001-6](https://doi.org/10.1016/S0422-9894(06)74001-6)
- Bartels, M., Titschack, J., Fahl, K., Stein, R., Seidenkrantz, M.-S.S., Hillaire-Marcel, C., Hebbeln, D., 2017. Atlantic Water advection vs glacier dynamics in northern Spitsbergen since early deglaciation. *Clim. Past Discuss.* 13, 1–53. <https://doi.org/10.5194/cp-2017-53>
- Batchelor, C.L., Dowdeswell, J.A., 2015. Ice-sheet grounding-zone wedges (GZWs) on high-latitude continental margins. *Mar. Geol.* 363, 65–92. <https://doi.org/10.1016/j.margeo.2015.02.001>
- Batchelor, C.L., Dowdeswell, J.A., 2014. The physiography of High Arctic cross-shelf troughs. *Quat.*

Sci. Rev. 92, 68–96. <https://doi.org/10.1016/j.quascirev.2013.05.025>

- Batchelor, C.L., Margold, M., Krapp, M., Murton, D.K., Dalton, A.S., Gibbard, P.L., Stokes, C.R., Murton, J.B., Manica, A., 2019. The configuration of Northern Hemisphere ice sheets through the Quaternary. *Nat. Commun.* 10, 1–10. <https://doi.org/10.1038/s41467-019-11601-2>
- Bennett, M.R., 2003. Ice streams as the arteries of an ice sheet: their mechanics, stability and significance. *Earth-Science Rev.* 61, 309–339.
- Bennett, R., Campbell, D., Furze, M.F.A., 2013. The shallow stratigraphy and geohazards of the northern Baffin Island shelf: studies to 2012. *Geol. Mag.* 150, 217–231. <https://doi.org/10.4095/292614>
- Bennett, R., Campbell, D.C., Furze, M.F.A., 2014. The shallow stratigraphy and geohazards of the Northeast Baffin Shelf and Lancaster Sound. *Bull. Can. Pet. Geol.* 62, 217–231. <https://doi.org/10.2113/gscpgbull.62.4.217>
- Berger, A., Loutre, M.F., 1991. Insolation values for the climate of the last 10 million years. *Quat. Sci. Rev.* 10, 297–317. [https://doi.org/10.1016/0277-3791\(91\)90033-Q](https://doi.org/10.1016/0277-3791(91)90033-Q)
- Berger, A., Mélice, J.L., Loutre, M.F., 2005. On the origin of the 100-kyr cycles in the astronomical forcing. *Paleoceanography* 20. <https://doi.org/10.1029/2005PA001173>
- Bjørk, A.A., Kjær, K.H., Korsgaard, N.J., Khan, S.A., Kjeldsen, K.K., Andresen, C.S., Box, J.E., Larsen, N.K., Funder, S., 2012. An aerial view of 80 years of climate-related glacier fluctuations in southeast Greenland. *Nat. Geosci.* 5, 427–432. <https://doi.org/10.1038/ngeo1481>
- Blake, W.J., Jackson, H., Currie, C., 1996. Seafloor evidence for glaciation, northernmost Baffin Bay. *Bull. Geol. Soc. Denmark* 23, 157–168.
- Bohm, E., Lippold, J., Gutjahr, M., Frank, M., Blaser, P., Antz, B., Fohlmeister, J., Frank, N., Andersen, M.B., Deininger, M., 2015. Strong and deep Atlantic meridional overturning circulation during the last glacial cycle. *Nature* 517, 73–76. <https://doi.org/10.1038/nature14059>
- Bowen, D.Q., Richmond, G.M., Fullerton, D.S., Šibrava, V., Fulton, R.J., Velichko, A.A., 1986. Correlation of Quaternary glaciations in the northern hemisphere. *Quat. Sci. Rev.* 5, 509–510. [https://doi.org/10.1016/0277-3791\(86\)90218-0](https://doi.org/10.1016/0277-3791(86)90218-0)
- Box, J.E., Colgan, W.T., Christensen, T.R., Schmidt, N.M., Lund, M., Parmentier, F.J.W., Brown, R., Bhatt, U.S., Euskirchen, E.S., Romanovsky, V.E., Walsh, J.E., Overland, J.E., Wang, M., Corell, R.W., Meier, W.N., Wouters, B., Mernild, S., Mård, J., Pawlak, J., Olsen, M.S., 2019. Key indicators of Arctic climate change: 1971–2017. *Environ. Res. Lett.* 14. <https://doi.org/10.1088/1748-9326/aafc1b>
- Boxberg, F., Asendorf, S., Bartholomä, A., Schnetger, B., de Lange, W.P., Hebbeln, D., 2020. Historical anthropogenic heavy metal input to the south-eastern North Sea. *Geo-Marine Lett.* 40, 135–148. <https://doi.org/10.1007/s00367-019-00592-0>
- Briner, J.P., Bini, A.C., Anderson, R.S., 2009a. Rapid early Holocene retreat of a Laurentide outlet glacier through an Arctic fjord. *Nat. Geosci.* 2, 496–499. <https://doi.org/10.1038/ngeo556>
- Briner, J.P., Cuzzone, J.K., Badgley, J.A., Young, N.E., Steig, E.J., Morlighem, M., Schlegel, N.J., Hakim, G.J., Schaefer, J.M., Johnson, J. V., Lesnek, A.J., Thomas, E.K., Allan, E., Bennike, O., Cluett, A.A., Csatho, B., de Vernal, A., Downs, J., Larour, E., Nowicki, S., 2020. Rate of mass loss from the Greenland Ice Sheet will exceed Holocene values this century. *Nature* 586, 70–74. <https://doi.org/10.1038/s41586-020-2742-6>
- Briner, J.P., Davis, P.T., Miller, G.H., 2009b. Latest Pleistocene and Holocene glaciation of Baffin Island, Arctic Canada: key patterns and chronologies. *Quat. Sci. Rev.* 28, 2075–2087. <https://doi.org/10.1016/j.quascirev.2008.09.017>
- Briner, J.P., McKay, N.P., Axford, Y., Bennike, O., Bradley, R.S., de Vernal, A., Fisher, D., Francus, P., Fréchette, B., Gajewski, K., Jennings, A., Kaufman, D.S., Miller, G., Rouston, C., Wagner, B., 2016. Holocene climate change in Arctic Canada and Greenland. *Quat. Sci. Rev.* 147, 340–364.

<https://doi.org/10.1016/j.quascirev.2016.02.010>

- Briner, J.P., Michelutti, N., Francis, D.R., Miller, G.H., Axford, Y., Wooller, M.J., Wolfe, A.P., 2006. A multi-proxy lacustrine record of Holocene climate change on northeastern Baffin Island, Arctic Canada. *Quat. Res.* 65, 431–442. <https://doi.org/10.1016/j.yqres.2005.10.005>
- Briner, J.P., Miller, G.H., Davis, P., Finkel, R.C., Thompson Davis, P., Finkel, R.C., 2005. Cosmogenic exposure dating in Arctic glacial landscapes: implications for the glacial history of Northeastern Baffin Island, Arctic Canada. *Can. J. Earth Sci.* 42, 67–84. <https://doi.org/10.1139/e04-102>
- Briner, J.P., Overeem, I., Miller, G., Finkel, R., 2007. The deglaciation of Clyde Inlet, northeastern Baffin Island, Arctic Canada. *J. Quat. Sci.* 22, 223–232. <https://doi.org/https://doi.org/10.1002/jqs.1057>
- Brouard, E., Lajeunesse, P., 2019. Glacial to postglacial submarine landform assemblages in fiords of northeastern Baffin Island. *Geomorphology* 330, 40–56. <https://doi.org/10.1016/j.geomorph.2019.01.007>
- Brouard, E., Lajeunesse, P., 2017. Maximum extent and decay of the Laurentide Ice Sheet in Western Baffin Bay during the Last glacial episode. *Sci. Rep.* 7. <https://doi.org/10.1038/s41598-017-11010-9>
- Butzin, M., Köhler, P., Lohmann, G., 2017. Marine radiocarbon reservoir age simulations for the past 50,000 years. *Geophys. Res. Lett.* 44, 8473–8480. <https://doi.org/10.1002/2017GL074688>
- Campbell, D.C., Jenner, K.A., Higgins, J., Piper, D.J.W., 2017. Analysis of piston cores and high-resolution sub-bottom profiler data, Baffin Bay slope, Nunavut; Geological Survey of Canada Open File 8135, 179 p. <https://doi.org/10.4095/300835>
- Caron, M., Montero-Serrano, J., St-Onge, G., Rochon, A., 2020. Quantifying provenance and transport pathways of Holocene sediments from the northwestern Greenland margin, *Paleoceanography and Paleoclimatology*. <https://doi.org/10.1029/2019pa003809>
- Caron, M., Rochon, A., Montero-Serrano, J.C., St-Onge, G., 2019. Evolution of sea-surface conditions on the northwestern Greenland margin during the Holocene. *J. Quat. Sci.* 34, 569–580. <https://doi.org/10.1002/jqs.3146>
- Castro De La Guardia, L., Hu, X., Myers, P.G., 2015. Potential positive feedback between Greenland Ice Sheet melt and Baffin Bay heat content on the west Greenland shelf. *Geophys. Res. Lett.* 42, 4922–4930. <https://doi.org/10.1002/2015GL064626>
- Chen, J., Zhang, Q., Kjellström, E., Lu, Z., Chen, F., 2022. The Contribution of Vegetation-Climate Feedback and Resultant Sea Ice Loss to Amplified Arctic Warming During the Mid-Holocene. *Geophys. Res. Lett.* 49. <https://doi.org/10.1029/2022gl098816>
- Clapperton, C.M., 1990. Quaternary glaciations in the southern hemisphere: An overview. *Quat. Sci. Rev.* 9, 299–304. [https://doi.org/https://doi.org/10.1016/0277-3791\(90\)90024-5](https://doi.org/https://doi.org/10.1016/0277-3791(90)90024-5)
- Cohen, J., Pfeiffer, K., Francis, J.A., 2018a. Warm Arctic episodes linked with increased frequency of extreme winter weather in the United States. *Nat. Commun.* 9, 1–12. <https://doi.org/10.1038/s41467-018-02992-9>
- Cohen, J., Screen, J.A., Furtado, J.C., Barlow, M., Whittleston, D., Coumou, D., Francis, J., Dethloff, K., Entekhabi, D., Overland, J., Jones, J., 2014. Recent Arctic amplification and extreme mid-latitude weather. *Nat. Geosci.* 7, 627–637. <https://doi.org/10.1038/ngeo2234>
- Cohen, J., Zhang, X., Francis, J., Jung, T., Kwok, R., Overland, J., Ballinger, T., Blackport, R., Bhatt, U.S., Chen, H., Coumou, D., Feldstein, S., Handorf, D., Hell, M., Henderson, G., Ionita, M., Kretschmer, M., Laliberte, F., Lee, S., Linderholm, H., Maslowski, W., Rigor, I., Routson, C., Screen, J., Semmler, T., Singh, D., Smith, D., Stroeve, J., Taylor, P.C., Vihma, T., Wang, M., Wang, S., Wu, Y., Wendisch, M., Yoon, J., 2018b. Arctic change and possible influence on mid-latitude climate and weather. *US CLIVAR reports* 45. <https://doi.org/10.5065/D6TH8KGW.CONTRIBUTORS>

- Colville, E.J., Carlson, A.E., Beard, B.L., Hatfield, R.G., Stoner, J.S., Reyes, A. V, Ullman, D.J., 2011. Sr-Nd-Pb isotope evidence for ice-sheet presence on southern Greenland during the Last Interglacial. *Science* 333, 620–623. <https://doi.org/10.1126/science.1204673>
- Comiso, J.C., 2012. Large decadal decline of the arctic multiyear ice cover. *J. Clim.* 25, 1176–1193. <https://doi.org/10.1175/JCLI-D-11-00113.1>
- Comiso, J.C., 2002. A rapidly declining perennial sea ice cover in the Arctic. *Geophys. Res. Lett.* 29, 2–5. <https://doi.org/10.1029/2002GL015650>
- Couette, P.O., Lajeunesse, P., Ghienne, J.F., Dorschel, B., Gebhardt, C., Hebbeln, D., Brouard, E., 2023. Retreat and stabilization of a marine-based ice margin along a high arctic fjord-cross-shelf trough system. *Quat. Sci. Rev.* 302, 107949. <https://doi.org/10.1016/j.quascirev.2022.107949>
- Couette, P.O., Lajeunesse, P., Ghienne, J.F., Dorschel, B., Gebhardt, C., Hebbeln, D., Brouard, E., 2022. Evidence for an extensive ice shelf in northern Baffin Bay during the Last Glacial Maximum. *Commun. Earth Environ.* 3, 1–12. <https://doi.org/10.1038/s43247-022-00559-7>
- Coulthard, R.D., 2012. The complexity of marine 14C chronologies in Arctic Canada: variable ΔR values, enhanced deep water reservoirs, and the Portlandia effect. *Quat. Int.* 279–280, 99. <https://doi.org/10.1016/j.quaint.2012.07.437>
- Coulthard, R.D., Furze, M.F.A., Pieńkowski, A.J., Chantel Nixon, F., England, J.H., 2010. New marine ΔR values for Arctic Canada. *Quat. Geochronol.* 5, 419–434. <https://doi.org/10.1016/j.quageo.2010.03.002>
- Dalton, A.S., Margold, M., Stokes, C.R., Tarasov, L., Dyke, A.S., Adams, R.S., Allard, S., Arends, H.E., Atkinson, N., Attig, J.W., Barnett, P.J., Barnett, R.L., Batterson, M., Bernatchez, P., Borns, H.W., Breckenridge, A., Briner, J.P., Brouard, E., Campbell, J.E., Carlson, A.E., Clague, J.J., Curry, B.B., Daigneault, R.-A.A., Dubé-Loubert, H., Easterbrook, D.J., Franzi, D.A., Friedrich, H.G., Funder, S., Gauthier, M.S., Gowan, A.S., Harris, K.L., Hétu, B., Hooyer, T.S., Jennings, C.E., Johnson, M.D., Kehew, A.E., Kelley, S.E., Kerr, D., King, E.L., Kjeldsen, K.K., Knaeble, A.R., Lajeunesse, P., Lakeman, T.R., Lamothe, M., Larson, P., Lavoie, M., Loope, H.M., Lowell, T. V., Lusardi, B.A., Manz, L., McMartin, I., Nixon, F.C., Occhietti, S., Parkhill, M.A., Piper, D.J.W., Pronk, A.G., Richard, P.J.H., Ridge, J.C., Ross, M., Roy, M., Seaman, A., Shaw, J., Stea, R.R., Teller, J.T., Thompson, W.B., Thorleifson, L.H., Utting, D.J., Veillette, J.J., Ward, B.C., Weddle, T.K., Wright, H.E., 2020. An updated radiocarbon-based ice margin chronology for the last deglaciation of the North American Ice Sheet Complex. *Quat. Sci. Rev.* 234, 106223. <https://doi.org/10.1016/j.quascirev.2020.106223>
- Dalton, A.S., Stokes, C.R., Batchelor, C.L., 2022. Evolution of the Laurentide and Innuitian ice sheets prior to the Last Glacial Maximum (115 ka to 25 ka). *Earth-Science Rev.* 224, 103875. <https://doi.org/10.1016/j.earscirev.2021.103875>
- Dawes, P.R., 2009. Precambrian - Palaeozoic geology of Smith Sound, Canada and Greenland: Key constraint to palaeogeographic reconstructions of northern Laurentia and the North Atlantic region. *Terra Nov.* 21, 1–13. <https://doi.org/10.1111/j.1365-3121.2008.00845.x>
- Deniel, C., Pin, C., 2001. Single-stage method for the simultaneous isolation of lead and strontium from silicate samples for isotopic measurements. *Anal. Chim. Acta* 426, 95–103. [https://doi.org/10.1016/S0003-2670\(00\)01185-5](https://doi.org/10.1016/S0003-2670(00)01185-5)
- Dethleff, D., 2005. Entrainment and export of Laptev Sea ice sediments, Siberian Arctic. *J. Geophys. Res. Ocean.* <https://doi.org/10.1029/2004JC002740>
- Ding, Q., Schweiger, A., L’Heureux, M., Steig, E.J., Battisti, D.S., Johnson, N.C., Blanchard-Wrigglesworth, E., Po-Chedley, S., Zhang, Q., Harnos, K., Bushuk, M., Markle, B., Baxter, I., 2019. Fingerprints of internal drivers of Arctic sea ice loss in observations and model simulations. *Nat. Geosci.* 12, 28–33. <https://doi.org/10.1038/s41561-018-0256-8>
- Ding, Q., Wallace, J.M., Battisti, D.S., Steig, E.J., Gallant, A.J.E., Kim, H.J., Geng, L., 2014. Tropical

- forcing of the recent rapid Arctic warming in northeastern Canada and Greenland. *Nature* 509, 209–212. <https://doi.org/10.1038/nature13260>
- Dorschel, B., Allan, E., Bartels, M., Campbell, C.D., Couette, P., Diekamp, V., Dreutter, S., Duboc, Q., Geils, J., Greco, M., Lenz, K., Lübben, B., Lütjens, M., Madaj, L., Perez, L., Recinos, B., Saini, J., Schade, T., Täuber, F., Ulner, L., Warnke, F., Weiser, J., 2017. WESTBAFF - Reconstruction of the Laurentide Ice sheet drainage into the northwest Baffin Bay and the palaeoceanography of the west Baffin Bay, Cruise No. MSM66, 22nd of July 2017 - 28th of August 2017, Nuuk (Greenland) - Reykjavik (Iceland), MARIA S. MERIAN-Berichte. Gutachterpanel Forschungsschiffe MSM66.
- Dowdeswell, J.A., Canals, M., Jakobsson, M., Todd, B.J., Dowdeswell, E.K., Hogan, K.A., 2016a. Introduction: An Atlas of Submarine Glacial Landforms. *Geol. Soc. Mem.* 46, 3–14. <https://doi.org/10.1144/M46.171>
- Dowdeswell, J.A., Elverhfi, A., Spielhagen, R., 1998. Glacimarine sedimentary processes and facies on the Polar North Atlantic margins. *Quat. Sci. Rev.* 17, 243–272. [https://doi.org/https://doi.org/10.1016/S0277-3791\(97\)00071-1](https://doi.org/https://doi.org/10.1016/S0277-3791(97)00071-1)
- Dowdeswell, J.A., Fugelli, E.M.G., 2012. The seismic architecture and geometry of grounding-zone wedges formed at the marine margins of past ice sheets. *Geol. Soc. Am. Bull.* 124, 1750–1761.
- Dowdeswell, J.A., Hogan, K.A., Cofaigh, C., 2016b. Submarine glacial-landform distribution across the West Greenland margin: A fjord-shelf-slope transect through the Uummannaq system (70–71° N). *Geol. Soc. Mem.* 46, 453–460. <https://doi.org/10.1144/M46.150>
- Dowdeswell, J.A., Hogan, K.A., Ó Cofaigh, C., Fugelli, E.M.G., Evans, J., Noormets, R., 2014. Late Quaternary ice flow in a West Greenland fjord and cross-shelf trough system: Submarine landforms from Rink Isbrae to Uummannaq shelf and slope. *Quat. Sci. Rev.* 92, 292–309. <https://doi.org/10.1016/j.quascirev.2013.09.007>
- Dunlap, E., Tang, C.C.L., 2006. Modelling the mean circulation of Baffin Bay. *Atmos. - Ocean* 44, 99–109. <https://doi.org/10.3137/ao.440107>
- Dyke, A.S., 2004. An outline of North American deglaciation with emphasis on central and northern Canada. *Dev. Quat. Sci.* 2, 373–424. [https://doi.org/10.1016/S1571-0866\(04\)80209-4](https://doi.org/10.1016/S1571-0866(04)80209-4)
- Dyke, A.S., 1999. Last Glacial Maximum and deglaciation of Devon Island, Arctic Canada: Support for an Inuitian ice sheet. *Quat. Sci. Rev.* 18, 393–420. [https://doi.org/10.1016/S0277-3791\(98\)00005-5](https://doi.org/10.1016/S0277-3791(98)00005-5)
- Dyke, A.S., Andrews, J.T., Clark, P.U., England, J.H., Miller, G.H., Shaw, J., Veillette, J.J., 2002. The Laurentide and Inuitian ice sheets during the Last Glacial Maximum. *Quat. Sci. Rev.* 21, 9–31. [https://doi.org/10.1016/S0277-3791\(01\)00095-6](https://doi.org/10.1016/S0277-3791(01)00095-6)
- Dyke, A.S., Moore, A., Robertson, L., 2003. Deglaciation of North America Open File 1547. <https://doi.org/10.4095/214399>
- Dyke, A.S., Morris, T.F., Green, D.E.C., 1991. Postglacial Tectonic and Sea Level History of the Central Canadian Arctic, Bulletin (Commission géologique du Canada : Édition anglaise). Energy, Mines, and Resources Canada.
- Eicken, H., Kolatschek, J., Freitag, J., Lindemann, F., Kassens, H., Dmitrenko, I., 2000. A key source area and constraints on entrainment for basin-scale sediment transport by Arctic sea ice. *Geophys. Res. Lett.* <https://doi.org/10.1029/1999GL011132>
- Eisenhauer, A., Meyer, H., Rachold, V., Tütken, T., Wiegand, B., Hansen, B.T., Spielhagen, R.F., Lindemann, F., Kassens, H., 1999. Grain size separation and sediment mixing in Arctic Ocean sediments: evidence from the strontium isotope systematic. *Chem. Geol.* 158, 173–188. [https://doi.org/https://doi.org/10.1016/S0009-2541\(99\)00026-1](https://doi.org/https://doi.org/10.1016/S0009-2541(99)00026-1)
- England, J., 1999. Coalescent Greenland and Inuitian ice during the Last Glacial Maximum: Revising the Quaternary of the Canadian High Arctic. *Quat. Sci. Rev.* 18, 421–456. [https://doi.org/10.1016/S0277-3791\(98\)00070-5](https://doi.org/10.1016/S0277-3791(98)00070-5)

- England, J., Atkinson, N., Bednarski, J., Dyke, A.S., Hodgson, D.A., Ó Cofaigh, C., 2006. The Inuitian Ice Sheet: configuration, dynamics and chronology. *Quat. Sci. Rev.* 25, 689–703. <https://doi.org/10.1016/j.quascirev.2005.08.007>
- England, M.R., Eisenman, I., Lutsko, N.J., Wagner, T.J.W., 2021. The Recent Emergence of Arctic Amplification. *Geophys. Res. Lett.* 48. <https://doi.org/10.1029/2021GL094086>
- Faure, G., Powell, J.L., 2012. *Strontium Isotope Geology, Minerals, Rocks and Mountains*. Springer Berlin Heidelberg.
- Filippova, A., Frank, M., Kienast, M., Gutjahr, M., Hathorne, E.C., Hillaire-Marcel, C., 2023. Authigenic and Detrital Carbonate Nd Isotope Records Reflect Pulses of Detrital Material Input to the Labrador Sea During the Heinrich Stadials. *Paleoceanogr. Paleoclimatology* 38, 1–23. <https://doi.org/10.1029/2022PA004470>
- Fisher, D., Zheng, J., Burgess, D., Zdanowicz, C., Kinnard, C., Sharp, M., Bourgeois, J., 2012. Recent melt rates of Canadian arctic ice caps are the highest in four millennia. *Glob. Planet. Change* 84–85, 3–7. <https://doi.org/10.1016/j.gloplacha.2011.06.005>
- Fisher, D.A., Koerner, R.M., Reeh, N., 1995. Holocene climatic records from Agassiz Ice Cap, Ellesmere Island, NWT, Canada. *The Holocene* 5, 19–24. <https://doi.org/10.1177/095968369500500103>
- Francis, J., Skific, N., 2015. Evidence linking rapid Arctic warming to mid-latitude weather patterns. *Philos. Trans. R. Soc. A Math. Phys. Eng. Sci.* 373. <https://doi.org/10.1098/rsta.2014.0170>
- Francis, J.A., Vavrus, S.J., Cohen, J., 2017. Amplified Arctic warming and mid-latitude weather: new perspectives on emerging connections. *Wiley Interdiscip. Rev. Clim. Chang.* 8, 1–11. <https://doi.org/10.1002/wcc.474>
- Funder, S., Kjeldsen, K.K., Kjær, K.H., Colm, O., Ó Cofaigh, C., 2011. The Greenland Ice Sheet During the Past 300,000 Years: A Review. *Dev. Quat. Sci.* 15, 699–713. <https://doi.org/10.1016/B978-0-444-53447-7.00050-7>
- Furze, M.F.A., Pieńkowski, A.J., McNeely, M.A., Bennett, R., Cage, A.G., 2018. Deglaciation and ice shelf development at the northeast margin of the Laurentide Ice Sheet during the Younger Dryas chronozone. *Boreas* 47, 271–296. <https://doi.org/10.1111/bor.12265>
- Gajewski, K., 2015. Quantitative reconstruction of Holocene temperatures across the Canadian Arctic and Greenland. *Glob. Planet. Change* 128, 14–23. <https://doi.org/10.1016/j.gloplacha.2015.02.003>
- Garcia, H.E., Boyer, T.P., Baranova, O.K., Locarnini, R.A., Mishonov, A.V., Grodskyy, A., Paver, C.R., Weathers, K.W., Smolyar, I.V., Reagan, J.R., Seidov, D., Zweng, M.M., 2019. *World Ocean Atlas 2018: Product Documentation* 20pp.
- Garçon, M., Chauvel, C., France-Lanord, C., Limonta, M., Garzanti, E., 2014. Which minerals control the Nd–Hf–Sr–Pb isotopic compositions of river sediments? *Chem. Geol.* 364, 42–55. <https://doi.org/10.1016/j.chemgeo.2013.11.018>
- Georgiadis, E., Giraudeau, J., Jennings, A., Limoges, A., Jackson, R., Ribeiro, S., Massé, G., 2020. Local and regional controls on Holocene sea ice dynamics and oceanography in Nares Strait, Northwest Greenland. *Mar. Geol.* 422, 106115. <https://doi.org/10.1016/j.margeo.2020.106115>
- Georgiadis, E., Giraudeau, J., Martinez, P., Lajeunesse, P., St-Onge, G., Schmidt, S., Massé, G., 2018. Deglacial to postglacial history of Nares Strait, Northwest Greenland: A marine perspective from Kane Basin. *Clim. Past* 14, 1991–2010. <https://doi.org/10.5194/cp-14-1991-2018>
- Gibb, O.T., Hillaire-Marcel, C., de Vernal, A., 2014. Oceanographic regimes in the northwest Labrador Sea since Marine Isotope Stage 3 based on dinocyst and stable isotope proxy records. *Quat. Sci. Rev.* 92, 269–279. <https://doi.org/10.1016/j.quascirev.2013.12.010>
- Gibb, O.T., Steinhauer, S., Fréchette, B., de Vernal, A., Hillaire-Marcel, C., 2015. Diachronous evolution of sea surface conditions in the Labrador sea and Baffin Bay since the last deglaciation.

- Holocene 25, 1882–1897. <https://doi.org/10.1177/0959683615591352>
- Giraudeau, J., Georgiadis, E., Caron, M., Martinez, P., St-Onge, G., Billy, I., Lebleu, P., Ther, O., Massé, G., 2020. A high-resolution elemental record of post-glacial lithic sedimentation in Upernavik Trough, western Greenland: History of ice-sheet dynamics and ocean circulation changes over the last 9100 years. *Glob. Planet. Change* 191, 103217. <https://doi.org/10.1016/j.gloplacha.2020.103217>
- Grenier, M., Brown, K.A., Colombo, M., Belhadj, M., Baconnais, I., Pham, V., Soon, M., Myers, P.G., Jeandel, C., Franc, R., 2022. Controlling factors and impacts of river-borne neodymium isotope signatures and rare earth element concentrations supplied to the Canadian Arctic Archipelago. *Earth Planet. Sci. Lett.* 578. <https://doi.org/10.1016/j.epsl.2021.117341>
- Gutjahr, M., Frank, M., Stirling, C.H., Klemm, V., van de Flierdt, T., Halliday, A.N., 2007. Reliable extraction of a deepwater trace metal isotope signal from Fe-Mn oxyhydroxide coatings of marine sediments. *Chem. Geol.* 242, 351–370. <https://doi.org/10.1016/j.chemgeo.2007.03.021>
- Hanna, E., Jones, J.M., Cappelen, J., Mernild, S.H., Wood, L., Steffen, K., Huybrechts, P., 2013. The influence of North Atlantic atmospheric and oceanic forcing effects on 1900–2010 Greenland summer climate and ice melt/runoff. *Int. J. Climatol.* 33, 862–880. <https://doi.org/10.1002/joc.3475>
- Harrison, J.C., Brent, T.A., Oakey, G.N., 2011a. Chapter 40: Baffin Fan and its inverted rift system of Arctic eastern Canada: Stratigraphy, tectonics and petroleum resource potential. *Geol. Soc. Mem.* 35, 595–626. <https://doi.org/10.1144/M35.40>
- Harrison, J.C., St Onge, M.R., Petrov, O.V., Strel'nikov, S.I., Lopatin, B.G., Wilson, F.H., Tella, S., Paul, D., Lynds, T., Shokalsky, S.P., Hulst, C.K., Bergman, S., Jepsen, H.F., Solli, A., 2011b. Geological map of the Arctic; Geological Survey of Canada, Map 2159A, scale 1/5 000 000 1–5.
- Hasholt, B., 1996. Sediment transport in Greenland. *IAHS-AISH Publ.* 236, 105–114.
- Hasholt, B., van As, D., Mikkelsen, A.B., Mernild, S.H., Yde, J.C., 2018. Observed sediment and solute transport from the Kangerlussuaq sector of the Greenland Ice Sheet (2006–2016). *Arctic, Antarct. Alp. Res.* 50. <https://doi.org/10.1080/15230430.2018.1433789>
- Hauser, D.D.W., Laidre, K.L., Stern, H.L., 2018. Vulnerability of arctic marine mammals to vessel traffic in the increasingly ice-free northwest passage and Northern Sea Route. *Proc. Natl. Acad. Sci. U. S. A.* 115, 7617–7622. <https://doi.org/10.1073/pnas.1803543115>
- Heaton, T.J., Bard, E., Bronk Ramsey, C., Butzin, M., Hatté, C., Hughen, K.A., Köhler, P., Reimer, P.J., 2023a. a Response To Community Questions on the Marine20 Radiocarbon Age Calibration Curve: Marine Reservoir Ages and the Calibration of 14C Samples From the Oceans. *Radiocarbon* 65, 247–273. <https://doi.org/10.1017/RDC.2022.66>
- Heaton, T.J., Butzin, M., Bard, E., Bronk Ramsey, C., Hughen, K.A., Köhler, P., Reimer, P.J., 2023b. Marine Radiocarbon Calibration in Polar Regions: A Simple Approximate Approach using Marine20. *Radiocarbon* 65, 848–875. <https://doi.org/DOI:10.1017/RDC.2023.42>
- Heaton, T.J., Köhler, P., Butzin, M., Bard, E., Reimer, R.W., Austin, W.E.N., Bronk Ramsey, C., Grootes, P.M., Hughen, K.A., Kromer, B., Reimer, P.J., Adkins, J., Burke, A., Cook, M.S., Olsen, J., Skinner, L.C., 2020. Marine20 - The Marine Radiocarbon Age Calibration Curve (0–55,000 cal BP). *Radiocarbon* 62, 779–820. <https://doi.org/10.1017/RDC.2020.68>
- Hebbeln, D., 2000. Flux of ice-rafted detritus from sea ice in the Fram Strait. *Deep. Res. Part II Top. Stud. Oceanogr.* 47, 1773–1790. [https://doi.org/10.1016/S0967-0645\(00\)00006-0](https://doi.org/10.1016/S0967-0645(00)00006-0)
- Heinrich, H., 1988. Origin and consequences of cyclic ice rafting in the Northeast Atlantic Ocean during the past 130,000 years. *Quat. Res.* 29, 142–152. [https://doi.org/10.1016/0033-5894\(88\)90057-9](https://doi.org/10.1016/0033-5894(88)90057-9)
- Hingst, J; Stein, R; Kasemann, S. A.: Late Quaternary Sr-Nd-Pb isotope composition of the siliciclastic sediment fraction of the marine sediment core PS72/287-3 from Barrow Strait, Canadian Arctic Archipelago. PANGAEA, <https://doi.pangaea.de/10.1594/PANGAEA.962323> (dataset in review).

- Hiscott, R.N., Aksu, A.E., Nielsen, O.B., 1989. Provenance and dispersal patterns, Pliocene-Pleistocene section at Site 645, Baffin Bay. *Proc., Sci. results, ODP, Leg 105, Baffin Bay Labrador Sea 105*, 31–52.
- Hodell, D.A., Channeil, J.E.T., Curtis, J.H., Romero, O.E., Röhl, U., 2008. Onset of “Hudson Strait” Heinrich events in the eastern North Atlantic at the end of the middle Pleistocene transition (~640 ka)? *Paleoceanography* 23, 1–16. <https://doi.org/10.1029/2008PA001591>
- Hofmann, J.C., Knutz, P.C., Nielsen, T., Kuijpers, A., 2016. Seismic architecture and evolution of the Disko Bay trough-mouth fan, central West Greenland margin. *Quat. Sci. Rev.* 147, 69–90. <https://doi.org/10.1016/j.quascirev.2016.05.019>
- Hogan, K.A., Dowdeswell, J.A., ÓCofaigh, C., 2012. Glacimarine sedimentary processes and depositional environments in an embayment fed by West Greenland ice streams. *Mar. Geol.* 311–314, 1–16. <https://doi.org/10.1016/j.margeo.2012.04.006>
- Hogan, K.A., Jakobsson, M., Mayer, L., Reilly, B.T., Jennings, A.E., Stoner, J.S., Nielsen, T., Andresen, K.J., Nørmark, E., Heirman, K.A., Kamla, E., Jerram, K., Stranne, C., Mix, A., 2020. Glacial sedimentation, fluxes and erosion rates associated with ice retreat in Petermann Fjord and Nares Strait, north-west Greenland. *Cryosphere* 14, 261–286. <https://doi.org/10.5194/tc-14-261-2020>
- Hogan, K.A., Ó Cofaigh, C., Jennings, A.E., Dowdeswell, J.A., Hiemstra, J.F., 2016. Deglaciation of a major palaeo-ice stream in Disko Trough, West Greenland. *Quat. Sci. Rev.* 147, 5–26. <https://doi.org/10.1016/j.quascirev.2016.01.018>
- Holland, D.M., Thomas, R.H., De Young, B., Ribergaard, M.H., Lyberth, B., 2008. Acceleration of Jakobshavn Isbr triggered by warm subsurface ocean waters. *Nat. Geosci.* 1, 659–664. <https://doi.org/10.1038/ngeo316>
- Holland, M.M., Bitz, C.M., 2003. Polar amplification of climate change in coupled models. *Clim. Dyn.* 21, 221–232. <https://doi.org/10.1007/s00382-003-0332-6>
- Holland, M.M., Bitz, C.M., Eby, M., Weaver, A.J., 2001. The role of ice-ocean interactions in the variability of the North Atlantic thermohaline circulation. *J. Clim.* 14, 656–675. [https://doi.org/10.1175/1520-0442\(2001\)014<0656:TROIOI>2.0.CO;2](https://doi.org/10.1175/1520-0442(2001)014<0656:TROIOI>2.0.CO;2)
- Holland, M.M., Bitz, C.M., Tremblay, B., 2006. Future abrupt reductions in the summer Arctic sea ice. *Geophys. Res. Lett.* 33, 1–5. <https://doi.org/10.1029/2006GL028024>
- Höppner, N., Lucassen, F., Chiessi, C.M., Sawakuchi, A.O., Kasemann, S.A., 2018. Holocene provenance shift of suspended particulate matter in the Amazon River basin. *Quat. Sci. Rev.* 190, 66–80. <https://doi.org/10.1016/j.quascirev.2018.04.021>
- Ingram, R.G., Bâcle, J., Barber, D.G., Gratton, Y., Melling, H., 2002. An overview of physical processes in the North Water. *Deep. Res. Part II Top. Stud. Oceanogr.* 49, 4893–4906. [https://doi.org/10.1016/S0967-0645\(02\)00169-8](https://doi.org/10.1016/S0967-0645(02)00169-8)
- Intergovernmental Panel on Climate Change (IPCC), 2022. The Ocean and Cryosphere in a Changing Climate, *The Ocean and Cryosphere in a Changing Climate*. <https://doi.org/10.1017/9781009157964>
- Jackson, G., Berman, R., 2000. Precambrian metamorphic and tectonic evolution of northern Baffin Island, Nunavut, Canada. *Can. Mineral. - CAN Mineral.* 38, 399–421. <https://doi.org/10.2113/gscanmin.38.2.399>
- Jackson, R., Carlson, A.E., Hillaire-Marcel, C., Wacker, L., Vogt, C., Kucera, M., 2017. Asynchronous instability of the North American-Arctic and Greenland ice sheets during the last deglaciation. *Quat. Sci. Rev.* 164, 140–153. <https://doi.org/10.1016/j.quascirev.2017.03.020>
- Jackson, R., Frederichs, T., Schulz, H., Kucera, M., 2023. Chronology of detrital carbonate events in Baffin Bay reveals different timing but similar average recurrence time of North American-Arctic and Laurentide ice sheet collapse events during MIS 3. *Earth Planet. Sci. Lett.* 613, 118191. <https://doi.org/10.1016/J.EPSL.2023.118191>

- Jackson, R., Kvorning, A.B., Limoges, A., Georgiadis, E., Olsen, S.M., Tallberg, P., Andersen, T.J., Mikkelsen, N., Giraudeau, J., Massé, G., Wacker, L., Ribeiro, S., 2021. Holocene polynya dynamics and their interaction with oceanic heat transport in northernmost Baffin Bay. *Sci. Rep.* 11. <https://doi.org/10.1038/s41598-021-88517-9>
- Jacob, T., Wahr, J., Pfeffer, W.T., Swenson, S., 2012. Recent contributions of glaciers and ice caps to sea level rise. *Nature* 482, 514–518. <https://doi.org/10.1038/nature10847>
- Jacobsen, S.B., Wasserburg, G.J., 1980. Sm-Nd isotopic evolution of chondrites. *Earth Planet. Sci. Lett.* 50, 139–155. [https://doi.org/10.1016/0012-821X\(80\)90125-9](https://doi.org/10.1016/0012-821X(80)90125-9)
- Jakobsson, M., Mayer, L., Coakley, B., Dowdeswell, J.A., Forbes, S., Fridman, B., Hodnesdal, H., Noormets, R., Pedersen, R., Rebesco, M., Schenke, H.W., Zarayskaya, Y., Accettella, D., Armstrong, A., Anderson, R.M., Bienhoff, P., Camerlenghi, A., Church, I., Edwards, M., Gardner, J. V., Hall, J.K., Hell, B., Hestvik, O., Kristoffersen, Y., Marcussen, C., Mohammad, R., Mosher, D., Nghiem, S. V., Pedrosa, M.T., Travaglini, P.G., Weatherall, P., 2012. The International Bathymetric Chart of the Arctic Ocean (IBCAO) Version 3.0. *Geophys. Res. Lett.* <https://doi.org/10.1029/2012GL052219>
- Jenkins, M., Dai, A., 2021. The Impact of Sea-Ice Loss on Arctic Climate Feedbacks and Their Role for Arctic Amplification. *Geophys. Res. Lett.* 48, 1–9. <https://doi.org/10.1029/2021GL094599>
- Jenner, K.A., Campbell, D.C., Piper, D.J.W., 2018. Along-slope variations in sediment lithofacies and depositional processes since the Last Glacial Maximum on the northeast Baffin margin, Canada. *Mar. Geol.* 405, 92–107. <https://doi.org/10.1016/j.margeo.2018.07.012>
- Jennings, A., Reilly, B., Andrews, J., Hogan, K., Walczak, M., Jakobsson, M., Stoner, J., Mix, A., Nicholls, K.W., Regan, M.O., Prins, M.A., Troelstra, S.R., 2022. Modern and early Holocene ice shelf sediment facies from Petermann Fjord and northern Nares Strait, northwest Greenland. *Quat. Sci. Rev.* 283, 107460. <https://doi.org/10.1016/j.quascirev.2022.107460>
- Jennings, A.E., Andrews, J.T., Ó Cofaigh, C., Onge, G.S., Sheldon, C., Belt, S.T., Cabedo-Sanz, P., Hillaire-Marcel, C., 2017. Ocean forcing of Ice Sheet retreat in central west Greenland from LGM to the early Holocene. *Earth Planet. Sci. Lett.* 472, 1–13. <https://doi.org/10.1016/j.epsl.2017.05.007>
- Jennings, A.E., Andrews, J.T., Ó Cofaigh, C., St-Onge, G., Belt, S., Cabedo-Sanz, P., Pearce, C., Hillaire-Marcel, C., Calvin Campbell, D., 2018. Baffin Bay paleoenvironments in the LGM and HS1: Resolving the ice-shelf question. *Mar. Geol.* 402, 5–16. <https://doi.org/10.1016/j.margeo.2017.09.002>
- Jennings, A.E., Andrews, J.T., Oliver, B., Walczak, M., Mix, A., 2019. Retreat of the Smith Sound Ice Stream in the Early Holocene. *Boreas* 48, 825–840. <https://doi.org/10.1111/bor.12391>
- Jennings, A.E., Sheldon, C., Cronin, T.M., Francus, P., Stoner, J., Andrews, J., Jennings, A.E., Sheldon, C., Cronin, T.M., Francus, P., Stoner, J., Andrews, J., 2011. The holocene history of nares strait. *Oceanography* 24, 26–41. <https://doi.org/10.5670/oceanog.2011.52>
- Jennings, A.E., Walton, M.E., Ó Cofaigh, C., Kilfeather, A., Andrews, J.T., Ortiz, J.D., De Vernal, A., Dowdeswell, J.A., 2014. Paleoenvironments during Younger Dryas-Early Holocene retreat of the Greenland Ice Sheet from outer Disko Trough, central west Greenland. *J. Quat. Sci.* 29, 27–40. <https://doi.org/10.1002/jqs.2652>
- Jokat, W., 2009. The Expedition of the Research Vessel Polarstern to the Arctic in 2008 (ARK-XXIII/3), *Berichte zur Polar- und Meeresforschung = Reports on Polar and Marine Research*. Alfred-Wegener-Institut für Polar- und Meeresforschung, Bremerhaven, Germany. https://doi.org/10.2312/BzPM_0597_2009
- Jung, T., Doblas-Reyes, F., Goessling, H., Guemas, V., Bitz, C., Buontempo, C., Caballero, R., Jakobson, E., Jungclaus, J., Karcher, M., Koenigk, T., Matei, D., Overland, J., Spengler, T., Yang, S., 2015. Polar lower-latitude linkages and their role in weather and climate prediction. *Bull. Am. Meteorol. Soc.* 96, ES197–ES200. <https://doi.org/10.1175/BAMS-D-15-00121.1>

- Kaufman, D.S., Ager, T.A., Anderson, N.J., Anderson, P.M., Andrews, J.T., Bartlein, P.J., Brubaker, L.B., Coats, L.L., Cwynar, L.C., Duvall, M.L., Dyke, A.S., Edwards, M.E., Eisner, W.R., Gajewski, K., Geirsdóttir, A., Hu, F.S., Jennings, A.E., Kaplan, M.R., Kerwin, M.W., Lozhkin, A. V., MacDonald, G.M., Miller, G.H., Mock, C.J., Oswald, W.W., Otto-Bliesner, B.L., Porinchu, D.F., Rühland, K., Smol, J.P., Steig, E.J., Wolfe, B.B., 2004. Holocene thermal maximum in the western Arctic (0-180°W). *Quat. Sci. Rev.* 23, 529–560. <https://doi.org/10.1016/j.quascirev.2003.09.007>
- Kelleher, R., Jennings, A., Andrews, J., Brooks, N.K.S., Marchitto, T., Feng, S., Woelders, L., Normandeau, A., Jenner, K., Bennett, R., Brookins, S., 2022. Late glacial retreat of the Lancaster Sound Ice Stream and early Holocene onset of Arctic/Atlantic throughflow in the Arctic Island channels, Arctic, Antarctic, and Alpine Research. Taylor & Francis. <https://doi.org/10.1080/15230430.2022.2110689>
- King, M.D., Howat, I.M., Candela, S.G., Noh, M.J., Jeong, S., Noël, B.P.Y., van den Broeke, M.R., Wouters, B., Negrete, A., 2020. Dynamic ice loss from the Greenland Ice Sheet driven by sustained glacier retreat. *Commun. Earth Environ.* 1, 1–7. <https://doi.org/10.1038/s43247-020-0001-2>
- Kirillova, V., 2017. Radiogenic isotopes on marine sediments from the Baffin Bay: implications for the sediment supply during the last deglaciation. Dissertation, Geosciences, University Bremen, Bremen, Germany.
- Knudsen, K.L., Stabell, B., Seidenkrantz, M.S., Eiríksson, J., Blake, W., 2008. Deglacial and Holocene conditions in northernmost Baffin Bay: Sediments, foraminifera, diatoms and stable isotopes. *Boreas* 37, 346–376. <https://doi.org/10.1111/j.1502-3885.2008.00035.x>
- Knutz, P., Gregersen, U., Harrison, C., Brent, T., Hopper, J., Nøhr-Hansen, H., 2021. Baffin Bay Composite Tectono-Sedimentary Element. *Geol. Soc. London, Mem.* 57, M57-2016. <https://doi.org/10.1144/M57-2016-7>
- Knutz, P.C., Newton, A.M.W., Hopper, J.R., Huuse, M., Gregersen, U., Sheldon, E., Dybkjær, K., 2019. Eleven phases of Greenland Ice Sheet shelf-edge advance over the past 2.7 million years. *Nat. Geosci.* 12, 361–368. <https://doi.org/10.1038/s41561-019-0340-8>
- Koppes, M., Hallet, B., Rignot, E., Mouginot, J., Wellner, J.S., Boldt, K., 2015. Observed latitudinal variations in erosion as a function of glacier dynamics. *Nature* 526, 100–103. <https://doi.org/10.1038/nature15385>
- Laberg, J.S., Vorren, T.O., 1995. Late Weichselian submarine debris flow deposits on the Bear Island Trough Mouth Fan. *Mar. Geol.* 127, 45–72. [https://doi.org/10.1016/0025-3227\(95\)00055-4](https://doi.org/10.1016/0025-3227(95)00055-4)
- Land Farmer, G., Barber, D., Andrews, J., 2003. Provenance of Late Quaternary ice-proximal sediments in the North Atlantic: Nd, Sr and Pb isotopic evidence. *Earth Planet. Sci. Lett.* 209, 227–243. [https://doi.org/10.1016/S0012-821X\(03\)00068-2](https://doi.org/10.1016/S0012-821X(03)00068-2)
- Laskar, J., Robutel, P., Joutel, F., Gastineau, M., Correia, A.C.M., Levrard, B., 2004. A long-term numerical solution for the insolation quantities of the Earth. *Astron. Astrophys.* 428, 261–285. <https://doi.org/10.1051/0004-6361:20041335>
- Lecavalier, B.S., Milne, G.A., Simpson, M.J.R., Wake, L., Huybrechts, P., Tarasov, L., Kjeldsen, K.K., Funder, S., Long, A.J., Woodroffe, S., Dyke, A.S., Larsen, N.K., 2014. A model of Greenland ice sheet deglaciation constrained by observations of relative sea level and ice extent. *Quat. Sci. Rev.* 102, 54–84. <https://doi.org/10.1016/j.quascirev.2014.07.018>
- Ledu, D., Rochon, A., De Vernal, A., Barletta, F., St-Onge, G., 2010. Holocene sea ice history and climate variability along the main axis of the Northwest Passage, Canadian Arctic. *Paleoceanography* 25, 1–21. <https://doi.org/10.1029/2009PA001817>
- Ledu, D., Rochon, A., De Vernal, A., St-Onge, G., 2008. Palynological evidence of Holocene climate change in the eastern Arctic: A possible shift in the Arctic oscillation at the millennial time scale. *Can. J. Earth Sci.* 45, 1363–1375. <https://doi.org/10.1139/E08-043>

- Leger, T.P.M., Clark, C.D., Huynh, C., Jones, S., Ely, J.C., Sarah, L., Diemont, C., Hughes, A.L.C., 2023. A Greenland-wide empirical reconstruction of paleo ice-sheet retreat informed by ice extent markers : PaleoGrIS version 1 . 0 1–97.
- Lemos, A., Shepherd, A., McMillan, M., Hogg, A.E., Hatton, E., Joughin, I., 2018. Ice velocity of Jakobshavn Isbræ, Petermann Glacier, Nioghalvfjerdsfjorden, and Zachariæ Isstrøm, 2015-2017, from Sentinel 1-a/b SAR imagery. *Cryosphere* 12, 2087–2097. <https://doi.org/10.5194/tc-12-2087-2018>
- Lévesque, Y., St-Onge, G., Lajeunesse, P., Desiagne, P.A., Brouard, E., 2020. Defining the maximum extent of the Laurentide Ice Sheet in Home Bay (eastern Arctic Canada) during the Last Glacial episode. *Boreas* 49, 52–70. <https://doi.org/10.1111/bor.12415>
- Li, G., Piper, D.J.W., Calvin Campbell, D., 2011. The Quaternary Lancaster Sound trough-mouth fan, NW Baffin Bay. *J. Quat. Sci.* 26, 511–522. <https://doi.org/10.1002/jqs.1479>
- Limoges, A., Weckström, K., Ribeiro, S., Georgiadis, E., Hansen, K.E., Martinez, P., Seidenkrantz, M.S., Giraudeau, J., Crosta, X., Massé, G., 2020. Learning from the past: Impact of the Arctic Oscillation on sea ice and marine productivity off northwest Greenland over the last 9,000 years. *Glob. Chang. Biol.* 26, 6767–6786. <https://doi.org/10.1111/gcb.15334>
- Lougheed, B.C., Obrochta, S.P., 2019. A Rapid, Deterministic Age-Depth Modeling Routine for Geological Sequences With Inherent Depth Uncertainty. *Paleoceanogr. Paleoclimatology* 34, 122–133. <https://doi.org/10.1029/2018PA003457>
- Lougheed, B.C., Obrochta, S.P., 2016. MatCal : Open Source Bayesian Matlab. *J. Open Res. Softw.* 4, 1–4.
- Lyle, M., Oliarez Lyle, A., Gorgas, T., Holbourn, A., Westerhold, T., Hathorne, E., Kimoto, K., Yamamoto, S., 2012. Data report: raw and normalized elemental data along the Site U1338 splice from X-ray fluorescence scanning 320. <https://doi.org/10.2204/iodp.proc.320321.203.2012>
- Maccali, J., Hillaire-Marcel, C., Not, C., 2018. Radiogenic isotope (Nd, Pb, Sr) signatures of surface and sea ice-transported sediments from the Arctic Ocean under the present interglacial conditions. *Polar Res.* 37. <https://doi.org/10.1080/17518369.2018.1442982>
- MacLean, B., Blasco, S., Bennett, R., Lakeman, T., Pieńkowski, A.J., Furze, M.F.A., Hughes Clarke, J., Patton, E., 2017. Seafloor features delineate Late Wisconsinan ice stream configurations in eastern Parry Channel, Canadian Arctic Archipelago. *Quat. Sci. Rev.* 160, 67–84. <https://doi.org/10.1016/j.quascirev.2017.02.001>
- Maclean, B., Williams, G L., Srivastava, S.P., 1990. Geology of Baffin Bay and Davis Strait, in: Keen, M.J., Williams, G L (Eds.), *Geology of the Continental Margin of Eastern Canada*. Geological Survey of Canada, pp. 325–348. <https://doi.org/10.4095/132710>
- Madaj, L., 2021. Holocene Ice Sheet Dynamics and Detrital Provenance Shifts Along the West Greenland Margin Recorded by Radiogenic Isotopes. Dissertation, Geosciences, University of Bremen, Bremen, Germany.
- Margold, M., Stokes, C.R., Clark, C.D., 2018. Reconciling records of ice streaming and ice margin retreat to produce a palaeogeographic reconstruction of the deglaciation of the Laurentide Ice Sheet. *Quat. Sci. Rev.* 189, 1–30. <https://doi.org/10.1016/j.quascirev.2018.03.013>
- Margold, M., Stokes, C.R., Clark, C.D., 2015. Ice streams in the Laurentide Ice Sheet: Identification, characteristics and comparison to modern ice sheets. *Earth-Science Rev.* 143, 117–146. <https://doi.org/10.1016/j.earscirev.2015.01.011>
- McCulloch, M.T., Wasserburg, G.J., 1978. Sm-Nd and Rb-Sr Chronology of Continental Crust Formation. *Science* (80-.). 200, 1003–1011. <https://doi.org/10.1126/science.200.4345.1003>
- McGregor, H. V., Dupont, L., Stuut, J.B.W., Kuhlmann, H., 2009. Vegetation change, goats, and religion: a 2000-year history of land use in southern Morocco. *Quat. Sci. Rev.* 28, 1434–1448. <https://doi.org/10.1016/j.quascirev.2009.02.012>

- McKay, N.P., Kaufman, D.S., Routsos, C.C., Erb, M.P., Zander, P.D., 2018. The Onset and Rate of Holocene Neoglacial Cooling in the Arctic. *Geophys. Res. Lett.* 45, 12,487–12,496. <https://doi.org/10.1029/2018GL079773>
- Melia, N., Haines, K., Hawkins, E., 2016. Sea ice decline and 21st century trans-Arctic shipping routes. *Geophys. Res. Lett.* 43, 9720–9728. <https://doi.org/10.1002/2016GL069315>
- Melling, H., Gratton, Y., Ingram, G., 2001. Ocean circulation within the North Water polynya of Baffin Bay. *Atmos. - Ocean* 39, 301–325. <https://doi.org/10.1080/07055900.2001.9649683>
- Meyer, I., Davies, G.R., Stuut, J.-B.B.W., 2011. Grain size control on Sr-Nd isotope provenance studies and impact on paleoclimate reconstructions: An example from deep-sea sediments offshore NW Africa. *Geochemistry Geophys. Geosystems - GEOCHEM Geophys GEOSYST* 12, 1–14. <https://doi.org/10.1029/2010GC003355>
- Miller, G.H., Brigham-Grette, J., Alley, R.B., Anderson, L., Bauch, H.A., Douglas, M.S.V., Edwards, M.E., Elias, S.A., Finney, B.P., Fitzpatrick, J.J., Funder, S. V., Herbert, T.D., Hinzman, L.D., Kaufman, D.S., MacDonald, G.M., Polyak, L., Robock, A., Serreze, M.C., Smol, J.P., Spielhagen, R., White, J.W.C., Wolfe, A.P., Wolff, E.W., 2010. Temperature and precipitation history of the Arctic. *Quat. Sci. Rev.* 29, 1679–1715. <https://doi.org/10.1016/j.quascirev.2010.03.001>
- Miller, G.H., Wolfe, A.P., Briner, J.P., Sauer, P.E., Nesje, A., 2005. Holocene glaciation and climate evolution of Baffin Island, Arctic Canada. *Quat. Sci. Rev.* 24, 1703–1721. <https://doi.org/10.1016/j.quascirev.2004.06.021>
- Mollenhauer, G., Grotheer, H., Gentz, T., Bonk, E., Hefter, J., 2021. Standard operation procedures and performance of the MICADAS radiocarbon laboratory at Alfred Wegener Institute (AWI), Germany. *Nucl. Instruments Methods Phys. Res. Sect. B Beam Interact. with Mater. Atoms* 496, 45–51. <https://doi.org/10.1016/j.nimb.2021.03.016>
- Moore, J.J., Hughen, K.A., Miller, G.H., Overpeck, J.T., 2001. Little Ice Age recorded in summer temperature reconstruction from varved sediments of Donard Lake, Baffin Island, Canada. *J. Paleolimnol.* 25, 503–517. <https://doi.org/10.1023/A:1011181301514>
- Muench, R.D., 1973. Physical Oceanographic Observations in Baffin Bay and Davis Strait. *Arctic* 26, 73–76.
- Münchow, A., Falkner, K.K., Melling, H., 2015. Baffin Island and West Greenland Current Systems in northern Baffin Bay. *Prog. Oceanogr.* 132, 305–317. <https://doi.org/10.1016/j.pocean.2014.04.001>
- Naughton, F., Sánchez-Goñi, M.F., Landais, A., Rodrigues, T., Riveiros, N.V., Toucanne, S., 2023. The Bølling–Allerød Interstadial. *Eur. Glacial Landscapes Last Deglaciation* 45–50. <https://doi.org/10.1016/B978-0-323-91899-2.00015-2>
- Newton, A.M.W., Knutz, P.C., Huuse, M., Gannon, P., Brocklehurst, S.H., Clausen, O.R., Gong, Y., 2017. Ice stream reorganization and glacial retreat on the northwest Greenland shelf. *Geophys. Res. Lett.* 44, 7826–7835. <https://doi.org/10.1002/2017GL073690>
- Nghiem, S. V., Rigor, I.G., Perovich, D.K., Clemente-Colón, P., Weatherly, J.W., Neumann, G., 2007. Rapid reduction of Arctic perennial sea ice. *Geophys. Res. Lett.* 34, 1–6. <https://doi.org/10.1029/2007GL031138>
- Niessen, F., Matthiessen, J., Stein, R., 2009. Sedimentary environment and glacial history of the northwest passage (Canadian arctic archipelago) reconstructed from high-resolution acoustic data. *Polarforschung* 79, 65–80.
- Notz, D., Community, S., 2020. Arctic Sea Ice in CMIP6. *Geophys. Res. Lett.* 47, 1–11. <https://doi.org/10.1029/2019GL086749>
- Notz, D., Stroeve, J., 2018. The Trajectory Towards a Seasonally Ice-Free Arctic Ocean. *Curr. Clim. Chang. Reports* 4, 407–416. <https://doi.org/10.1007/s40641-018-0113-2>
- Notz, D., Stroeve, J., 2016. Observed Arctic sea-ice loss directly follows anthropogenic CO₂ emission.

- Science (80-). 354, 747–750. <https://doi.org/10.1126/science.aag2345>
- Nürnberg, D., Wollenburg, I., Dethleff, D., Eicken, H., Kassens, H., Letzig, T., Reimnitz, E., Thiede, J., 1994. Sediments in Arctic sea ice: Implications for entrainment, transport and release. *Mar. Geol.* 119, 185–214. [https://doi.org/10.1016/0025-3227\(94\)90181-3](https://doi.org/10.1016/0025-3227(94)90181-3)
- Ó Cofaigh, C., Andrews, J.T., Jennings, A.E., Dowdeswell, J.A., Hogan, K.A., Kilfeather, A.A., Sheldon, C., 2013a. Glacimarine lithofacies, provenance and depositional processes on a West Greenland trough-mouth fan. *J. Quat. Sci.* 28, 13–26. <https://doi.org/10.1002/jqs.2569>
- Ó Cofaigh, C., Dowdeswell, J.A., Jennings, A.E., Hogan, K.A., Kilfeather, A., Hiemstra, J.F., Noormets, R., Evans, J., McCarthy, D.J., Andrews, J.T., Lloyd, J.M., Moros, M., 2013b. An extensive and dynamic ice sheet on the west greenland shelf during the last glacial cycle. *Geology* 41, 219–222. <https://doi.org/10.1130/G33759.1>
- Ó Cofaigh, C., Dowdeswell, J.A., Jennings, A.E., Hogan, K.A., Kilfeather, A., Hiemstra, J.F., Noormets, R., Evans, J., McCarthy, D.J., Andrews, J.T., Lloyd, J.M., Moros, M., Cofaigh, C.Ó., Dowdeswell, J.A., Jennings, A.E., Hogan, K.A., Kilfeather, A., Hiemstra, J.F., Noormets, R., Evans, J., Ó Cofaigh, C., Dowdeswell, J.A., Jennings, A.E., Hogan, K.A., Kilfeather, A., Hiemstra, J.F., Noormets, R., Evans, J., McCarthy, D.J., Andrews, J.T., Lloyd, J.M., Moros, M., 2013c. An extensive and dynamic ice sheet on the west greenland shelf during the last glacial cycle. *Geology* 41, 219–222. <https://doi.org/10.1130/G33759.1>
- Ó Cofaigh, C., Taylor, J., Dowdeswell, J., Pudsey, C., 2003. Palaeo-ice streams, trough mouth fans and high-latitude continental slope sedimentation. *Boreas* 32, 37–55. <https://doi.org/10.1080/03009480310001858>
- Okuma, E., Hingst, J., Weiser, J., Madaj, L., Titschack, J., Vogt, C., Kienast, M., Hillaire-Marcel, C., Hebbeln, D., Kasemann, S.A., 2023. Deglacial and Holocene sediment dynamics and provenances off Lancaster Sound: Implications for paleoenvironmental conditions in northern Baffin Bay. *Quat. Sci. Rev.* 309, 108101. <https://doi.org/10.1016/j.quascirev.2023.108101>
- Olsen, I.L., Laberg, J.S., Forwick, M., Rydningen, T.A., Husum, K., 2022. Late Weichselian and Holocene behavior of the Greenland Ice Sheet in the Kejser Franz Josef Fjord system, NE Greenland. *Quat. Sci. Rev.* 284, 107504. <https://doi.org/https://doi.org/10.1016/j.quascirev.2022.107504>
- Ottesen, D., Batchelor, C.L., Bjarnadóttir, L.R., Wiberg, D.H., Dowdeswell, J.A., 2022. Glacial landforms reveal dynamic ice-sheet behaviour along the mid-Norwegian margin during the last glacial-deglacial cycle. *Quat. Sci. Rev.* 285. <https://doi.org/10.1016/j.quascirev.2022.107462>
- Overeem, I., Hudson, B.D., Syvitski, J.P.M., Mikkelsen, A.B., Hasholt, B., Van Den Broeke, M.R., Noel, B.P.Y., Morlighem, M., 2017. Substantial export of suspended sediment to the global oceans from glacial erosion in Greenland. *Nat. Geosci.* 10, 859–863. <https://doi.org/10.1038/NGEO3046>
- Overland, J., Dunlea, E., Box, J.E., Corell, R., Forsius, M., Kattsov, V., Olsen, M.S., Pawlak, J., Reiersen, L.O., Wang, M., 2019. The urgency of Arctic change. *Polar Sci.* 21, 6–13. <https://doi.org/10.1016/j.polar.2018.11.008>
- Owensworth, E., Selby, D., Lloyd, J., Knutz, P., Szidat, S., Andrews, J., Ó Cofaigh, C., 2023. Tracking sediment delivery to central Baffin Bay during the past 40 kyrs: Insights from a multiproxy approach and new age model. *Quat. Sci. Rev.* 308. <https://doi.org/10.1016/j.quascirev.2023.108082>
- Perner, K., Moros, M., Jennings, A., Lloyd, J.M., Knudsen, K.L., 2013. Holocene palaeoceanographic evolution off West Greenland. *Holocene* 23, 374–387. <https://doi.org/10.1177/0959683612460785>
- Petschick, R., Kuhn, G., Gingele, F., 1996. Clay mineral distribution in surface sediments of the South Atlantic: Sources, transport, and relation to oceanography. *Mar. Geol.* 130, 203–229. [https://doi.org/10.1016/0025-3227\(95\)00148-4](https://doi.org/10.1016/0025-3227(95)00148-4)
- Pieńkowski, A.J., Coulthard, R.D., Furze, M.F.A., 2022. Revised marine reservoir offset (ΔR) values

for molluscs and marine mammals from Arctic North America . *Boreas*.
<https://doi.org/10.1111/bor.12606>

- Pieńkowski, A.J., England, J.H., Furze, M.F.A., Blasco, S., Mudie, P.J., MacLean, B., 2013. 11,000yrs of environmental change in the northwest passage: A multiproxy core record from central parry channel, canadian high arctic. *Mar. Geol.* 341, 68–85. <https://doi.org/10.1016/j.margeo.2013.04.008>
- Pieńkowski, A.J., England, J.H., Furze, M.F.A., MacLean, B., Blasco, S., 2014. The late Quaternary environmental evolution of marine Arctic Canada: Barrow Strait to Lancaster Sound. *Quat. Sci. Rev.* 91, 184–203. <https://doi.org/10.1016/j.quascirev.2013.09.025>
- Pieńkowski, A.J., England, J.H., Furze, M.F.A., Marret, F., Eynaud, F., Vilks, G., MacLean, B., Blasco, S., Scourse, J.D., 2012. The deglacial to postglacial marine environments of SE Barrow Strait, Canadian Arctic Archipelago, *Boreas*. <https://doi.org/10.1111/j.1502-3885.2011.00227.x>
- Pin, C., Briot, D., Bassin, C., Poitrasson, F., 1994. Concomitant separation of strontium and samarium-neodymium for isotopic analysis in silicate samples, based on specific extraction chromatography. *Anal. Chim. Acta* 298, 209–217. [https://doi.org/10.1016/0003-2670\(94\)00274-6](https://doi.org/10.1016/0003-2670(94)00274-6)
- Piper, D.J.W., Farre, J.A., Shor, A., 1985. Late Quaternary slumps and debris flows on the Scotian Slope. *Geol. Soc. Am. Bull.* 96, 1508–1517. [https://doi.org/10.1130/0016-7606\(1985\)96<1508:LQSADF>2.0.CO;2](https://doi.org/10.1130/0016-7606(1985)96<1508:LQSADF>2.0.CO;2)
- Polyakov, I. V., Walsh, J.E., Kwok, R., 2012. Recent changes of Arctic multiyear sea ice coverage and the likely causes. *Bull. Am. Meteorol. Soc.* 93, 145–151. <https://doi.org/10.1175/BAMS-D-11-00070.1>
- Praeg, D., Maclean, B., Sonnichsen, G., 2007. Quaternary Geology of the Northeast Baffin Island Continental Shelf, Cape Aston to Buchan Gulf (70° to 72°N). Geological Survey of Canada Open File 5409 1–98.
- Previdi, M., Smith, K.L., Polvani, L.M., 2021. Arctic amplification of climate change: A review of underlying mechanisms. *Environ. Res. Lett.* 16. <https://doi.org/10.1088/1748-9326/ac1c29>
- Radić, V., Bliss, A., Beedlow, A.C., Hock, R., Miles, E., Cogley, J.G., 2014. Regional and global projections of twenty-first century glacier mass changes in response to climate scenarios from global climate models. *Clim. Dyn.* 42, 37–58. <https://doi.org/10.1007/s00382-013-1719-7>
- Rantanen, M., Karpechko, A.Y., Lipponen, A., Nordling, K., Hyvärinen, O., Ruosteenoja, K., Vihma, T., Laaksonen, A., 2022. The Arctic has warmed nearly four times faster than the globe since 1979. *Commun. Earth Environ.* 3, 1–10. <https://doi.org/10.1038/s43247-022-00498-3>
- Rasmussen, S.O., Bigler, M., Blockley, S.P., Blunier, T., Buchardt, S.L., Clausen, H.B., Cvijanovic, I., Dahl-Jensen, D., Johnsen, S.J., Fischer, H., Gkinis, V., Guillevic, M., Hoek, W.Z., Lowe, J.J., Pedro, J.B., Popp, T., Seierstad, I.K., Steffensen, J.P., Svensson, A.M., Vallelonga, P., Vinther, B.M., Walker, M.J.C., Wheatley, J.J., Winstrup, M., 2014. A stratigraphic framework for abrupt climatic changes during the Last Glacial period based on three synchronized Greenland ice-core records: Refining and extending the INTIMATE event stratigraphy. *Quat. Sci. Rev.* 106, 14–28. <https://doi.org/10.1016/j.quascirev.2014.09.007>
- Reimer, P.J., Bard, E., Bayliss, A., Beck, J.W., Blackwell, P.G., Ramsey, C.B., Buck, C.E., Cheng, H., Edwards, R.L., Friedrich, M., Grootes, P.M., Guilderson, T.P., Hafliðason, H., Hajdas, I., Hatté, C., Heaton, T.J., Hoffmann, D.L., Hogg, A.G., Hughen, K.A., Kaiser, K.F., Kromer, B., Manning, S.W., Niu, M., Reimer, R.W., Richards, D.A., Scott, E.M., Southon, J.R., Staff, R.A., Turney, C.S.M., van der Plicht, J., 2013. IntCal13 and Marine13 Radiocarbon Age Calibration Curves 0–50,000 Years cal BP. *Radiocarbon* 55, 1869–1887. https://doi.org/10.2458/azu_js_rc.55.16947
- Ren, H., Shokr, M., Li, X., Zhang, Z., Hui, F., 2022. Estimation of Sea Ice Production in the North Water Polynya Based on Ice Arch Duration in Winter During 2006 – 2019 *Journal of Geophysical Research : Oceans*. <https://doi.org/10.1029/2022JC018764>

- Reyes, A. V., Carlson, A.E., Beard, B.L., Hatfield, R.G., Stoner, J.S., Winsor, K., Welke, B., Ullman, D.J., 2014. South Greenland ice-sheet collapse during Marine Isotope Stage 11. *Nature* 510, 525–528. <https://doi.org/10.1038/nature13456>
- Rignot, E., Kanagaratnam, P., 2006. Changes in the velocity structure of the Greenland Ice Sheet. *Science* (80-.). 311, 986–990. <https://doi.org/10.1126/science.1121381>
- Ritz, S.P., Stocker, T.F., Grimalt, J.O., Menviel, L., Timmermann, A., 2013. Estimated strength of the Atlantic overturning circulation during the last deglaciation. *Nat. Geosci.* 6, 208–212. <https://doi.org/10.1038/ngeo1723>
- Saini, J., Stein, R., Fahl, K., Weiser, J., Hebbeln, D., Hillaire-Marcel, C., de Vernal, A., 2020. Holocene variability in sea ice and primary productivity in the northeastern Baffin Bay. *Arktos* 1–19. <https://doi.org/10.1007/s41063-020-00075-y>
- Saini, J., Stein, R., Fahl, K., Weiser, J., Hebbeln, D., Madaj, L., 2022. Holocene variability in sea-ice conditions in the eastern Baffin Bay-Labrador Sea – A north–south biomarker transect study. *Boreas* 51, 553–572. <https://doi.org/10.1111/bor.12583>
- Schlitzer, R., 2019. Ocean Data View. <http://odv.awi.de>. <https://doi.org/10.5670/oceanog.1998.04>
- Scott, D.J., de Kemp, E.A., 1998. Bedrock geology compilation, northern Baffin Island and northern Melville Peninsula, Northwest Territories. Geological Survey of Canada, Open File 3633. <https://doi.org/10.4095/210024>
- Screen, J.A., 2017. Climate science: Far-flung effects of Arctic warming. *Nat. Geosci.* 10, 253–254. <https://doi.org/10.1038/ngeo2924>
- Screen, J.A., Deser, C., Simmonds, I., 2012. Local and remote controls on observed Arctic warming. *Geophys. Res. Lett.* 39, 1–5. <https://doi.org/10.1029/2012GL051598>
- Serreze, M.C., Barrett, A.P., Stroeve, J.C., Kindig, D.N., Holland, M.M., 2009. The emergence of surface-based Arctic amplification. *Cryosphere* 3, 11–19. <https://doi.org/10.5194/tc-3-11-2009>
- Serreze, M.C., Francis, J.A., 2006. The arctic amplification debate. *Clim. Change* 76, 241–264. <https://doi.org/10.1007/s10584-005-9017-y>
- Sheldon, C., Jennings, A., Andrews, J.T., Ó Cofaigh, C., Hogan, K., Dowdeswell, J.A., Seidenkrantz, M.S., 2016. Ice stream retreat following the LGM and onset of the west Greenland current in Ummannaq Trough, west Greenland. *Quat. Sci. Rev.* 147, 27–46. <https://doi.org/10.1016/j.quascirev.2016.01.019>
- Shen, Z., Zhou, W., Li, J., Chan, J.C.L., 2023. A frequent ice-free Arctic is likely to occur before the mid-21st century. *npj Clim. Atmos. Sci.* 6, 1–7. <https://doi.org/10.1038/s41612-023-00431-1>
- Simon, Q., Hillaire-Marcel, C., St-Onge, G., Andrews, J.T., 2014. North-eastern Laurentide, western Greenland and southern Inuitian ice stream dynamics during the last glacial cycle. *J. Quat. Sci.* 29, 14–26. <https://doi.org/10.1002/jqs.2648>
- Simon, Q., St-Onge, G., Hillaire-Marcel, C., 2012. Late Quaternary chronostratigraphic framework of deep Baffin Bay glaciomarine sediments from high-resolution paleomagnetic data. *Geochemistry, Geophys. Geosystems* 13, 1–24. <https://doi.org/10.1029/2012GC004272>
- Simon, Q., Thouveny, N., Bourlès, D.L., Nuttin, L., Hillaire-Marcel, C., St-Onge, G., 2016. Authigenic $^{10}\text{Be}/^{9}\text{Be}$ ratios and ^{10}Be -fluxes (^{230}Th -normalized) in central Baffin Bay sediments during the last glacial cycle: Paleoenvironmental implications. *Quat. Sci. Rev.* 140, 142–162. <https://doi.org/10.1016/j.quascirev.2016.03.027>
- Skinner, L.C., Bard, E., 2022. Radiocarbon as a Dating Tool and Tracer in Paleoceanography. *Rev. Geophys.* 60, 1–64. <https://doi.org/10.1029/2020RG000720>
- Slabon, P., Dorschel, B., Jokat, W., Myklebust, R., Hebbeln, D., Gebhardt, C., 2016. Greenland ice sheet retreat history in the northeast Baffin Bay based on high-resolution bathymetry. *Quat. Sci. Rev.* 154, 182–198. <https://doi.org/10.1016/j.quascirev.2016.10.022>

- Slater, D.A., Straneo, F., 2022. Submarine melting of glaciers in Greenland amplified by atmospheric warming. *Nat. Geosci.* 15, 794–799. <https://doi.org/10.1038/s41561-022-01035-9>
- Smith, D.M., Screen, J.A., Deser, C., Cohen, J., Fyfe, J.C., García-Serrano, J., Jung, T., Kattsov, V., Matei, D., Msadek, R., Peings, Y., Sigmond, M., Ukita, J., Zhang, X., 2019. The Polar Amplification Model Intercomparison Project (PAMIP) contribution to CMIP6: Investigating the causes and consequences of polar amplification. *Geosci. Model Dev.* 12, 1139–1164. <https://doi.org/10.5194/gmd-12-1139-2019>
- Smith, L.C., Stephenson, S.R., 2013. New Trans-Arctic shipping routes navigable by midcentury. *Proc. Natl. Acad. Sci. U. S. A.* 110, 6–10. <https://doi.org/10.1073/pnas.1214212110>
- St-Onge, M., van Gool, J., Garde, A., Scott, D., 2009. Correlation of Archaean and Palaeoproterozoic units between northeastern Canada and western Greenland: Constraining the pre-collisional upper late accretionary history of the Trans-Hudson orogen. *Geol. Soc. London, Spec. Publ.* 318, 193–235. <https://doi.org/10.1144/SP318.7>
- St-Onge, M.P., St-Onge, G., 2014. Environmental changes in Baffin Bay during the Holocene based on the physical and magnetic properties of sediment cores. *J. Quat. Sci.* 29, 41–56. <https://doi.org/10.1002/jqs.2674>
- Stalling, D., Westerhoff, M., Hege, H.C., 2005. Amira: A highly interactive system for visual data analysis, *Visualization Handbook*. Elsevier Inc. <https://doi.org/10.1016/B978-012387582-2/50040-X>
- Stearns, L.A., Hamilton, G.S., 2007. Rapid volume loss from two East Greenland outlet glaciers quantified using repeat stereo satellite imagery. *Geophys. Res. Lett.* 34, 1–5. <https://doi.org/10.1029/2006GL028982>
- Stein, R., 2008a. Arctic Ocean Sediments: Processes, Proxies, and Paleoenvironment. [https://doi.org/10.1016/s1572-5480\(08\)00014-6](https://doi.org/10.1016/s1572-5480(08)00014-6)
- Stein, R., 2008b. Chapter Three Glacio-Marine Sedimentary Processes. *Dev. Mar. Geol.* 2, 87–132. [https://doi.org/10.1016/S1572-5480\(08\)00003-1](https://doi.org/10.1016/S1572-5480(08)00003-1)
- Stein, R., Niessen, F., Matthiessen, J., 2009: Marine Geology.- In: W. Jokat (ed), *The Expedition of the Research Vessel “Polarstern” to the Arctic in 2008 (ARK-XXIII/3)*, Rep. Polar Mar, Res. 597: 12–15.
- Stevenard, N., Montero-Serrano, J.C., Eynaud, F., St-Onge, G., Zaragosi, S., Copland, L., 2022. Lateglacial and Holocene sedimentary dynamics in northwestern Baffin Bay as recorded in sediment cores from Cape Norton Shaw Inlet (Nunavut, Canada). *Boreas* 51, 532–552. <https://doi.org/10.1111/bor.12575>
- Stevenard, N., St-onge, G., Ed, F.R., Bay, B., 2021. Lateglacial and Holocene sedimentary dynamics in northwestern Baffin Bay as recorded in sediment cores from Cape Norton Shaw Inlet (Nunavut , Canada) Ellesmere Island. <https://doi.org/10.1111/bor.12575>
- Stokes, C.R., Tarasov, L., Blomdin, R., Cronin, T.M., Fisher, T.G., Gyllencreutz, R., Hättstrand, C., Heyman, J., Hindmarsh, R.C.A., Hughes, A.L.C., Jakobsson, M., Kirchner, N., Livingstone, S.J., Margold, M., Murton, J.B., Noormets, R., Peltier, W.R., Peteet, D.M., Piper, D.J.W., Preusser, F., Renssen, H., Roberts, D.H., Roche, D.M., Saint-Ange, F., Stroeven, A.P., Teller, J.T., 2015. On the reconstruction of palaeo-ice sheets: Recent advances and future challenges. *Quat. Sci. Rev.* 125, 15–49. <https://doi.org/10.1016/j.quascirev.2015.07.016>
- Stokes, C.R., Tarasov, L., Dyke, A.S., 2012. Dynamics of the North American Ice Sheet Complex during its inception and build-up to the Last Glacial Maximum. *Quat. Sci. Rev.* 50, 86–104. <https://doi.org/10.1016/j.quascirev.2012.07.009>
- Streuff, K., Ó Cofaigh, C., Hogan, K., Jennings, A., Lloyd, J.M., Noormets, R., Nielsen, T., Kuijpers, A., Dowdeswell, J.A., Weinrebe, W., 2017. Seafloor geomorphology and glacimarine sedimentation associated with fast-flowing ice sheet outlet glaciers in Disko Bay, West Greenland.

- Quat. Sci. Rev. 169, 206–230. <https://doi.org/10.1016/j.quascirev.2017.05.021>
- Stroeve, J.C., Kattsov, V., Barrett, A., Serreze, M., Pavlova, T., Holland, M., Meier, W.N., 2012. Trends in Arctic sea ice extent from CMIP5, CMIP3 and observations. *Geophys. Res. Lett.* 39, 1–7. <https://doi.org/10.1029/2012GL052676>
- Stuiver, M., Reimer, P.J., 1993. Extended program. *Radiocarbon* 35, 215–230.
- Syvitski, J.P.M., 1991. Towards an understanding of sediment deposition on glaciated continental shelves. *Cont. Shelf Res.* 11, 897–937. [https://doi.org/10.1016/0278-4343\(91\)90085-K](https://doi.org/10.1016/0278-4343(91)90085-K)
- Tang, C.C.L., Ross, C.K., Yao, T., Petrie, B., DeTracey, B.M., Dunlap, E., 2004. The circulation, water masses and sea-ice of Baffin Bay. *Prog. Oceanogr.* 63, 183–228. <https://doi.org/10.1016/j.pocean.2004.09.005>
- Thomas, E.K., Castañeda, I.S., McKay, N.P., Briner, J.P., Salacup, J.M., Nguyen, K.Q., Schweinsberg, A.D., 2018. A Wetter Arctic Coincident With Hemispheric Warming 8,000 Years Ago. *Geophys. Res. Lett.* 45, 10,637–10,647. <https://doi.org/10.1029/2018GL079517>
- Thomas, E.K., Cluett, A.A., Erb, M.P., McKay, N.P., Jason, P., Castañeda, I.S., Corcoran, M.C., Cowling, O.C., Gorbey, D.B., Lindberg, K.R., Prince, K.K., Salacup, J., 2023. Early Holocene Laurentide Ice Sheet Retreat Influenced Summer Atmospheric Circulation in Baffin Bay *Geophysical Research Letters*. <https://doi.org/10.1029/2023GL103428>
- Thomas, E.K., Szymanski, J.S., Briner, J.P., 2010. Holocene alpine glaciation inferred from lacustrine sediments on northeastern Baffin Island, Arctic Canada. *J. Quat. Sci.* 25.
- Tjallingii, R., Röhl, U., Kölling, M., Bickert, T., 2007. Influence of the water content on X-ray fluorescence corescanning measurements in soft marine sediments. *Geochemistry, Geophys. Geosystems* 8, 1–12. <https://doi.org/10.1029/2006GC001393>
- Tütken, T., Eisenhauer, A., Wiegand, B., Hansen, B., 2002. Glacial–interglacial cycles in Sr and Nd isotopic composition of Arctic marine sediments triggered by the Svalbard/Barents Sea ice sheet. *Mar. Geol.* 182, 351–372. [https://doi.org/10.1016/S0025-3227\(01\)00248-1](https://doi.org/10.1016/S0025-3227(01)00248-1)
- Vare, L.L., Massé, G., Gregory, T.R., Smart, C.W., Belt, S.T., 2009. Sea ice variations in the central Canadian Arctic Archipelago during the Holocene. *Quat. Sci. Rev.* 28, 1354–1366. <https://doi.org/10.1016/j.quascirev.2009.01.013>
- Vasskog, K., Langebroek, P.M., Andrews, J.T., Nilsen, J.E.Ø., Nesje, A., 2015. The Greenland Ice Sheet during the last glacial cycle: Current ice loss and contribution to sea-level rise from a palaeoclimatic perspective. *Earth-Science Rev.* 150, 45–67. <https://doi.org/10.1016/j.earscirev.2015.07.006>
- Vinther, B.M., Clausen, H.B., Johnsen, S.J., Rasmussen, S.O., Andersen, K.K., Buchardt, S.L., Dahl-Jensen, D., Seierstad, I.K., Siggaard-Andersen, M.L., Steffensen, J.P., Svensson, A., Olsen, J., Heinemeier, J., 2006. A synchronized dating of three Greenland ice cores throughout the Holocene. *J. Geophys. Res. Atmos.* 111, 1–11. <https://doi.org/10.1029/2005JD006921>
- Vogt, C., Lauterjung, J., Fischer, R.X., 2002. Investigation of the clay fraction (<2 µm) of the clay minerals society reference clays. *Clays Clay Miner.* 50, 388–400. <https://doi.org/10.1346/000986002760833765>
- Vorren, T.O., Laberg, J.A.N.S., Blaume, F., Dowdeswell, J.A., Kenyon, N.H., Mienert, J., Rumohr, J.A.N., Werner, F., 1998. The Norwegian–Greenland Sea Continental Margins: Morphology and Late Quaternary Sedimentary Processes and Environment. *Quat. Sci. Rev.* 17, 273–302. [https://doi.org/https://doi.org/10.1016/S0277-3791\(97\)00072-3](https://doi.org/https://doi.org/10.1016/S0277-3791(97)00072-3)
- Wang, M., Overland, J.E., 2012. A sea ice free summer Arctic within 30 years: An update from CMIP5 models. *Geophys. Res. Lett.* 39. <https://doi.org/10.1029/2012GL052868>
- Weatherall, P., Marks, K.M., Jakobsson, M., Schmitt, T., Tani, S., Arndt, J.E., Rovere, M., Chayes, D., Ferrini, V., Wigley, R., 2015. A new digital bathymetric model of the world’s oceans. *Earth Sp.*

Sci. 2, 331–345. <https://doi.org/https://doi.org/10.1002/2015EA000107>

- Weidick, A., Bennike, O., 2007. Quaternary glaciation history and glaciology of Jakobshavn Isbræ and the Disko Bugt region, West Greenland: A review, Geological Survey of Denmark and Greenland Bulletin.
- Weiser, J., Titschack, J., Hebbeln, D., 2023. The deglaciation of Upernavik trough, West Greenland, and its Holocene sediment infill: processes and provenance. *Boreas*. <https://doi.org/10.1111/bor.12626>
- Weiser, J., Titschack, J., Kienast, M., McCave, I.N., Lochte, A.A., Saini, J., Stein, R., Hebbeln, D., 2021. Atlantic water inflow to Labrador Sea and its interaction with ice sheet dynamics during the Holocene. *Quat. Sci. Rev.* 256, 106833. <https://doi.org/10.1016/j.quascirev.2021.106833>
- Weltje, G., Bloemsa, M., Tjallingii, R., Heslop, D., Röhl, U., Croudace, Ian, Croudace, I, 2015. Prediction of Geochemical Composition from XRF Core Scanner Data: A New Multivariate Approach Including Automatic Selection of Calibration Samples and Quantification of Uncertainties. pp. 507–534. https://doi.org/10.1007/978-94-017-9849-5_21
- Weltje, G.J., Tjallingii, R., 2008. Calibration of XRF core scanners for quantitative geochemical logging of sediment cores: Theory and application. *Earth Planet. Sci. Lett.* 274, 423–438. <https://doi.org/10.1016/j.epsl.2008.07.054>
- Yadav, J., Kumar, A., Mohan, R., 2020. Dramatic decline of Arctic sea ice linked to global warming. *Nat. Hazards* 103, 2617–2621. <https://doi.org/10.1007/s11069-020-04064-y>
- Young, N.E., Briner, J.P., Maurer, J., Schaefer, J.M., 2016. 10Be measurements in bedrock constrain erosion beneath the Greenland Ice Sheet margin. *Geophys. Res. Lett.* 43, 11,708–11,719. <https://doi.org/10.1002/2016GL070258>
- Young, N.E., Briner, J.P., Rood, D.H., Finkel, R.C., 2012. Glacier extent during the Younger Dryas and 8.2-ka event on Baffin Island, Arctic Canada. *Science* 337, 1330–1333. <https://doi.org/10.1126/science.1222759>
- Zreda, M., England, J., Phillips, F., Elmore, D., Sharma, P., 1999. Unblocking of the Nares Strait by Greenland and Ellesmere ice-sheet retreat 10,000 years ago. *Nature* 398, 139–142. <https://doi.org/10.1038/18197>

Chapter 9

9. Appendices

9.1 Supplement to Manuscript I (Chapter 4)

Table 9.1.1: Sr and Nd isotope composition of the detrital sediment fraction of core GeoB22336-4 from the mouth of Lancaster Sound in northern Baffin Bay. ϵNd values were calculated using the CHUR value of 0.512638 (Jacobsen & Wasserburg, 1980). Uncertainties (2SD_{mean}) are given for the last digit.

Sample ID	Depth [cm]		Age [ka BP]	Radiogenic isotope data [dt fraction]		
	Top	Bottom		$^{87}\text{Sr}/^{86}\text{Sr}$	$^{143}\text{Nd}/^{144}\text{Nd}$	ϵNd
JH38	20	21	0.567	0.737083±10	0.511384±6	-24.46
JH39	60	61	1.700	0.738320±8	0.511336±7	-25.40
JH74	80	81	2.3	0.739444±11	0.511486±4	-22.47
JH40	100	101	2.978	0.740838±8	0.511467±6	-22.84
JH75	120	121	3.627	0.740862±11	0.511495±6	-22.30
JH76	140	141	4.235	0.741112±10	0.511488±5	-22.43
JH41	160	161	4.9	0.741854±8	0.511283±8	-26.43
JH42	200	201	6.137	0.742466±9	0.511472±5	-22.75
JH77	230	231	6.728	0.741940±9	0.511492±6	-22.35
JH43	260	261	7.376	0.742783±7	0.511472±7	-22.75
JH78	280	281	7.791	0.742551±7	0.511488±5	-22.43
JH44	300	301	8.273	0.742471±8	0.511482±5	-22.55
JH79	310	311	8.575	0.740623±9	0.511547±6	-21.28

JH80	320	321	8.887	0.738791±9	0.511591±4	-20.42
JH81	330	331	9.217	0.739496±9	0.511567±5	-20.89
JH82	340	341	9.546	0.739833±11	0.511553±4	-21.17
JH83	350	351	9.916	0.740025±8	0.511575±6	-20.74
JH45	360	361	10.149	0.742119±8	0.511488±5	-22.43
JH46	380	381	10.436	0.741508±8	0.511286±6	-26.37
JH47	400	401	10.707	0.743261±9	0.511429±4	-23.58
JH48	420	421	10.997	0.745302±8	0.511321±4	-25.69
JH49	440	441	11.300	0.746470±8	0.511279±5	-26.51
JH84	450	451	11.441	0.746333±8	0.511342±4	-25.28
JH50	470	471	11.665	0.733335±9	0.511676±5	-18.77
JH51	490	491	12.374	0.736263±8	0.511174±8	-28.56
JH52	500	501	12.748	0.745270±7	0.511301±4	-26.08
JH53	520	521	13.196	0.741352±9	0.511282±6	-26.45
JH85	530	531	13.403	0.741204±9	0.511331±4	-25.50
JH54	540	541	13.611	0.746604±8	0.511560±5	-21.03
JH55	550	551	13.833	0.742983±7	0.511298±5	-26.14
JH56	580	581	14.543	0.738149±9	0.511285±6	-26.39
JH57	600	601	15.023	0.738269±9	0.511262±5	-26.84

Table 9.1.2: Sr and Nd isotope composition of the detrital sediment fraction of core PS72/287-3 from Barrow Strait. Chronology estimation is based on Parasound data and correlation with the dated core ARC-3 (Vare et al., 2009; Stein et al., 2009; Niessen et al., 2010). ϵNd values were calculated using the CHUR value of 0.512638 (Jacobsen & Wasserburg, 1980). Uncertainties (2SD_{mean}) are given for the last digit.

Sample ID	Depth [cm]		Time Interval	Radiogenic isotope data (dt fraction)		
	Top	Bottom		$^{87}\text{Sr}/^{86}\text{Sr}$	$^{143}\text{Nd}/^{144}\text{Nd}$	ϵNd
JH 58	10	11	Holocene	0.736352±8	0.511718±5	-17.9
JH 59	30	31	Holocene	0.736225±8	0.511715±6	-18.0
JH 60	50	51	Holocene	0.736881±8	0.511724±5	-17.8
JH 61	103	104	Holocene	0.736056±7	0.511674±4	-18.8
JH 62	150	151	Holocene	0.733013±8	0.511807±5	-16.2
JH 63	200	201	Holocene	0.733351±8	0.511779±5	-16.8
JH 64	250	251	Holocene	0.734265±9	0.511716±5	-18.0

Table 9.1.3: Sr and Nd isotope composition of the detrital sediment fraction of core GeoB22357-3 from the Clyde inlet shelf. ϵNd values were calculated using the CHUR value of 0.512638 (Jacobsen & Wasserburg, 1980). Uncertainties (2SD_{mean}) are given for the last digit.

Sample ID	Depth [cm]		Radiogenic isotope data (dt fraction)		
	Top	Bottom	$^{87}\text{Sr}/^{86}\text{Sr}$	$^{143}\text{Nd}/^{144}\text{Nd}$	ϵNd
JH14	10	11	0.747755±7	0.510877±5	-34.4
JH15	29	30	0.744270±8	0.510931±5	-33.3
JH16	54	55	0.743368±8	0.510925±6	-33.4
JH17	104	105	0.748314±9	0.510843±6	-35.0

JH18	154	155	0.749524±8	0.510821±6	-35.4
JH19	204	205	0.751774±8	0.510789±5	-36.1
JH20	254	255	0.749871±8	0.510802±6	-35.8
JH21	263	264	0.749620±8	0.510812±6	-35.6
JH22	304	305	0.753249±8	0.510759±5	-36.7
JH23	354	355	0.755961±9	0.510757±9	-36.7
JH24	381	382	0.759324±8	0.510694±5	-37.9
JH25	404	405	0.758853±9	0.510710±6	-37.6
JH26	454	455	0.757921±9	0.510742±5	-37.0
JH27	504	505	0.759452±8	0.510748±5	-36.9
JH28	554	555	0.758465±9	0.510687±5	-38.1
JH29	604	605	0.761015±8	0.510653±5	-38.7
JH30	654	655	0.753654±9	0.510731±6	-37.2
JH31	704	705	0.760297±8	0.510663±6	-38.5
JH32	726	727	0.749546±9	0.510772±5	-36.4
JH33	752	753	0.745626±8	0.510852±5	-34.8
JH34	778	779	0.750817±9	0.510766±5	-36.5
JH35	804	805	0.755883±9	0.510738±6	-37.1
JH36	841	842	0.749074±8	0.510815±5	-35.6
JH37	876	877	0.743568±8	0.510942±5	-33.1

Table 9.1.4: Compilation of AMS radiocarbon dates from sediment cores 144PC (Pieńkowski et al., 2012), 154PC (Pieńkowski et al., 2014), 49PC (Kelleher et al., 2022), 42PC (St-Onge and St-Onge, 2014), 117Q (Jackson et al., 2021), GeoB19948-3 (Saini et al., 2022), 14PC (Jennings et al., 2019), 05GC (Jennings et al., 2011), and Kane2B (Georgiadis et al., 2018) re-calibrated here to calculate sedimentation rates on a common age scale as shown in Figure S4.1. (see Figure 1 for core locations). All ^{14}C ages were calibrated using the Marine20 dataset (Heaton et al., 2020) and applying a regional reservoir correction (ΔR) of 81 ± 18 years (after Pieńkowski et al., 2022) for mid and late-Holocene ages and variable ΔR values, described in the text, for older ages (after Kelleher et al., 2022). Calibrated ages are the median age and 95% confidence interval (in parenthesis) based on Calib 8.20 (Stuiver & Reimer, 1993). Abbreviations: BF, benthic foraminifera; PF, planktic foraminifera; MBF, mixed benthic foraminifera; MBPF, mixed benthic and planktic foraminifera; O, ostracods.

Core ID	Location	Lab ID	Depth	^{14}C Age	^{14}C -error	ΔR	Calibrated age (yrs BP)	Material
			(cm)	(yrs)	(yrs)	(yrs)	Median (2 σ range)	
144PC	Barrow Strait	OS-70925	31–34	4540	55	81 ± 18	4440 (4219 – 4676)	MBF
144PC	Barrow Strait	UCIAMS-37923	82–85	5820	30	81 ± 18	5949 (5763 – 6125)	MBF
144PC	Barrow Strait	TO-752	168–175	8380	70	141 ± 50	8564 (8333 – 8863)	<i>Bathyarca glacialis</i>
144PC	Barrow Strait	TO-1863	215–216	9450	190	311 ± 50	9721 (9221 – 10230)	<i>Portlandia arctica</i>
144PC	Barrow Strait	OS-77147	247–248	9900	45	366 ± 50	10235 (10008 – 10848)	<i>Yoldiella fraterna</i>
144PC	Barrow Strait	UCIAMS-37924	302–305	10610	80	411 ± 50	11149 (10794 – 11457)	MBF
154PC	Barrow Strait	OS-78360	0–2	2310	40	81 ± 18	1651 (1489 – 1825)	BF (<i>Dentalina sp.</i>)
154PC	Barrow Strait	OS-71079	20–24	7070	60	81 ± 18	7304 (7131 – 7478)	Mollusc shell
154PC	Barrow Strait	OS-70904	67–70	9340	50	281 ± 50	9588 (9398 – 9854)	<i>Yoldiella fraterna</i>
154PC	Barrow Strait	OS-70883	154–156	9790	50	351 ± 50	10105 (9838 – 10342)	<i>Yoldiella fraterna</i>
154PC	Barrow Strait	OS-79109	196–200	10500	60	411 ± 50	10998 (10717 – 11221)	O (<i>Heterocyprideis sorbyana</i>)
154PC	Barrow Strait	OS-78357	229–231	10750	60	411 ± 50	11337 (11102 – 11635)	MBF
49PC	N. Baffin Bay	NSRL-39519	195	8410	40	81 ± 18	8678 (8484 – 8910)	Algae (Seaweed)
49PC	N. Baffin Bay	NSRL-39504	215	8605	54	171 ± 50	8819 (8565 – 9060)	MBF (<i>I. norcrossi</i> , <i>N. labradorica</i> , <i>C. neoteretis</i>)

49PC	N. Baffin Bay	NSRL-41641	245	9510	64	311 ± 50	9759 (9516 – 10071)	MBF (<i>I. norcrossi</i> , <i>N. labradorica</i>)
49PC	N. Baffin Bay	NSRL-41642	265	9770	64	351 ± 50	10074 (9773 – 10328)	MBF (<i>I. norcrossi</i> , <i>N. labradorica</i>)
49PC	N. Baffin Bay	NSRL-39506	295	10150	56	411 ± 50	10492 (10232 – 10737)	Mollusc (<i>Yoldiella lenticula</i>)
49PC	N. Baffin Bay	NSRL-39507	325	10575	56	411 ± 50	11106 (10795 – 11323)	BF (<i>E. clavatum</i>)
49PC	N. Baffin Bay	NSRL-39509	408	10710	56	411 ± 50	11283 (11066 – 11583)	MBF (<i>I. norcrossi</i> , <i>C. reniforme</i>)
42PC	N. Baffin Bay	CAMS-150984	42	975	55	81 ± 18	356 (177 – 505)	Shell fragments
42PC	N. Baffin Bay	UCIAMS-61336	598	6305	55	81 ± 18	6461 (6281 – 6649)	Shell fragments
42PC	N. Baffin Bay	UCIAMS-61334	622	6505	55	81 ± 18	6685 (6480 – 6887)	Pelecypod valve
42PC	N. Baffin Bay	UCIAMS-61332	810	8155	55	111 ± 50	8339 (8139 – 8549)	Pelecypod
117Q	N. Baffin Bay	ETH-87284.1.1	199.5	4725	70	81 ± 18	4674 (4422 – 4875)	MBF
117Q	N. Baffin Bay	UA-56315	240.5	5310	30	81 ± 18	5400 (5264 – 5563)	Bivalve shell fragments
117Q	N. Baffin Bay	ETH-87283.1.1	283.5	6300	60	81 ± 18	6456 (6273 – 6652)	MBF
117Q	N. Baffin Bay	ETH-87282.1.1	343.5	6765	60	81 ± 18	6986 (6765 – 7184)	MBF
117Q	N. Baffin Bay	ETH-87281.3.1	403.5	8010	70	81 ± 18	8220 (8013 – 8396)	MBF
117Q	N. Baffin Bay	UA-56314	480.5	9610	40	321 ± 50	9906 (9651 – 10153)	Bivalve shell fragments
117Q	N. Baffin Bay	UA-56313	492.5	9675	40	331 ± 50	9984 (9726 – 10195)	Bivalve shell fragments
117Q	N. Baffin Bay	ETH-90546.1.1	524.5	9970	90	381 ± 50	10310 (10003 – 10632)	MBF
GeoB19948-3	N. Baffin Bay	AWI-1252.1.1	14	2443	108	81 ± 18	1815 (1522 – 2117)	MBPF
GeoB19948-3	N. Baffin Bay	AWI-1253.1.1	150	5427	114	81 ± 18	5520 (5253 – 5836)	PF (<i>N. pachyderma</i> sin)
GeoB19948-3	N. Baffin Bay	AWI-1475.1.1	274	7789	184	81 ± 18	7994 (7600 – 8379)	MBPF

14PC	Smith Sound	UCIAMS-171868	9–10	1625	20	81 ± 18	931 (781 – 1067)	BF (<i>N. labradorica</i>)
14PC	Smith Sound	UCIAMS-163876	40–41	7215	15	81 ± 18	7438 (7307 – 7563)	BF (<i>N. labradorica</i>)
14PC	Smith Sound	UCIAMS-171869	87–91.5	8535	30	156 ± 50	8749 (8541 – 8975)	MBF
14PC	Smith Sound	UCIAMS-171870	116–118	9015	45	234 ± 50	9274 (9048 – 9463)	MBF
14PC	Smith Sound	UCIAMS-163867	147–151	10035	25	381 ± 50	10378 (10189 – 10576)	MBF
14PC	Smith Sound	UCIAMS-163868	187–189	10240	30	411 ± 50	10622 (10362 – 10890)	BF (<i>C. neoteretis</i>)
05GC	Nares Strait	NOS-71686	8–10	3100	35	81 ± 18	2634 (2444 – 2775)	PF (<i>N. pachyderma</i> sin)
05GC	Nares Strait	NOS-71688	58–60	6870	45	81 ± 18	7099 (6913 – 7269)	PF (<i>N. pachyderma</i> sin)
05GC	Nares Strait	AA-81310	68–70	7302	61	81 ± 18	7513 (7341 – 7673)	PF (<i>N. pachyderma</i> sin)
05GC	Nares Strait	NOS-72574	96–98	8290	50	81 ± 18	8516 (8346 – 8721)	PF (<i>N. pachyderma</i> sin)
05GC	Nares Strait	NOS-71689	345–349	9320	45	181 ± 50	9684 (9473 – 9943)	MBPF
Kane2B	Nares Strait	UGAMS-24305	62	3010	25	81 ± 18	2530 (2357 – 2690)	Mollusc shell
Kane2B	Nares Strait	UCIAMS-173009	139	4540	20	81 ± 18	4440 (4262 – 4612)	Mollusc shell
Kane2B	Nares Strait	UGAMS-24307	186	5445	25	81 ± 18	5537 (5380 – 5700)	Mollusc shell
Kane2B	Nares Strait	UGAMS-24295	207.5	6005	25	81 ± 18	6148 (5984 – 6288)	Mollusc shell
Kane2B	Nares Strait	SacA-46002	251.5	7250	60	81 ± 18	7468 (7296 – 7627)	MBF
Kane2B	Nares Strait	SacA-45999	273.5	7870	50	81 ± 18	8072 (7913 – 8260)	MBF
Kane2B	Nares Strait	Beta-467584	297.5	7980	30	81 ± 18	8192 (8028 – 8333)	MBF
Kane2B	Nares Strait	Beta-467583	327.5	8160	30	111 ± 50	8344 (8170 – 8523)	MBF
Kane2B	Nares Strait	SacA-46001	333.5	8200	60	111 ± 50	8390 (8173 – 8596)	MBF
Kane2B	Nares Strait	UCIAMS-173007	358.5	8450	20	156 ± 50	8630 (8420 – 8866)	Mollusc shell
Kane2B	Nares Strait	UCIAMS-173008	362.5	8520	20	156 ± 50	8728 (8531 – 8962)	Mollusc shell
Kane2B	Nares Strait	UGAMS-24296	407.5	8640	30	171 ± 50	8867 (8627 – 9079)	Mollusc shell

9.2 Supplement to Manuscript II (Chapter 5)

Table 9.2.1: Sr, Pb, and, Nd isotope compositions of core GeoB22346-3 from the Clyde Inlet head. Pb (corr.) isotope values were corrected by a bulk uncertainty of 0.1 % per atomic mass unit. ϵ Nd values were calculated using the CHUR value of 0.512638 (Jacobsen and Wasserburg, 1980). Uncertainties (2SDmean) are given for the last digit.

Sample ID	Depth [cm]		Age [ka BP]	Radiogenic isotope data (dt fraction)				
	Top	Bottom		$^{87}\text{Sr}/^{86}\text{Sr}$	$^{206}\text{Pb}/^{204}\text{Pb}$	$^{206}\text{Pb}/^{204}\text{Pb}$ corr.	$^{143}\text{Nd}/^{144}\text{Nd}$	ϵ Nd
JH01	20	21	0.2	0.776481±8	19.9247±6	19.94	0.510684±6	-38.12
JH02	123	124	1.5	0.752798±8	20.9174±9	20.94	0.511062±6	-30.74
JH03	128	129	1.5	0.755534±8	20.0946±7	20.11	0.511020±6	-31.56
JH04	172	173	2.1	0.753255±8	18.0059±5	18.02	0.511004±6	-31.87
JH05	270	271	3.8	0.796260±9	22.9801±10	23.00	0.510789±6	-36.07
JH06	345	346	5.1	0.819383±8	24.2218±9	24.25	0.510852±5	-34.84
JH07	420	421	6.2	0.801938±9	22.1984±9	22.22	0.510795±5	-35.95
JH08	500	501	7.1	0.756788±8	17.8445±7	17.86	0.510958±5	-32.77
JH09	560	561	7.7	0.795990±9	20.7038±8	20.72	0.510820±6	-35.46
JH10	568	569	7.8	0.762168±7	18.2336±6	18.25	0.510923±5	-33.45
JH11	630	631	8.3	0.789833±8	20.2926±9	20.31	0.510851±5	-34.86
JH12	680	681	8.6	0.783038±8	20.1933±5	20.21	0.510876±6	-34.37

Table 9.2.2: Sr, Pb, and, Nd isotope compositions of the detrital sediment fraction of core GeoB22357-3 from the Clyde Inlet shelf. Pb (corr.) isotope values were corrected by a bulk uncertainty of 0.1 % per atomic mass unit. ϵ Nd values were calculated using the CHUR value of 0.512638 (Jacobsen and Wasserburg, 1980). Uncertainties (2SDmean) are given for the last digit.

Sample ID	Depth [cm]		Age [ka BP]	Radiogenic isotope data (dt fraction)				
	Top	Bottom		$^{87}\text{Sr}/^{86}\text{Sr}$	$^{206}\text{Pb}/^{204}\text{Pb}$	$^{206}\text{Pb}/^{204}\text{Pb}$ corr.	$^{143}\text{Nd}/^{144}\text{Nd}$	ϵNd
JH14	10	11	8.2	0.747755±7	17.5049±10	17.52	0.510877±5	-34.35
JH15	29	30	8.4	0.744270±8	17.2238±16	17.24	0.510931±5	-33.30
JH16	54	55	8.7	0.743368±8	17.0084±5	17.03	0.510925±6	-33.42
JH17	104	105	9.2	0.748314±9	17.7903±12	17.81	0.510843±6	-35.01
JH18	154	155	9.7	0.749524±8	17.6228±11	17.64	0.510821±6	-35.44
JH19	204	205	10.2	0.751774±8	17.7297±9	17.75	0.510789±5	-36.07
JH20	254	255	10.6	0.749871±8	17.8141±12	17.83	0.510802±6	-35.81
JH21	263	264	10.6	0.749620±8	17.9818±9	18.00	0.510812±6	-35.62
JH22	304	305	10.8	0.753249±8	17.7375±10	17.76	0.510759±5	-36.65
JH23	354	355	11	0.755961±9	18.0266±11	18.04	0.510757±9	-36.69
JH24	381	382	11	0.759324±8	17.8214±14	17.84	0.510694±5	-37.92
JH25	404	405	11.1	0.758853±9	17.7441±12	17.76	0.510710±6	-37.61
JH26	454	455	11.3	0.757921±9	17.7531±16	17.77	0.510742±5	-36.99
JH27	504	505	11.5	0.759452±8	17.8454±15	17.86	0.510748±5	-36.87
JH28	554	555	11.7	0.758465±9	17.6219±9	17.64	0.510687±5	-38.06
JH29	604	605	11.8	0.761015±8	17.6905±11	17.71	0.510653±5	-38.72
JH30	654	655	12	0.753654±9	17.4680±11	17.49	0.510731±6	-37.20
JH31	704	705	12.2	0.760297±8	17.3724±11	17.39	0.510663±6	-38.53
JH32	726	727	12.3	0.749546±9	17.4082±11	17.43	0.510772±5	-36.40

JH33	752	753	12.4	0.745626±8	17.4012±14	17.42	0.510852±5	-34.84
JH34	778	779	12.5	0.750817±9	17.5013±11	17.52	0.510766±5	-36.52
JH35	804	805	12.6	0.755883±9	17.7540±11	17.77	0.510738±6	-37.06
JH36	841	842	12.7	0.749074±8	17.3620±7	17.38	0.510815±5	-35.56
JH37	876	877	12.8	0.743568±8	16.6804±13	16.70	0.510942±5	-33.08

Table 9.2.3: Mineralogical composition of the < 63 µm sediment fraction of core GeoB22346-3 from the Clyde Inlet head.

Sample ID	Sediment Depth [cm]		Mineral Content [%]						
	Top	Bottom	Quartz	Albite	K-feldspar	Mica	Other Phyllosilicates	Amphibole + Pyroxene	Others
JH01	20	21	33	24	12	13	10	6	2
JH02	123	124	27	16	11	33	9	3	0
JH03	128	129	31	31	8	21	2	7	1
JH04	172	173	36	27	10	5	1	10	10
JH05	270	271	23	14	9	39	7	4	5
JH06	345	346	21	14	17	27	7	4	9
JH07	420	421	23	18	11	24	10	7	6
JH08	500	501	33	31	12	9	2	9	4
JH09	560	561	27	21	12	17	8	7	8
JH10	568	569	27	36	10	15	2	5	5
JH11	630	631	27	29	10	15	9	7	5
JH12	680	681	31	26	10	11	13	10	0

Table 9.2.4: Mineralogical composition of the < 63 µm sediment fraction of core GeoB22357-3 from the Baffin Island shelf.

Sample ID	Sediment Depth [cm]		Mineral Content [%]							
	Top	Bottom	Quartz	Albite	K-feldspar	Mica	Other Phyllosilicates	Amphibole + Pyroxene	Carbonates	Others
JH14	10	11	31	26	16	16	1	7	3	
JH16	54	55	32	22	12	21	2	9	3	
JH18	154	155	31	27	13	15	4	7	4	
JH20	254	255	32	26	12	13	2	5	9	
JH22	304	305	36	27	13	10	2	6	6	
JH24	381	382	28	23	25	9	4	7	4	
JH26	454	455	28	25	13	18	4	7		4
JH28	554	555	26	30	15	19	4	7		
JH29	604	605	31	29	16	18	4	2		
JH30	654	655	34	24	11	18	3	8		
JH31	704	705	33	30	14	10	4	8		
JH32	726	727	39	25	12	15	3	7		
JH33	752	753	43	20	14	11	5	6		
JH34	778	779	44	24	13	11	2	5		
JH35	804	805	28	29	12	20	4	2		6
JH36	841	842	33	29	15	13	0	9		1
JH37	876	877	43	32	17	0	1	7		

9.3 Supplement to Manuscript III (Chapter 6)

Table 9.3.1: Compilation of radiocarbon-dated sediment cores from Baffin Bay and related publications. Core numbers correspond to those in Figure 6.1c. PC = piston core; GC = gravity core; VC = vibro core; RC = rumohr core; TWC = trigger-weight core.

Core No. in Fig. 1c	Core ID	Lat	Lon	Location	Region	Depocenter in Fig. 1c	Type	Core Length (cm)	Water Depth (m)	No Of ¹⁴ C Dates	Citation
1	HU77029-006	73.201667	-67.8235	NE Baffin Island	Central Baffin Bay	Deep Basin	PC	~500	2200	2	Andrews et al., 1998
2	HU76029-034	71.768333	-64.37	central Baffin Bay	Central Baffin Bay	Deep Basin	PC	~430	2275	3	Andrews et al., 1998
3	HE-0006-4-2PC	71.22	-61.49	Uummannaq Trough TMF	Central Baffin Bay	Deep Basin	PC	1409	1829	2	O Cofaigh et al., 2013a
4	HU2008-029-016PC	70.769	-65.09616667	E Baffin Island	Central Baffin Bay	Deep Basin	PC	741	2063	3	Simon et al., 2012
5	HU76029-040	70.703333	-64.978333	E Baffin Island	Central Baffin Bay	Deep Basin	PC	~430	2041	2	Andrews et al., 1998
6	JR175-GC01	69.9335	-63.056667	central Baffin Bay	Central Baffin Bay	Deep Basin	GC	1680	2034	12	Owensworth et al., 2023
7	HU76029-025	69.205	-62.425	central Baffin Bay	Central Baffin Bay	Deep Basin	PC	~450	1910	3	Andrews et al., 1998
8	64PC	72.426113	-72.769305	NE Baffin Island	Baffin Bay Slope	Slope	PC	713	875	8	Kelleher et al., 2022; Jenner et al., 2018
9	2018042-48	68.793684	-63.882891	Home Bay, SE Baffin Island	Baffin Bay Slope	Slope	PC	758.5	1511.4	4	This study

10	SL 174	68.531333	-63.330333	SE Baffin Island	Baffin Bay Slope	Slope	GC	777.5	1559	15	Jackson et al., 2023; Jackson et al., 2017
11	77	68.308682	-63.794663	SE Baffin Island	Baffin Bay Slope	Slope	PC	649.5	1153	3	Jenner et al., 2018
12	2018042-64	68.19245	-63.427283	Home Bay, SE Baffin Island	Baffin Bay Slope	Slope	PC	740	1265	4	This study
13	2018042-65	67.890084	-62.353189	Home Bay, SE Baffin Island	Baffin Bay Slope	Slope	PC	759	1130	2	This study
14	JR175-VC45	70.5665	-60.3075	Uummannaq Trough TMF	Baffin Bay Slope	Slope	VC	141	648	2	Sheldon et al., 2016
15	JR175-VC46	70.468833	-61.0485	Uummannaq Trough TMF	Baffin Bay Slope	Slope	VC	558	845	3	Jennings et al., 2017
16	SL 170	68.969167	-59.426333	Disko Bay TMF	Baffin Bay Slope	Slope	GC	683	1078	21	Jackson et al., 2017
17	GeoB22304-3	68.903	-59.477	Disko Bay TMF	Baffin Bay Slope	Slope	GC	1144	1149	4	This study
18	HU2008029-012PC	68.66662	-60.00044	Disko Bay TMF	Baffin Bay Slope	Slope	PC	~1140	1475	12	Jennings et al., 2017
19	JR175-VC29	68.1225	-59.739333	Disko Bay TMF	Baffin Bay Slope	Slope	VC	580	1064	11	Jennings et al., 2017
20	JR175-VC35	67.7005	-59.34233333	Disko Bay TMF	Baffin Bay Slope	Slope	VC	536	1267	2	O' Cofaigh et al., 2013b, 2018; Jennings et al. (2013)
21	JR175-VC34	67.556	-59.88383333	Disko Bay TMF	Baffin Bay Slope	Slope	VC	345	1476	6	O' Cofaigh et al., 2013b, 2018
22	HU77027-17PC	66.9015	-58.295	Disko Bay TMF	Baffin Bay Slope	Slope	PC	1073	935	4	Andrews et al., 1998

23	JR175-VC20	68.20166667	-57.75666667	Disko Bay Trough	West Greenland	Outer Shelf	VC	421	424	8	O'Cofaigh et al., 2013b
24	70PC	68.22833333	-57.61666667	Disko Bay Trough	West Greenland	Outer Shelf	PC	245	444	6	Jennings et al., 2014
25	70TWC	68.22833333	-57.61666667	Disko Bay Trough	West Greenland	Outer Shelf	TWC	208	444	5	Jennings et al., 2014
26	VC01	68.39833333	-55.89833333	Disko Bay Trough	West Greenland	Mid Shelf	VC	270	545	2	Hogan et al., 2016a
27	JR175-VC24	68.44833333	-55.25333333	Disko Bay Trough	West Greenland	Mid Shelf	VC	563	432	3	Andrews et al., 2015; Hogan et al., 2016a
28	343340-GC	68.39725	-55.12965	Disko Bay Trough	West Greenland	Mid Shelf	GC	~1050	461	7	Perner et al., 2013b
29	MSM343300	68.47185	-54.001967	Disko Bay Trough	West Greenland	Inner Shelf	GC	1132	519	26	Quellet-Bernier et al., 2014; Perner et al., 2013b
30	MSM 343310	68.647683	-53.824883	Disko Bay Trough	West Greenland	Inner Shelf	GC	939	855	20	Perner et al., 2011
31	DA00-02P	68.86466667	-53.32866667	Disko Bay Trough	West Greenland	Inner Shelf	PC	861	840	11	Seidenkrantz et al., 2008
32	343330-GC	68.967933	-53.185083	Disko Bay Trough	West Greenland	Inner Shelf	GC	~740	830	8	Perner et al., 2013b
33	DA00-03P	69	-53.13333333	Disko Bay Trough	West Greenland	Inner Shelf	PC	1008	852	8	Seidenkrantz et al., 2008
34	DA05	68.71533333	-51.107	Disko Bay Trough	West Greenland	Inner Shelf	PC	1048	335	7	Lloyd et al., 2007
35	DA00-04P	68.737	-51.0105	Disko Bay Trough	West Greenland	Inner Shelf	PC	897.5	265	8	Kuijpers et al., 2001; Seidenkrantz et al., 2013

36	VC05	69.16	-51.527167	Disko Bay Trough	West Greenland	Inner Shelf	VC	587	389	8	Streuff et al., 2017b
37	VC09	69.0965	-51.394167	Disko Bay Trough	West Greenland	Inner Shelf	VC	598	294	6	Streuff et al., 2017b
38	DA00-06	69.1725	-51.388056	Disko Bay Trough	West Greenland	Inner Shelf	PC	960	363	6	Rooney et al., 2016
39	ACDC2014-001	69.28666667	-51.27	Disko Bay Trough	West Greenland	Inner Shelf	RC	162	391	9	Wangner et al. , 2018; Wangner, 2019; Vermassen, 2019
40	ACDC2014-003	69.313	-51.3305	Disko Bay Trough	West Greenland	Inner Shelf	RC	173	380	4	Wangner et al. , 2018; Wangner, 2019; Vermassen, 2019
41	POR18	69.192333	-51.823	Disko Bay Trough	West Greenland	Inner Shelf	GC	120	379	2	Lloyd et al., 2005
42	VC06	69.149	-52.069	Disko Bay Trough	West Greenland	Inner Shelf	VC	494	439	2	Streuff et al., 2017b
43	VC07	69.14366884	-52.31465847	Disko Bay Trough	West Greenland	Inner Shelf	VC	546	439	2	Streuff et al., 2017b
44	DA06-139G	70.091433	-52.893083	Disko Bay Trough	West Greenland	Inner Shelf	GC	446	384	12	Andresen et al., 2011
45	343390-GC	70.2196	-53.053233	Disko Bay Trough	West Greenland	Inner Shelf	GC	~500	537	3	Perner et al., 2013b
46	MSM-343520_G	70.81585	-56.8483	Uummanaq Trough	West Greenland	Mid Shelf	GC	989	545.7	10	McCarthy, 2011
47	GeoB19973-2	72.8235	-60.04716667	Upernavik Trough	West Greenland	Mid Shelf	GC	817	754	9	Weiser et al., 2023
48	AMD14-204C	73.26105	-57.899783	Upernavik Trough	West Greenland	Inner Shelf	GC	738	987	15	Hansen et al., 2020; Caron et al., 2019

49	GeoB19920-1	73.26533333	-57.84916667	Upernavik Trough	West Greenland	Inner Shelf	GC	1108	998	7	Weiser et al., 2023; Slabon et al., 2016
50	GeoB19927-3	73.587667	-58.094333	Upernavik Trough	West Greenland	Inner Shelf	GC	1147	932	14	Weiser et al., 2023; Saini et al. 2020
51	GeoB19969-1	936	-57.24066667	Upernavik Trough	West Greenland	Inner Shelf	GC	936	720	11	Weiser et al., 2023
52	AMD14-210	73.26105	-57.899783	Melville By Trough	West Greenland	Inner Shelf	GC	596	1155	3	Caron et al., 2019
53	GeoB19946-4	75.83316667	-62.51633333	Melville By Trough	West Greenland	Inner Shelf	GC	1372	718.3	7	This study
54	GeoB19948-3	75.768333	-64.142833	Melville By Trough	West Greenland	Inner Shelf	GC	1018	778	7	Saini et al., 2022
55	91-039-012P	76.805	-71.858333	Hvalsund	Northern Baffin Bay	Inner Shelf	PC	~240	823	7	Knudsen et al., 2008; Levac et al., 2001
56	GeoB22315-2	76.92	-71.96	Hvalsund	Northern Baffin Bay	Inner Shelf	GC	758	907	9	This study
57	117Q	77.004833	-72.138667	Hvalsund	Northern Baffin Bay	Inner Shelf	GC	599	963	17	Jackson et al., 2021
58	2001LSSL-014PC	77.733333	-75.066667	Smith Sound	Northern Baffin Bay	Inner Shelf	PC	429	657.5	6	Jennings et al., 2019
59	91-039-008P	77.266667	-74.331667	Smith Sound	Northern Baffin Bay	Inner Shelf	PC	~835	663	7	Knudsen et al., 2008
60	CASQ1	77.250583	-74.425	Smith Sound	Northern Baffin Bay	Inner Shelf	GC	543	692	11	Jackson et al., 2021
61	38PC	76.57349	-73.955535	Smith Sound	Northern Baffin Bay	Inner Shelf	PC	846	680	9	St Onge & St Onge, 2014

62	HU2008-029-34	76.32905	-71.418998	Smith Sound	Northern Baffin Bay	Inner Shelf	PC	710	696	4	Kelleher et al., 2022; St Onge & St Onge, 2014
63	01PC	76.48925	-78.725017	Smith Sound	Northern Baffin Bay	Inner Shelf	PC	198	119	9	Stevenard et al., 2021
64	LSSL2001-006	75.58333333	-78.68333333	Jones Sound	Northern Baffin Bay	Inner Shelf	PC	1150	561	3	Mudie et al., 2006
65	42PC	75.57939	-78.629571	Jones Sound	Northern Baffin Bay	Inner Shelf	PC	1059	580	5	St Onge & St Onge, 2014
66	2004-804-009 PC	74.186667	-81.195	Lancaster Sound	Northern Baffin Bay	Inner Shelf	PC	600	781	4	Ledu et al., 2008
67	2011804-0010PC	73.808333	-80.009	Lancaster Sound	Northern Baffin Bay	Inner Shelf	PC	275.5	837	3	Furze et al., 2018
68	2011804-0010TWC	73.808333	-80.009	Lancaster Sound	Northern Baffin Bay	Inner Shelf	TWC	175	837	3	Furze et al., 2018
69	GeoB22336-4	74.073833	-77.449833	Lancaster Sound	Northern Baffin Bay	Mid Shelf	GC	613	839	13	Okuma et al., 2023
70	49PC	74.026178	-77.125263	Lancaster Sound	Northern Baffin Bay	Mid Shelf	PC	594	868	12	Kelleher et al., 2022; Bennett et al., 2015
71	2013029-66	72.849098	-77.441545	Pond Inlet NE Baffin Island	Baffin Island	Inner Shelf	PC	629.5	880	3	Broom, 2017
72	2013029-65	72.814891	-77.676665	Pond Inlet NE Baffin Island	Baffin Island	Inner Shelf	PC	817	1035	5	Broom, 2017
73	2013029-67	72.815566	-77.426285	Pond Inlet NE Baffin Island	Baffin Island	Inner Shelf	PC	1087	1076	2	Broom, 2017

74	GeoB22346-3	69.903	-70.2257	Clyde Fjord	Baffin Island	Inner Shelf	GC	783	203	8	This study; Couette et al., 2023
75	GeoB22357-3	70.604667	-67.893833	Clyde Trough	Baffin Island	Mid Shelf	GC	902	315	6	This study
76	2018042-67	67.725993	-63.443412	Broughton Trough, Off Qikiqtarjuaq, Baffin Island	Baffin Island	Mid Shelf	PC	239	592	3	This study
77	2018042-16	67.23184	-62.269741	Padloping Island, SE Baffin Island	Baffin Island	Mid Shelf	PC	242	356	4	This study
78	2018042-24	66.757516	-62.338508	Southwind Fjord SE Baffin Island	Baffin Island	Inner Shelf	PC	335.5	97.8	3	This study
79	HU82-SU5	66.555	-61.71	SE Baffin Island	Baffin Island	Inner Shelf	PC	770	146	3	Andrews, 1987

Table 9.3.2: List of radiocarbon data obtained in sediment cores retrieved from Baffin Bay and associated publications. Only cores with a minimum of two ^{14}C dates are included here. All ^{14}C ages were re-calibrated within UNDATABLE software (Lougheed & Obrochta, 2019) using Marine20 dataset (Heaton et al., 2020) and regional-specific reservoir correction (ΔR) values (in years; Pieńkowski et al., 2022) of 188 ± 91 (NW CAA), 81 ± 18 (NE Baffin Island), and -93 ± 111 (west Greenland) for ages $<15,000$; older ages were calibrated with a higher ΔR (250 ± 100 ; Jackson et al., 2023).

CoreID	Depth interval (cm)		Depth (cm)	LabID	Material dated	^{14}C age (yrs)	^{14}C error (yrs)	Citation	Comment	Bulk organic ^{14}C age after correction	Used in age model	ΔR (yrs)
77	137	142	139.5	OS-117723	Mixed benthics	10550	40	Jenner et al., 2018			yes	81 ± 18
77	200	205	202.5	OS-118359	Mixed planktics	12750	55	Jenner et al., 2018			yes	81 ± 18
77	638	643.5	640.75	UCIAMS-181265	Nps	37900	1600	Jenner et al., 2018			yes	250 ± 100
01PC			3	UCIAMS-233557	Shell fragment	-6	0	Stevenard et al., 2021			No	188 ± 91
01PC			10	UCIAMS-233558	Shell fragment	1385	15	Stevenard et al., 2021			yes	188 ± 91
01PC			23	UCIAMS-233556	Shell fragment	2210	15	Stevenard et al., 2021			yes	188 ± 91
01PC			31	UCIAMS-233559	Shell fragment	2480	15	Stevenard et al., 2021			yes	188 ± 91
01PC			53	UCIAMS-233555	Shell fragment	5805	20	Stevenard et al., 2021			yes	188 ± 91
01PC			80	UCIAMS-233560	Shell fragment	9725	20	Stevenard et al., 2021			yes	188 ± 91
01PC			87	UCIAMS-233561	Shell fragment	9795	20	Stevenard et al., 2021			yes	188 ± 91
01PC			100	UCIAMS-233562	Shell fragment	9960	20	Stevenard et al., 2021			yes	188 ± 91

01PC			120	UCIAMS-239490	Mixed-benthic foram	10095	20	Stevenard et al., 2021			yes	188±91
01PC			160	*UCIAMS-239489	Shell fragment	42000	810	Stevenard et al., 2021	reworked		No	250±100
117Q			18.5	Beta-507517	Bulk organic carbon	2370	30	Jackson et al., 2021	Bulk Organic C	199	No	-93±111
117Q			68.5	Beta-507518	Bulk organic carbon	3560	30	Jackson et al., 2021	Bulk Organic C	1377	No	-93±111
117Q			98.5	Beta-507519	Bulk organic carbon	4310	30	Jackson et al., 2021	Bulk Organic C	2119	No	-93±111
117Q			144.5	Beta-507520	Bulk organic carbon	5620	30	Jackson et al., 2021	Bulk Organic C	3416	No	-93±111
117Q			199.5	ETH-87284.1.1	Mixed benthic foram	4725	70	Jackson et al., 2021			yes	-93±111
117Q			240.5	UA-56315	Bivalve shell fragments	5310	30	Jackson et al., 2021			yes	-93±111
117Q			283.5	ETH-87283.1.1	BF (mixed spe-	6300	60	Jackson et al., 2021			yes	-93±111
117Q			343.5	ETH-87282.1.1	Benthic foram (mixed spe-	6765	60	Jackson et al., 2021			yes	-93±111
117Q			403.5	ETH-87281.1.1	Benthic foram (mixed spe-	7705	70	Jackson et al., 2021			yes	-93±111
117Q			403.5	ETH-87281.3.1	BF (mixed species) (duplicate)	8010	70	Jackson et al., 2021			yes	-93±111
117Q			480.5	UA-56314	Bivalve shell fragments	9610	40	Jackson et al., 2021			yes	-93±111
117Q			492.5	UA-56313	Bivalve shell fragments	9675	40	Jackson et al., 2021			yes	-93±111
117Q			524.5	ETH-90546.1.1	Benthic foram (mixed spe-	9970	90	Jackson et al., 2021			yes	-93±111

117Q			524.5	ETH-90547.1.1	PF (N. pachyderma sin.)	9875	90	Jackson et al., 2021		yes	-93±111
117Q			524.5	ETH-90548.1.1	Bivalve shell fragments	9800	90	Jackson et al., 2021		yes	-93±111
117Q			564.5	ETH-90544.1.1**	BF (mostly C. neoteretis)	11585	90	Jackson et al., 2021		yes	-93±111
117Q			564.5	ETH-90545.1.1**	Benthic foram (mixed spe-	30160	290	Jackson et al., 2021	reworked	No	250±100
2001LSSL-014PC	9	10	9.5	UCIAMS-171868	BF (N. labradorica)	1625	20	Jennings et al., 2019		yes	188±91
2001LSSL-014PC	40	41	40.5	UCIAMS-163876	BF (N. labradorica)	7215	15	Jennings et al., 2019		yes	188±91
2001LSSL-014PC	87	91.5	89.25	UCIAMS-171869	MBF	8535	30	Jennings et al., 2019		yes	188±91
2001LSSL-014PC	116	118	117	UCIAMS-171870	MBF	9015	45	Jennings et al., 2019		yes	188±91
2001LSSL-014PC	147	151	149	UCIAMS-163867	MBF	10035	25	Jennings et al., 2019		yes	188±91
2001LSSL-014PC	187	189	188	UCIAMS-163868	BF (C. neoteretis)	10240	30	Jennings et al., 2019		yes	188±91
2004-804-009 PC	217	220	218.5	Beta-02317	Mixed benthic foraminifers	6370	30	Ledu et al., 2008		yes	81±18
2004-804-009 PC	317		317	Beta-203496	Bivalve fragments shell	8490	40	Ledu et al., 2008		yes	81±18
2004-804-009 PC	525		525	Beta-203498	Bivalve fragments shell	9770	50	Ledu et al., 2008		yes	81±18
2004-804-009 PC	571	572	571.5	Beta-02318	Mixed benthic foraminifers	10480	40	Ledu et al., 2008		yes	81±18

2011804-0010PC	10	12	11	OS-101670	Foram: Islandiella norcrossi	10050	60	Furze et al., 2018		yes	81±18
2011804-0010PC	130	132	131	OS-101671	Foram: mixed benthics	11000	75	Furze et al., 2018		yes	81±18
2011804-0010PC	270	272	271	OS-101672	Foram: mixed benthics	11750	65	Furze et al., 2018		yes	81±18
2011804-0010TWC	10	12	11	OS-101659	Foram: Islandiella norcrossi	10000	55	Furze et al., 2018		yes	81±18
2011804-0010TWC	80	82	81	OS-101754	Foram: mixed benthics	11000	170	Furze et al., 2018		yes	81±18
2011804-0010TWC	170	172	171	OS-101653	Foram: mixed benthics	10950	60	Furze et al., 2018		yes	81±18
2013029-65			53		Forams	1580	35	Broom, 2017		yes	81±18
2013029-65			123		Forams	2630	40	Broom, 2017		yes	81±18
2013029-65			208		Forams	3005	15	Broom, 2017		yes	81±18
2013029-65			250		Forams	3840	25	Broom, 2017		yes	81±18
2013029-65			769		Forams	9450	30	Broom, 2017		yes	81±18
2013029-66			16		Forams	1580	50	Broom, 2017		yes	81±18
2013029-66			127		Forams	3970	20	Broom, 2017		yes	81±18
2013029-66			532		Forams	8990	30	Broom, 2017		yes	81±18
2013029-67			165		Shell	2250	15	Broom, 2017		yes	81±18
2013029-67			590		Shell	3675	20	Broom, 2017		yes	81±18
2018042-16	68	69	68.5	Beta518505	(shell): acid etch	9260	30	This study		yes	81±18
2018042-16	116	117	116.5	Beta518506	(shell): acid etch	10000	30	This study		yes	81±18
2018042-16	149		149	Beta518507	(shell - Portlandia	12860	40	This study	Portlandia effect	No	81±18

					Arctica): acid etch							
2018042-16	160	165	162.5	Keck260276	forams	10775	30	This study			yes	81±18
2018042-24	68	68	68	Beta518502	(shell): acid etch	1020	30	This study			yes	81±18
2018042-24	127	128	127.5	Beta518503	(shell): acid etch	1030	30	This study			yes	81±18
2018042-24	159	159	159	Beta518504	(shell): acid etch	1190	30	This study			yes	81±18
2018042-48	200	204	202	KECK257096	forams	13750	130	This study			yes	81±18
2018042-48	422	427	424.5	Keck247720	Forams	35250	280	This study			yes	250±100
2018042-48	507	513	510	Keck247727	Forams	38940	980	This study			yes	250±100
2018042-48	708	713	710.5	Keck247730	Forams	44000	3600	This study			yes	250±100
2018042-64	204	208	206	KECK257097	forams	14260	70	This study			yes	81±18
2018042-64	272	277	274.5	Keck260275	forams	15690	60	This study			yes	250±100
2018042-64	362	365	363.5	Keck247728	Forams	21110	160	This study			yes	250±100
2018042-64	502	505	503.5	Keck247729	Forams	22270	130	This study			yes	250±100
2018042-65	170	172	171	Keck260280	forams	11065	30	This study			yes	81±18
2018042-65	344	349	346.5	Keck260279	forams	14250	40	This study			yes	81±18
2018042-67	37	39	38	Keck260271	forams	10390	25	This study			yes	81±18
2018042-67	40	42	41	Keck247726	Forams	10725	20	This study			yes	81±18
2018042-67	506	511	508.5	Keck260270	forams	23890	120	This study	Subglacial till deposit, reworked?		No	250±100
343330-GC	98	100	99	Poz-42495	Mix benthic foram	3730	60	Perner et al, 2013b			yes	-93±111
343330-GC	198	200	199	Poz-42491	Mix benthic foram	4980	50	Perner et al, 2013b			yes	-93±111
343330-GC	278	280	279	Poz-35734	Mix benthic foram	5410	40	Perner et al, 2013b			yes	-93±111

343330-GC	308	310	309	Poz-42492	Mix benthic foram	5370	50	Perner et al, 2013b		yes	-93±111
343330-GC	396	400	398	Poz-35735	Mix benthic foram	5670	50	Perner et al, 2013b		yes	-93±111
343330-GC	420	424	422	LuS 9920	Mix benthic foram	5745	75	Perner et al, 2013b		yes	-93±111
343330-GC	496	502	499	Poz-42493	Mix benthic foram	8150	120	Perner et al, 2013b		yes	-93±111
343330-GC	532	536	534	LuS 9921	Mix benthic foram	8085	80	Perner et al, 2013b		yes	-93±111
343340-GC	53	58	55.5	Poz-22361	Mollusc	2555	30	Perner et al, 2013b		yes	-93±111
343340-GC	86	94	90	LuS	Mix benthic foram	5310	80	Perner et al, 2013b		yes	-93±111
343340-GC	129	129	129	Poz-30988	Mollusc	8240	50	Perner et al, 2013b		yes	-93±111
343340-GC	276	276	276	SUERC-26760	Mollusc	8730	39	Perner et al, 2013b		yes	-93±111
343340-GC	456	457	456.5	Poz-30989	Mollusc (Nuculana sp.)	9790	50	Perner et al, 2013b		yes	-93±111
343340-GC	632	634	633	Poz-30990	Mollusc	10260	60	Perner et al, 2013b		yes	-93±111
343340-GC	901	902.5	901.75	Poz-30991	Mollusc (Portlandia arctica)	10840	60	Perner et al, 2013b	Portlandian effect	No	-93±111
343390-GC	250	250	250	AA82362	Yoldia agularis	1308	35	Perner et al., 2013b		yes	-93±111
343390-GC	281	283	282	AA82361	Nucula lenticula	1447	38	Perner et al., 2013b		yes	-93±111
343390-GC	498	500	499	AA82363	Turitella polaris	2352	37	Perner et al., 2013b		yes	-93±111
38PC	195	195	195	UCIAMS-61333	Pelecypod fragments	3490	55	St Onge & St Onge, 2014		yes	-93±111
38PC	253	253	253	UCIAMS-61335	Entire pelecypod shell	3875	55	St Onge & St Onge, 2014		yes	-93±111

38PC	509	509	509	UCIAMS-61340	Pelecypod	5000	55	St Onge & St Onge, 2014		yes	-93±111
38PC	528	528	528	UCIAMS-61339	Pelecypod	5075	55	St Onge & St Onge, 2014		yes	-93±111
38PC	543	543	543	UCIAMS-61338	Shell fragments	5115	55	St Onge & St Onge, 2014		yes	-93±111
38PC	586	586	586	UCIAMS-61341	Pelecypod fragments	5480	55	St Onge & St Onge, 2014		yes	-93±111
38PC	740	740	740	UCIAMS-61343	Shell fragments	6425	55	St Onge & St Onge, 2014		yes	-93±111
38PC	801	801	801	UCIAMS-61342	Shell fragments	7110	55	St Onge & St Onge, 2014		yes	-93±111
42PC	24		24	CAMS-150983	Shell fragments	810	55	St Onge & St Onge, 2014		yes	188±91
42PC	42		42	CAMS-150984	Shell fragments	975	55	St Onge & St Onge, 2014		yes	188±91
42PC	547 (598)		598	UCIAMS-61336	Shell fragments	6305	55	St Onge & St Onge, 2014		yes	188±91
42PC	571 (622)		622	UCIAMS-61334	Pelecypod valve	6505	55	St Onge & St Onge, 2014		yes	188±91
42PC	766 (810)		810	UCIAMS-61332	Pelecypod	8155	55	St Onge & St Onge, 2014		yes	188±91
49PC	195	195	195	NSRL-39519	Algae (Seaweed)	8410	40	Kelleher et al. 2022		yes	81±18
49PC	215	215	215	NSRL-39504	Benthic foram (Islandiella norcrossi, Nonionella labradorica, Cassidulina neoteretis)	8605	54	Kelleher et al. 2022		yes	81±18

49PC	245	245	245	NSRL-41641	Benthic foram (Islandiella norcrossi, Nonionella labradorica)	9510	64	Kelleher et al. 2022		yes	81±18
49PC	265	265	265	NSRL-41642	Benthic foram (Islandiella norcrossi, Nonionella labradorica)	9770	64	Kelleher et al. 2022		yes	81±18
49PC	285	285	285	NSRL-41643	Planktic foram (N. pachyderma sinistral)	9845	45	Kelleher et al. 2022		yes	81±18
49PC	285	285	285	NSRL-39505	Benthic foram (Islandiella norcrossi, Nonionella labradorica, Cassidulina neoteretis)	10175	56	Kelleher et al. 2022		yes	81±18
49PC	295	295	295	NSRL-39506	Mollusc (Yoldiella lenticula)	10150	56	Kelleher et al. 2022		yes	81±18
49PC	325	325	325	NSRL-39507	Benthic foram (Elphidium clavatum)	10575	56	Kelleher et al. 2022		yes	81±18
49PC	332	332	332	Unknown	Mollusc (Yoldiella nana)	11060	71	Bennett et al., 2015.		yes	81±18
49PC	345	345	345	NSRL-39508	Mollusc (Thyasira gouldi)	10965	56	Kelleher et al. 2022		yes	81±18
49PC	408	408	408	NSRL-39509	Benthic foram (Islandiella norcrossi,	10710	56	Kelleher et al. 2022		yes	81±18

					Cassidulina reniforme)						
49PC	408	408	408	NSRL-39510	Benthic foram (Elphidium clavatum)	10865	56	Kelleher et al. 2022		yes	81±18
64PC	111	111	111	NSRL-39523	Seaweed	8435	35	Kelleher et al. 2022		yes	81±18
64PC	135	140	137.5	OS-118358a	MBF	9200	35	Jenner et al., 2018		yes	81±18
64PC	141	141	141	NSRL-39515	MBF (I. norcrossi, N. labradorica, C. neoteretis, M. barleeanus)	9270	25	Kelleher et al. 2022		yes	81±18
64PC	171	171	171	NSRL-39517	PF (N. pachyderma sin.)	9615	25	Kelleher et al. 2022		yes	81±18
64PC	171	171	171	NSRL-39516	MBF (I. norcrossi, N. labradorica, C. neoteretis, M. barleeanus)	9995	25	Kelleher et al. 2022		yes	81±18
64PC	191	191	191	NSRL-39518	BF (C. neoteretis)	10300	25	Kelleher et al. 2022		yes	81±18
64PC	275	280	277.5	OS-118649a	MBF	13850	95	Jenner et al., 2018		yes	81±18
64PC	330	335	332.5	OS-117862a	MBF	12500	45	Jenner et al., 2018		yes	81±18
70PC	14	15	14.5	SUERC-25672	Seaweed	7501	40	Jennings et al., 2014		yes	-93±111
70PC	55	56	55.5	SUERC-30590	Shell fragments	8830	39	Jennings et al., 2014		yes	-93±111
70PC	142	144.5	143.25	AA-84711	Bivalve shell fragments	9831	44	Jennings et al., 2014		yes	-93±111
70PC	169	170	169.5	AA-84712	Paired bivalve	10190	160	Jennings et al., 2014		yes	-93±111
70PC	188	189	188.5	AA-84713	Paired bivalve	10174	43	Jennings et al., 2014		yes	-93±111

70PC	209	211	210	AA-84714	Large paired bivalve	10545	45	Jennings et al., 2014		yes	-93±111
70TWC	82	83	82.5	AA-84708	Single valve	3197	43	Jennings et al., 2014		yes	-93±111
70TWC	97	98	97.5	AA-84709	Paired valves	3252	37	Jennings et al., 2014		yes	-93±111
70TWC	134	135	134.5	SUERC-25670	Seaweed	5913	39	Jennings et al., 2014		yes	-93±111
70TWC	172	172	172	AA-84710	Paired valves, large	7898	54	Jennings et al., 2014		yes	-93±111
70TWC	194	195	194.5	SUERC-3058	Seaweed	8464	40	Jennings et al., 2014		yes	-93±111
91-039-008P	14	22	18	Ua-10256	Benthic foram	720	85	Knudsen et al., 2008		yes	-93±111
91-039-008P	72	73	72.5	Ua-2832	Megayoldia thraciaeformis	2885	60	Knudsen et al., 2008		yes	-93±111
91-039-008P	461	464	462.5	Ua-2833	Megayoldia thraciaeformis	4065	50	Knudsen et al., 2008		yes	-93±111
91-039-008P	527	529	528	Ua-4118	Megayoldia thraciaeformis	4190	60	Knudsen et al., 2008		yes	-93±111
91-039-008P	704	705	704.5	Ua-4450	Clinocardium ciliatum	5110	55	Knudsen et al., 2008		yes	-93±111
91-039-008P	831	834	832.5	Ua-2834	Clinocardium ciliatum	6675	75	Knudsen et al., 2008		yes	-93±111
91-039-008P	832	834	833	Ua-4119	Benthic foram	6800	60	Knudsen et al., 2008		yes	-93±111
91-039-012P	15	18	16.5	Ua-11797	Benthic foram	7755	100	Knudsen et al., 2008; Levac et al, 2001		yes	-93±111
91-039-012P	24	27	25.5	Ua-4447	Benthic foram	8230	70	Knudsen et al., 2008; Levac et al, 2001		yes	-93±111
91-039-012P	105	108	106.5	Ua-4448	Benthic foram	9675	110	Knudsen et al., 2008; Levac et al, 2001		yes	-93±111
91-039-012P	117	120	118.5	Ua-4449	Pelecypod fragments	9885	115	Knudsen et al., 2008; Levac et al, 2001		yes	-93±111
91-039-012P	184	188	186	Ua-3366	Benthic foram	10930	105	Knudsen et al., 2008; Levac et al, 2001		yes	-93±111
91-039-012P	188	194	191	Ua-3367	Benthic foram	10805	145	Knudsen et al., 2008; Levac et al, 2001		yes	-93±111

91-039-012P	190	195	192.5	Ua-4998	Benthic foram	10815	130	Knudsen et al., 2008; Levac et al, 2001	yes	-93±111
ACDC2014-001	37	37	37	#-31834		845	30	Wangner et al. (2018), Wangner (2019), Vermassen (2019)	yes	-93±111
ACDC2014-001	81	81	81	#-31835		1045	30	Wangner et al. (2018), Wangner (2019), Vermassen (2019)	yes	-93±111
ACDC2014-001	85	85	85	Beta-431619		950	30	Wangner et al. (2018), Wangner (2019), Vermassen (2019)	yes	-93±111
ACDC2014-001	89	89	89	Beta-431620		980	30	Wangner et al. (2018), Wangner (2019), Vermassen (2019)	yes	-93±111
ACDC2014-001	102	102	102	#-31836		1515	30	Wangner et al. (2018), Wangner (2019), Vermassen (2019)	yes	-93±111
ACDC2014-001	111	111	111	#-31837		1640	30	Wangner et al. (2018), Wangner (2019), Vermassen (2019)	yes	-93±111
ACDC2014-001	112	112	112	#-31838		1650	30	Wangner et al. (2018), Wangner (2019), Vermassen (2019)	yes	-93±111
ACDC2014-001	117	117	117	#-31839		1725	30	Wangner et al. (2018), Wangner (2019), Vermassen (2019)	yes	-93±111
ACDC2014-001	126	126	126	#-31840		1925	30	Wangner et al. (2018), Wangner (2019), Vermassen (2019)	yes	-93±111
ACDC2014-003	70	70	70	003_70		875	35	Wangner et al. (2018), Wangner (2019), Vermassen (2019)	yes	-93±111
ACDC2014-003	108	108	108	003_108		3435	45	Wangner et al. (2018), Wangner (2019), Vermassen (2019)	yes	-93±111
ACDC2014-003	133	133	133	003_133		1710	45	Wangner et al. (2018), Wangner (2019), Vermassen (2019)	yes	-93±111
ACDC2014-003	161	161	161	003_161		2040	35	Wangner et al. (2018), Wangner (2019), Vermassen (2019)	yes	-93±111
AMD14-204C	4.5	4.5	4.5	ETH-92277	Mixed benthic foram	705	50	Hansen et al., 2020	yes	-93±111

AMD14-204C	70.5	70.5	70.5	ETH-92279	Mixed benthic foram	1795	50	Hansen et al., 2020		yes	-93±111
AMD14-204C	70.5	70.5	70.5	ETH-92278	Mixed planktonic foram	1710	50	Hansen et al., 2020		yes	-93±111
AMD14-204C	169	170	169.5	SacA 46004	Mixed benthic & planktonic foram	3555	35	Caron et al. 2019; Hansen et al., 2020		yes	-93±111
AMD14-204C	251	253	252	BETA 467785	Mixed benthic & planktonic foram	4300	30	Caron et al. 2019; Hansen et al., 2020		yes	-93±111
AMD14-204C	310.5	310.5	310.5	ETH-92281	Mixed benthic foram	4950	60	Hansen et al., 2020		yes	-93±111
AMD14-204C	310.5	310.5	310.5	ETH-92280	Mixed planktonic	4940	70	Hansen et al., 2020		yes	-93±111
AMD14-204C	410.5	410.5	410.5	ETH-92283	Mixed benthic	5805	60	Hansen et al., 2020		yes	-93±111
AMD14-204C	410.5	410.5	410.5	ETH-92282	Mixed planktonic	5825	60	Hansen et al., 2020		yes	-93±111
AMD14-204C	500	503	501.5	BETA 488641	Mixed benthic	6400	30	Caron et al. 2019; Hansen et al., 2020		yes	-93±111
AMD14-204C	580.5	580.5	580.5	ETH-92285	Mixed benthic	7155	70	Hansen et al., 2020		yes	-93±111
AMD14-204C	580.5	580.5	580.5	ETH-92284	Mixed planktonic	7005	60	Hansen et al., 2020		yes	-93±111
AMD14-204C	609	611	610	SacA 46005	Mixed benthic	7445	50	Caron et al. 2019; Hansen et al., 2020		yes	-93±111
AMD14-204C	700.5	700.5	700.5	ETH-92286	Mixed benthic	8270	389	Hansen et al., 2020		yes	-93±111
AMD14-204C	737.5	737.5	737.5	ETH-92287	Mixed benthic	8489	154	Hansen et al., 2020		yes	-93±111

AMD14-210	119	121	120	GIFA17340	Mixed benthic and planktonic foram	5530	70	Caron et al. 2019		yes	-93±111
AMD14-210	200	201	200.5	BETA463137	Mixed benthic and planktonic foram	7440	30	Caron et al. 2019		yes	-93±111
AMD14-210	291	292	291.5	GIFA17339	Mixed benthic and planktonic foram	7990	70	Caron et al. 2019		yes	-93±111
CASQ1	117.5	117.5	117.5	ULA-6034	Bivalve shell fragments	1570	20	Jackson et al., 2021		yes	-93±111
CASQ1	176.5	176.5	176.5	ULA-5837	Bivalve shell fragments	1850	20	Jackson et al., 2021		yes	-93±111
CASQ1	263.5	263.5	263.5	ULA-6035	Bivalve shell fragments	2370	20	Jackson et al., 2021		yes	-93±111
CASQ1	332.5	332.5	332.5	ULA-5836	Bivalve shell fragments	2660	25	Jackson et al., 2021		yes	-93±111
CASQ1	341.5	341.5	341.5	ULA-6036	Bivalve shell fragments	2705	20	Jackson et al., 2021		yes	-93±111
CASQ1	393.5	393.5	393.5	ULA-6037	Bivalve shell fragments	2970	25	Jackson et al., 2021		yes	-93±111
CASQ1	405.5	405.5	405.5	ULA-6044	Bivalve shell fragments	3505	20	Jackson et al., 2021		yes	-93±111
CASQ1	460.5	460.5	460.5	ULA-6045	Bivalve shell fragments	3505	20	Jackson et al., 2021		yes	-93±111
CASQ1	472.5	472.5	472.5	ULA-6046	Bivalve shell fragments	3775	20	Jackson et al., 2021		yes	-93±111
CASQ1	501.5	501.5	501.5	ULA-6047	Bivalve shell fragments	3485	25	Jackson et al., 2021		yes	-93±111
CASQ1	543.5	543.5	543.5	ULA-5835	Bivalve shell fragments	3745	25	Jackson et al., 2021		yes	-93±111

DA00-02P	0	5	2.5	KIA 23363	Plant remains	735	30	Seidenkrantz et al 2008		yes	-93±111
DA00-02P	70	70	70	KIA 23362	Plant remains	975	35	Seidenkrantz et al 2008		yes	-93±111
DA00-02P	140	140	140	KIA 23361	Plant remains	1315	50	Seidenkrantz et al 2008		yes	-93±111
DA00-02P	185	185	185	Poz-8169	Shell	1465	35	Seidenkrantz et al 2008		yes	-93±111
DA00-02P	256	256	256	AAR-7512	Shell	1810	47	Seidenkrantz et al 2008		yes	-93±111
DA00-02P	419	419	419	KIA 23364	Shell	2025	25	Seidenkrantz et al 2008		yes	-93±111
DA00-02P	475	477	476	AAR-9814	Shell	2145	41	Seidenkrantz et al 2008		yes	-93±111
DA00-02P	579	581	580	AAR-9813	Shell	2617	41	Seidenkrantz et al 2008		yes	-93±111
DA00-02P	621	621	621	KIA 23365	Shell	2945	35	Seidenkrantz et al 2008		yes	-93±111
DA00-02P	677	679	678	AAR-9857	Shell	3303	43	Seidenkrantz et al 2008		yes	-93±111
DA00-02P	861	861	861	AAR-6882	Mixed benthic foram	3332	54	Seidenkrantz et al 2008		yes	-93±111
DA00-03P	128	128	128	AAR-7508	Bivalve	1415	40	Seidenkrantz et al 2008		yes	-93±111
DA00-03P	239	239	239	CAMS-86752	Shell	1594	42	Seidenkrantz et al 2008		yes	-93±111
DA00-03P	404	404	404	CAMS-82824	Bivalve	1940	40	Seidenkrantz et al 2008		yes	-93±111
DA00-03P	500	500	500	AAR-6833	Mixed benthic foram	2065	40	Seidenkrantz et al 2008		yes	-93±111
DA00-03P	642	642	642	AAR-6834	Gastropod	2445	40	Seidenkrantz et al 2008		yes	-93±111
DA00-03P	738	738	738	AAR-44949	Shell	2745	45	Seidenkrantz et al 2008		yes	-93±111
DA00-03P	982	982	982	CAMS-91944	Shell	3265	45	Seidenkrantz et al 2008		yes	-93±111
DA00-03P	1002	1002	1002	CAMS-91935	Mixed benthic foram	3351	44	Seidenkrantz et al 2008		yes	-93±111
DA00-04P	120	125	122.5	Poz-8110	Plant remains (sea grass)	2125	35	Kuijpers et al. (2001); Seidenkrantz et al. (2013)		yes	-93±111
DA00-04P	175	175	175	AAR-9810	Plant remains (sea grass)	3432	44	Kuijpers et al. (2001); Seidenkrantz et al. (2013)		yes	-93±111

DA00-04P	235	235	235	Poz-8109	Plant remains (sea grass)	4380	40	Kuijpers et al. (2001); Seidenkrantz et al. (2013)	yes	-93±111
DA00-04P	322	322	322	AAR-7513	Plant remains (sea grass)	5620	70	Kuijpers et al. (2001); Seidenkrantz et al. (2013)	yes	-93±111
DA00-04P	390	400	395	Poz-8141	Benthic foram. fauna	6120	40	Kuijpers et al. (2001); Seidenkrantz et al. (2013)	yes	-93±111
DA00-04P	456	456	456	Poz-8143	Shell + benthic foram. fauna	6320	40	Kuijpers et al. (2001); Seidenkrantz et al. (2013)	yes	-93±111
DA00-04P	635	635	635	Poz-8168	Shell + benthic foram. fauna	7370	70	Kuijpers et al. (2001); Seidenkrantz et al. (2013)	yes	-93±111
DA00-04P	730	730	730	KIA23366	Benthic foram. fauna	7310	40	Kuijpers et al. (2001); Seidenkrantz et al. (2013)	yes	-93±111
DA00-06	5	7	6	KIA-17925	Benthic foram	1500	90	Rooney et al. 2016	yes	-93±111
DA00-06	72	76	74	B203723	Benthic foram	6300	40	Rooney et al. 2016	yes	-93±111
DA00-06	159	159	159	AAR-6837	Shell	7350	68	Rooney et al. 2016	yes	-93±111
DA00-06	426	434	430	KIA-23024	Benthic foram	7270	45	Rooney et al. 2016	yes	-93±111
DA00-06	646	654	650	KIA-23025	Benthic foram	7430	70	Rooney et al. 2016	yes	-93±111
DA00-06	891	891	891	AAR-6839	Shell	7843	72	Rooney et al. 2016	yes	-93±111
DA05	50	50	50	AAR-7509	Plant remains	1705	38	Lloyd et al 2007	yes	-93±111
DA05	106	106	106	AAR-7510	Plant remains	2004	36	Lloyd et al 2007	yes	-93±111
DA05	262	262	262	AAR-7511	Plant remains	3200	60	Lloyd et al 2007	yes	-93±111
DA05	327	327	327	AAR-8283	Plant remains	3600	120	Lloyd et al 2007	yes	-93±111
DA05	592	592	592	AAR-6835	Plant remains	4200	50	Lloyd et al 2007	yes	-93±111
DA05	812	812	812	AAR8297	Plant remains	5350	100	Lloyd et al 2007	yes	-93±111
DA05	1017	1017	1017	AAR-6836	Plant remains	6300	75	Lloyd et al 2007	yes	-93±111
DA06-139G	7	8	7.5	AAR 10953	Bivalve fragment	1013	35	Andresen et al. 2011	yes	-93±111

DA06-139G	27	28	27.5	AAR13060	Bivalve fragment	607	22	Andresen et al. 2011		yes	-93±111
DA06-139G	58	60	59	AAR 10952	Bivalve fragment	903	35	Andresen et al. 2011		yes	-93±111
DA06-139G	99	99	99	AAR 13552	Marine plant fragm.	1356	27	Andresen et al. 2011		yes	-93±111
DA06-139G	132	136	134	AAR 10951	Marine plant fragm.	1797	40	Andresen et al. 2011		yes	-93±111
DA06-139G	152	152	152	AAR 13553	Marine plant fragm.	1899	33	Andresen et al. 2011		yes	-93±111
DA06-139G	180	180	180	AAR 13059	Marine plant fragm.	1913	27	Andresen et al. 2011		yes	-93±111
DA06-139G	199	200	199.5	AAR 10950	Marine plant fragm.	2090	42	Andresen et al. 2011		yes	-93±111
DA06-139G	302	304	303	AAR 13061	Benthic forams	3030	90	Andresen et al. 2011		yes	-93±111
DA06-139G	385	385	385	AAR 10949	Bivalve fragment	3976	38	Andresen et al. 2011		yes	-93±111
DA06-139G	390	393	391.5	AAR 10948	Marine plant fragm.	3833	43	Andresen et al. 2011		yes	-93±111
DA06-139G	435	435	435	AAR 10947	Bivalve fragment	4709	40	Andresen et al. 2011		yes	-93±111
GeoB19920-1	50	50	50	AWI 6235.1.1	mixed foram	1670	63	Weiser et al., 2023		yes	-93±111
GeoB19920-1	321	321	321	AWI 6395.1.1	mixed foram	4618	78	Weiser et al., 2023		yes	-93±111
GeoB19920-1	620	620	620	AWI 6236.1.1	mixed foram	7063	87	Weiser et al., 2023		yes	-93±111
GeoB19920-1	959	959	959	AWI 6237.1.1	mixed foram	8524	94	Weiser et al., 2023		yes	-93±111
GeoB19920-1	1006	1006	1006	AWI 6238.1.1	mollusk shell (fragment)	7939	26	Weiser et al., 2023		yes	-93±111
GeoB19920-1	1105	1105	1105	ETH-66277	mixed planktic foram	7915	70	Slabon et al., 2016		yes	-93±111

GeoB19920-1	1105	1105	1105	ETH-66276	mixed benthic forams	7925	75	Slabon et al., 2016		yes	-93±111
GeoB19927-3	33	33	33	AWI-1468.1.1	Mixed benthic forams	1821	176	Saini et al. 2020		yes	-93±111
GeoB19927-3	62	62	62	AWI-1469.1.1	Mixed benthic forams	2072	177	Saini et al. 2020		yes	-93±111
GeoB19927-3	199	199	199	Poz-85919	Mollusk shells	3360	30	Saini et al. 2020		yes	-93±111
GeoB19927-3	410	410	410	AWI-1259.1.1	Mixed benthic forams	4692	197	Saini et al. 2020		yes	-93±111
GeoB19927-3	411	411	411	AWI-1261.1.1	Mixed benthic forams	4836	192	Saini et al. 2020	reversal	No	-93±111
GeoB19927-3	538	538	538	Poz-85920	Mollusk shells	5495	35	Saini et al. 2020		yes	-93±111
GeoB19927-3	561	561	561	Poz-85921	Mollusk shells	5720	35	Saini et al. 2020		yes	-93±111
GeoB19927-3	607	607	607	Poz-85924	Mollusk shells	5885	35	Saini et al. 2020		yes	-93±111
GeoB19927-3	689	689	689	Poz-85925	Mollusk shells	6670	50	Saini et al. 2020		yes	-93±111
GeoB19927-3	767	767	767	Poz-85926	Mollusk shells	7410	10	Saini et al. 2020		yes	-93±111
GeoB19927-3	790	790	790	Poz-85927	Mollusk shells	7640	50	Saini et al. 2020		yes	-93±111
GeoB19927-3	1000	1000	1000	AWI-1260.1.1	Planktonic (N. pachyderma sin.) and mixed benthic	8831	205	Saini et al. 2020		yes	-93±111
GeoB19927-3	1053	1053	1053	AWI 6394.1.1	mixed benthic foram	10504	94	Weiser et al., 2023		yes	-93±111
GeoB19927-3	1117	1117	1117	AWI 6393.1.1	mixed benthic foram	9877	94	Weiser et al., 2023		yes	-93±111
GeoB19946-4	74	74	74	AWI_1914.1.1	benthic forams	4906	118	This study		yes	-93±111
GeoB19946-4	150	150	150	AWI_1248.1.1	mixed forams	6414	122	This study		yes	-93±111
GeoB19946-4	315	315	315	AWI_1915.1.1	benthic forams	8359	126	This study		yes	-93±111

GeoB19946-4	689	689	689	AWI_1473.1.1	benthic forams	9071	193	This study			yes	-93±111
GeoB19946-4	800	800	800	AWI_1250.1.1	mixed forams	8967	209	This study			yes	-93±111
GeoB19946-4	950	950	950	AWI_1251.1.1	benthic forams	9454	209	This study			yes	-93±111
GeoB19946-4	1372	1372	1372	AWI_1474.1.1	benthic forams	10079	195	This study			yes	-93±111
GeoB19948-3	14	14	14	AWI-1252.1.1	Mixed foram	2443	108	Saini et al. 2022			yes	-93±111
GeoB19948-3	150	150	150	1253.2.1	N. pachyderma sin	5431	198	Saini et al. 2022			yes	-93±111
GeoB19948-3	150	150	150	1253.1.1	Mixed benthic foram	5427	114	Saini et al. 2022			yes	-93±111
GeoB19948-3	274	274	274	1475.1.1	Mixed foram	7789	184	Saini et al. 2022			yes	-93±111
GeoB19948-3	678	678	678	AWI 1254.1.1	N. pachyderma sin	8965	199	Saini et al. 2022			yes	-93±111
GeoB19948-3	678	678	678	AWI 1254.2.1	mixed benthic	9044	199	Saini et al. 2022			yes	-93±111
GeoB19948-3	802	802	802	AWI 1255.1.1	mixed foram	8583	141	Saini et al. 2022			yes	-93±111
GeoB19969-1	20	20	20	AWI 6239.1.1	mixed foram	1256	101	Weiser et al., 2023			yes	-93±111
GeoB19969-1	100	100	100	AWI 6240.1.1	mixed foram	2114	59	Weiser et al., 2023			yes	-93±111
GeoB19969-1	400	400	400	AWI 6396.1.1	mixed foram	4512	81	Weiser et al., 2023			yes	-93±111
GeoB19969-1	712	712	712	Poz-85928	mollusk shell (fragment)	6140	40	Weiser et al., 2023			yes	-93±111
GeoB19969-1	757	757	757	Poz-85930	mollusk shell (fragment)	6360	40	Weiser et al., 2023			yes	-93±111
GeoB19969-1	780	780	780	Poz-85931	mollusk shell (fragment)	6650	40	Weiser et al., 2023			yes	-93±111
GeoB19969-1	858	858	858	Poz-85984	mollusk shell (fragment)	7510	50	Weiser et al., 2023			yes	-93±111
GeoB19969-1	888	888	888	Poz-85985	mollusk shell (fragment)	7880	50	Weiser et al., 2023	reversal		No	-93±111

GeoB19969-1	927	927	927	Poz-85986	mollusk shell (fragment)	7570	50	Weiser et al., 2023		yes	-93±111
GeoB19969-1	933	933	933	Poz-85987	mollusk shell (fragment)	8190	50	Weiser et al., 2023	reversal	No	-93±111
GeoB19969-1	935	935	935	Poz-85988	mollusk shell (fragment)	8150	50	Weiser et al., 2023		yes	-93±111
GeoB19973-2	10	10	10	AWI 1472.1.1	mixed benthic foram	1594	175	Weiser et al., 2023		yes	-93±111
GeoB19973-2	60	60	60	AWI 1919.1.1	mixed benthic foram	3405	113	Weiser et al., 2023		yes	-93±111
GeoB19973-2	170	170	170	AWI 1920.1.1	mixed benthic foram	5680	120	Weiser et al., 2023		yes	-93±111
GeoB19973-2	240	240	240	AWI 1256.1.1	mixed foram	6500	199	Weiser et al., 2023		yes	-93±111
GeoB19973-2	320	320	320	AWI 1257.1.1	mixed planktic foram	7870	197	Weiser et al., 2023		yes	-93±111
GeoB19973-2	320	320	320	AWI 1257.2.1	mixed benthic foram	8205	197	Weiser et al., 2023		yes	-93±111
GeoB19973-2	400	400	400	AWI 1258.1.1	mixed foram	9222	201	Weiser et al., 2023		yes	-93±111
GeoB19973-2	480	480	480	AWI 7147.1.1	mixed foram	10380	111	Weiser et al., 2023		yes	-93±111
GeoB19973-2	720	720	720	AWI 1470.1.1	mollusk shell (fragment)	44474	2076	Weiser et al., 2023	reworked	No	250±100
GeoB22304-3	478	479	478.5	AWI-6965.1.1	Mixed Planktic Foram	17109	66	This study		yes	250±100
GeoB22304-3	798	799	798.5	AWI-6964.1.1	Mixed Planktic Foram	20985	252	This study		yes	250±100
GeoB22304-3	828	829	828.5	AWI-6963.1.1	Mixed Planktic Foram	23078	309	This study		yes	250±100
GeoB22304-3	1048	1049	1048.5	AWI-6962.1.1	Mixed Planktic Foram	26781	362	This study		yes	250±100

GeoB22315-2	193	194	193.5	AWI-5481.1.1	Mixed Planktic & Benthic Foram	3559	69	This study			yes	-93±111
GeoB22315-2	194.5	195.5	195	AWI-5482.1.1	Mixed Benthic Foram	3379	70	This study			yes	-93±111
GeoB22315-2	278	279	278.5	AWI-5483.1.1	Mixed Benthic Foram	4142	71	This study			yes	-93±111
GeoB22315-2	373	374	373.5	AWI-5484.1.1	Mixed Benthic Foram	4972	72	This study			yes	-93±111
GeoB22315-2	468	469	468.5	AWI-5485.1.1	Mixed Planktic & Benthic Foram	5172	80	This study			yes	-93±111
GeoB22315-2	578	579	578.5	AWI-5486.1.1	Mixed Benthic Foram	6938	81	This study			yes	-93±111
GeoB22315-2	638	639	638.5	AWI-6217.1.1	Mixed Planktic & Benthic Foram	8349	29	This study			yes	-93±111
GeoB22315-2	668	669	668.5	AWI-6218.1.1	Mixed Planktic & Benthic Foram	9213	98	This study			yes	-93±111
GeoB22315-2	698	699	698.5	AWI-5487.1.1	Mixed Planktic & Benthic Foram	23967	231	This study	reworked, subglacial till deposit?		No	250±100
GeoB22336-4	65	69	67	AWI-6220.1.1	MBF	2513	65	Okuma et al., 2023			yes	81±18
GeoB22336-4	108	109	108.5	AWI-5488.1.1	MBPF	3736	69	Okuma et al., 2023			yes	81±18
GeoB22336-4	109.5	110.5	110	AWI-5489.1.1	MBPF	3640	69	Okuma et al., 2023			yes	81±18
GeoB22336-4	198	199	198.5	AWI-5490.1.1	MBPF	6004	79	Okuma et al., 2023			yes	81±18
GeoB22336-4	258	259	258.5	AWI-5491.1.1	MBPF	7111	79	Okuma et al., 2023			yes	81±18
GeoB22336-4	273	274	273.5	AWI-5492.1.1	MBPF	7493	84	Okuma et al., 2023			yes	81±18
GeoB22336-4	290	291	290.5	AWI 1724.1.1	MBF	7729	120	Okuma et al., 2023			yes	81±18

GeoB22336-4	323	324	323.5	AWI-6221.1.1	MBPF	8696	92	Okuma et al., 2023		yes	81±18
GeoB22336-4	353	354	353.5	AWI-5493.1.1	MBPF	9655	84	Okuma et al., 2023		yes	81±18
GeoB22336-4	443	444	443.5	AWI-7625.1.1	MBF	10904	126	Okuma et al., 2023		yes	81±18
GeoB22336-4	473	474	473.5	AWI-5494.1.1	MBF & Ostra.	10945	104	Okuma et al., 2023		yes	81±18
GeoB22336-4	498	499	498.5	AWI 1725.1.1	MBF	11811	136	Okuma et al., 2023		yes	81±18
GeoB22336-4	568	569	568.5	AWI-5495.1.1	MBPF	12968	119	Okuma et al., 2023		yes	81±18
GeoB22346-3	32	36	34	AWI-6222.1.1	MBF	2688	212	This study		yes	81±18
GeoB22346-3	152	155	153.5	AWI-6223.1.1	MBF	2442	71	This study		yes	81±18
GeoB22346-3	243	245	244	AWI-6224.1.1	MBF	3614	71	This study		yes	81±18
GeoB22346-3	387	387	387	AWI-1726.1.1	Mollusc shell	5929	51	Couette et al., 2023		yes	81±18
GeoB22346-3	483	485	484	AWI-6225.1.1	MBF	6833	85	This study		yes	81±18
GeoB22346-3	603	604	603.5	AWI-6226.1.1	MBF	8471	91	This study		yes	81±18
GeoB22346-3	723	724	723.5	AWI-6227.1.1	MBF	8421	102	This study		yes	81±18
GeoB22346-3	767	768	767.5	AWI-1727.1.1	Foram	8902	193	Couette et al., 2023		yes	81±18
GeoB22357-3	128	129	128.5	AWI-6229.1.1	MBF	9044	99	This study		yes	81±18
GeoB22357-3	218	219	218.5	AWI-6230.1.1	MBF	9915	98	This study		yes	81±18
GeoB22357-3	248	249	248.5	AWI-6231.1.1	MBF	9894	38	This study		yes	81±18
GeoB22357-3	308	309	308.5	AWI-6232.1.1	MBF	10025	33	This study		yes	81±18
GeoB22357-3	368	369	368.5	AWI-6233.1.1	MBF	10442	95	This study		yes	81±18
GeoB22357-3	398	399	398.5	AWI-6234.1.1	MBF	10246	36	This study		yes	81±18
HE-0006-4-2PC	25	27	26	KCC-50860	Planktonic foram, N. pachyderma (s)	9730	55	Ö Cofaigh et al. (2013a)		yes	-93±111
HE-0006-4-2PC	315	317	316	AA-82697	Planktonic foram, N. pachyderma (s)	21440	55	O Cofaigh et al. (2013a)		yes	250±100

HU2008029-012PC	110	112	111	CURL14071	NPS	11955	40	Jennings et al., 2017	reversal		No	-93±111
HU2008029-012PC	110	112	111	CURL14052	NPS	11690	30	Jennings et al., 2017	reversal		No	-93±111
HU2008029-012PC	111	112	111.5	CURL14506	Cassidulina neoteretis	10525	30	Jennings et al., 2017	reversal		No	-93±111
HU2008029-012PC	201	202	201.5	CURL14065	NPS	10760	35	Jennings et al., 2017			yes	-93±111
HU2008029-012PC	201	202	201.5	CURL16679	Cassidulina neoteretis	10490	40	Jennings et al., 2017	reversal		No	-93±111
HU2008029-012PC	201	202	201.5	CURL14055	Cassidulina neoteretis	10540	25	Jennings et al., 2017	reversal		No	-93±111
HU2008029-012PC	251	252	251.5	AA90386	NPS	12666	61	Jennings et al., 2017			yes	-93±111
HU2008029-012PC	469	470	469.5	CURL16671	NPS	14030	40	Jennings et al., 2017			yes	-93±111
HU2008029-012PC	571	572	571.5	CURL18165	NPS	15150	60	Jennings et al., 2017			yes	250±100
HU2008029-012PC	690	691	690.5	CURL14067	NPS	16660	45	Jennings et al., 2017			yes	250±100
HU2008029-012PC	780	781	780.5	CURL16663	NPS	16600	50	Jennings et al., 2017			yes	250±100
HU2008029-012PC	859	860	859.5	CURL18628	NPS	18540	80	Jennings et al., 2017			yes	250±100
HU2008-029-016PC	66	67	66.5	CAMS-151299	planktonic foram (Npl)	11905	40	Simon et al., 2012			yes	81±18
HU2008-029-016PC	79	80	79.5	CAMS-151297	planktonic foram (Npl)	12470	40	Simon et al., 2012			yes	81±18
HU2008-029-016PC	111	112	111.5	CAMS-151300	planktonic foram (Npl)	13820	130	Simon et al., 2012			yes	81±18

HU2008-029-34	157	157	157	UCIAMS-61330	Pelecypod fragments	4265	55	St Onge & St Onge2014		yes	-93±111
HU2008-029-34	280	280	280	UCIAMS-61331	Gastropod	5555	55	St Onge & St Onge2014		yes	-93±111
HU2008-029-34	513.5	513.5	513.5	NSRL-41637	PF (N. pachyderma sin.)	8290	35	Kelleher et al. 2022		yes	-93±111
HU2008-029-34	513.5	513.5	513.5	NSRL-41638	MBF	8340	60	Kelleher et al. 2022		yes	-93±111
HU76029-025	73.5	73.5	73.5	AA-17385	Plank forams	12830	95	Andrews et al. 1998		yes	81±18
HU76029-025	201	201	201	AA-21751	Plank forams	31710	1900	Andrews et al. 1998		yes	250±100
HU76029-025	596	596	596	CAMS-18937	Plank forams	40870	710	Andrews et al. 1998		yes	250±100
HU76029-034	37	37	37	AA-18388	Plank forams	12380	105	Andrews et al. 1998		yes	81±18
HU76029-034	300	300	300	AA-17386	Plank forams	49900	2000	Andrews et al. 1998	carbon dead	No	250±100
HU76029-034	411	411	411	AA-18389	Plank forams	40000	2000	Andrews et al. 1998		yes	250±100
HU77027-17PC	52.5	52.5	52.5	CAMS-19389	Gastropod	10800	50	Andrews et al. 1998		yes	-93±111
HU77027-17PC	127	127	127	AA-17388	Bivalve	11830	90	Andrews et al. 1998		yes	-93±111
HU77027-17PC	900	900	900	CAMS-17400	Plank forams	17990	110	Andrews et al. 1998		yes	250±100
HU77027-17PC	902	902	902	AA-18386	Plank forams	17930	210	Andrews et al. 1998		yes	250±100
HU82-SU5	165	165	165	AA-712	Shell	5800	330	Andrews et al. 1985; Andrews 1987		yes	81±18
HU82-SU5	275	279	277	AA-412	Shell	9410	400	Andrews et al. 1985; Andrews 1987		yes	81±18
HU82-SU5	618	618	618	AA-264	Shell	10490	450	Andrews et al. 1985; Andrews 1987		yes	81±18
JR175-GC01	27	29	28	Beta468820	C. neoteretis* + Trioculina*	10560	40	Owensworth et al., 2023		yes	81±18

JR175-GC01	38	41	39.5	Beta521060	C. neoteretis* + Trioculina*	10750	30	Owensworth et al., 2023		yes	81±18
JR175-GC01	57	59	58	Beta470332	N. pachyderma#	12310	40	Owensworth et al., 2023		yes	81±18
JR175-GC01	74	77	75.5	Beta521061	C. neoteretis*	12800	30	Owensworth et al., 2023		yes	81±18
JR175-GC01	97	99	98	BE-14923.1.1	N. pachyderma#	13425	78	Owensworth et al., 2023		yes	81±18
JR175-GC01	106	106	106	Beta483066	N. pachyderma#	14080	40	Owensworth et al., 2023		yes	81±18
JR175-GC01	106	106	106	BE-14924.1.1	N. pachyderma#	14053	65	Owensworth et al., 2023		yes	81±18
JR175-GC01	111	113	112	BE-14925.1.1	N. pachyderma#	14047	150	Owensworth et al., 2023		yes	81±18
JR175-GC01	118	120	119	BE-12425.1.1	N. pachyderma#	13637	139	Owensworth et al., 2023		yes	81±18
JR175-GC01	126	128	127	BE-12426.1.1	N. pachyderma# + C. neoteretis*	18608	209	Owensworth et al., 2023		yes	250±100
JR175-GC01	154	154	154	Beta483067	N. pachyderma#	35850	280	Owensworth et al., 2023		yes	250±100
JR175-GC01	168	168	168	BE-14926.1.1	N. pachyderma#	30996	730	Owensworth et al., 2023		yes	250±100
JR175-VC20	80	81	80.5	AA-90387	Seaweed	7464	66	O’Cofaigh et al. 2013b		yes	-93±111
JR175-VC20	110	111	110.5	AA-90388	Seaweed	8300	180	O’Cofaigh et al. 2013b		yes	-93±111
JR175-VC20	140	141	140.5	AA-90389	Seaweed	9030	200	O’Cofaigh et al. 2013b		yes	-93±111
JR175-VC20	261	262	261.5	BETA-265214	Paired bivalve	9700	50	O’Cofaigh et al. 2013b		yes	-93±111
JR175-VC20	301	303	302	BETA-265215	Paired bivalve	9780	50	O’Cofaigh et al. 2013b		yes	-93±111
JR175-VC20	408	409	408.5	AA-91731	Mollusc fragment	10914	59	O’Cofaigh et al. 2013b		yes	-93±111
JR175-VC20	477.5	478	477.75	BETA-265216	Shell fragment	10840	60	O’Cofaigh et al. 2013b		yes	-93±111
JR175-VC20	524	525	524.5	BETA-265217	Single valve	10910	60	O’Cofaigh et al. 2013b		yes	-93±111
JR175-VC24	149	150	149.5	CURL16082	Single valve, pelecypod	10525	42	Andrews et al. (2015), Hogan et al. (2016a)		yes	-93±111
JR175-VC24	165	165	165	CURL16666	(Yoldiella intermedia)	10455	42	Andrews et al. (2015), Hogan et al. (2016a)		yes	-93±111

JR175-VC24	217	218	217.5	CURL17355	Paired bivalve shell (sp. not known)	10680	46	Andrews et al. (2015), Hogan et al. (2016a)	yes	-93±111
JR175-VC29	54	57	55.5	CURL18625	Mixed benthic sp.	10160	40	Jennings et al., 2017	yes	-93±111
JR175-VC29	137	137	137	SUERC30594	Paired bivalve	10057	39	Jennings et al., 2017	yes	-93±111
JR175-VC29	225	226	225.5	CURL17354	Mixed benthic sp.	10570	40	Jennings et al., 2017	yes	-93±111
JR175-VC29	249	250	249.5	CURL17344	2 small gastropods	10690	40	Jennings et al., 2017	yes	-93±111
JR175-VC29	249	251	250	CURL17358	Cassidulina neoteretis	10710	35	Jennings et al., 2017	yes	-93±111
JR175-VC29	400	400	400	SUERC30596	Paired bivalve	12494	41	Jennings et al., 2017	yes	-93±111
JR175-VC29	424	427	425.5	CURL17359	Cassidulina neoteretis	12805	50	Jennings et al., 2017	yes	-93±111
JR175-VC29	424	426	425	CURL16675	NPS	12710	45	Jennings et al., 2017	yes	-93±111
JR175-VC29	494	494	494	SUERC30597	Paired bivalve	13194	63	Jennings et al., 2017	yes	-93±111
JR175-VC29	515	516	515.5	CURL16087	NPS	13255	40	Jennings et al., 2017	yes	-93±111
JR175-VC29	574	577	575.5	CURL17352	NPS	13760	60	Jennings et al., 2017	yes	-93±111
JR175-VC34	99	99	99	BETA-272267	Shell fragment	12490	70	Ö Cofaigh et al. (2013b, 2018)	yes	-93±111
JR175-VC34	130	132	131	BETA-272268	Shell fragment	12050	60	Ö Cofaigh et al. (2013b, 2018)	yes	-93±111
JR175-VC34	160	161	160.5	BETA-272269	Shell fragment	12550	70	Ö Cofaigh et al. (2013b, 2018)	yes	-93±111
JR175-VC34	183	183	183	BETA-272270	Shell fragment	12740	70	Ö Cofaigh et al. (2013b, 2018)	yes	-93±111
JR175-VC34	253	254	253.5	BETA-265220	Shell fragment (Nuculana pernula)	21770	100	Ö Cofaigh et al. (2013b, 2018)	yes	250±100
JR175-VC34	316	316	316	BETA-265221	Shell fragment	23310	160	Ö Cofaigh et al. (2013b, 2018)	yes	250±100

JR175-VC35	174.5	176.5	175.5	BETA-272271	Shell fragment	10940	60	Ö Cofaigh et al. (2013b, 2018), Jennings et al. (2013)	yes	-93±111
JR175-VC35	482	483	482.5	BETA-265222	Nuculana pernula (single valve)	15380	70	Ö Cofaigh et al. (2013b, 2018), Jennings et al. (2013)	yes	250±100
JR175-VC45	93	95	94	CURL-14050	I. norcrossi	12555	30	Sheldon et al., 2016	yes	-93±111
JR175-VC45	125	127	126	AA-89913	Mixed benthic foram	13211	92	Sheldon et al., 2016	yes	-93±111
JR175-VC46	120	121	120.5	CURL14068	Cassidulina	12770	30	Jennings et al., 2017	yes	-93±111
JR175-VC46	139	140	139.5	CURL16077	Echinoid spines	12930	40	Jennings et al., 2017	yes	-93±111
JR175-VC46	262	267	264.5	CURL16656	NPS	14570	60	Jennings et al., 2017	yes	-93±111
LSSL2001- 006	518	518	518	AAR-505	Shell	3405	55	Mudie et al. (2006)	yes	188±91
LSSL2001- 006	530	530	530	AAR-506	Shell	3375	42	Mudie et al. (2006)	yes	188±91
LSSL2001- 006	1080	1080	1080	AAR-507	Shell	6315	60	Mudie et al. (2006)	yes	188±91
MSM 343310	6	10	8	Poz-33417	Mix benthic forams	671	29	Perner et al, 2011	yes	-93±111
MSM 343310	18	20	19	Poz-33412	Mix benthic forams	659	33	Perner et al, 2011	yes	-93±111
MSM 343310	18	19	18.5	Poz-22357	Mollusc shell	682	32	Perner et al, 2011	yes	-93±111
MSM 343310	90	92	91	Poz-33453	Mix benthic forams	909	35	Perner et al, 2011	yes	-93±111
MSM 343310	149	151	150	Poz-33411	Mix benthic forams	1216	30	Perner et al, 2011	yes	-93±111
MSM 343310	204	205	204.5	Poz-30969	Mollusc shell	1384	27	Perner et al, 2011	yes	-93±111
MSM 343310	269	271	270	Poz-33413	Mix benthic forams	1526	34	Perner et al, 2011	yes	-93±111

MSM 343310	340	342	341	Poz-33488	Mix benthic forams	1768	46	Perner et al, 2011		yes	-93±111
MSM 343310	400	401	400.5	Poz-33414	Mix benthic forams	2074	29	Perner et al, 2011		yes	-93±111
MSM 343310	401	402	401.5	Poz-22359	Mollusc shell	2029	28	Perner et al, 2011		yes	-93±111
MSM 343310	457	458	457.5	Poz-30970	Mix benthic forams	2198	31	Perner et al, 2011		yes	-93±111
MSM 343310	519	521	520	Poz-33416	Mix benthic forams	2356	35	Perner et al, 2011		yes	-93±111
MSM 343310	600	601	600.5	Poz-30971	Mollusc shell	2733	30	Perner et al, 2011		yes	-93±111
MSM 343310	633	634	633.5	AAR-1699	Mollusc shell	2845	37	Perner et al, 2011		yes	-93±111
MSM 343310	691	692	691.5	Poz-30972	Mollusc shell	2956	30	Perner et al, 2011		yes	-93±111
MSM 343310	740	742	741	Poz-33418	Mix benthic forams	3217	34	Perner et al, 2011		yes	-93±111
MSM 343310	782	783	782.5	Poz-30973	Mollusc shell	3430	33	Perner et al, 2011		yes	-93±111
MSM 343310	856	857	856.5	Poz-30974	Mollusc shell	3544	32	Perner et al, 2011		yes	-93±111
MSM 343310	855	857	856	Poz-33419	Mix benthic forams	3541	36	Perner et al, 2011		yes	-93±111
MSM 343310	905	906	905.5	Poz-30975	Mollusc shell	3746	26	Perner et al, 2011		yes	-93±111
MSM343300	4	7	5.5	Poz-39052	Mix benthic foram	1415	35	Perner et al, 2013b		yes	-93±111
MSM343300	29	31	30	Poz-39051	Mix benthic foram	1645	30	Perner et al, 2013b		yes	-93±111
MSM343300	71	71	71	Poz-33489	Mix benthic foram	1990	50	Perner et al, 2013b		yes	-93±111
MSM343300	100	101	100.5	Poz-39047	Mix benthic foram	2305	30	Perner et al, 2013b		yes	-93±111

MSM343300	149	150	149.5	Poz-39048	Mix benthic foram	2750	60	Perner et al, 2013b		yes	-93±111
MSM343300	169	170	169.5	Poz-43445	Mix benthic foram	3005	35	Perner et al, 2013b		yes	-93±111
MSM343300	190	192	191	AA-81304	Paired Yoldia limatula	3248	44	Perner et al, 2013b		yes	-93±111
MSM343300	213	214	213.5	Poz-30985	Globobulimina auriculata arctica and Nonionellina labradorica	3715	35	Perner et al, 2013b		yes	-93±111
MSM343300	219	220	219.5	Poz-43446	Mix benthic foram	3820	50	Perner et al, 2013b		yes	-93±111
MSM343300	239	240	239.5	Poz-43447	Mix benthic foram	4410	50	Perner et al, 2013b		yes	-93±111
MSM343300	261.5	261.5	261.5	Poz-33456	G. auriculata arctica and N. labradorica	4490	40	Perner et al, 2013b		yes	-93±111
MSM343300	297.5	297.5	297.5	Poz-33457	N. labradorica	4970	40	Perner et al, 2013b		yes	-93±111
MSM343300	319	320	319.5	Poz-39053	Mix benthic foram	5440	40	Perner et al, 2013b		yes	-93±111
MSM343300	340	342	341	AA-81307	G. auriculata arctica and N. labradorica	5822	57	Perner et al, 2013b		yes	-93±111
MSM343300	358	360	359	Poz-39054	Mix benthic foram	6500	50	Perner et al, 2013b		yes	-93±111
MSM343300	381	381	381	LuS 9918	Mix benthic foram	6380	80	Quellet-Bernier et al.2014		yes	-93±111
MSM343300	399	400	399.5	Poz-39055	Mix benthic foram	7390	50	Perner et al, 2013b		yes	-93±111

MSM343300	434	434	434	LuS 9704	Mix benthic foram	7025	70	Quellet-Bernier et al.2014		yes	-93±111
MSM343300	455	457	456	LuS 9919	Mix benthic foram	7780	80	Perner et al, 2013b		yes	-93±111
MSM343300	467	467	467	Poz-30986	Shell fragments	8420	50	Perner et al, 2013b		yes	-93±111
MSM343300	540	543	541.5	LuS 9705	Mix benthic foram	8585	75	Perner et al, 2013b		yes	-93±111
MSM343300	597	598	597.5	Poz-33458	Unid gastropod	9390	60	Perner et al, 2013b		yes	-93±111
MSM343300	655	657	656	AA-81305	Paired Yoldia. chalky	9473	57	Perner et al, 2013b		yes	-93±111
MSM343300	667	669	668	LuS 9706	Mix benthic foram	9475	80	Perner et al, 2013b		yes	-93±111
MSM343300	976.5	976.5	976.5	LuS 9707	Mix benthic foram	9295	80	Quellet-Bernier et al.2014		yes	-93±111
MSM343300	1107	1119	1113	LuS 9708	Mix benthic foram	9455	90	Perner et al, 2013b		yes	-93±111
MSM-343520_G	41	41	41	Poz 22364	Shell	1205	30	McCarthy, 2011 (E-Diss. Chp. 6)		yes	-93±111
MSM-343520_G	161	161	161	Poz 22365	Shell	2260	30	McCarthy, 2011 (E-Diss. Chp. 6)		yes	-93±111
MSM-343520_G	216	218	217	LuS 8601	Benthic foram	3055	60	McCarthy, 2011 (E-Diss. Chp. 6)		yes	-93±111
MSM-343520_G	328	330	329	Lus 8550	Benthic foram	4730	70	McCarthy, 2011 (E-Diss. Chp. 6)		yes	-93±111
MSM-343520_G	452	456	454	Lus 8549	Benthic foram	6125	65	McCarthy, 2011 (E-Diss. Chp. 6)		yes	-93±111
MSM-343520_G	480	480	480	AAR 11700	Bivalve	6326	43	McCarthy, 2011 (E-Diss. Chp. 6)		yes	-93±111
MSM-343520_G	556	560	558	Lus 8548	Benthic	7065	70	McCarthy, 2011 (E-Diss. Chp. 6)		yes	-93±111

MSM-343520_G	640	642	641	Poz 30962	Bivalve	7900	40	McCarthy, 2011 (E-Diss. Chp. 6)	yes	-93±111
MSM-343520_G	692	694	693	Lus 8547	Benthic foram	8340	70	McCarthy, 2011 (E-Diss. Chp. 6)	yes	-93±111
MSM-343520_G	896	906	901	Lus 7707	Benthic foram	9970	100	McCarthy, 2011 (E-Diss. Chp. 6)	yes	-93±111
SL 170	24	27	25.5	ETH-55678	mixed benthic	9668	112	Jackson et al., 2017	yes	-93±111
SL 170	35	37	36	ETH-55679	mixed benthic	9460	80	Jackson et al., 2017	yes	-93±111
SL 170	55	57	56	ETH-55680	mixed benthic	9833	83	Jackson et al., 2017	yes	-93±111
SL 170	74	76	75	ETH-55682.2	planktonic (N. pachyderma)	10090	97	Jackson et al., 2017	yes	-93±111
SL 170	74	76	75	ETH-55682.1	mixed benthic	10028	87	Jackson et al., 2017	yes	-93±111
SL 170	74	76	75	ETH-55681	mixed benthic (replicate)	9901	82	Jackson et al., 2017	yes	-93±111
SL 170	98	100	99	ETH-55683.2	mixed benthic	10232	137	Jackson et al., 2017	yes	-93±111
SL 170	98	100	99	ETH-55683.1	mixed benthic (replicate)	10243	80	Jackson et al., 2017	yes	-93±111
SL 170	116	118	117	ETH-55685	planktonic (N. pachyderma)	10274	86	Jackson et al., 2017	yes	-93±111
SL 170	116	118	117	**ETH-55684	mixed benthic	11042	107	Jackson et al., 2017	yes	-93±111
SL 170	136	139	137.5	**ETH-55686	mollusc fragments	12990	117	Jackson et al., 2017	yes	-93±111
SL 170	136	139	137.5	**Beta - 344504	mixed benthic	10080	50	Jackson et al., 2017	yes	-93±111
SL 170	159	160	159.5	ETH-58352	mollusc fragments	10905	85	Jackson et al., 2017	yes	-93±111
SL 170	159	160	159.5	ETH-58351	mixed benthic	10755	85	Jackson et al., 2017	yes	-93±111
SL 170	180	181	180.5	ETH-58353	mixed benthic	10671	85	Jackson et al., 2017	yes	-93±111

SL 170	266	267	266.5	ETH-55687	mixed benthic	11267	100	Jackson et al., 2017		yes	-93±111
SL 170	288	289	288.5	ETH-58354	mixed benthic	11150	75	Jackson et al., 2017		yes	-93±111
SL 170	399	402	400.5	ETH-55689	planktonic (N. pachyderma)	11944	92	Jackson et al., 2017		yes	-93±111
SL 170	399	402	400.5	ETH-55688	mixed benthic	11597	104	Jackson et al., 2017		yes	-93±111
SL 170	484	488	486	KIA 40766	planktonic (N. pachyderma)	12730	60	Jackson et al., 2017		yes	-93±111
SL 170	636	637	636.5	ETH-58355	planktonic (N. pachyderma)	14640	130	Jackson et al., 2017		yes	-93±111
SL 174	97	100	98.5	ETH-55690	planktonic (N.pachyderma) and mixed benthic	9793	120	Jackson et al., 2017		yes	-93±111
SL 174	122	125	123.5	Beta-344508	planktonic (N.pachyderma) and mixed benthic	10390	40	Jackson et al., 2017		yes	-93±111
SL 174	142	145	143.5	ETH-55691	mixed benthic	10997	110	Jackson et al., 2017		yes	-93±111
SL 174	169	170	169.5	ETH-58356	mixed benthic	11010	85	Jackson et al., 2017		yes	-93±111
SL 174	196	199	197.5	Beta - 344505	planktonic (N. pachyderma)	11410	50	Jackson et al., 2017		yes	-93±111
SL 174	196	199	197.5	Beta - 344506	mixed benthic	11150	50	Jackson et al., 2017		yes	-93±111
SL 174	215	219	217	KIA 40767	planktonic (N. pachyderma)	12000	80	Jackson et al., 2017		yes	-93±111
SL 174	233	236	234.5	Beta - 344507	planktonic (N. pachyderma)	12580	60	Jackson et al., 2017		yes	-93±111
SL 174	278	279	278.5	ETH-58357	planktonic (N. pachyderma)	14510	120	Jackson et al., 2017		yes	-93±111
SL 174	294	295	294.5	ETH-58358	planktonic (N. pachyderma)	15060	110	Jackson et al., 2017		yes	250±100

SL 174	384	385	384.5	*ETH-58360.1	planktonic (N. pachyderma)	22380	289	Jackson et al. (2023)		yes	250±100
SL 174	384	385	384.5	*ETH-58360.3	planktonic (N. pachyderma) replicate	22640	190	Jackson et al. (2023)		yes	250±100
SL 174	400	401	400.5	ETH-64602	planktonic (N. pachyderma)	24010	310	Jackson et al. (2023)		yes	250±100
SL 174	455	456	455.5	*ETH-64603	planktonic (N. pachyderma)	24970	360	Jackson et al. (2023)		yes	250±100
SL 174	765	766	765.5	ETH-58362	mixed benthic	46370	3370	Jackson et al. (2023)		yes	250±100
VC01	24.5	24.5	24.5	CURL16085	Small shell fragments	1230	20	Hogan et al. (2016a)		yes	-93±111
VC01	180	181	180.5	CURL16084	Large shell fragments	2785	20	Hogan et al. (2016a)		yes	-93±111
VC05	20	22	21	AA-90391	Seaweed	1079	78	Streuff et al 2017b		yes	-93±111
VC05	50	52	51	AA-90392	Seaweed	1575	88	Streuff et al 2017b		yes	-93±111
VC05	112	113	112.5	Beta-434927	Seaweed	3930	30	Streuff et al 2017b		yes	-93±111
VC05	130	131	130.5	AA-90393	Seaweed	4159	50	Streuff et al 2017b		yes	-93±111
VC05	170	171	170.5	AA-90394	Seaweed	6322	60	Streuff et al 2017b		yes	-93±111
VC05	220	221	220.5	AA-90395	Seaweed	7250	380	Streuff et al 2017b		yes	-93±111
VC05	340	341	340.5	AA-90396	Seaweed	6370	180	Streuff et al 2017b		yes	-93±111
VC05	478	479	478.5	AA-90396	Paired Bivalve	8710	50	Streuff et al 2017b		yes	-93±111
VC07	140	142	141	Beta-434930	Foraminifera	9300	30	Streuff et al 2017b		yes	-93±111
VC07	280	281	280.5	Betae434931	Paired Bivalve	9850	30	Streuff et al 2017b		yes	-93±111
VC09	48	48	48	Beta-434933	Seaweed	6700	30	Streuff et al 2017b		yes	-93±111
VC09	137	137	137	Betae434934	Paired Bivalve	7330	30	Streuff et al 2017b		yes	-93±111
VC09	195	195	195	Betae434935	Paired Bivalve	7400	30	Streuff et al 2017b		yes	-93±111

VC09	316	318	317	Betae434936	Foraminifera	7800	30	Streuff et al 2017b		yes	-93±111
VC09	476	476	476	Betae265208	Paired Bivalve	7490	50	Streuff et al 2017b		yes	-93±111
VC09	575	575	575	Betae265209	Paired Bivalve	7970	50	Streuff et al 2017b		yes	-93±111
HU77029-006	25.5	25.5	25.5	AA-17384	Plank.Forams	12835	110	Andrews et al., 1998		yes	81±18
HU77029-006	384	384	384	CAMS-19388	Plank forams	48000	2000	Andrews et al., 1998		yes	250±100
HU76029-040	75	75	75	AA-17387	Plank forams	13170	125	Andrews et al., 1998		yes	81±18
HU76029-040	300	300	300	CAMS-19390	Plank forams	43800	1400	Andrews et al., 1998		yes	250±100
POR18	56	56	56	Beta161262	Bivalve	8700	40	Lloyd et al 2005		yes	-93±111
POR18	120	120	120	AA37711	Forams	9483	65	Lloyd et al 2005		yes	-93±111
VC06	250	250	250	Beta-434928	Single Bivalve	5580	30	Streuff et al 2017b		yes	-93±111
VC06	270	273	271.5	Betae434929	Seaweed	6280	30	Streuff et al 2017b		yes	-93±111

Table 9.3.3: Binned sedimentation rates (1 kyr slices) for the individual cores from Baffin Bay.

Core No in Fig. 1c	Core ID	Region	Depocenter	Location	Bin (ka BP)	Mean SR (cm/ka)
1	HU77029-006	Central Baffin Bay	Deep basin	NE Baffin Island	0.5	1.8
1	HU77029-006	Central Baffin Bay	Deep basin	NE Baffin Island	1.5	1.7
1	HU77029-006	Central Baffin Bay	Deep basin	NE Baffin Island	2.5	1.7
1	HU77029-006	Central Baffin Bay	Deep basin	NE Baffin Island	3.5	1.7
1	HU77029-006	Central Baffin Bay	Deep basin	NE Baffin Island	4.5	1.7
1	HU77029-006	Central Baffin Bay	Deep basin	NE Baffin Island	5.5	1.7
1	HU77029-006	Central Baffin Bay	Deep basin	NE Baffin Island	6.5	1.7
1	HU77029-006	Central Baffin Bay	Deep basin	NE Baffin Island	7.5	1.8
1	HU77029-006	Central Baffin Bay	Deep basin	NE Baffin Island	8.5	1.7

1	HU77029-006	Central Baffin Bay	Deep basin	NE Baffin Island	9.5	1.8
1	HU77029-006	Central Baffin Bay	Deep basin	NE Baffin Island	10.5	1.8
1	HU77029-006	Central Baffin Bay	Deep basin	NE Baffin Island	11.5	1.8
1	HU77029-006	Central Baffin Bay	Deep basin	NE Baffin Island	12.5	1.8
1	HU77029-006	Central Baffin Bay	Deep basin	NE Baffin Island	13.5	1.8
1	HU77029-006	Central Baffin Bay	Deep basin	NE Baffin Island	14.5	8.7
1	HU77029-006	Central Baffin Bay	Deep basin	NE Baffin Island	15.5	9.9
1	HU77029-006	Central Baffin Bay	Deep basin	NE Baffin Island	16.5	9.9
1	HU77029-006	Central Baffin Bay	Deep basin	NE Baffin Island	17.5	9.9
1	HU77029-006	Central Baffin Bay	Deep basin	NE Baffin Island	18.5	9.9
1	HU77029-006	Central Baffin Bay	Deep basin	NE Baffin Island	19.5	9.9
1	HU77029-006	Central Baffin Bay	Deep basin	NE Baffin Island	20.5	9.9
1	HU77029-006	Central Baffin Bay	Deep basin	NE Baffin Island	21.5	9.9
1	HU77029-006	Central Baffin Bay	Deep basin	NE Baffin Island	22.5	9.9
1	HU77029-006	Central Baffin Bay	Deep basin	NE Baffin Island	23.5	9.9
1	HU77029-006	Central Baffin Bay	Deep basin	NE Baffin Island	24.5	9.8
1	HU77029-006	Central Baffin Bay	Deep basin	NE Baffin Island	25.5	9.9
1	HU77029-006	Central Baffin Bay	Deep basin	NE Baffin Island	26.5	9.9
1	HU77029-006	Central Baffin Bay	Deep basin	NE Baffin Island	27.5	9.9
1	HU77029-006	Central Baffin Bay	Deep basin	NE Baffin Island	28.5	9.9
1	HU77029-006	Central Baffin Bay	Deep basin	NE Baffin Island	29.5	9.9
1	HU77029-006	Central Baffin Bay	Deep basin	NE Baffin Island	30.5	9.9
1	HU77029-006	Central Baffin Bay	Deep basin	NE Baffin Island	31.5	10.0
1	HU77029-006	Central Baffin Bay	Deep basin	NE Baffin Island	32.5	10.0
1	HU77029-006	Central Baffin Bay	Deep basin	NE Baffin Island	33.5	10.1

1	HU77029-006	Central Baffin Bay	Deep basin	NE Baffin Island	34.5	10.0
1	HU77029-006	Central Baffin Bay	Deep basin	NE Baffin Island	35.5	10.0
1	HU77029-006	Central Baffin Bay	Deep basin	NE Baffin Island	36.5	10.0
1	HU77029-006	Central Baffin Bay	Deep basin	NE Baffin Island	37.5	10.0
1	HU77029-006	Central Baffin Bay	Deep basin	NE Baffin Island	38.5	10.1
1	HU77029-006	Central Baffin Bay	Deep basin	NE Baffin Island	39.5	10.1
1	HU77029-006	Central Baffin Bay	Deep basin	NE Baffin Island	40.5	10.0
1	HU77029-006	Central Baffin Bay	Deep basin	NE Baffin Island	41.5	10.0
1	HU77029-006	Central Baffin Bay	Deep basin	NE Baffin Island	42.5	10.1
1	HU77029-006	Central Baffin Bay	Deep basin	NE Baffin Island	43.5	10.0
1	HU77029-006	Central Baffin Bay	Deep basin	NE Baffin Island	44.5	10.1
1	HU77029-006	Central Baffin Bay	Deep basin	NE Baffin Island	45.5	10.0
1	HU77029-006	Central Baffin Bay	Deep basin	NE Baffin Island	46.5	9.8
1	HU77029-006	Central Baffin Bay	Deep basin	NE Baffin Island	47.5	9.7
1	HU77029-006	Central Baffin Bay	Deep basin	NE Baffin Island	48.5	9.6
1	HU77029-006	Central Baffin Bay	Deep basin	NE Baffin Island	49.5	9.5
1	HU77029-006	Central Baffin Bay	Deep basin	NE Baffin Island	50.5	9.4
2	HU76029-034	Central Baffin Bay	Deep basin	central Baffin Bay	0.5	2.9
2	HU76029-034	Central Baffin Bay	Deep basin	central Baffin Bay	1.5	2.7
2	HU76029-034	Central Baffin Bay	Deep basin	central Baffin Bay	2.5	2.7
2	HU76029-034	Central Baffin Bay	Deep basin	central Baffin Bay	3.5	2.7
2	HU76029-034	Central Baffin Bay	Deep basin	central Baffin Bay	4.5	2.7
2	HU76029-034	Central Baffin Bay	Deep basin	central Baffin Bay	5.5	2.7
2	HU76029-034	Central Baffin Bay	Deep basin	central Baffin Bay	6.5	2.7
2	HU76029-034	Central Baffin Bay	Deep basin	central Baffin Bay	7.5	2.7

2	HU76029-034	Central Baffin Bay	Deep basin	central Baffin Bay	8.5	2.7
2	HU76029-034	Central Baffin Bay	Deep basin	central Baffin Bay	9.5	2.7
2	HU76029-034	Central Baffin Bay	Deep basin	central Baffin Bay	10.5	2.7
2	HU76029-034	Central Baffin Bay	Deep basin	central Baffin Bay	11.5	2.7
2	HU76029-034	Central Baffin Bay	Deep basin	central Baffin Bay	12.5	2.7
2	HU76029-034	Central Baffin Bay	Deep basin	central Baffin Bay	13.5	11.0
2	HU76029-034	Central Baffin Bay	Deep basin	central Baffin Bay	14.5	13.0
2	HU76029-034	Central Baffin Bay	Deep basin	central Baffin Bay	15.5	13.0
2	HU76029-034	Central Baffin Bay	Deep basin	central Baffin Bay	16.5	13.0
2	HU76029-034	Central Baffin Bay	Deep basin	central Baffin Bay	17.5	13.0
2	HU76029-034	Central Baffin Bay	Deep basin	central Baffin Bay	18.5	13.0
2	HU76029-034	Central Baffin Bay	Deep basin	central Baffin Bay	19.5	13.0
2	HU76029-034	Central Baffin Bay	Deep basin	central Baffin Bay	20.5	13.0
2	HU76029-034	Central Baffin Bay	Deep basin	central Baffin Bay	21.5	13.0
2	HU76029-034	Central Baffin Bay	Deep basin	central Baffin Bay	22.5	13.0
2	HU76029-034	Central Baffin Bay	Deep basin	central Baffin Bay	23.5	13.0
2	HU76029-034	Central Baffin Bay	Deep basin	central Baffin Bay	24.5	13.0
2	HU76029-034	Central Baffin Bay	Deep basin	central Baffin Bay	25.5	13.0
2	HU76029-034	Central Baffin Bay	Deep basin	central Baffin Bay	26.5	12.9
2	HU76029-034	Central Baffin Bay	Deep basin	central Baffin Bay	27.5	12.8
2	HU76029-034	Central Baffin Bay	Deep basin	central Baffin Bay	28.5	12.7
2	HU76029-034	Central Baffin Bay	Deep basin	central Baffin Bay	29.5	12.6
2	HU76029-034	Central Baffin Bay	Deep basin	central Baffin Bay	30.5	12.5
2	HU76029-034	Central Baffin Bay	Deep basin	central Baffin Bay	31.5	12.5
2	HU76029-034	Central Baffin Bay	Deep basin	central Baffin Bay	32.5	12.5

2	HU76029-034	Central Baffin Bay	Deep basin	central Baffin Bay	33.5	12.5
2	HU76029-034	Central Baffin Bay	Deep basin	central Baffin Bay	34.5	12.5
2	HU76029-034	Central Baffin Bay	Deep basin	central Baffin Bay	35.5	12.5
2	HU76029-034	Central Baffin Bay	Deep basin	central Baffin Bay	36.5	12.6
2	HU76029-034	Central Baffin Bay	Deep basin	central Baffin Bay	37.5	12.7
2	HU76029-034	Central Baffin Bay	Deep basin	central Baffin Bay	38.5	12.8
2	HU76029-034	Central Baffin Bay	Deep basin	central Baffin Bay	39.5	12.8
2	HU76029-034	Central Baffin Bay	Deep basin	central Baffin Bay	40.5	12.8
2	HU76029-034	Central Baffin Bay	Deep basin	central Baffin Bay	41.5	12.5
2	HU76029-034	Central Baffin Bay	Deep basin	central Baffin Bay	42.5	12.3
3	HE-0006-4-2PC	Central Baffin Bay	Deep basin	Uummannaq Trough	0.5	2.5
3	HE-0006-4-2PC	Central Baffin Bay	Deep basin	Uummannaq Trough	1.5	2.4
3	HE-0006-4-2PC	Central Baffin Bay	Deep basin	Uummannaq Trough	2.5	2.4
3	HE-0006-4-2PC	Central Baffin Bay	Deep basin	Uummannaq Trough	3.5	2.4
3	HE-0006-4-2PC	Central Baffin Bay	Deep basin	Uummannaq Trough	4.5	2.4
3	HE-0006-4-2PC	Central Baffin Bay	Deep basin	Uummannaq Trough	5.5	2.4
3	HE-0006-4-2PC	Central Baffin Bay	Deep basin	Uummannaq Trough	6.5	2.4
3	HE-0006-4-2PC	Central Baffin Bay	Deep basin	Uummannaq Trough	7.5	2.4
3	HE-0006-4-2PC	Central Baffin Bay	Deep basin	Uummannaq Trough	8.5	2.4
3	HE-0006-4-2PC	Central Baffin Bay	Deep basin	Uummannaq Trough	9.5	2.4
3	HE-0006-4-2PC	Central Baffin Bay	Deep basin	Uummannaq Trough	10.5	16.9
3	HE-0006-4-2PC	Central Baffin Bay	Deep basin	Uummannaq Trough	11.5	20.9
3	HE-0006-4-2PC	Central Baffin Bay	Deep basin	Uummannaq Trough	12.5	21.1
3	HE-0006-4-2PC	Central Baffin Bay	Deep basin	Uummannaq Trough	13.5	21.0
3	HE-0006-4-2PC	Central Baffin Bay	Deep basin	Uummannaq Trough	14.5	21.0

3	HE-0006-4-2PC	Central Baffin Bay	Deep basin	Uummannaq Trough	15.5	21.0
3	HE-0006-4-2PC	Central Baffin Bay	Deep basin	Uummannaq Trough	16.5	21.0
3	HE-0006-4-2PC	Central Baffin Bay	Deep basin	Uummannaq Trough	17.5	21.0
3	HE-0006-4-2PC	Central Baffin Bay	Deep basin	Uummannaq Trough	18.5	21.0
3	HE-0006-4-2PC	Central Baffin Bay	Deep basin	Uummannaq Trough	19.5	21.0
3	HE-0006-4-2PC	Central Baffin Bay	Deep basin	Uummannaq Trough	20.5	21.0
3	HE-0006-4-2PC	Central Baffin Bay	Deep basin	Uummannaq Trough	21.5	21.0
3	HE-0006-4-2PC	Central Baffin Bay	Deep basin	Uummannaq Trough	22.5	21.0
3	HE-0006-4-2PC	Central Baffin Bay	Deep basin	Uummannaq Trough	23.5	21.1
3	HE-0006-4-2PC	Central Baffin Bay	Deep basin	Uummannaq Trough	24.5	19.1
4	HU2008-029-016PC	Central Baffin Bay	Deep basin	central Baffin Bay	0.5	5.1
4	HU2008-029-016PC	Central Baffin Bay	Deep basin	central Baffin Bay	1.5	5.0
4	HU2008-029-016PC	Central Baffin Bay	Deep basin	central Baffin Bay	2.5	5.0
4	HU2008-029-016PC	Central Baffin Bay	Deep basin	central Baffin Bay	3.5	5.0
4	HU2008-029-016PC	Central Baffin Bay	Deep basin	central Baffin Bay	4.5	5.0
4	HU2008-029-016PC	Central Baffin Bay	Deep basin	central Baffin Bay	5.5	5.0
4	HU2008-029-016PC	Central Baffin Bay	Deep basin	central Baffin Bay	6.5	5.0
4	HU2008-029-016PC	Central Baffin Bay	Deep basin	central Baffin Bay	7.5	5.0
4	HU2008-029-016PC	Central Baffin Bay	Deep basin	central Baffin Bay	8.5	5.0
4	HU2008-029-016PC	Central Baffin Bay	Deep basin	central Baffin Bay	9.5	5.0
4	HU2008-029-016PC	Central Baffin Bay	Deep basin	central Baffin Bay	10.5	5.0
4	HU2008-029-016PC	Central Baffin Bay	Deep basin	central Baffin Bay	11.5	5.0
4	HU2008-029-016PC	Central Baffin Bay	Deep basin	central Baffin Bay	12.5	5.0
4	HU2008-029-016PC	Central Baffin Bay	Deep basin	central Baffin Bay	13.5	19.1
4	HU2008-029-016PC	Central Baffin Bay	Deep basin	central Baffin Bay	14.5	16.5

4	HU2008-029-016PC	Central Baffin Bay	Deep basin	central Baffin Bay	15.5	15.9
5	HU76029-040	Central Baffin Bay	Deep basin	E Baffin Island	0.5	5.1
5	HU76029-040	Central Baffin Bay	Deep basin	E Baffin Island	1.5	5.0
5	HU76029-040	Central Baffin Bay	Deep basin	E Baffin Island	2.5	5.0
5	HU76029-040	Central Baffin Bay	Deep basin	E Baffin Island	3.5	5.0
5	HU76029-040	Central Baffin Bay	Deep basin	E Baffin Island	4.5	5.0
5	HU76029-040	Central Baffin Bay	Deep basin	E Baffin Island	5.5	5.0
5	HU76029-040	Central Baffin Bay	Deep basin	E Baffin Island	6.5	5.0
5	HU76029-040	Central Baffin Bay	Deep basin	E Baffin Island	7.5	5.0
5	HU76029-040	Central Baffin Bay	Deep basin	E Baffin Island	8.5	5.0
5	HU76029-040	Central Baffin Bay	Deep basin	E Baffin Island	9.5	5.0
5	HU76029-040	Central Baffin Bay	Deep basin	E Baffin Island	10.5	5.0
5	HU76029-040	Central Baffin Bay	Deep basin	E Baffin Island	11.5	5.0
5	HU76029-040	Central Baffin Bay	Deep basin	E Baffin Island	12.5	5.0
5	HU76029-040	Central Baffin Bay	Deep basin	E Baffin Island	13.5	5.0
5	HU76029-040	Central Baffin Bay	Deep basin	E Baffin Island	14.5	5.3
5	HU76029-040	Central Baffin Bay	Deep basin	E Baffin Island	15.5	7.3
5	HU76029-040	Central Baffin Bay	Deep basin	E Baffin Island	16.5	7.3
5	HU76029-040	Central Baffin Bay	Deep basin	E Baffin Island	17.5	7.3
5	HU76029-040	Central Baffin Bay	Deep basin	E Baffin Island	18.5	7.3
5	HU76029-040	Central Baffin Bay	Deep basin	E Baffin Island	19.5	7.3
5	HU76029-040	Central Baffin Bay	Deep basin	E Baffin Island	20.5	7.3
5	HU76029-040	Central Baffin Bay	Deep basin	E Baffin Island	21.5	7.3
5	HU76029-040	Central Baffin Bay	Deep basin	E Baffin Island	22.5	7.3
5	HU76029-040	Central Baffin Bay	Deep basin	E Baffin Island	23.5	7.3

5	HU76029-040	Central Baffin Bay	Deep basin	E Baffin Island	24.5	7.3
5	HU76029-040	Central Baffin Bay	Deep basin	E Baffin Island	25.5	7.3
5	HU76029-040	Central Baffin Bay	Deep basin	E Baffin Island	26.5	7.3
5	HU76029-040	Central Baffin Bay	Deep basin	E Baffin Island	27.5	7.3
5	HU76029-040	Central Baffin Bay	Deep basin	E Baffin Island	28.5	7.3
5	HU76029-040	Central Baffin Bay	Deep basin	E Baffin Island	29.5	7.3
5	HU76029-040	Central Baffin Bay	Deep basin	E Baffin Island	30.5	7.3
5	HU76029-040	Central Baffin Bay	Deep basin	E Baffin Island	31.5	7.3
5	HU76029-040	Central Baffin Bay	Deep basin	E Baffin Island	32.5	7.3
5	HU76029-040	Central Baffin Bay	Deep basin	E Baffin Island	33.5	7.4
5	HU76029-040	Central Baffin Bay	Deep basin	E Baffin Island	34.5	7.4
5	HU76029-040	Central Baffin Bay	Deep basin	E Baffin Island	35.5	7.3
5	HU76029-040	Central Baffin Bay	Deep basin	E Baffin Island	36.5	7.3
5	HU76029-040	Central Baffin Bay	Deep basin	E Baffin Island	37.5	7.4
5	HU76029-040	Central Baffin Bay	Deep basin	E Baffin Island	38.5	7.4
5	HU76029-040	Central Baffin Bay	Deep basin	E Baffin Island	39.5	7.4
5	HU76029-040	Central Baffin Bay	Deep basin	E Baffin Island	40.5	7.4
5	HU76029-040	Central Baffin Bay	Deep basin	E Baffin Island	41.5	7.5
5	HU76029-040	Central Baffin Bay	Deep basin	E Baffin Island	42.5	7.4
5	HU76029-040	Central Baffin Bay	Deep basin	E Baffin Island	43.5	7.3
5	HU76029-040	Central Baffin Bay	Deep basin	E Baffin Island	44.5	7.2
5	HU76029-040	Central Baffin Bay	Deep basin	E Baffin Island	45.5	7.1
6	JR175-GC01	Central Baffin Bay	Deep basin	central Baffin Bay	0.5	2.4
6	JR175-GC01	Central Baffin Bay	Deep basin	central Baffin Bay	1.5	2.4
6	JR175-GC01	Central Baffin Bay	Deep basin	central Baffin Bay	2.5	2.4

6	JR175-GC01	Central Baffin Bay	Deep basin	central Baffin Bay	3.5	2.4
6	JR175-GC01	Central Baffin Bay	Deep basin	central Baffin Bay	4.5	2.4
6	JR175-GC01	Central Baffin Bay	Deep basin	central Baffin Bay	5.5	2.4
6	JR175-GC01	Central Baffin Bay	Deep basin	central Baffin Bay	6.5	2.4
6	JR175-GC01	Central Baffin Bay	Deep basin	central Baffin Bay	7.5	2.4
6	JR175-GC01	Central Baffin Bay	Deep basin	central Baffin Bay	8.5	2.4
6	JR175-GC01	Central Baffin Bay	Deep basin	central Baffin Bay	9.5	2.4
6	JR175-GC01	Central Baffin Bay	Deep basin	central Baffin Bay	10.5	2.4
6	JR175-GC01	Central Baffin Bay	Deep basin	central Baffin Bay	11.5	25.4
6	JR175-GC01	Central Baffin Bay	Deep basin	central Baffin Bay	12.5	11.4
6	JR175-GC01	Central Baffin Bay	Deep basin	central Baffin Bay	13.5	22.0
6	JR175-GC01	Central Baffin Bay	Deep basin	central Baffin Bay	14.5	23.7
6	JR175-GC01	Central Baffin Bay	Deep basin	central Baffin Bay	15.5	39.7
6	JR175-GC01	Central Baffin Bay	Deep basin	central Baffin Bay	16.5	1.4
6	JR175-GC01	Central Baffin Bay	Deep basin	central Baffin Bay	17.5	1.4
6	JR175-GC01	Central Baffin Bay	Deep basin	central Baffin Bay	18.5	1.5
6	JR175-GC01	Central Baffin Bay	Deep basin	central Baffin Bay	19.5	1.5
6	JR175-GC01	Central Baffin Bay	Deep basin	central Baffin Bay	20.5	1.9
6	JR175-GC01	Central Baffin Bay	Deep basin	central Baffin Bay	21.5	2.9
6	JR175-GC01	Central Baffin Bay	Deep basin	central Baffin Bay	22.5	3.2
6	JR175-GC01	Central Baffin Bay	Deep basin	central Baffin Bay	23.5	3.2
6	JR175-GC01	Central Baffin Bay	Deep basin	central Baffin Bay	24.5	3.2
6	JR175-GC01	Central Baffin Bay	Deep basin	central Baffin Bay	25.5	3.2
6	JR175-GC01	Central Baffin Bay	Deep basin	central Baffin Bay	26.5	3.2
6	JR175-GC01	Central Baffin Bay	Deep basin	central Baffin Bay	27.5	3.1

6	JR175-GC01	Central Baffin Bay	Deep basin	central Baffin Bay	28.5	3.0
6	JR175-GC01	Central Baffin Bay	Deep basin	central Baffin Bay	29.5	3.0
6	JR175-GC01	Central Baffin Bay	Deep basin	central Baffin Bay	30.5	3.0
6	JR175-GC01	Central Baffin Bay	Deep basin	central Baffin Bay	31.5	3.0
6	JR175-GC01	Central Baffin Bay	Deep basin	central Baffin Bay	32.5	3.0
6	JR175-GC01	Central Baffin Bay	Deep basin	central Baffin Bay	33.5	2.9
6	JR175-GC01	Central Baffin Bay	Deep basin	central Baffin Bay	34.5	2.9
7	HU76029-025	Central Baffin Bay	Deep basin	central Baffin Bay	0.5	5.1
7	HU76029-025	Central Baffin Bay	Deep basin	central Baffin Bay	1.5	5.1
7	HU76029-025	Central Baffin Bay	Deep basin	central Baffin Bay	2.5	5.1
7	HU76029-025	Central Baffin Bay	Deep basin	central Baffin Bay	3.5	5.1
7	HU76029-025	Central Baffin Bay	Deep basin	central Baffin Bay	4.5	5.1
7	HU76029-025	Central Baffin Bay	Deep basin	central Baffin Bay	5.5	5.1
7	HU76029-025	Central Baffin Bay	Deep basin	central Baffin Bay	6.5	5.1
7	HU76029-025	Central Baffin Bay	Deep basin	central Baffin Bay	7.5	5.1
7	HU76029-025	Central Baffin Bay	Deep basin	central Baffin Bay	8.5	5.1
7	HU76029-025	Central Baffin Bay	Deep basin	central Baffin Bay	9.5	5.1
7	HU76029-025	Central Baffin Bay	Deep basin	central Baffin Bay	10.5	5.1
7	HU76029-025	Central Baffin Bay	Deep basin	central Baffin Bay	11.5	5.1
7	HU76029-025	Central Baffin Bay	Deep basin	central Baffin Bay	12.5	5.1
7	HU76029-025	Central Baffin Bay	Deep basin	central Baffin Bay	13.5	5.2
7	HU76029-025	Central Baffin Bay	Deep basin	central Baffin Bay	14.5	5.7
7	HU76029-025	Central Baffin Bay	Deep basin	central Baffin Bay	15.5	6.0
7	HU76029-025	Central Baffin Bay	Deep basin	central Baffin Bay	16.5	6.0
7	HU76029-025	Central Baffin Bay	Deep basin	central Baffin Bay	17.5	6.0

7	HU76029-025	Central Baffin Bay	Deep basin	central Baffin Bay	18.5	6.0
7	HU76029-025	Central Baffin Bay	Deep basin	central Baffin Bay	19.5	6.0
7	HU76029-025	Central Baffin Bay	Deep basin	central Baffin Bay	20.5	6.0
7	HU76029-025	Central Baffin Bay	Deep basin	central Baffin Bay	21.5	6.0
7	HU76029-025	Central Baffin Bay	Deep basin	central Baffin Bay	22.5	6.0
7	HU76029-025	Central Baffin Bay	Deep basin	central Baffin Bay	23.5	6.1
7	HU76029-025	Central Baffin Bay	Deep basin	central Baffin Bay	24.5	6.1
7	HU76029-025	Central Baffin Bay	Deep basin	central Baffin Bay	25.5	6.2
7	HU76029-025	Central Baffin Bay	Deep basin	central Baffin Bay	26.5	6.1
7	HU76029-025	Central Baffin Bay	Deep basin	central Baffin Bay	27.5	6.1
7	HU76029-025	Central Baffin Bay	Deep basin	central Baffin Bay	28.5	6.1
7	HU76029-025	Central Baffin Bay	Deep basin	central Baffin Bay	29.5	6.0
7	HU76029-025	Central Baffin Bay	Deep basin	central Baffin Bay	30.5	6.0
7	HU76029-025	Central Baffin Bay	Deep basin	central Baffin Bay	31.5	5.9
7	HU76029-025	Central Baffin Bay	Deep basin	central Baffin Bay	32.5	5.9
7	HU76029-025	Central Baffin Bay	Deep basin	central Baffin Bay	33.5	5.8
7	HU76029-025	Central Baffin Bay	Deep basin	central Baffin Bay	34.5	5.8
7	HU76029-025	Central Baffin Bay	Deep basin	central Baffin Bay	35.5	45.1
7	HU76029-025	Central Baffin Bay	Deep basin	central Baffin Bay	36.5	49.0
7	HU76029-025	Central Baffin Bay	Deep basin	central Baffin Bay	37.5	48.7
7	HU76029-025	Central Baffin Bay	Deep basin	central Baffin Bay	38.5	51.3
7	HU76029-025	Central Baffin Bay	Deep basin	central Baffin Bay	39.5	56.8
7	HU76029-025	Central Baffin Bay	Deep basin	central Baffin Bay	40.5	55.3
7	HU76029-025	Central Baffin Bay	Deep basin	central Baffin Bay	41.5	55.0
7	HU76029-025	Central Baffin Bay	Deep basin	central Baffin Bay	42.5	54.6

7	HU76029-025	Central Baffin Bay	Deep basin	central Baffin Bay	43.5	51.4
8	64PC	Baffin Bay slope	Slope	NE Baffin Island	0.5	12.7
8	64PC	Baffin Bay slope	Slope	NE Baffin Island	1.5	12.7
8	64PC	Baffin Bay slope	Slope	NE Baffin Island	2.5	12.7
8	64PC	Baffin Bay slope	Slope	NE Baffin Island	3.5	12.7
8	64PC	Baffin Bay slope	Slope	NE Baffin Island	4.5	12.7
8	64PC	Baffin Bay slope	Slope	NE Baffin Island	5.5	12.7
8	64PC	Baffin Bay slope	Slope	NE Baffin Island	6.5	12.7
8	64PC	Baffin Bay slope	Slope	NE Baffin Island	7.5	12.7
8	64PC	Baffin Bay slope	Slope	NE Baffin Island	8.5	20.5
8	64PC	Baffin Bay slope	Slope	NE Baffin Island	9.5	32.9
8	64PC	Baffin Bay slope	Slope	NE Baffin Island	10.5	35.2
8	64PC	Baffin Bay slope	Slope	NE Baffin Island	11.5	53.5
8	64PC	Baffin Bay slope	Slope	NE Baffin Island	12.5	53.1
8	64PC	Baffin Bay slope	Slope	NE Baffin Island	13.5	51.3
9	2018042-48	Baffin Bay slope	Slope	SE Baffin Island	-0.5	11.9
9	2018042-48	Baffin Bay slope	Slope	SE Baffin Island	0.5	12.9
9	2018042-48	Baffin Bay slope	Slope	SE Baffin Island	1.5	12.9
9	2018042-48	Baffin Bay slope	Slope	SE Baffin Island	2.5	12.9
9	2018042-48	Baffin Bay slope	Slope	SE Baffin Island	3.5	12.9
9	2018042-48	Baffin Bay slope	Slope	SE Baffin Island	4.5	12.9
9	2018042-48	Baffin Bay slope	Slope	SE Baffin Island	5.5	12.8
9	2018042-48	Baffin Bay slope	Slope	SE Baffin Island	6.5	12.9
9	2018042-48	Baffin Bay slope	Slope	SE Baffin Island	7.5	12.9
9	2018042-48	Baffin Bay slope	Slope	SE Baffin Island	8.5	12.9

9	2018042-48	Baffin Bay slope	Slope	SE Baffin Island	9.5	12.9
9	2018042-48	Baffin Bay slope	Slope	SE Baffin Island	10.5	12.9
9	2018042-48	Baffin Bay slope	Slope	SE Baffin Island	11.5	12.9
9	2018042-48	Baffin Bay slope	Slope	SE Baffin Island	12.5	12.9
9	2018042-48	Baffin Bay slope	Slope	SE Baffin Island	13.5	12.9
9	2018042-48	Baffin Bay slope	Slope	SE Baffin Island	14.5	12.9
9	2018042-48	Baffin Bay slope	Slope	SE Baffin Island	15.5	11.9
9	2018042-48	Baffin Bay slope	Slope	SE Baffin Island	16.5	10.5
9	2018042-48	Baffin Bay slope	Slope	SE Baffin Island	17.5	10.5
9	2018042-48	Baffin Bay slope	Slope	SE Baffin Island	18.5	10.5
9	2018042-48	Baffin Bay slope	Slope	SE Baffin Island	19.5	10.5
9	2018042-48	Baffin Bay slope	Slope	SE Baffin Island	20.5	10.5
9	2018042-48	Baffin Bay slope	Slope	SE Baffin Island	21.5	10.5
9	2018042-48	Baffin Bay slope	Slope	SE Baffin Island	22.5	10.5
9	2018042-48	Baffin Bay slope	Slope	SE Baffin Island	23.5	10.5
9	2018042-48	Baffin Bay slope	Slope	SE Baffin Island	24.5	10.5
9	2018042-48	Baffin Bay slope	Slope	SE Baffin Island	25.5	10.3
9	2018042-48	Baffin Bay slope	Slope	SE Baffin Island	26.5	10.0
9	2018042-48	Baffin Bay slope	Slope	SE Baffin Island	27.5	9.8
9	2018042-48	Baffin Bay slope	Slope	SE Baffin Island	28.5	9.5
9	2018042-48	Baffin Bay slope	Slope	SE Baffin Island	29.5	9.5
9	2018042-48	Baffin Bay slope	Slope	SE Baffin Island	30.5	9.5
9	2018042-48	Baffin Bay slope	Slope	SE Baffin Island	31.5	9.5
9	2018042-48	Baffin Bay slope	Slope	SE Baffin Island	32.5	9.4
9	2018042-48	Baffin Bay slope	Slope	SE Baffin Island	33.5	9.2

9	2018042-48	Baffin Bay slope	Slope	SE Baffin Island	34.5	8.8
9	2018042-48	Baffin Bay slope	Slope	SE Baffin Island	35.5	8.5
9	2018042-48	Baffin Bay slope	Slope	SE Baffin Island	36.5	7.9
9	2018042-48	Baffin Bay slope	Slope	SE Baffin Island	37.5	7.5
9	2018042-48	Baffin Bay slope	Slope	SE Baffin Island	38.5	26.5
9	2018042-48	Baffin Bay slope	Slope	SE Baffin Island	39.5	38.3
9	2018042-48	Baffin Bay slope	Slope	SE Baffin Island	40.5	22.4
9	2018042-48	Baffin Bay slope	Slope	SE Baffin Island	41.5	18.2
9	2018042-48	Baffin Bay slope	Slope	SE Baffin Island	42.5	36.4
9	2018042-48	Baffin Bay slope	Slope	SE Baffin Island	43.5	39.1
9	2018042-48	Baffin Bay slope	Slope	SE Baffin Island	44.5	37.2
9	2018042-48	Baffin Bay slope	Slope	SE Baffin Island	45.5	33.4
9	2018042-48	Baffin Bay slope	Slope	SE Baffin Island	46.5	33.1
9	2018042-48	Baffin Bay slope	Slope	SE Baffin Island	47.5	33.7
10	SL 174	Baffin Bay slope	Slope	SE Baffin Island	0.5	9.1
10	SL 174	Baffin Bay slope	Slope	SE Baffin Island	1.5	9.1
10	SL 174	Baffin Bay slope	Slope	SE Baffin Island	2.5	9.1
10	SL 174	Baffin Bay slope	Slope	SE Baffin Island	3.5	9.1
10	SL 174	Baffin Bay slope	Slope	SE Baffin Island	4.5	9.2
10	SL 174	Baffin Bay slope	Slope	SE Baffin Island	5.5	9.1
10	SL 174	Baffin Bay slope	Slope	SE Baffin Island	6.5	9.1
10	SL 174	Baffin Bay slope	Slope	SE Baffin Island	7.5	9.2
10	SL 174	Baffin Bay slope	Slope	SE Baffin Island	8.5	9.2
10	SL 174	Baffin Bay slope	Slope	SE Baffin Island	9.5	9.2
10	SL 174	Baffin Bay slope	Slope	SE Baffin Island	10.5	20.6

10	SL 174	Baffin Bay slope	Slope	SE Baffin Island	11.5	34.3
10	SL 174	Baffin Bay slope	Slope	SE Baffin Island	12.5	67.8
10	SL 174	Baffin Bay slope	Slope	SE Baffin Island	13.5	26.7
10	SL 174	Baffin Bay slope	Slope	SE Baffin Island	14.5	18.6
10	SL 174	Baffin Bay slope	Slope	SE Baffin Island	15.5	18.0
10	SL 174	Baffin Bay slope	Slope	SE Baffin Island	16.5	24.6
10	SL 174	Baffin Bay slope	Slope	SE Baffin Island	17.5	20.0
10	SL 174	Baffin Bay slope	Slope	SE Baffin Island	18.5	10.4
10	SL 174	Baffin Bay slope	Slope	SE Baffin Island	19.5	10.7
10	SL 174	Baffin Bay slope	Slope	SE Baffin Island	20.5	10.8
10	SL 174	Baffin Bay slope	Slope	SE Baffin Island	21.5	10.8
10	SL 174	Baffin Bay slope	Slope	SE Baffin Island	22.5	10.9
10	SL 174	Baffin Bay slope	Slope	SE Baffin Island	23.5	10.9
10	SL 174	Baffin Bay slope	Slope	SE Baffin Island	24.5	10.8
10	SL 174	Baffin Bay slope	Slope	SE Baffin Island	25.5	11.4
10	SL 174	Baffin Bay slope	Slope	SE Baffin Island	26.5	11.9
10	SL 174	Baffin Bay slope	Slope	SE Baffin Island	27.5	47.1
10	SL 174	Baffin Bay slope	Slope	SE Baffin Island	28.5	23.7
10	SL 174	Baffin Bay slope	Slope	SE Baffin Island	29.5	13.7
10	SL 174	Baffin Bay slope	Slope	SE Baffin Island	30.5	13.9
10	SL 174	Baffin Bay slope	Slope	SE Baffin Island	31.5	14.2
10	SL 174	Baffin Bay slope	Slope	SE Baffin Island	32.5	14.3
10	SL 174	Baffin Bay slope	Slope	SE Baffin Island	33.5	14.6
10	SL 174	Baffin Bay slope	Slope	SE Baffin Island	34.5	14.7
10	SL 174	Baffin Bay slope	Slope	SE Baffin Island	35.5	14.8

10	SL 174	Baffin Bay slope	Slope	SE Baffin Island	36.5	14.9
10	SL 174	Baffin Bay slope	Slope	SE Baffin Island	37.5	15.3
10	SL 174	Baffin Bay slope	Slope	SE Baffin Island	38.5	15.6
10	SL 174	Baffin Bay slope	Slope	SE Baffin Island	39.5	15.8
10	SL 174	Baffin Bay slope	Slope	SE Baffin Island	40.5	15.6
10	SL 174	Baffin Bay slope	Slope	SE Baffin Island	41.5	15.5
10	SL 174	Baffin Bay slope	Slope	SE Baffin Island	42.5	15.2
10	SL 174	Baffin Bay slope	Slope	SE Baffin Island	43.5	14.9
10	SL 174	Baffin Bay slope	Slope	SE Baffin Island	44.5	14.7
10	SL 174	Baffin Bay slope	Slope	SE Baffin Island	45.5	14.5
10	SL 174	Baffin Bay slope	Slope	SE Baffin Island	46.5	14.4
10	SL 174	Baffin Bay slope	Slope	SE Baffin Island	47.5	14.3
10	SL 174	Baffin Bay slope	Slope	SE Baffin Island	48.5	14.3
10	SL 174	Baffin Bay slope	Slope	SE Baffin Island	49.5	14.6
11	77	Baffin Bay slope	Slope	SE Baffin Island	0.5	12.1
11	77	Baffin Bay slope	Slope	SE Baffin Island	1.5	12.1
11	77	Baffin Bay slope	Slope	SE Baffin Island	2.5	12.1
11	77	Baffin Bay slope	Slope	SE Baffin Island	3.5	12.1
11	77	Baffin Bay slope	Slope	SE Baffin Island	4.5	12.1
11	77	Baffin Bay slope	Slope	SE Baffin Island	5.5	12.1
11	77	Baffin Bay slope	Slope	SE Baffin Island	6.5	12.1
11	77	Baffin Bay slope	Slope	SE Baffin Island	7.5	12.1
11	77	Baffin Bay slope	Slope	SE Baffin Island	8.5	12.1
11	77	Baffin Bay slope	Slope	SE Baffin Island	9.5	12.1
11	77	Baffin Bay slope	Slope	SE Baffin Island	10.5	12.0

11	77	Baffin Bay slope	Slope	SE Baffin Island	11.5	19.8
11	77	Baffin Bay slope	Slope	SE Baffin Island	12.5	24.0
11	77	Baffin Bay slope	Slope	SE Baffin Island	13.5	24.0
11	77	Baffin Bay slope	Slope	SE Baffin Island	14.5	17.0
11	77	Baffin Bay slope	Slope	SE Baffin Island	15.5	16.1
11	77	Baffin Bay slope	Slope	SE Baffin Island	16.5	16.1
11	77	Baffin Bay slope	Slope	SE Baffin Island	17.5	16.1
11	77	Baffin Bay slope	Slope	SE Baffin Island	18.5	16.1
11	77	Baffin Bay slope	Slope	SE Baffin Island	19.5	16.1
11	77	Baffin Bay slope	Slope	SE Baffin Island	20.5	16.1
11	77	Baffin Bay slope	Slope	SE Baffin Island	21.5	16.1
11	77	Baffin Bay slope	Slope	SE Baffin Island	22.5	16.1
11	77	Baffin Bay slope	Slope	SE Baffin Island	23.5	16.1
11	77	Baffin Bay slope	Slope	SE Baffin Island	24.5	16.1
11	77	Baffin Bay slope	Slope	SE Baffin Island	25.5	16.1
11	77	Baffin Bay slope	Slope	SE Baffin Island	26.5	16.2
11	77	Baffin Bay slope	Slope	SE Baffin Island	27.5	16.2
11	77	Baffin Bay slope	Slope	SE Baffin Island	28.5	16.3
11	77	Baffin Bay slope	Slope	SE Baffin Island	29.5	16.1
11	77	Baffin Bay slope	Slope	SE Baffin Island	30.5	16.2
11	77	Baffin Bay slope	Slope	SE Baffin Island	31.5	16.3
11	77	Baffin Bay slope	Slope	SE Baffin Island	32.5	16.1
11	77	Baffin Bay slope	Slope	SE Baffin Island	33.5	16.2
11	77	Baffin Bay slope	Slope	SE Baffin Island	34.5	16.2
11	77	Baffin Bay slope	Slope	SE Baffin Island	35.5	16.2

11	77	Baffin Bay slope	Slope	SE Baffin Island	36.5	16.3
11	77	Baffin Bay slope	Slope	SE Baffin Island	37.5	16.2
11	77	Baffin Bay slope	Slope	SE Baffin Island	38.5	16.0
11	77	Baffin Bay slope	Slope	SE Baffin Island	39.5	15.8
11	77	Baffin Bay slope	Slope	SE Baffin Island	40.5	15.5
11	77	Baffin Bay slope	Slope	SE Baffin Island	41.5	15.5
12	2018042-64	Baffin Bay slope	Slope	SE Baffin Island	0.5	12.6
12	2018042-64	Baffin Bay slope	Slope	SE Baffin Island	1.5	12.6
12	2018042-64	Baffin Bay slope	Slope	SE Baffin Island	2.5	12.6
12	2018042-64	Baffin Bay slope	Slope	SE Baffin Island	3.5	12.6
12	2018042-64	Baffin Bay slope	Slope	SE Baffin Island	4.5	12.6
12	2018042-64	Baffin Bay slope	Slope	SE Baffin Island	5.5	12.6
12	2018042-64	Baffin Bay slope	Slope	SE Baffin Island	6.5	12.6
12	2018042-64	Baffin Bay slope	Slope	SE Baffin Island	7.5	12.6
12	2018042-64	Baffin Bay slope	Slope	SE Baffin Island	8.5	12.6
12	2018042-64	Baffin Bay slope	Slope	SE Baffin Island	9.5	12.6
12	2018042-64	Baffin Bay slope	Slope	SE Baffin Island	10.5	12.6
12	2018042-64	Baffin Bay slope	Slope	SE Baffin Island	11.5	12.6
12	2018042-64	Baffin Bay slope	Slope	SE Baffin Island	12.5	12.6
12	2018042-64	Baffin Bay slope	Slope	SE Baffin Island	13.5	12.6
12	2018042-64	Baffin Bay slope	Slope	SE Baffin Island	14.5	12.6
12	2018042-64	Baffin Bay slope	Slope	SE Baffin Island	15.5	12.6
12	2018042-64	Baffin Bay slope	Slope	SE Baffin Island	16.5	27.2
12	2018042-64	Baffin Bay slope	Slope	SE Baffin Island	17.5	42.7
12	2018042-64	Baffin Bay slope	Slope	SE Baffin Island	18.5	27.1

12	2018042-64	Baffin Bay slope	Slope	SE Baffin Island	19.5	19.0
12	2018042-64	Baffin Bay slope	Slope	SE Baffin Island	20.5	15.2
12	2018042-64	Baffin Bay slope	Slope	SE Baffin Island	21.5	13.5
12	2018042-64	Baffin Bay slope	Slope	SE Baffin Island	22.5	12.8
12	2018042-64	Baffin Bay slope	Slope	SE Baffin Island	23.5	86.3
12	2018042-64	Baffin Bay slope	Slope	SE Baffin Island	24.5	93.4
12	2018042-64	Baffin Bay slope	Slope	SE Baffin Island	25.5	50.4
13	2018042-65	Baffin Bay slope	Slope	SE Baffin Island	0.5	14.0
13	2018042-65	Baffin Bay slope	Slope	SE Baffin Island	1.5	13.9
13	2018042-65	Baffin Bay slope	Slope	SE Baffin Island	2.5	13.9
13	2018042-65	Baffin Bay slope	Slope	SE Baffin Island	3.5	13.9
13	2018042-65	Baffin Bay slope	Slope	SE Baffin Island	4.5	13.9
13	2018042-65	Baffin Bay slope	Slope	SE Baffin Island	5.5	13.9
13	2018042-65	Baffin Bay slope	Slope	SE Baffin Island	6.5	13.8
13	2018042-65	Baffin Bay slope	Slope	SE Baffin Island	7.5	13.8
13	2018042-65	Baffin Bay slope	Slope	SE Baffin Island	8.5	13.8
13	2018042-65	Baffin Bay slope	Slope	SE Baffin Island	9.5	13.8
13	2018042-65	Baffin Bay slope	Slope	SE Baffin Island	10.5	13.8
13	2018042-65	Baffin Bay slope	Slope	SE Baffin Island	11.5	13.8
13	2018042-65	Baffin Bay slope	Slope	SE Baffin Island	12.5	40.1
13	2018042-65	Baffin Bay slope	Slope	SE Baffin Island	13.5	44.4
13	2018042-65	Baffin Bay slope	Slope	SE Baffin Island	14.5	44.3
13	2018042-65	Baffin Bay slope	Slope	SE Baffin Island	15.5	44.2
13	2018042-65	Baffin Bay slope	Slope	SE Baffin Island	16.5	40.7
14	JR175-VC45	Baffin Bay slope	Slope	Uummannaq Trough	0.5	6.7

14	JR175-VC45	Baffin Bay slope	Slope	Uummannaq Trough	1.5	6.6
14	JR175-VC45	Baffin Bay slope	Slope	Uummannaq Trough	2.5	6.6
14	JR175-VC45	Baffin Bay slope	Slope	Uummannaq Trough	3.5	6.6
14	JR175-VC45	Baffin Bay slope	Slope	Uummannaq Trough	4.5	6.6
14	JR175-VC45	Baffin Bay slope	Slope	Uummannaq Trough	5.5	6.6
14	JR175-VC45	Baffin Bay slope	Slope	Uummannaq Trough	6.5	6.6
14	JR175-VC45	Baffin Bay slope	Slope	Uummannaq Trough	7.5	6.6
14	JR175-VC45	Baffin Bay slope	Slope	Uummannaq Trough	8.5	6.6
14	JR175-VC45	Baffin Bay slope	Slope	Uummannaq Trough	9.5	6.6
14	JR175-VC45	Baffin Bay slope	Slope	Uummannaq Trough	10.5	6.6
14	JR175-VC45	Baffin Bay slope	Slope	Uummannaq Trough	11.5	6.6
14	JR175-VC45	Baffin Bay slope	Slope	Uummannaq Trough	12.5	6.6
14	JR175-VC45	Baffin Bay slope	Slope	Uummannaq Trough	13.5	6.8
14	JR175-VC45	Baffin Bay slope	Slope	Uummannaq Trough	14.5	30.4
14	JR175-VC45	Baffin Bay slope	Slope	Uummannaq Trough	15.5	26.8
15	JR175-VC46	Baffin Bay slope	Slope	Uummannaq Trough	0.5	8.6
15	JR175-VC46	Baffin Bay slope	Slope	Uummannaq Trough	1.5	8.6
15	JR175-VC46	Baffin Bay slope	Slope	Uummannaq Trough	2.5	8.6
15	JR175-VC46	Baffin Bay slope	Slope	Uummannaq Trough	3.5	8.6
15	JR175-VC46	Baffin Bay slope	Slope	Uummannaq Trough	4.5	8.6
15	JR175-VC46	Baffin Bay slope	Slope	Uummannaq Trough	5.5	8.5
15	JR175-VC46	Baffin Bay slope	Slope	Uummannaq Trough	6.5	8.5
15	JR175-VC46	Baffin Bay slope	Slope	Uummannaq Trough	7.5	8.4
15	JR175-VC46	Baffin Bay slope	Slope	Uummannaq Trough	8.5	8.4
15	JR175-VC46	Baffin Bay slope	Slope	Uummannaq Trough	9.5	8.4

15	JR175-VC46	Baffin Bay slope	Slope	Uummannaq Trough	10.5	8.3
15	JR175-VC46	Baffin Bay slope	Slope	Uummannaq Trough	11.5	8.1
15	JR175-VC46	Baffin Bay slope	Slope	Uummannaq Trough	12.5	7.9
15	JR175-VC46	Baffin Bay slope	Slope	Uummannaq Trough	13.5	7.8
15	JR175-VC46	Baffin Bay slope	Slope	Uummannaq Trough	14.5	48.5
15	JR175-VC46	Baffin Bay slope	Slope	Uummannaq Trough	15.5	58.7
15	JR175-VC46	Baffin Bay slope	Slope	Uummannaq Trough	16.5	57.0
16	SL 170	Baffin Bay slope	Slope	Disko Bay	0.5	3.4
16	SL 170	Baffin Bay slope	Slope	Disko Bay	1.5	3.3
16	SL 170	Baffin Bay slope	Slope	Disko Bay	2.5	3.3
16	SL 170	Baffin Bay slope	Slope	Disko Bay	3.5	3.3
16	SL 170	Baffin Bay slope	Slope	Disko Bay	4.5	3.3
16	SL 170	Baffin Bay slope	Slope	Disko Bay	5.5	3.5
16	SL 170	Baffin Bay slope	Slope	Disko Bay	6.5	3.6
16	SL 170	Baffin Bay slope	Slope	Disko Bay	7.5	3.7
16	SL 170	Baffin Bay slope	Slope	Disko Bay	8.5	3.6
16	SL 170	Baffin Bay slope	Slope	Disko Bay	9.5	3.9
16	SL 170	Baffin Bay slope	Slope	Disko Bay	10.5	66.9
16	SL 170	Baffin Bay slope	Slope	Disko Bay	11.5	96.3
16	SL 170	Baffin Bay slope	Slope	Disko Bay	12.5	178.4
16	SL 170	Baffin Bay slope	Slope	Disko Bay	13.5	116.4
16	SL 170	Baffin Bay slope	Slope	Disko Bay	14.5	65.7
16	SL 170	Baffin Bay slope	Slope	Disko Bay	15.5	60.4
16	SL 170	Baffin Bay slope	Slope	Disko Bay	16.5	59.3
17	GeoB22304-3	Baffin Bay slope	Slope	Disko Bay	0.5	24.7

17	GeoB22304-3	Baffin Bay slope	Slope	Disko Bay	1.5	24.6
17	GeoB22304-3	Baffin Bay slope	Slope	Disko Bay	2.5	24.6
17	GeoB22304-3	Baffin Bay slope	Slope	Disko Bay	3.5	24.6
17	GeoB22304-3	Baffin Bay slope	Slope	Disko Bay	4.5	24.6
17	GeoB22304-3	Baffin Bay slope	Slope	Disko Bay	5.5	24.6
17	GeoB22304-3	Baffin Bay slope	Slope	Disko Bay	6.5	24.6
17	GeoB22304-3	Baffin Bay slope	Slope	Disko Bay	7.5	24.6
17	GeoB22304-3	Baffin Bay slope	Slope	Disko Bay	8.5	24.6
17	GeoB22304-3	Baffin Bay slope	Slope	Disko Bay	9.5	24.6
17	GeoB22304-3	Baffin Bay slope	Slope	Disko Bay	10.5	24.6
17	GeoB22304-3	Baffin Bay slope	Slope	Disko Bay	11.5	24.6
17	GeoB22304-3	Baffin Bay slope	Slope	Disko Bay	12.5	24.6
17	GeoB22304-3	Baffin Bay slope	Slope	Disko Bay	13.5	24.6
17	GeoB22304-3	Baffin Bay slope	Slope	Disko Bay	14.5	24.6
17	GeoB22304-3	Baffin Bay slope	Slope	Disko Bay	15.5	24.6
17	GeoB22304-3	Baffin Bay slope	Slope	Disko Bay	16.5	24.6
17	GeoB22304-3	Baffin Bay slope	Slope	Disko Bay	17.5	24.7
17	GeoB22304-3	Baffin Bay slope	Slope	Disko Bay	18.5	24.8
17	GeoB22304-3	Baffin Bay slope	Slope	Disko Bay	19.5	50.2
17	GeoB22304-3	Baffin Bay slope	Slope	Disko Bay	20.5	60.7
17	GeoB22304-3	Baffin Bay slope	Slope	Disko Bay	21.5	62.7
17	GeoB22304-3	Baffin Bay slope	Slope	Disko Bay	22.5	68.0
17	GeoB22304-3	Baffin Bay slope	Slope	Disko Bay	23.5	60.3
17	GeoB22304-3	Baffin Bay slope	Slope	Disko Bay	24.5	48.0
17	GeoB22304-3	Baffin Bay slope	Slope	Disko Bay	25.5	39.9

17	GeoB22304-3	Baffin Bay slope	Slope	Disko Bay	26.5	52.7
17	GeoB22304-3	Baffin Bay slope	Slope	Disko Bay	27.5	57.4
17	GeoB22304-3	Baffin Bay slope	Slope	Disko Bay	28.5	51.3
17	GeoB22304-3	Baffin Bay slope	Slope	Disko Bay	29.5	48.3
18	HU2008029-012PC	Baffin Bay slope	Slope	Disko Bay	-0.5	16.3
18	HU2008029-012PC	Baffin Bay slope	Slope	Disko Bay	0.5	16.5
18	HU2008029-012PC	Baffin Bay slope	Slope	Disko Bay	1.5	16.6
18	HU2008029-012PC	Baffin Bay slope	Slope	Disko Bay	2.5	16.5
18	HU2008029-012PC	Baffin Bay slope	Slope	Disko Bay	3.5	16.5
18	HU2008029-012PC	Baffin Bay slope	Slope	Disko Bay	4.5	16.5
18	HU2008029-012PC	Baffin Bay slope	Slope	Disko Bay	5.5	16.6
18	HU2008029-012PC	Baffin Bay slope	Slope	Disko Bay	6.5	16.6
18	HU2008029-012PC	Baffin Bay slope	Slope	Disko Bay	7.5	16.6
18	HU2008029-012PC	Baffin Bay slope	Slope	Disko Bay	8.5	16.6
18	HU2008029-012PC	Baffin Bay slope	Slope	Disko Bay	9.5	16.7
18	HU2008029-012PC	Baffin Bay slope	Slope	Disko Bay	10.5	16.7
18	HU2008029-012PC	Baffin Bay slope	Slope	Disko Bay	11.5	16.5
18	HU2008029-012PC	Baffin Bay slope	Slope	Disko Bay	12.5	29.1
18	HU2008029-012PC	Baffin Bay slope	Slope	Disko Bay	13.5	21.1
18	HU2008029-012PC	Baffin Bay slope	Slope	Disko Bay	14.5	107.3
18	HU2008029-012PC	Baffin Bay slope	Slope	Disko Bay	15.5	102.5
18	HU2008029-012PC	Baffin Bay slope	Slope	Disko Bay	16.5	100.9
18	HU2008029-012PC	Baffin Bay slope	Slope	Disko Bay	17.5	92.3
18	HU2008029-012PC	Baffin Bay slope	Slope	Disko Bay	18.5	165.6
18	HU2008029-012PC	Baffin Bay slope	Slope	Disko Bay	19.5	29.6

18	HU2008029-012PC	Baffin Bay slope	Slope	Disko Bay	20.5	42.4
18	HU2008029-012PC	Baffin Bay slope	Slope	Disko Bay	21.5	41.9
19	JR175-VC29	Baffin Bay slope	Slope	Disko Bay	0.5	11.1
19	JR175-VC29	Baffin Bay slope	Slope	Disko Bay	1.5	11.1
19	JR175-VC29	Baffin Bay slope	Slope	Disko Bay	2.5	11.1
19	JR175-VC29	Baffin Bay slope	Slope	Disko Bay	3.5	11.1
19	JR175-VC29	Baffin Bay slope	Slope	Disko Bay	4.5	11.2
19	JR175-VC29	Baffin Bay slope	Slope	Disko Bay	5.5	12.1
19	JR175-VC29	Baffin Bay slope	Slope	Disko Bay	6.5	13.4
19	JR175-VC29	Baffin Bay slope	Slope	Disko Bay	7.5	13.8
19	JR175-VC29	Baffin Bay slope	Slope	Disko Bay	8.5	13.8
19	JR175-VC29	Baffin Bay slope	Slope	Disko Bay	9.5	13.8
19	JR175-VC29	Baffin Bay slope	Slope	Disko Bay	10.5	13.2
19	JR175-VC29	Baffin Bay slope	Slope	Disko Bay	11.5	125.5
19	JR175-VC29	Baffin Bay slope	Slope	Disko Bay	12.5	75.2
19	JR175-VC29	Baffin Bay slope	Slope	Disko Bay	13.5	77.9
19	JR175-VC29	Baffin Bay slope	Slope	Disko Bay	14.5	100.9
19	JR175-VC29	Baffin Bay slope	Slope	Disko Bay	15.5	100.0
20	JR175-VC35	Baffin Bay slope	Slope	Disko Bay	0.5	14.3
20	JR175-VC35	Baffin Bay slope	Slope	Disko Bay	1.5	14.2
20	JR175-VC35	Baffin Bay slope	Slope	Disko Bay	2.5	14.2
20	JR175-VC35	Baffin Bay slope	Slope	Disko Bay	3.5	14.2
20	JR175-VC35	Baffin Bay slope	Slope	Disko Bay	4.5	14.2
20	JR175-VC35	Baffin Bay slope	Slope	Disko Bay	5.5	14.2
20	JR175-VC35	Baffin Bay slope	Slope	Disko Bay	6.5	14.2

20	JR175-VC35	Baffin Bay slope	Slope	Disko Bay	7.5	14.2
20	JR175-VC35	Baffin Bay slope	Slope	Disko Bay	8.5	14.2
20	JR175-VC35	Baffin Bay slope	Slope	Disko Bay	9.5	14.2
20	JR175-VC35	Baffin Bay slope	Slope	Disko Bay	10.5	14.2
20	JR175-VC35	Baffin Bay slope	Slope	Disko Bay	11.5	14.1
20	JR175-VC35	Baffin Bay slope	Slope	Disko Bay	12.5	53.9
20	JR175-VC35	Baffin Bay slope	Slope	Disko Bay	13.5	60.2
20	JR175-VC35	Baffin Bay slope	Slope	Disko Bay	14.5	60.0
20	JR175-VC35	Baffin Bay slope	Slope	Disko Bay	15.5	59.9
20	JR175-VC35	Baffin Bay slope	Slope	Disko Bay	16.5	59.9
20	JR175-VC35	Baffin Bay slope	Slope	Disko Bay	17.5	57.5
21	JR175-VC34	Baffin Bay slope	Slope	Disko Bay	-0.5	9.5
21	JR175-VC34	Baffin Bay slope	Slope	Disko Bay	0.5	9.7
21	JR175-VC34	Baffin Bay slope	Slope	Disko Bay	1.5	9.7
21	JR175-VC34	Baffin Bay slope	Slope	Disko Bay	2.5	9.7
21	JR175-VC34	Baffin Bay slope	Slope	Disko Bay	3.5	9.7
21	JR175-VC34	Baffin Bay slope	Slope	Disko Bay	4.5	9.7
21	JR175-VC34	Baffin Bay slope	Slope	Disko Bay	5.5	9.7
21	JR175-VC34	Baffin Bay slope	Slope	Disko Bay	6.5	9.7
21	JR175-VC34	Baffin Bay slope	Slope	Disko Bay	7.5	9.7
21	JR175-VC34	Baffin Bay slope	Slope	Disko Bay	8.5	9.7
21	JR175-VC34	Baffin Bay slope	Slope	Disko Bay	9.5	9.7
21	JR175-VC34	Baffin Bay slope	Slope	Disko Bay	10.5	9.7
21	JR175-VC34	Baffin Bay slope	Slope	Disko Bay	11.5	9.7
21	JR175-VC34	Baffin Bay slope	Slope	Disko Bay	12.5	9.7

21	JR175-VC34	Baffin Bay slope	Slope	Disko Bay	13.5	44.3
21	JR175-VC34	Baffin Bay slope	Slope	Disko Bay	14.5	39.5
21	JR175-VC34	Baffin Bay slope	Slope	Disko Bay	15.5	7.1
21	JR175-VC34	Baffin Bay slope	Slope	Disko Bay	16.5	7.2
21	JR175-VC34	Baffin Bay slope	Slope	Disko Bay	17.5	7.6
21	JR175-VC34	Baffin Bay slope	Slope	Disko Bay	18.5	7.5
21	JR175-VC34	Baffin Bay slope	Slope	Disko Bay	19.5	6.9
21	JR175-VC34	Baffin Bay slope	Slope	Disko Bay	20.5	6.6
21	JR175-VC34	Baffin Bay slope	Slope	Disko Bay	21.5	6.6
21	JR175-VC34	Baffin Bay slope	Slope	Disko Bay	22.5	6.5
21	JR175-VC34	Baffin Bay slope	Slope	Disko Bay	23.5	6.5
21	JR175-VC34	Baffin Bay slope	Slope	Disko Bay	24.5	27.2
21	JR175-VC34	Baffin Bay slope	Slope	Disko Bay	25.5	41.4
21	JR175-VC34	Baffin Bay slope	Slope	Disko Bay	26.5	26.5
22	HU77027-17PC	Baffin Bay slope	Slope	Davis Strait	0.5	4.4
22	HU77027-17PC	Baffin Bay slope	Slope	Davis Strait	1.5	4.3
22	HU77027-17PC	Baffin Bay slope	Slope	Davis Strait	2.5	4.3
22	HU77027-17PC	Baffin Bay slope	Slope	Davis Strait	3.5	4.3
22	HU77027-17PC	Baffin Bay slope	Slope	Davis Strait	4.5	4.3
22	HU77027-17PC	Baffin Bay slope	Slope	Davis Strait	5.5	4.3
22	HU77027-17PC	Baffin Bay slope	Slope	Davis Strait	6.5	4.3
22	HU77027-17PC	Baffin Bay slope	Slope	Davis Strait	7.5	4.3
22	HU77027-17PC	Baffin Bay slope	Slope	Davis Strait	8.5	4.3
22	HU77027-17PC	Baffin Bay slope	Slope	Davis Strait	9.5	4.3
22	HU77027-17PC	Baffin Bay slope	Slope	Davis Strait	10.5	4.3

22	HU77027-17PC	Baffin Bay slope	Slope	Davis Strait	11.5	4.2
22	HU77027-17PC	Baffin Bay slope	Slope	Davis Strait	12.5	77.8
22	HU77027-17PC	Baffin Bay slope	Slope	Davis Strait	13.5	102.8
22	HU77027-17PC	Baffin Bay slope	Slope	Davis Strait	14.5	108.2
22	HU77027-17PC	Baffin Bay slope	Slope	Davis Strait	15.5	107.3
22	HU77027-17PC	Baffin Bay slope	Slope	Davis Strait	16.5	107.6
22	HU77027-17PC	Baffin Bay slope	Slope	Davis Strait	17.5	107.0
22	HU77027-17PC	Baffin Bay slope	Slope	Davis Strait	18.5	106.8
22	HU77027-17PC	Baffin Bay slope	Slope	Davis Strait	19.5	106.1
22	HU77027-17PC	Baffin Bay slope	Slope	Davis Strait	20.5	98.3
23	JR175-VC20	West Greenland	Outer Shelf	Disko Bay	0.5	10.2
23	JR175-VC20	West Greenland	Outer Shelf	Disko Bay	1.5	10.2
23	JR175-VC20	West Greenland	Outer Shelf	Disko Bay	2.5	10.2
23	JR175-VC20	West Greenland	Outer Shelf	Disko Bay	3.5	10.2
23	JR175-VC20	West Greenland	Outer Shelf	Disko Bay	4.5	10.2
23	JR175-VC20	West Greenland	Outer Shelf	Disko Bay	5.5	10.2
23	JR175-VC20	West Greenland	Outer Shelf	Disko Bay	6.5	10.3
23	JR175-VC20	West Greenland	Outer Shelf	Disko Bay	7.5	18.7
23	JR175-VC20	West Greenland	Outer Shelf	Disko Bay	8.5	34.3
23	JR175-VC20	West Greenland	Outer Shelf	Disko Bay	9.5	100.7
23	JR175-VC20	West Greenland	Outer Shelf	Disko Bay	10.5	132.7
23	JR175-VC20	West Greenland	Outer Shelf	Disko Bay	11.5	138.6
23	JR175-VC20	West Greenland	Outer Shelf	Disko Bay	12.5	181.2
24	70PC	West Greenland	Outer Shelf	Disko Bay	0.5	1.9
24	70PC	West Greenland	Outer Shelf	Disko Bay	1.5	1.8

24	70PC	West Greenland	Outer Shelf	Disko Bay	2.5	1.8
24	70PC	West Greenland	Outer Shelf	Disko Bay	3.5	1.8
24	70PC	West Greenland	Outer Shelf	Disko Bay	4.5	1.8
24	70PC	West Greenland	Outer Shelf	Disko Bay	5.5	1.8
24	70PC	West Greenland	Outer Shelf	Disko Bay	6.5	1.8
24	70PC	West Greenland	Outer Shelf	Disko Bay	7.5	19.7
24	70PC	West Greenland	Outer Shelf	Disko Bay	8.5	28.0
24	70PC	West Greenland	Outer Shelf	Disko Bay	9.5	60.4
24	70PC	West Greenland	Outer Shelf	Disko Bay	10.5	66.3
24	70PC	West Greenland	Outer Shelf	Disko Bay	11.5	66.5
25	70TWC	West Greenland	Outer Shelf	Disko Bay	-0.5	28.1
25	70TWC	West Greenland	Outer Shelf	Disko Bay	0.5	29.3
25	70TWC	West Greenland	Outer Shelf	Disko Bay	1.5	28.9
25	70TWC	West Greenland	Outer Shelf	Disko Bay	2.5	32.5
25	70TWC	West Greenland	Outer Shelf	Disko Bay	3.5	36.8
25	70TWC	West Greenland	Outer Shelf	Disko Bay	4.5	12.0
25	70TWC	West Greenland	Outer Shelf	Disko Bay	5.5	12.4
25	70TWC	West Greenland	Outer Shelf	Disko Bay	6.5	19.5
25	70TWC	West Greenland	Outer Shelf	Disko Bay	7.5	17.2
25	70TWC	West Greenland	Outer Shelf	Disko Bay	8.5	27.9
26	VC01	West Greenland	Mid Shelf	Disko Bay	0.5	59.7
26	VC01	West Greenland	Mid Shelf	Disko Bay	1.5	91.4
26	VC01	West Greenland	Mid Shelf	Disko Bay	2.5	87.1
27	JR175-VC24	West Greenland	Mid Shelf	Disko Bay	-0.5	13.7
27	JR175-VC24	West Greenland	Mid Shelf	Disko Bay	0.5	14.0

27	JR175-VC24	West Greenland	Mid Shelf	Disko Bay	1.5	14.0
27	JR175-VC24	West Greenland	Mid Shelf	Disko Bay	2.5	14.0
27	JR175-VC24	West Greenland	Mid Shelf	Disko Bay	3.5	14.0
27	JR175-VC24	West Greenland	Mid Shelf	Disko Bay	4.5	14.0
27	JR175-VC24	West Greenland	Mid Shelf	Disko Bay	5.5	13.7
27	JR175-VC24	West Greenland	Mid Shelf	Disko Bay	6.5	13.6
27	JR175-VC24	West Greenland	Mid Shelf	Disko Bay	7.5	13.5
27	JR175-VC24	West Greenland	Mid Shelf	Disko Bay	8.5	13.6
27	JR175-VC24	West Greenland	Mid Shelf	Disko Bay	9.5	14.4
27	JR175-VC24	West Greenland	Mid Shelf	Disko Bay	10.5	16.3
27	JR175-VC24	West Greenland	Mid Shelf	Disko Bay	11.5	120.4
28	343340-GC	West Greenland	Mid Shelf	Disko Bay	-0.5	21.0
28	343340-GC	West Greenland	Mid Shelf	Disko Bay	0.5	25.5
28	343340-GC	West Greenland	Mid Shelf	Disko Bay	1.5	25.5
28	343340-GC	West Greenland	Mid Shelf	Disko Bay	2.5	13.5
28	343340-GC	West Greenland	Mid Shelf	Disko Bay	3.5	10.2
28	343340-GC	West Greenland	Mid Shelf	Disko Bay	4.5	9.9
28	343340-GC	West Greenland	Mid Shelf	Disko Bay	5.5	13.8
28	343340-GC	West Greenland	Mid Shelf	Disko Bay	6.5	13.4
28	343340-GC	West Greenland	Mid Shelf	Disko Bay	7.5	11.1
28	343340-GC	West Greenland	Mid Shelf	Disko Bay	8.5	195.5
28	343340-GC	West Greenland	Mid Shelf	Disko Bay	9.5	167.4
28	343340-GC	West Greenland	Mid Shelf	Disko Bay	10.5	187.9
28	343340-GC	West Greenland	Mid Shelf	Disko Bay	11.5	249.6
29	MSM343300	West Greenland	Inner Shelf	Disko Bay	0.5	61.9

29	MSM343300	West Greenland	Inner Shelf	Disko Bay	1.5	96.4
29	MSM343300	West Greenland	Inner Shelf	Disko Bay	2.5	76.8
29	MSM343300	West Greenland	Inner Shelf	Disko Bay	3.5	42.2
29	MSM343300	West Greenland	Inner Shelf	Disko Bay	4.5	59.7
29	MSM343300	West Greenland	Inner Shelf	Disko Bay	5.5	50.3
29	MSM343300	West Greenland	Inner Shelf	Disko Bay	6.5	59.4
29	MSM343300	West Greenland	Inner Shelf	Disko Bay	7.5	72.2
29	MSM343300	West Greenland	Inner Shelf	Disko Bay	8.5	161.7
29	MSM343300	West Greenland	Inner Shelf	Disko Bay	9.5	522.7
29	MSM343300	West Greenland	Inner Shelf	Disko Bay	10.5	559.8
30	MSM 343310	West Greenland	Inner Shelf	Disko Bay	-0.5	101.6
30	MSM 343310	West Greenland	Inner Shelf	Disko Bay	0.5	296.1
30	MSM 343310	West Greenland	Inner Shelf	Disko Bay	1.5	272.8
30	MSM 343310	West Greenland	Inner Shelf	Disko Bay	2.5	226.9
30	MSM 343310	West Greenland	Inner Shelf	Disko Bay	3.5	280.6
31	DA00-02P	West Greenland	Inner Shelf	Disko Bay	0.5	253.3
31	DA00-02P	West Greenland	Inner Shelf	Disko Bay	1.5	393.6
31	DA00-02P	West Greenland	Inner Shelf	Disko Bay	2.5	408.3
31	DA00-02P	West Greenland	Inner Shelf	Disko Bay	3.5	565.6
32	343330-GC	West Greenland	Inner Shelf	Disko Bay	0.5	27.4
32	343330-GC	West Greenland	Inner Shelf	Disko Bay	1.5	27.4
32	343330-GC	West Greenland	Inner Shelf	Disko Bay	2.5	27.5
32	343330-GC	West Greenland	Inner Shelf	Disko Bay	3.5	53.4
32	343330-GC	West Greenland	Inner Shelf	Disko Bay	4.5	66.9
32	343330-GC	West Greenland	Inner Shelf	Disko Bay	5.5	237.2

32	343330-GC	West Greenland	Inner Shelf	Disko Bay	6.5	69.2
32	343330-GC	West Greenland	Inner Shelf	Disko Bay	7.5	49.2
32	343330-GC	West Greenland	Inner Shelf	Disko Bay	8.5	53.6
33	DA00-03P	West Greenland	Inner Shelf	Disko Bay	-0.5	161.9
33	DA00-03P	West Greenland	Inner Shelf	Disko Bay	0.5	267.8
33	DA00-03P	West Greenland	Inner Shelf	Disko Bay	1.5	450.2
33	DA00-03P	West Greenland	Inner Shelf	Disko Bay	2.5	360.2
33	DA00-03P	West Greenland	Inner Shelf	Disko Bay	3.5	171.9
34	DA05	West Greenland	Inner Shelf	Disko Bay	0.5	42.3
34	DA05	West Greenland	Inner Shelf	Disko Bay	1.5	127.9
34	DA05	West Greenland	Inner Shelf	Disko Bay	2.5	116.9
34	DA05	West Greenland	Inner Shelf	Disko Bay	3.5	250.5
34	DA05	West Greenland	Inner Shelf	Disko Bay	4.5	210.7
34	DA05	West Greenland	Inner Shelf	Disko Bay	5.5	184.1
34	DA05	West Greenland	Inner Shelf	Disko Bay	6.5	197.7
35	DA00-04P	West Greenland	Inner Shelf	Disko Bay	-0.5	64.6
35	DA00-04P	West Greenland	Inner Shelf	Disko Bay	0.5	75.1
35	DA00-04P	West Greenland	Inner Shelf	Disko Bay	1.5	64.6
35	DA00-04P	West Greenland	Inner Shelf	Disko Bay	2.5	34.2
35	DA00-04P	West Greenland	Inner Shelf	Disko Bay	3.5	48.0
35	DA00-04P	West Greenland	Inner Shelf	Disko Bay	4.5	58.8
35	DA00-04P	West Greenland	Inner Shelf	Disko Bay	5.5	81.7
35	DA00-04P	West Greenland	Inner Shelf	Disko Bay	6.5	203.8
35	DA00-04P	West Greenland	Inner Shelf	Disko Bay	7.5	285.2
36	VC05	West Greenland	Inner Shelf	Disko Bay	0.5	44.9

36	VC05	West Greenland	Inner Shelf	Disko Bay	1.5	31.3
36	VC05	West Greenland	Inner Shelf	Disko Bay	2.5	23.5
36	VC05	West Greenland	Inner Shelf	Disko Bay	3.5	31.1
36	VC05	West Greenland	Inner Shelf	Disko Bay	4.5	29.4
36	VC05	West Greenland	Inner Shelf	Disko Bay	5.5	14.7
36	VC05	West Greenland	Inner Shelf	Disko Bay	6.5	485.4
36	VC05	West Greenland	Inner Shelf	Disko Bay	7.5	50.5
36	VC05	West Greenland	Inner Shelf	Disko Bay	8.5	64.0
36	VC05	West Greenland	Inner Shelf	Disko Bay	9.5	65.5
37	VC09	West Greenland	Inner Shelf	Disko Bay	0.5	6.9
37	VC09	West Greenland	Inner Shelf	Disko Bay	1.5	6.7
37	VC09	West Greenland	Inner Shelf	Disko Bay	2.5	6.7
37	VC09	West Greenland	Inner Shelf	Disko Bay	3.5	6.7
37	VC09	West Greenland	Inner Shelf	Disko Bay	4.5	6.7
37	VC09	West Greenland	Inner Shelf	Disko Bay	5.5	6.7
37	VC09	West Greenland	Inner Shelf	Disko Bay	6.5	6.6
37	VC09	West Greenland	Inner Shelf	Disko Bay	7.5	1007.8
37	VC09	West Greenland	Inner Shelf	Disko Bay	8.5	249.7
38	DA00-06	West Greenland	Inner Shelf	Disko Bay	0.5	6.5
38	DA00-06	West Greenland	Inner Shelf	Disko Bay	1.5	13.5
38	DA00-06	West Greenland	Inner Shelf	Disko Bay	2.5	13.5
38	DA00-06	West Greenland	Inner Shelf	Disko Bay	3.5	12.4
38	DA00-06	West Greenland	Inner Shelf	Disko Bay	4.5	10.8
38	DA00-06	West Greenland	Inner Shelf	Disko Bay	5.5	10.9
38	DA00-06	West Greenland	Inner Shelf	Disko Bay	6.5	291.5

38	DA00-06	West Greenland	Inner Shelf	Disko Bay	7.5	698.6
38	DA00-06	West Greenland	Inner Shelf	Disko Bay	8.5	615.8
39	ACDC2014-001	West Greenland	Inner Shelf	Disko Bay	-0.5	133.3
39	ACDC2014-001	West Greenland	Inner Shelf	Disko Bay	0.5	180.3
39	ACDC2014-001	West Greenland	Inner Shelf	Disko Bay	1.5	42.9
40	ACDC2014-003	West Greenland	Inner Shelf	Disko Bay	-0.5	143.9
40	ACDC2014-003	West Greenland	Inner Shelf	Disko Bay	0.5	133.4
40	ACDC2014-003	West Greenland	Inner Shelf	Disko Bay	1.5	78.5
41	POR18	West Greenland	Inner Shelf	Jakobshavn Isfjord	0.5	6.1
41	POR18	West Greenland	Inner Shelf	Jakobshavn Isfjord	1.5	6.0
41	POR18	West Greenland	Inner Shelf	Jakobshavn Isfjord	2.5	6.0
41	POR18	West Greenland	Inner Shelf	Jakobshavn Isfjord	3.5	6.0
41	POR18	West Greenland	Inner Shelf	Jakobshavn Isfjord	4.5	6.0
41	POR18	West Greenland	Inner Shelf	Jakobshavn Isfjord	5.5	6.0
41	POR18	West Greenland	Inner Shelf	Jakobshavn Isfjord	6.5	6.0
41	POR18	West Greenland	Inner Shelf	Jakobshavn Isfjord	7.5	6.0
41	POR18	West Greenland	Inner Shelf	Jakobshavn Isfjord	8.5	6.0
41	POR18	West Greenland	Inner Shelf	Jakobshavn Isfjord	9.5	62.8
41	POR18	West Greenland	Inner Shelf	Jakobshavn Isfjord	10.5	60.2
42	VC06	West Greenland	Inner Shelf	Disko	-0.5	40.0
42	VC06	West Greenland	Inner Shelf	Disko	0.5	42.5
42	VC06	West Greenland	Inner Shelf	Disko	1.5	42.5
42	VC06	West Greenland	Inner Shelf	Disko	2.5	42.6
42	VC06	West Greenland	Inner Shelf	Disko	3.5	42.6
42	VC06	West Greenland	Inner Shelf	Disko	4.5	42.7

42	VC06	West Greenland	Inner Shelf	Disko	5.5	40.6
42	VC06	West Greenland	Inner Shelf	Disko	6.5	29.2
43	VC07	West Greenland	Inner Shelf	Disko Bay	0.5	15.2
43	VC07	West Greenland	Inner Shelf	Disko Bay	1.5	14.2
43	VC07	West Greenland	Inner Shelf	Disko Bay	2.5	14.2
43	VC07	West Greenland	Inner Shelf	Disko Bay	3.5	14.2
43	VC07	West Greenland	Inner Shelf	Disko Bay	4.5	14.1
43	VC07	West Greenland	Inner Shelf	Disko Bay	5.5	13.9
43	VC07	West Greenland	Inner Shelf	Disko Bay	6.5	13.8
43	VC07	West Greenland	Inner Shelf	Disko Bay	7.5	13.8
43	VC07	West Greenland	Inner Shelf	Disko Bay	8.5	13.9
43	VC07	West Greenland	Inner Shelf	Disko Bay	9.5	14.0
43	VC07	West Greenland	Inner Shelf	Disko Bay	10.5	182.0
44	DA06-139G	West Greenland	Inner Shelf	Disko Bay	-0.5	156.6
44	DA06-139G	West Greenland	Inner Shelf	Disko Bay	0.5	118.3
44	DA06-139G	West Greenland	Inner Shelf	Disko Bay	1.5	131.4
44	DA06-139G	West Greenland	Inner Shelf	Disko Bay	2.5	89.4
44	DA06-139G	West Greenland	Inner Shelf	Disko Bay	3.5	80.8
44	DA06-139G	West Greenland	Inner Shelf	Disko Bay	4.5	41.3
45	343390-GC	West Greenland	Inner Shelf	Disko Bay	-0.5	300.8
45	343390-GC	West Greenland	Inner Shelf	Disko Bay	0.5	310.2
45	343390-GC	West Greenland	Inner Shelf	Disko Bay	1.5	220.7
46	MSM-343520_G	West Greenland	Mid Shelf	Uummannaq Trough	0.5	74.8
46	MSM-343520_G	West Greenland	Mid Shelf	Uummannaq Trough	1.5	102.0
46	MSM-343520_G	West Greenland	Mid Shelf	Uummannaq Trough	2.5	58.8

46	MSM-343520_G	West Greenland	Mid Shelf	Uummannaq Trough	3.5	55.3
46	MSM-343520_G	West Greenland	Mid Shelf	Uummannaq Trough	4.5	57.5
46	MSM-343520_G	West Greenland	Mid Shelf	Uummannaq Trough	5.5	83.2
46	MSM-343520_G	West Greenland	Mid Shelf	Uummannaq Trough	6.5	90.3
46	MSM-343520_G	West Greenland	Mid Shelf	Uummannaq Trough	7.5	102.2
46	MSM-343520_G	West Greenland	Mid Shelf	Uummannaq Trough	8.5	97.0
46	MSM-343520_G	West Greenland	Mid Shelf	Uummannaq Trough	9.5	99.6
46	MSM-343520_G	West Greenland	Mid Shelf	Uummannaq Trough	10.5	96.7
47	GeoB19973-2	West Greenland	Mid Shelf	Upernavik Trough	0.5	9.0
47	GeoB19973-2	West Greenland	Mid Shelf	Upernavik Trough	1.5	26.7
47	GeoB19973-2	West Greenland	Mid Shelf	Upernavik Trough	2.5	23.6
47	GeoB19973-2	West Greenland	Mid Shelf	Upernavik Trough	3.5	41.7
47	GeoB19973-2	West Greenland	Mid Shelf	Upernavik Trough	4.5	40.4
47	GeoB19973-2	West Greenland	Mid Shelf	Upernavik Trough	5.5	41.7
47	GeoB19973-2	West Greenland	Mid Shelf	Upernavik Trough	6.5	65.3
47	GeoB19973-2	West Greenland	Mid Shelf	Upernavik Trough	7.5	53.3
47	GeoB19973-2	West Greenland	Mid Shelf	Upernavik Trough	8.5	51.9
47	GeoB19973-2	West Greenland	Mid Shelf	Upernavik Trough	9.5	54.0
47	GeoB19973-2	West Greenland	Mid Shelf	Upernavik Trough	10.5	51.3
47	GeoB19973-2	West Greenland	Mid Shelf	Upernavik Trough	11.5	49.7
48	AMD14-204C	West Greenland	Inner Shelf	Upernavik Trough	0.5	60.4
48	AMD14-204C	West Greenland	Inner Shelf	Upernavik Trough	1.5	54.1
48	AMD14-204C	West Greenland	Inner Shelf	Upernavik Trough	2.5	47.5
48	AMD14-204C	West Greenland	Inner Shelf	Upernavik Trough	3.5	76.0
48	AMD14-204C	West Greenland	Inner Shelf	Upernavik Trough	4.5	76.2

48	AMD14-204C	West Greenland	Inner Shelf	Upernavik Trough	5.5	100.6
48	AMD14-204C	West Greenland	Inner Shelf	Upernavik Trough	6.5	125.5
48	AMD14-204C	West Greenland	Inner Shelf	Upernavik Trough	7.5	107.6
48	AMD14-204C	West Greenland	Inner Shelf	Upernavik Trough	8.5	105.5
48	AMD14-204C	West Greenland	Inner Shelf	Upernavik Trough	9.5	97.3
49	GeoB19920-1	West Greenland	Inner Shelf	Upernavik Trough	0.5	43.2
49	GeoB19920-1	West Greenland	Inner Shelf	Upernavik Trough	1.5	74.9
49	GeoB19920-1	West Greenland	Inner Shelf	Upernavik Trough	2.5	78.6
49	GeoB19920-1	West Greenland	Inner Shelf	Upernavik Trough	3.5	73.9
49	GeoB19920-1	West Greenland	Inner Shelf	Upernavik Trough	4.5	95.1
49	GeoB19920-1	West Greenland	Inner Shelf	Upernavik Trough	5.5	127.6
49	GeoB19920-1	West Greenland	Inner Shelf	Upernavik Trough	6.5	97.1
49	GeoB19920-1	West Greenland	Inner Shelf	Upernavik Trough	7.5	530.6
49	GeoB19920-1	West Greenland	Inner Shelf	Upernavik Trough	8.5	553.1
50	GeoB19927-3	West Greenland	Inner Shelf	Upernavik Trough	0.5	26.5
50	GeoB19927-3	West Greenland	Inner Shelf	Upernavik Trough	1.5	80.4
50	GeoB19927-3	West Greenland	Inner Shelf	Upernavik Trough	2.5	91.8
50	GeoB19927-3	West Greenland	Inner Shelf	Upernavik Trough	3.5	122.9
50	GeoB19927-3	West Greenland	Inner Shelf	Upernavik Trough	4.5	122.2
50	GeoB19927-3	West Greenland	Inner Shelf	Upernavik Trough	5.5	134.9
50	GeoB19927-3	West Greenland	Inner Shelf	Upernavik Trough	6.5	125.0
50	GeoB19927-3	West Greenland	Inner Shelf	Upernavik Trough	7.5	106.9
50	GeoB19927-3	West Greenland	Inner Shelf	Upernavik Trough	8.5	141.4
50	GeoB19927-3	West Greenland	Inner Shelf	Upernavik Trough	9.5	115.7
50	GeoB19927-3	West Greenland	Inner Shelf	Upernavik Trough	10.5	93.3

51	GeoB19969-1	West Greenland	Inner Shelf	Upernavik Trough	0.5	60.1
51	GeoB19969-1	West Greenland	Inner Shelf	Upernavik Trough	1.5	98.3
51	GeoB19969-1	West Greenland	Inner Shelf	Upernavik Trough	2.5	107.3
51	GeoB19969-1	West Greenland	Inner Shelf	Upernavik Trough	3.5	98.2
51	GeoB19969-1	West Greenland	Inner Shelf	Upernavik Trough	4.5	135.6
51	GeoB19969-1	West Greenland	Inner Shelf	Upernavik Trough	5.5	170.8
51	GeoB19969-1	West Greenland	Inner Shelf	Upernavik Trough	6.5	141.8
51	GeoB19969-1	West Greenland	Inner Shelf	Upernavik Trough	7.5	177.7
51	GeoB19969-1	West Greenland	Inner Shelf	Upernavik Trough	8.5	21.0
52	AMD14-210	West Greenland	Inner Shelf	Melville Bay	0.5	20.6
52	AMD14-210	West Greenland	Inner Shelf	Melville Bay	1.5	20.6
52	AMD14-210	West Greenland	Inner Shelf	Melville Bay	2.5	20.6
52	AMD14-210	West Greenland	Inner Shelf	Melville Bay	3.5	20.6
52	AMD14-210	West Greenland	Inner Shelf	Melville Bay	4.5	20.6
52	AMD14-210	West Greenland	Inner Shelf	Melville Bay	5.5	26.3
52	AMD14-210	West Greenland	Inner Shelf	Melville Bay	6.5	40.9
52	AMD14-210	West Greenland	Inner Shelf	Melville Bay	7.5	92.9
52	AMD14-210	West Greenland	Inner Shelf	Melville Bay	8.5	160.4
53	GeoB19946-4	West Greenland	Inner Shelf	Melville Bay	0.5	14.5
53	GeoB19946-4	West Greenland	Inner Shelf	Melville Bay	1.5	14.4
53	GeoB19946-4	West Greenland	Inner Shelf	Melville Bay	2.5	14.4
53	GeoB19946-4	West Greenland	Inner Shelf	Melville Bay	3.5	14.4
53	GeoB19946-4	West Greenland	Inner Shelf	Melville Bay	4.5	14.2
53	GeoB19946-4	West Greenland	Inner Shelf	Melville Bay	5.5	51.4
53	GeoB19946-4	West Greenland	Inner Shelf	Melville Bay	6.5	77.9

53	GeoB19946-4	West Greenland	Inner Shelf	Melville Bay	7.5	92.4
53	GeoB19946-4	West Greenland	Inner Shelf	Melville Bay	8.5	376.3
53	GeoB19946-4	West Greenland	Inner Shelf	Melville Bay	9.5	414.3
53	GeoB19946-4	West Greenland	Inner Shelf	Melville Bay	10.5	443.5
53	GeoB19946-4	West Greenland	Inner Shelf	Melville Bay	11.5	434.3
54	GeoB19948-3	West Greenland	Inner Shelf	Melville Bay	0.5	6.9
54	GeoB19948-3	West Greenland	Inner Shelf	Melville Bay	1.5	6.6
54	GeoB19948-3	West Greenland	Inner Shelf	Melville Bay	2.5	38.3
54	GeoB19948-3	West Greenland	Inner Shelf	Melville Bay	3.5	38.8
54	GeoB19948-3	West Greenland	Inner Shelf	Melville Bay	4.5	36.3
54	GeoB19948-3	West Greenland	Inner Shelf	Melville Bay	5.5	59.6
54	GeoB19948-3	West Greenland	Inner Shelf	Melville Bay	6.5	59.1
54	GeoB19948-3	West Greenland	Inner Shelf	Melville Bay	7.5	41.5
54	GeoB19948-3	West Greenland	Inner Shelf	Melville Bay	8.5	552.4
54	GeoB19948-3	West Greenland	Inner Shelf	Melville Bay	9.5	351.1
55	91-039-012P	Northern Baffin Bay	Inner Shelf	Hvalsund	0.5	2.0
55	91-039-012P	Northern Baffin Bay	Inner Shelf	Hvalsund	1.5	2.0
55	91-039-012P	Northern Baffin Bay	Inner Shelf	Hvalsund	2.5	2.0
55	91-039-012P	Northern Baffin Bay	Inner Shelf	Hvalsund	3.5	1.9
55	91-039-012P	Northern Baffin Bay	Inner Shelf	Hvalsund	4.5	1.9
55	91-039-012P	Northern Baffin Bay	Inner Shelf	Hvalsund	5.5	2.0
55	91-039-012P	Northern Baffin Bay	Inner Shelf	Hvalsund	6.5	2.0
55	91-039-012P	Northern Baffin Bay	Inner Shelf	Hvalsund	7.5	3.2
55	91-039-012P	Northern Baffin Bay	Inner Shelf	Hvalsund	8.5	32.8
55	91-039-012P	Northern Baffin Bay	Inner Shelf	Hvalsund	9.5	43.3

55	91-039-012P	Northern Baffin Bay	Inner Shelf	Hvalsund	10.5	44.8
55	91-039-012P	Northern Baffin Bay	Inner Shelf	Hvalsund	11.5	60.2
55	91-039-012P	Northern Baffin Bay	Inner Shelf	Hvalsund	12.5	30.9
56	GeoB22315-2	Northern Baffin Bay	Inner Shelf	Hvalsund	-0.5	59.0
56	GeoB22315-2	Northern Baffin Bay	Inner Shelf	Hvalsund	0.5	61.6
56	GeoB22315-2	Northern Baffin Bay	Inner Shelf	Hvalsund	1.5	62.0
56	GeoB22315-2	Northern Baffin Bay	Inner Shelf	Hvalsund	2.5	61.3
56	GeoB22315-2	Northern Baffin Bay	Inner Shelf	Hvalsund	3.5	86.0
56	GeoB22315-2	Northern Baffin Bay	Inner Shelf	Hvalsund	4.5	98.5
56	GeoB22315-2	Northern Baffin Bay	Inner Shelf	Hvalsund	5.5	165.8
56	GeoB22315-2	Northern Baffin Bay	Inner Shelf	Hvalsund	6.5	61.8
56	GeoB22315-2	Northern Baffin Bay	Inner Shelf	Hvalsund	7.5	54.5
56	GeoB22315-2	Northern Baffin Bay	Inner Shelf	Hvalsund	8.5	41.5
56	GeoB22315-2	Northern Baffin Bay	Inner Shelf	Hvalsund	9.5	29.7
57	117Q	Northern Baffin Bay	Inner Shelf	Hvalsund	-0.5	39.4
57	117Q	Northern Baffin Bay	Inner Shelf	Hvalsund	0.5	40.6
57	117Q	Northern Baffin Bay	Inner Shelf	Hvalsund	1.5	40.6
57	117Q	Northern Baffin Bay	Inner Shelf	Hvalsund	2.5	40.8
57	117Q	Northern Baffin Bay	Inner Shelf	Hvalsund	3.5	40.8
57	117Q	Northern Baffin Bay	Inner Shelf	Hvalsund	4.5	41.9
57	117Q	Northern Baffin Bay	Inner Shelf	Hvalsund	5.5	54.2
57	117Q	Northern Baffin Bay	Inner Shelf	Hvalsund	6.5	78.5
57	117Q	Northern Baffin Bay	Inner Shelf	Hvalsund	7.5	65.3
57	117Q	Northern Baffin Bay	Inner Shelf	Hvalsund	8.5	44.2
57	117Q	Northern Baffin Bay	Inner Shelf	Hvalsund	9.5	39.1

57	117Q	Northern Baffin Bay	Inner Shelf	Hvalsund	10.5	60.4
57	117Q	Northern Baffin Bay	Inner Shelf	Hvalsund	11.5	18.6
57	117Q	Northern Baffin Bay	Inner Shelf	Hvalsund	12.5	20.7
58	2001LSSL-014PC	Northern Baffin Bay	Inner Shelf	Smith Sound	-0.5	8.7
58	2001LSSL-014PC	Northern Baffin Bay	Inner Shelf	Smith Sound	0.5	10.0
58	2001LSSL-014PC	Northern Baffin Bay	Inner Shelf	Smith Sound	1.5	5.3
58	2001LSSL-014PC	Northern Baffin Bay	Inner Shelf	Smith Sound	2.5	5.3
58	2001LSSL-014PC	Northern Baffin Bay	Inner Shelf	Smith Sound	3.5	5.0
58	2001LSSL-014PC	Northern Baffin Bay	Inner Shelf	Smith Sound	4.5	4.3
58	2001LSSL-014PC	Northern Baffin Bay	Inner Shelf	Smith Sound	5.5	4.2
58	2001LSSL-014PC	Northern Baffin Bay	Inner Shelf	Smith Sound	6.5	4.3
58	2001LSSL-014PC	Northern Baffin Bay	Inner Shelf	Smith Sound	7.5	37.9
58	2001LSSL-014PC	Northern Baffin Bay	Inner Shelf	Smith Sound	8.5	35.4
58	2001LSSL-014PC	Northern Baffin Bay	Inner Shelf	Smith Sound	9.5	34.1
58	2001LSSL-014PC	Northern Baffin Bay	Inner Shelf	Smith Sound	10.5	80.8
59	91-039-008P	Northern Baffin Bay	Inner Shelf	Smith Sound	-0.5	45.4
59	91-039-008P	Northern Baffin Bay	Inner Shelf	Smith Sound	0.5	46.1
59	91-039-008P	Northern Baffin Bay	Inner Shelf	Smith Sound	1.5	22.0
59	91-039-008P	Northern Baffin Bay	Inner Shelf	Smith Sound	2.5	263.6
59	91-039-008P	Northern Baffin Bay	Inner Shelf	Smith Sound	3.5	242.5
59	91-039-008P	Northern Baffin Bay	Inner Shelf	Smith Sound	4.5	167.4
59	91-039-008P	Northern Baffin Bay	Inner Shelf	Smith Sound	5.5	131.1
59	91-039-008P	Northern Baffin Bay	Inner Shelf	Smith Sound	6.5	82.2
59	91-039-008P	Northern Baffin Bay	Inner Shelf	Smith Sound	7.5	68.2
60	CASQ1	Northern Baffin Bay	Inner Shelf	Smith Sound	-0.5	110.2

60	CASQ1	Northern Baffin Bay	Inner Shelf	Smith Sound	0.5	112.0
60	CASQ1	Northern Baffin Bay	Inner Shelf	Smith Sound	1.5	170.6
60	CASQ1	Northern Baffin Bay	Inner Shelf	Smith Sound	2.5	158.2
60	CASQ1	Northern Baffin Bay	Inner Shelf	Smith Sound	3.5	201.4
61	38PC	Northern Baffin Bay	Inner Shelf	Smith Sound	-0.5	57.4
61	38PC	Northern Baffin Bay	Inner Shelf	Smith Sound	0.5	58.9
61	38PC	Northern Baffin Bay	Inner Shelf	Smith Sound	1.5	59.2
61	38PC	Northern Baffin Bay	Inner Shelf	Smith Sound	2.5	59.1
61	38PC	Northern Baffin Bay	Inner Shelf	Smith Sound	3.5	136.4
61	38PC	Northern Baffin Bay	Inner Shelf	Smith Sound	4.5	187.8
61	38PC	Northern Baffin Bay	Inner Shelf	Smith Sound	5.5	137.4
61	38PC	Northern Baffin Bay	Inner Shelf	Smith Sound	6.5	136.2
61	38PC	Northern Baffin Bay	Inner Shelf	Smith Sound	7.5	96.1
62	HU2008-029-34	Northern Baffin Bay	Inner Shelf	Smith Sound	0.5	36.4
62	HU2008-029-34	Northern Baffin Bay	Inner Shelf	Smith Sound	1.5	36.4
62	HU2008-029-34	Northern Baffin Bay	Inner Shelf	Smith Sound	2.5	36.6
62	HU2008-029-34	Northern Baffin Bay	Inner Shelf	Smith Sound	3.5	36.4
62	HU2008-029-34	Northern Baffin Bay	Inner Shelf	Smith Sound	4.5	72.0
62	HU2008-029-34	Northern Baffin Bay	Inner Shelf	Smith Sound	5.5	80.3
62	HU2008-029-34	Northern Baffin Bay	Inner Shelf	Smith Sound	6.5	79.4
62	HU2008-029-34	Northern Baffin Bay	Inner Shelf	Smith Sound	7.5	81.0
62	HU2008-029-34	Northern Baffin Bay	Inner Shelf	Smith Sound	8.5	78.5
63	01PC	Northern Baffin Bay	Inner Shelf	Smith Sound	0.5	15.9
63	01PC	Northern Baffin Bay	Inner Shelf	Smith Sound	1.5	17.0
63	01PC	Northern Baffin Bay	Inner Shelf	Smith Sound	2.5	5.3

63	01PC	Northern Baffin Bay	Inner Shelf	Smith Sound	3.5	5.5
63	01PC	Northern Baffin Bay	Inner Shelf	Smith Sound	4.5	5.7
63	01PC	Northern Baffin Bay	Inner Shelf	Smith Sound	5.5	6.2
63	01PC	Northern Baffin Bay	Inner Shelf	Smith Sound	6.5	7.2
63	01PC	Northern Baffin Bay	Inner Shelf	Smith Sound	7.5	6.7
63	01PC	Northern Baffin Bay	Inner Shelf	Smith Sound	8.5	6.0
63	01PC	Northern Baffin Bay	Inner Shelf	Smith Sound	9.5	5.4
63	01PC	Northern Baffin Bay	Inner Shelf	Smith Sound	10.5	65.7
64	LSSL2001-006	Northern Baffin Bay	Inner Shelf	Jones Sound	-0.5	179.3
64	LSSL2001-006	Northern Baffin Bay	Inner Shelf	Jones Sound	0.5	188.1
64	LSSL2001-006	Northern Baffin Bay	Inner Shelf	Jones Sound	1.5	188.6
64	LSSL2001-006	Northern Baffin Bay	Inner Shelf	Jones Sound	2.5	178.8
64	LSSL2001-006	Northern Baffin Bay	Inner Shelf	Jones Sound	3.5	155.2
64	LSSL2001-006	Northern Baffin Bay	Inner Shelf	Jones Sound	4.5	157.1
64	LSSL2001-006	Northern Baffin Bay	Inner Shelf	Jones Sound	5.5	157.8
64	LSSL2001-006	Northern Baffin Bay	Inner Shelf	Jones Sound	6.5	153.3
65	42PC	Northern Baffin Bay	Inner Shelf	Jones Sound	-0.5	188.4
65	42PC	Northern Baffin Bay	Inner Shelf	Jones Sound	0.5	120.9
65	42PC	Northern Baffin Bay	Inner Shelf	Jones Sound	1.5	91.9
65	42PC	Northern Baffin Bay	Inner Shelf	Jones Sound	2.5	91.8
65	42PC	Northern Baffin Bay	Inner Shelf	Jones Sound	3.5	91.8
65	42PC	Northern Baffin Bay	Inner Shelf	Jones Sound	4.5	91.7
65	42PC	Northern Baffin Bay	Inner Shelf	Jones Sound	5.5	92.1
65	42PC	Northern Baffin Bay	Inner Shelf	Jones Sound	6.5	101.5
65	42PC	Northern Baffin Bay	Inner Shelf	Jones Sound	7.5	113.3

65	42PC	Northern Baffin Bay	Inner Shelf	Jones Sound	8.5	107.1
66	2004-804-009 PC	Northern Baffin Bay	Inner Shelf	Lancaster Sound	0.5	33.4
66	2004-804-009 PC	Northern Baffin Bay	Inner Shelf	Lancaster Sound	1.5	33.4
66	2004-804-009 PC	Northern Baffin Bay	Inner Shelf	Lancaster Sound	2.5	33.4
66	2004-804-009 PC	Northern Baffin Bay	Inner Shelf	Lancaster Sound	3.5	33.4
66	2004-804-009 PC	Northern Baffin Bay	Inner Shelf	Lancaster Sound	4.5	33.4
66	2004-804-009 PC	Northern Baffin Bay	Inner Shelf	Lancaster Sound	5.5	33.4
66	2004-804-009 PC	Northern Baffin Bay	Inner Shelf	Lancaster Sound	6.5	48.1
66	2004-804-009 PC	Northern Baffin Bay	Inner Shelf	Lancaster Sound	7.5	50.5
66	2004-804-009 PC	Northern Baffin Bay	Inner Shelf	Lancaster Sound	8.5	79.8
66	2004-804-009 PC	Northern Baffin Bay	Inner Shelf	Lancaster Sound	9.5	119.5
66	2004-804-009 PC	Northern Baffin Bay	Inner Shelf	Lancaster Sound	10.5	76.1
66	2004-804-009 PC	Northern Baffin Bay	Inner Shelf	Lancaster Sound	11.5	65.7
67	2011804-0010PC	Northern Baffin Bay	Inner Shelf	Lancaster Sound	0.5	1.5
67	2011804-0010PC	Northern Baffin Bay	Inner Shelf	Lancaster Sound	1.5	1.0
67	2011804-0010PC	Northern Baffin Bay	Inner Shelf	Lancaster Sound	2.5	1.0
67	2011804-0010PC	Northern Baffin Bay	Inner Shelf	Lancaster Sound	3.5	1.0
67	2011804-0010PC	Northern Baffin Bay	Inner Shelf	Lancaster Sound	4.5	1.0
67	2011804-0010PC	Northern Baffin Bay	Inner Shelf	Lancaster Sound	5.5	1.0
67	2011804-0010PC	Northern Baffin Bay	Inner Shelf	Lancaster Sound	6.5	1.0
67	2011804-0010PC	Northern Baffin Bay	Inner Shelf	Lancaster Sound	7.5	1.0
67	2011804-0010PC	Northern Baffin Bay	Inner Shelf	Lancaster Sound	8.5	1.0
67	2011804-0010PC	Northern Baffin Bay	Inner Shelf	Lancaster Sound	9.5	1.2
67	2011804-0010PC	Northern Baffin Bay	Inner Shelf	Lancaster Sound	10.5	76.6
67	2011804-0010PC	Northern Baffin Bay	Inner Shelf	Lancaster Sound	11.5	88.6

67	2011804-0010PC	Northern Baffin Bay	Inner Shelf	Lancaster Sound	12.5	172.5
68	2011804-0010TWC	Northern Baffin Bay	Inner Shelf	Lancaster Sound	0.5	1.5
68	2011804-0010TWC	Northern Baffin Bay	Inner Shelf	Lancaster Sound	1.5	1.0
68	2011804-0010TWC	Northern Baffin Bay	Inner Shelf	Lancaster Sound	2.5	1.0
68	2011804-0010TWC	Northern Baffin Bay	Inner Shelf	Lancaster Sound	3.5	1.0
68	2011804-0010TWC	Northern Baffin Bay	Inner Shelf	Lancaster Sound	4.5	1.0
68	2011804-0010TWC	Northern Baffin Bay	Inner Shelf	Lancaster Sound	5.5	1.0
68	2011804-0010TWC	Northern Baffin Bay	Inner Shelf	Lancaster Sound	6.5	1.0
68	2011804-0010TWC	Northern Baffin Bay	Inner Shelf	Lancaster Sound	7.5	1.0
68	2011804-0010TWC	Northern Baffin Bay	Inner Shelf	Lancaster Sound	8.5	1.0
68	2011804-0010TWC	Northern Baffin Bay	Inner Shelf	Lancaster Sound	9.5	1.2
68	2011804-0010TWC	Northern Baffin Bay	Inner Shelf	Lancaster Sound	10.5	73.1
68	2011804-0010TWC	Northern Baffin Bay	Inner Shelf	Lancaster Sound	11.5	128.2
68	2011804-0010TWC	Northern Baffin Bay	Inner Shelf	Lancaster Sound	12.5	166.3
69	GeoB22336-4	Northern Baffin Bay	Mid Shelf	Lancaster Sound	-0.5	32.9
69	GeoB22336-4	Northern Baffin Bay	Mid Shelf	Lancaster Sound	0.5	35.1
69	GeoB22336-4	Northern Baffin Bay	Mid Shelf	Lancaster Sound	1.5	34.3
69	GeoB22336-4	Northern Baffin Bay	Mid Shelf	Lancaster Sound	2.5	30.7
69	GeoB22336-4	Northern Baffin Bay	Mid Shelf	Lancaster Sound	3.5	31.7
69	GeoB22336-4	Northern Baffin Bay	Mid Shelf	Lancaster Sound	4.5	32.3
69	GeoB22336-4	Northern Baffin Bay	Mid Shelf	Lancaster Sound	5.5	30.6
69	GeoB22336-4	Northern Baffin Bay	Mid Shelf	Lancaster Sound	6.5	48.8
69	GeoB22336-4	Northern Baffin Bay	Mid Shelf	Lancaster Sound	7.5	48.3
69	GeoB22336-4	Northern Baffin Bay	Mid Shelf	Lancaster Sound	8.5	30.0
69	GeoB22336-4	Northern Baffin Bay	Mid Shelf	Lancaster Sound	9.5	26.4

69	GeoB22336-4	Northern Baffin Bay	Mid Shelf	Lancaster Sound	10.5	54.3
69	GeoB22336-4	Northern Baffin Bay	Mid Shelf	Lancaster Sound	11.5	58.4
69	GeoB22336-4	Northern Baffin Bay	Mid Shelf	Lancaster Sound	12.5	52.8
69	GeoB22336-4	Northern Baffin Bay	Mid Shelf	Lancaster Sound	13.5	47.5
69	GeoB22336-4	Northern Baffin Bay	Mid Shelf	Lancaster Sound	14.5	43.7
70	49PC	Northern Baffin Bay	Mid Shelf	Lancaster Sound	-0.5	21.8
70	49PC	Northern Baffin Bay	Mid Shelf	Lancaster Sound	0.5	22.4
70	49PC	Northern Baffin Bay	Mid Shelf	Lancaster Sound	1.5	22.5
70	49PC	Northern Baffin Bay	Mid Shelf	Lancaster Sound	2.5	22.4
70	49PC	Northern Baffin Bay	Mid Shelf	Lancaster Sound	3.5	22.5
70	49PC	Northern Baffin Bay	Mid Shelf	Lancaster Sound	4.5	22.4
70	49PC	Northern Baffin Bay	Mid Shelf	Lancaster Sound	5.5	22.5
70	49PC	Northern Baffin Bay	Mid Shelf	Lancaster Sound	6.5	22.4
70	49PC	Northern Baffin Bay	Mid Shelf	Lancaster Sound	7.5	22.4
70	49PC	Northern Baffin Bay	Mid Shelf	Lancaster Sound	8.5	46.6
70	49PC	Northern Baffin Bay	Mid Shelf	Lancaster Sound	9.5	28.1
70	49PC	Northern Baffin Bay	Mid Shelf	Lancaster Sound	10.5	56.6
70	49PC	Northern Baffin Bay	Mid Shelf	Lancaster Sound	11.5	194.9
71	2013029-66	Baffin Island	Inner Shelf	NE Baffin Island	0.5	22.7
71	2013029-66	Baffin Island	Inner Shelf	NE Baffin Island	1.5	39.7
71	2013029-66	Baffin Island	Inner Shelf	NE Baffin Island	2.5	39.8
71	2013029-66	Baffin Island	Inner Shelf	NE Baffin Island	3.5	53.1
71	2013029-66	Baffin Island	Inner Shelf	NE Baffin Island	4.5	71.1
71	2013029-66	Baffin Island	Inner Shelf	NE Baffin Island	5.5	70.8
71	2013029-66	Baffin Island	Inner Shelf	NE Baffin Island	6.5	70.7

71	2013029-66	Baffin Island	Inner Shelf	NE Baffin Island	7.5	70.7
71	2013029-66	Baffin Island	Inner Shelf	NE Baffin Island	8.5	70.8
71	2013029-66	Baffin Island	Inner Shelf	NE Baffin Island	9.5	69.3
72	2013029-65	Baffin Island	Inner Shelf	NE Baffin Island	-0.5	58.4
72	2013029-65	Baffin Island	Inner Shelf	NE Baffin Island	0.5	60.8
72	2013029-65	Baffin Island	Inner Shelf	NE Baffin Island	1.5	63.7
72	2013029-65	Baffin Island	Inner Shelf	NE Baffin Island	2.5	128.6
72	2013029-65	Baffin Island	Inner Shelf	NE Baffin Island	3.5	70.6
72	2013029-65	Baffin Island	Inner Shelf	NE Baffin Island	4.5	81.1
72	2013029-65	Baffin Island	Inner Shelf	NE Baffin Island	5.5	79.1
72	2013029-65	Baffin Island	Inner Shelf	NE Baffin Island	6.5	79.2
72	2013029-65	Baffin Island	Inner Shelf	NE Baffin Island	7.5	78.4
72	2013029-65	Baffin Island	Inner Shelf	NE Baffin Island	8.5	78.3
72	2013029-65	Baffin Island	Inner Shelf	NE Baffin Island	9.5	77.8
72	2013029-65	Baffin Island	Inner Shelf	NE Baffin Island	10.5	76.3
73	2013029-67	Baffin Island	Inner Shelf	NE Baffin Island	0.5	104.4
73	2013029-67	Baffin Island	Inner Shelf	NE Baffin Island	1.5	191.0
73	2013029-67	Baffin Island	Inner Shelf	NE Baffin Island	2.5	246.4
73	2013029-67	Baffin Island	Inner Shelf	NE Baffin Island	3.5	238.2
74	GeoB22346-3	Baffin Island	Inner Shelf	Clyde Trough	0.5	82.0
74	GeoB22346-3	Baffin Island	Inner Shelf	Clyde Trough	1.5	83.5
74	GeoB22346-3	Baffin Island	Inner Shelf	Clyde Trough	2.5	62.8
74	GeoB22346-3	Baffin Island	Inner Shelf	Clyde Trough	3.5	57.7
74	GeoB22346-3	Baffin Island	Inner Shelf	Clyde Trough	4.5	52.4
74	GeoB22346-3	Baffin Island	Inner Shelf	Clyde Trough	5.5	49.5

74	GeoB22346-3	Baffin Island	Inner Shelf	Clyde Trough	6.5	95.8
74	GeoB22346-3	Baffin Island	Inner Shelf	Clyde Trough	7.5	109.6
74	GeoB22346-3	Baffin Island	Inner Shelf	Clyde Trough	8.5	156.1
74	GeoB22346-3	Baffin Island	Inner Shelf	Clyde Trough	9.5	93.5
75	GeoB22357-3	Baffin Island	Mid Shelf	Clyde Trough	0.5	13.6
75	GeoB22357-3	Baffin Island	Mid Shelf	Clyde Trough	1.5	13.5
75	GeoB22357-3	Baffin Island	Mid Shelf	Clyde Trough	2.5	13.5
75	GeoB22357-3	Baffin Island	Mid Shelf	Clyde Trough	3.5	13.5
75	GeoB22357-3	Baffin Island	Mid Shelf	Clyde Trough	4.5	13.5
75	GeoB22357-3	Baffin Island	Mid Shelf	Clyde Trough	5.5	13.5
75	GeoB22357-3	Baffin Island	Mid Shelf	Clyde Trough	6.5	13.5
75	GeoB22357-3	Baffin Island	Mid Shelf	Clyde Trough	7.5	13.5
75	GeoB22357-3	Baffin Island	Mid Shelf	Clyde Trough	8.5	13.6
75	GeoB22357-3	Baffin Island	Mid Shelf	Clyde Trough	9.5	89.1
75	GeoB22357-3	Baffin Island	Mid Shelf	Clyde Trough	10.5	229.3
75	GeoB22357-3	Baffin Island	Mid Shelf	Clyde Trough	11.5	282.5
76	2018042-67	Baffin Island	Mid Shelf	Clyde Trough	0.5	3.4
76	2018042-67	Baffin Island	Mid Shelf	Clyde Trough	1.5	3.3
76	2018042-67	Baffin Island	Mid Shelf	Clyde Trough	2.5	3.3
76	2018042-67	Baffin Island	Mid Shelf	Clyde Trough	3.5	3.3
76	2018042-67	Baffin Island	Mid Shelf	Clyde Trough	4.5	3.3
76	2018042-67	Baffin Island	Mid Shelf	Clyde Trough	5.5	3.3
76	2018042-67	Baffin Island	Mid Shelf	Clyde Trough	6.5	3.3
76	2018042-67	Baffin Island	Mid Shelf	Clyde Trough	7.5	3.3
76	2018042-67	Baffin Island	Mid Shelf	Clyde Trough	8.5	3.3

76	2018042-67	Baffin Island	Mid Shelf	Clyde Trough	9.5	3.3
76	2018042-67	Baffin Island	Mid Shelf	Clyde Trough	10.5	3.4
76	2018042-67	Baffin Island	Mid Shelf	Clyde Trough	11.5	5.5
77	2018042-16	Baffin Island	Mid Shelf	SE Baffin Island	0.5	7.1
77	2018042-16	Baffin Island	Mid Shelf	SE Baffin Island	1.5	7.0
77	2018042-16	Baffin Island	Mid Shelf	SE Baffin Island	2.5	7.0
77	2018042-16	Baffin Island	Mid Shelf	SE Baffin Island	3.5	7.0
77	2018042-16	Baffin Island	Mid Shelf	SE Baffin Island	4.5	7.0
77	2018042-16	Baffin Island	Mid Shelf	SE Baffin Island	5.5	7.0
77	2018042-16	Baffin Island	Mid Shelf	SE Baffin Island	6.5	7.0
77	2018042-16	Baffin Island	Mid Shelf	SE Baffin Island	7.5	7.0
77	2018042-16	Baffin Island	Mid Shelf	SE Baffin Island	8.5	7.0
77	2018042-16	Baffin Island	Mid Shelf	SE Baffin Island	9.5	33.9
77	2018042-16	Baffin Island	Mid Shelf	SE Baffin Island	10.5	45.5
77	2018042-16	Baffin Island	Mid Shelf	SE Baffin Island	11.5	42.2
78	2018042-24	Baffin Island	Inner Shelf	SE Baffin Island	-0.5	248.4
78	2018042-24	Baffin Island	Inner Shelf	SE Baffin Island	0.5	359.2
79	HU82-SU5	Baffin Island	Inner Shelf	SE Baffin Island	-0.5	27.1
79	HU82-SU5	Baffin Island	Inner Shelf	SE Baffin Island	0.5	27.7
79	HU82-SU5	Baffin Island	Inner Shelf	SE Baffin Island	1.5	27.8
79	HU82-SU5	Baffin Island	Inner Shelf	SE Baffin Island	2.5	27.9
79	HU82-SU5	Baffin Island	Inner Shelf	SE Baffin Island	3.5	28.0
79	HU82-SU5	Baffin Island	Inner Shelf	SE Baffin Island	4.5	27.9
79	HU82-SU5	Baffin Island	Inner Shelf	SE Baffin Island	5.5	26.9
79	HU82-SU5	Baffin Island	Inner Shelf	SE Baffin Island	6.5	27.3

79	HU82-SU5	Baffin Island	Inner Shelf	SE Baffin Island	7.5	28.8
79	HU82-SU5	Baffin Island	Inner Shelf	SE Baffin Island	8.5	28.3
79	HU82-SU5	Baffin Island	Inner Shelf	SE Baffin Island	9.5	60.5
79	HU82-SU5	Baffin Island	Inner Shelf	SE Baffin Island	10.5	231.9
79	HU82-SU5	Baffin Island	Inner Shelf	SE Baffin Island	11.5	221.8

Table 9.3.4: Mean sedimentation rates, accumulation rates, and derived subglacial erosion rates for west Greenland during late deglacial and postglacial intervals.

West Greenland	Mean SR (cm/ka)		Mean SAR (g/cm ² /ka)		Trough Area** (cm ²)	Paleo-ice stream drainage basin Area (cm ²)	Mass accumulation (g/ka)		Sediment flux (cm ³ /ka)		Erosion rates (mm/yr)	
	Deglacial	Postglacial	Deglacial	Postglacial			Deglacial	Postglacial	Deglacial	Postglacial	Deglacial	Postglacial
Disko Bay	153.8	94.4	123.0	75.5	4.3x10 ¹⁰	1.0x10 ¹¹	5.2x10 ¹²	3.2x10 ¹²	1.9x10 ¹²	1.2x10 ¹²	0.19	0.12
Uummannaq ⁻	97.2	71.8	77.8	57.5	2.7x10 ¹⁰	9.5x10 ¹⁰	2.1x10 ¹²	1.6x10 ¹²	7.8x10 ¹¹	5.7x10 ¹¹	0.08	0.06
Upernavik ⁺	157.3	78.0	125.9	62.4	1.2x10 ¹⁰	4.5x10 ¹⁰	1.5x10 ¹²	7.5x10 ¹¹	5.6x10 ¹¹	2.8x10 ¹¹	0.12	0.06
Melville Bay [#]	218.4	24.4	174.7	19.5	2.5x10 ¹⁰	4.5x10 ¹⁰	4.4x10 ¹²	4.9x10 ¹¹	1.6x10 ¹²	1.8x10 ¹¹	0.36	0.04
WGS integration considering drainage basin extent												
2.9 x10 ¹¹	Deglacial	Postglacial										
0.3509	0.068	0.042										
0.3333	0.027	0.020										
0.1579	0.020	0.010										
0.1579	0.057	0.006										

Mean erosion rates (mm/yr)	0.17	0.08
----------------------------	------	------

Sediment density = 0.8 g/cm³

Rock density = 2.7 g/cm³

**Trough area = trough width * shelf width
(from Batchelor & Dowsdewell, 2014)

single core⁻

no outer shelf core⁺

Inner shelf cores[#]

Versicherung an Eides Statt / *Affirmation in lieu of an oath*

gem. § 5 Abs. 5 der Promotionsordnung vom 18.06.2018 /

according to § 5 (5) of the Doctoral Degree Rules and Regulations of 18 June, 2018

Ich / I, Emmanuel Okuma, Bremen, Germany, 3029305

(Vorname / *First Name*, Name / *Name*, Anschrift / *Address*, ggf. Matr.-Nr. / *student ID no.*, *if applicable*)

versichere an Eides Statt durch meine Unterschrift, dass ich die vorliegende Dissertation selbständig und ohne fremde Hilfe angefertigt und alle Stellen, die ich wörtlich dem Sinne nach aus Veröffentlichungen entnommen habe, als solche kenntlich gemacht habe, mich auch keiner anderen als der angegebenen Literatur oder sonstiger Hilfsmittel bedient habe und die zu Prüfungszwecken beigelegte elektronische Version (PDF) der Dissertation mit der abgegebenen gedruckten Version identisch ist. / *With my signature I affirm in lieu of an oath that I prepared the submitted dissertation independently and without illicit assistance from third parties, that I appropriately referenced any text or content from other sources, that I used only literature and resources listed in the dissertation, and that the electronic (PDF) and printed versions of the dissertation are identical.*

Ich versichere an Eides Statt, dass ich die vorgenannten Angaben nach bestem Wissen und Gewissen gemacht habe und dass die Angaben der Wahrheit entsprechen und ich nichts verschwiegen habe. / *I affirm in lieu of an oath that the information provided herein to the best of my knowledge is true and complete.*

Die Strafbarkeit einer falschen eidesstattlichen Versicherung ist mir bekannt, namentlich die Strafandrohung gemäß § 156 StGB bis zu drei Jahren Freiheitsstrafe oder Geldstrafe bei vorsätzlicher Begehung der Tat bzw. gemäß § 161 Abs. 1 StGB bis zu einem Jahr Freiheitsstrafe oder Geldstrafe bei fahrlässiger Begehung. / *I am aware that a false affidavit is a criminal offence which is punishable by law in accordance with § 156 of the German Criminal Code (StGB) with up to three years imprisonment or a fine in case of intention, or in accordance with § 161 (1) of the German Criminal Code with up to one year imprisonment or a fine in case of negligence.*

Bremen, 27.10.2023

Ort / *Place*, Datum / *Date*

Unterschrift / *Signature*